Bioavailability of Matrix-Bound Growth Factors in Cartilage Injury

---

Stuart Joseph Keppie

Supervised by
Professor Tonia Vincent

Magdalen College
University of Oxford

A thesis submitted in fulfilment of the requirements
for the degree of *Doctor of Philosophy*

Hilary Term 2021

Abstract

Bioavailability of Matrix-Bound Growth Factors in Cartilage Injury

Articular cartilage is a dense extracellular matrix-rich tissue that degrades following chronic mechanical stress, resulting in osteoarthritis. In this work, hepatoma-derived growth factor, previously uncharacterised in cartilage, was discovered to be bound to extracellular matrix heparan sulfate in cartilage. Previously described pericellular matrix growth factors fibroblast growth factor 2 (FGF2) and connective tissue growth factor (CTGF/CCN2), along with hepatoma-derived growth factor (HDGF) were all rapidly released upon injury, independent of cellular viability, and were displaced by exogenous NaCl. I hypothesised that matrix sodium, sequestered within the further removed, aggrecan-rich matrix, was responsible for displacing growth factors upon injury, thereby enhancing their bioavailability. This was confirmed by showing that NaCl was able to release growth factors from cartilage. Furthermore, growth factor release was abrogated by interleukin-1 mediated depletion of matrix aggrecan and sodium, and also in severely damaged human osteoarthritic cartilage with reduced matrix sodium. Finally, a flux in free matrix sodium upon mechanical compression of cartilage was directly visualised by ^{23}Na-MRI imaging. These data corroborate an increase in free matrix sodium upon mechanical injury, able to displace heparan sulfate-bound growth factors in healthy cartilage, which is lost in osteoarthritis. Preliminary data after inducing osteoarthritis in *Hdgf*$^{-/-}$ mice indicated that HDGF, like FGF2, is chondroprotective *in vivo*, with putative proliferative effects on mesenchymal stem cells. Together, these results describe a novel intrinsic repair mechanism,

mediated by free sodium, in which heparan sulfate-bound growth factors are released from cartilage upon injurious load. They identify aggrecan as a depot for sequestered sodium, and explain why osteoarthritic tissue loses its ability to repair. Treatments that restore matrix sodium to allow appropriate release of growth factors upon load may therefore restore intrinsic cartilage repair in osteoarthritis.

Declaration

I hereby declare that the experiments, as well as the writing up of this thesis are my own work. Wherever I received assistance or collaborated to produce results, I have appropriately acknowledged this within each chapter. All experimental work was undertaken in line with the regulations of the Kennedy Institute of Rheumatology and Doctoral Training Partnership at the University of Oxford.

Permissions for material used within this thesis that was not my own were requested and granted by all relevant authors and publishers. All material was appropriately cited and acknowledged in the relevant sections throughout this thesis.

Acknowledgements

First and foremost, I would like to thank my supervisor, Professor Tonia Vincent, for her continued inspiration and support throughout my DPhil. Tonia has challenged me, helped to develop my critical thinking and encouraged me to pursue and take ownership of my work and ideas.

My research was possible through the help of my lab members and collaborators. Therefore, I want to thank the Histology team at the Kennedy Institute of Rheumatology and lab members of the Oxford Centre for Osteoarthritis Pathogenesis for their invaluable input. Additionally, I would like to thank my external collaborators for hosting me at their institutions, and the Biotechnology and Biological Sciences Research Council and Doctoral Training Programme for funding my studies.

I am grateful for the opportunities throughout my DPhil at the University of Oxford. In academia, I mentored two students in the laboratory on independent projects and presented my work at conferences and STEM outreach events. Outside of academia, Oxford University TaeKwonDo provided an outlet to compete, teach and develop. Grading for my black belt and serving as President in 2018–2019 proved hard but rewarding, and these opportunities have all augmented my DPhil experience.

Contents

1 Introduction 1

1.1 Cartilage structure and function 1

1.1.1 Cartilage types 1

1.1.2 The chondrocyte 2

1.1.3 Extracellular matrix 3

1.1.3.1 Pericellular matrix 6

1.1.3.2 Heparan sulfate 7

1.1.3.3 Chondroitin sulfate 10

1.2 Cartilage fixed charge density 12

1.2.1 Ions in cartilage 13

1.2.2 Extracellular sodium in cartilage 14

1.2.3 Alternative cations ions in cartilage 15

1.2.4 Measuring charge in tissue 16

1.3 Protein-salt interactions 19

1.3.1 Salt precipitation 19

1.3.2 Ionic screening 20

1.4 Osteoarthritis 21

1.4.1 Matrix changes in osteoarthritis 22

1.4.2 Sulfation patterning in osteoarthritis 24

1.4.3 Mechanical changes in osteoarthritis 25

1.4.4 Models of osteoarthritis 26

1.5 Cartilage injury responses 28

1.5.1 Mechanoflammation 29

1.5.2 Cartilage tissue repair 32

1.5.3 Cartilage injury models 36

1.6 Cartilage matrix growth factors 37

1.6.1 Fibroblast growth factors 37
1.6.1.1 Fibroblast growth factor 2 40
1.6.2 Connective tissue growth factor 42
1.6.2.1 Transforming Growth Factor Beta 45
1.6.3 Hepatoma-derived growth factor 48
1.6.4 Other cartilage growth factors 52
1.6.5 Heparin-binding growth factors 54
1.7 Cartilage response to mechanical load 55
1.7.1 Chondrocyte mechanotransduction 57
1.7.2 Fluid flow 59
1.7.3 Ion fluxes 59
1.8 Research aims 61
2 Materials and Methods 62
2.1 Tissue culture 62
2.1.1 Cartilage explantation 62
2.1.2 Chondrocyte isolation 63
2.1.3 Chondron isolation 63
2.1.4 Adipose tissue derived mesenchymal stem cells 64
2.2 Cartilage Injury 64
2.2.1 Explantation Injury 64
2.2.2 Recut Injury 65
2.2.3 Mechanical loading 65
2.3 RNA extraction 66
2.3.1 Chondrocytes 66
2.3.2 Tissue explants 66
2.4 Real-time polymerase chain reaction (RT-PCR) 67
2.4.1 Reverse Transcription 67
2.4.2 Primer Design 67
2.4.3 Manual quantitative RT-PCR 68

2.4.4 Taqman gene array microfluidic cards 68
2.4.5 Relative gene expression quantification 68
2.5 Protein analysis 69
2.5.1 Protein extraction 69
2.5.2 Western blot 69
2.5.3 FGF2 ELISA 70
2.5.4 Immunohistochemistry 70
2.5.5 Heparin affinity chromatography 71
2.6 Histology 72
2.6.1 Paraffin embedding 72
2.6.2 Safranin O 72
2.6.3 Cryosectioning 72
2.7 Knockout mouse generation 73
2.8 Animal husbandry 73
2.8.1 Surgery 73
2.9 Statistics 74
3 HDGF Release upon Cartilage Injury 75
3.1 Introduction 75
3.2 Methods 77
3.2.1 Cartilage injury 77
3.2.1.1 Recutting model 77
3.2.1.2 Explantation model 77
3.2.2 Chondrocyte ablation and treatment 77
3.2.3 Red blood cell assay 78
3.2.4 Immunohistochemistry 78
3.2.5 Heparitinase treatment 79
3.2.6 Heparin column chromatography 79
3.3 Results 80
3.3.1 HDGF is released upon cartilage injury 81

3.3.2 HDGF mRNA is not regulated upon injury 86
3.3.3 Cartilage releases growth factors irrespective of chondrocyte viability 87
3.3.4 Release of growth factors upon injury is temperature and protease independent 88
3.3.5 Imaging HDGF in cartilage 89
3.3.6 Heparitinase treatment liberates HDGF from cartilage explants 94
3.3.7 Pericellular matrix growth factors bind to heparin-sepharose and are eluted with salt 96
3.4 Discussion 98
4 Sodium Mobilisation as a Mechanism for Release of Heparan Sulfate-Bound Growth Factors upon Cartilage Injury 104
4.1 Introduction 104
4.2 Methods 107
4.2.1 Cartilage injury 107
4.2.1.1 Recutting model 107
4.2.1.2 Explantation model 107
4.2.2 Sodium addition 108
4.2.3 IL-1 dependent sodium depletion 108
4.2.4 DMMB assay 108
4.2.5 Histology 109
4.2.6 Osteoarthritis disease scoring 109
4.2.7 CoroNa imaging 110
4.2.8 Sodium MRI imaging 111
4.3 Results 115
4.3.1 Exogenous sodium releases growth factors 115
4.3.2 Reduced fixed charge density reduces growth factor release 120
4.3.3 Fixed charge density and growth factor release are lost in osteoarthritis progression 131
4.3.4 SGK1 sodium-sensitivity 136

4.3.5 Fluorescent sodium imaging with CoroNa green 141
4.3.6 Sodium ^{23}Na-MRI imaging in cartilage 145
4.4 Discussion 148
5 Function of HDGF in Cartilage 162
5.1 Introduction 162
5.2 Methods 165
5.2.1 Cartilage injury 165
5.2.1.1 Hip avulsion model 165
5.2.1.2 Destabilisation of the medial meniscus 165
5.2.2 Histology 167
5.2.2.1 DMM staining 167
5.2.2.2 Histological OA scoring 168
5.2.2.3 Cartilage thickness 168
5.2.3 TaqMan microfluidic cards 169
5.2.4 Heparin column chromatography 173
5.2.5 Adipose tissue-derived mesenchymal stem cell stimulation 173
5.3 Results 175
5.3.1 Phenotype of the *Hdgf* $^{-/-}$ knockout joint 175
5.3.2 HDGF in a surgical model of osteoarthritis 177
5.3.3 Genetic substrain influence on mouse weight 180
5.3.4 Altered gene regulation in *Hdgf* knockout mice upon cartilage injury 181
5.3.5 Heparin-binding proteins from injury CM have proliferative effects on mesenchymal stem cells 185
5.4 Discussion 191
6 Discussion 204
7 Bibliography 215
8 Appendix 236
8.1 Achievements 237
8.2 Reagents 249

8.3 Equipment 250
8.4 Supplementary 251

List of Figures

Figure 1.1 Ultrastructure of articular cartilage. 2

Figure 1.2 Distinct matrix regions of the extracellular matrix of articular cartilage. .. 4

Figure 1.3 Structure of heparan sulfate and heparin disaccharide units. 9

Figure 1.4 Structure of chondroitin sulfate disaccharide units. 11

Figure 1.5 Aggrecan structure and aggrecanase cleavage. 23

Figure 1.6 Cartilage injury-activated pathways in the chondrocyte. 31

Figure 1.7 Canonical FGF:FGFR signalling. 39

Figure 1.8 Connective tissue growth factor (CTGF/CCN2) function in cartilage..... 44

Figure 1.9 Canonical TGFβ and BMP signalling pathways. 46

Figure 1.10 Illustrative structure and domains of HDGF. 49

Figure 1.11 Putative actions of hepatoma-derived growth factor. 52

Figure 3.1 Dry weight of explants from three independent porcine trotters. 82

Figure 3.2 HDGF release by recut injury. 83

Figure 3.3 HDGF release by explantation injury. 84

Figure 3.4 Mouse hip avulsion injury in *Hdgf*$^{-/-}$ mice releases CTGF and FGF2, but not HDGF. 85

Figure 3.5 Growth factors HDGF, CTGF and FGF2 are released upon injury from human cartilage. 86

Figure 3.6 *HDGF* mRNA is not regulated in porcine cartilage 24 h after explantation. 87

Figure 3.7 Growth factors are released from live and dead cartilage upon recutting injury. 88

Figure 3.8 Growth factors are released by recutting injury, independent of temperature, MMP activity and protease activity. 89
Figure 3.9 Confocal microscopy of HDGF and perlecan in human osteoarthritic tissue chondrons. 90
Figure 3.10 Human osteoarthritic whole tissue confocal of HDGF and perlecan. 91
Figure 3.11 Red blood cell exclusion assay validation of chondron isolation with 2 h collagenase and dispase. 92
Figure 3.12 Porcine pericellular matrix confocal imaging. 93
Figure 3.13 Porcine pericellular matrix confocal imaging. 94
Figure 3.14 Heparitinase treatment of cartilage releases growth factors HDGF, CTGF and FGF2. 95
Figure 3.15 Heparitinase treatment of porcine cartilage releases HDGF with time.. 95
Figure 3.16 Growth factors HDGF, CTGF and FGF2 bind heparin and can be eluted by NaCl. 97
Figure 4.1 Confocal imaging of PCM collagen VI and TM collagen II and aggrecan chondroitin sulfate. 115
Figure 4.2 Sodium addition releases growth factors from cartilage. 117
Figure 4.3 Sodium addition releases growth factors from dead cartilage. 119
Figure 4.4 Full charge depletion reduces growth factor release upon cartilage injury. 122
Figure 4.5 NaCl and RIPA extraction of 7 day untreated and IL-1 treated explants. 124
Figure 4.6 Growth factor mRNA regulation throughout 7 days of IL-1 treatment for proteoglycan depletion. 126

Figure 4.7 Porcine chondrocyte mRNA regulation by IL-1. 128
Figure 4.8 Partial charge depletion variably affects growth factor release upon cartilage injury. 130
Figure 4.9 Human cartilage loss of proteoglycan by Safranin O stain with osteoarthritis progression. 131
Figure 4.10 Macroscopic grading and biopsy dissection of human osteoarthritic articular cartilage 132
Figure 4.11 Fixed charge density inversely correlates with severity of disease in osteoarthritic cartilage samples. 133
Figure 4.12 Severely diseased regions of osteoarthritic cartilage release less growth factor upon injury compared with undamaged regions. 134
Figure 4.13 Severely diseased regions of osteoarthritic cartilage contain more matrix and whole tissue growth factor than undamaged regions. 136
Figure 4.14 *SGK1* mRNA regulation in porcine cartilage after explantation. 137
Figure 4.15 *SGK1* and *COX2* mRNA in porcine chondrocytes transiently stimulated with NaCl. 139
Figure 4.16 Phosphorylated SGK1 in porcine cartilage after explantation. 140
Figure 4.17 Phosphorylated SGK1 (Thr256 site) in porcine cartilage stimulated with NaCl. 140
Figure 4.18 Phosphorylated SGK1 (Ser422 site) in porcine cartilage stimulated with NaCl. 141
Figure 4.19 CoroNa green dye can detect physiological and supraphysiological sodium levels in solution. 142

Figure 4.20 CoroNa green dye does not robustly detect sodium changes in cartilage upon compression. 144
Figure 4.21 ^{23}Na-MRI imaging and spectroscopy of loaded articular cartilage. 147
Figure 4.22 Proposed injury response mechanism of sodium flux and growth factor release in normal and osteoarthritic cartilage. 156
Figure 5.1 Destabilisation of the medial meniscus surgery. 167
Figure 5.2 GAPDH is an inconsistent housekeeper, whereas 18S and BMPR2 are consistent housekeepers in mouse hip avulsion. 172
Figure 5.3 HDGF knockout mice gain more body weight than in-house C57BL6/J wildtype mice over time. 175
Figure 5.4 *Hdgf* $^{-/-}$ mice have cystic lesions in the bone marrow not present in wildtype mice. 176
Figure 5.5 *Hdgf* $^{-/-}$ C57BL6/N mice have thinner average cartilage and maximal cartilage measurements at 18 weeks than wildtype C57BL6/J mice at 22 weeks. .. 177
Figure 5.6 *Hdgf* knockout mice develop severe OA early after DMM surgery. 179
Figure 5.7 Body weight differences between *Hdgf* $^{-/-}$ and wildtype mice diminish when backcrossed onto a C57BL6/J background. 181
Figure 5.8 Significantly altered gene expression in *Hdgf* $^{-/-}$ mice compared to wildtype mice after hip avulsion cartilage injury. 185
Figure 5.9 Heparin-binding proteins induce proliferation in adipose tissue-derived mesenchymal stem cells 187
Figure 5.10 Adipose tissue derived mesenchymal stem cell proliferation in response to injury conditioned medium with FGFR and TGFβR1 inhibition. 189

Figure 5.11 20 minute rHDGF stimulation does not activate ERK in primary chondrocytes. 190
Figure 6.1 Example of theoretical negative polymer incorporation into osteoarthritic articular cartilage. 211
Figure 6.2 Chondroitin sulfate-mediated impact in spinal cord injury, inhibitory to repair. 214

List of Tables

Table 1.1 Proteoglycans and glycosaminoglycans in cartilage 5

Table 1.2 Comparison of heparin and heparan sulfate targeting enzymes 10

Table 1.3 Comparison of sodium ion imaging methods 17

Table 1.4 Animal models of osteoarthritis 27

Table 2.1 P value symbol assignment of statistical significance 74

Table 4.1 Disease scoring of osteoarthritic cartilage 110

Table 5.1 Modified OARSI histological osteoarthritis scoring system 168

Table 5.2 Microfluidic array gene list 169

Table 5.3 Adipose tissue-derived mesenchymal stem cell stimulation conditions.. 174

Table 5.4 Genes significantly regulated by hip avulsion injury in wildtype and *Hdgf* $^{-/-}$ mice compared to respective 0h baseline expression 183

Table 8.1 Listed reagents 249

Table 8.2 Listed antibodies 250

Table 8.3 Listed equipment 250

Table 8.4 Hepatoma-Derived Growth Factor published structures 251

Table 8.5 Microfluidic TaqMan array gene list 252

Abbreviations

αMEM	Alpha Minimum Essential Medium (+Glutamax)
18S	Eukaryotic rRNA 18S
^{23}Na	^{23}Sodium Isotope
ACLT	Anterior Cruciate Ligament Transection
ADAMTS	A Disintegrin and Metalloproteinase with Thrombospondin Motif
BMP	Bone Morphogenic Protein
CM	Conditioned Medium
CS	Chondroitin Sulfate
CTGF	Connective Tissue Growth Factor (CCN2)
DAPI	4’,6-Diamidino-2-Phenylindole, Dihydrochloride
DMEM	Dulbecco's Modified Eagle Medium
DMM	Destabilisation of the Medial Meniscus
DMMB	Dimethylmethylene Blue
ECL	Enhanced Chemiluminescence
ECM	Extracellular Matrix
FGF2	Fibroblast Growth Factor 2 (Basic FGF/ bFGF)
FT	Flowthrough
GAG	Glycosaminoglycan
H’ase	Heparitinase I (Heparinase III)
HDGF	Hepatoma-Derived Growth Factor (Heparin-Binding Growth Factor, HMG1L2)
Hdgf $^{-/-}$	*Hdgf* homozygous null mouse (constitutive whole-body knockout)
HS	Heparan Sulfate
IGF	Insulin-Like Growth Factor
LAP	Latency Associated Peptide

LTBP	Latent TGF-Beta Binding Protein
MAPK	Mitogen-Activated Protein Kinase
MCP	Metacarpophalangeal
MMP	Matrix Metalloproteinase
MRI	Magnetic Resonance Imaging
mRNA	Messenger RNA
MRS	Magnetic Resonance Spectroscopy
MSC	Mesenchymal Stem Cell
OA	Osteoarthritis
OARSI	Osteoarthritis Research Society International
PCM	Pericellular Matrix
PCR	Polymerase Chain Reaction
PVDF	Polyvinylidene Fluoride
qPCR	Quantitative Polymerase Chain Reaction
SF-DMEM	Serum-Free Dulbecco's Modified Eagle Medium
TGFβ	Transforming Growth Factor-Beta
TLDA	TaqMan Low-Density Array
WT	Wildtype (mouse)

1 Introduction

1.1 Cartilage structure and function

1.1.1 Cartilage types

There are three types of cartilage within the human body: hyaline cartilage, fibrocartilage and elastic cartilage. Hyaline cartilage is the most abundant type in the body, found on the surface of many joints, consisting of a substantial amount of collagen, making it a firm tissue. Fibrocartilage is the only type to contain large bundles of collagen I, as well as the typical collagen II composition of cartilage, and is found in the menisci of joints, between intervertebral discs and in the pubic symphysis. Elastic cartilage is histologically similar to hyaline cartilage, but is particularly resilient against bending due to elastin fibres, between which the chondrocytes reside.

This work focuses on articular cartilage, a form of hyaline cartilage that overlies the subchondral bone of articulating joints. Articular cartilage is the avascular, aneural connective tissue of diarthrodial joints that provides cushioning of the joint on loading and a smooth lubricated surface for articulation. Cartilage is paucicellular, composed of a sparse distribution of cells (chondrocytes) surrounded by an abundance of dense extracellular matrix (ECM).

Articular cartilage has a highly organised structure, which can be divided into four zones based on chondrocyte morphology and collagen fibre arrangement (Figure 1.1). The calcified zone lies directly above the subchondral bone, contains hypertrophic chondrocytes and matrix collagen fibres aligned perpendicular to the cartilage surface. The top of the calcified zone is marked by the tidemark. Above this is the deep zone,

which also contains collagen fibres that are parallel to the articular surface, but has a columnar arrangement of hypertrophic chondrocytes. The middle zone (also called the transitional zone) contains obliquely oriented collagen fibres with a less organised distribution of chondrocytes. The superficial zone contains chondrocytes with a more flattened shape, with collagen fibres that are organised parallel to the articular surface.

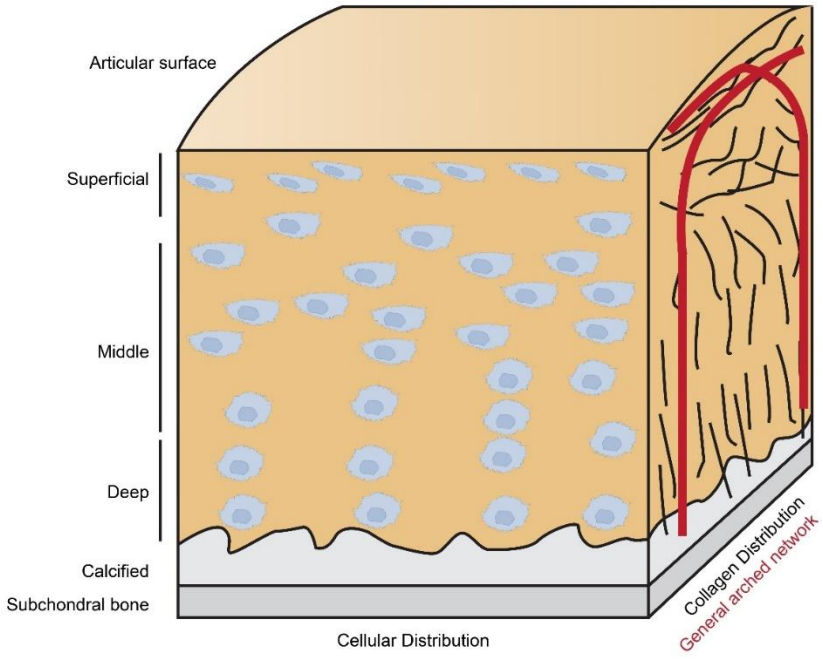

Figure 1.1 Ultrastructure of articular cartilage. Zones, cellular distribution and collagen distribution throughout the depths of articular cartilage. Deep chondrocytes exhibit a rounded phenotype, whilst superficial chondrocytes appear flattened. Collagen is highly aligned and organised in the superficial zone and middle–deep zone, in perpendicular directions, resulting in an overall arching of collagen ultrastructure.

1.1.2 The chondrocyte

Cartilage contains one principal cell type, the chondrocyte, which occupies between 5–10% of total cartilage volume (Roughley and Lee, 1994). These cells rely on the passive diffusion of nutrients, oxygen and waste products through the matrix due to a lack of cartilage vascularisation. They therefore reside in a variably hypoxic

environment and exhibit altered metabolism and cell survival responses. The main role of the chondrocyte in adult cartilage is the maintenance of the ECM by the turnover of its components. Chondrocytes are exquisitely sensitive to mechanical signals, through which they subsequent influence normal mechanoadaptive matrix homoeostasis (Vincent and Wann, 2018).

1.1.3 Extracellular matrix

The extracellular matrix makes up the bulk of cartilage tissue, surrounding the chondrocytes. The extracellular matrix predominantly consists of collagens, proteoglycans, and hyaluronic acid. There are three distinct regions of the cartilage extracellular matrix: the pericellular matrix thinly surrounding the chondrocyte cells, the larger territorial matrix region around the pericellular matrix, and the interterritorial matrix which makes up the bulk of cartilage tissue between the territorial matrix of each cell or cell cluster (Figure 1.2). The chondrocyte and its pericellular matrix make up the chondron. The territorial and interterritorial matrix are collectively referred to as the further removed matrix.

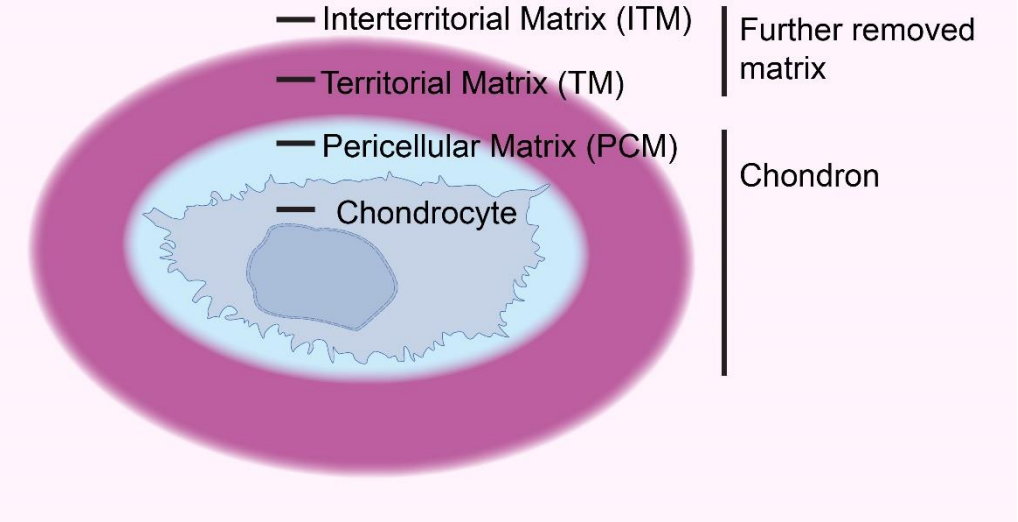

Figure 1.2 Distinct matrix regions of the extracellular matrix of articular cartilage. The extracellular matrix encompasses all the tissue matrix, excluding the chondrocyte. The chondron is the chondrocyte and the thin pericellular matrix region around the chondrocyte. The further removed matrix constitutes the territorial matrix and the interterritorial matrix.

Cartilage tissue contains up to 10% proteoglycan, residing in the extracellular matrix (Kiani *et al.*, 2002). The large chondroitin sulfate proteoglycan aggrecan is the most abundant proteoglycan in cartilage, which is attached to hyaluronic acid and link protein. Different proteoglycans are located in distinct regions of the cartilage matrix (Table 1.1).

Table 1.1 Proteoglycans and glycosaminoglycans in cartilage

Proteoglycan	Glycosaminoglycan Chains	Cell Surface?	PCM?	TM / ITM
	Hyaluronic acid / Hyaluronan (HA)	✗ (CD44)	✓ (unbound)	✓
Betaglycan (TGFBR3)	CS, HS	✓	✗	✗
Perlecan	HS	✗	✓	✗
Aggrecan	CS, KS (HA linkage)	✗	~	✓
Syndecan	HS	✓	✗	✗
Glypican	HS	✓	✗	✗
Decorin	CS, DS	✗	✓	✓ (ITM)
Biglycan	CS, DS	✗	✓	✗
Versican	CS, (KS)	✗	~	✓
Fibromodulin	KS	✗	✓	✓
Lumican	KS	✗	~	✓
Epiphycan	CS, DS	✗	~	✓

The pericellular matrix of cartilage is rich in the heparan sulfate proteoglycan perlecan and collagen VI. Collagen IX can also be found in the cartilage pericellular matrix, as well as other matrix macromolecules typically residing within basement membranes of other tissues such as fibronectin and laminin (Guilak *et al.*, 2018).

Some studies report the presence of hyaluronic acid in the pericellular matrix, mostly in isolated chondrocyte culture (Scrimgeour *et al.*, 2017). However, a newly formed pericellular matrix from cultured cells or chondrons is different to the pericellular matrix of enzymatically isolated tissue (Lee and Loeser, 1998). Fresh chondron isolation yields minimal hyaluronic acid (0.010 ± 0.001 pg cell^{-1}) within the cell and PCM (Wang, El Haj and Kuiper, 2008). Aggrecan, attached to hyaluronic acid, is predominantly in the territorial and interterritorial matrix.

1.1.3.1 Pericellular matrix

Chondrocytes are immediately surrounded by a distinct region of matrix containing an abundance of collagen VI and perlecan. This pericellular matrix (PCM) region, together with the chondrocyte, forms the chondron. Some studies include the pericellular matrix within their definition of the territorial matrix, but herein the pericellular matrix is referred to by collagen VI and perlecan localisation, distinctly separate from the territorial matrix and interterritorial matrix of the further removed matrix.

The pericellular matrix is visually defined by the colocalisation of Collagen VI and perlecan. Normal articular cartilage has a pericellular matrix devoid of type II collagen, which is found in the further removed matrix. This can be distinctly visualised by fluorescent microscopy imaging and electron microscopy using immuno-gold labelling of collagen VI (Sö *et al.*, 2002).

The average Young's modulus of the interterritorial matrix is greater than that of the pericellular matrix (636 ± 123 versus 265 ± 53 kPa), measured by atomic force microscopy (Allen and Mao, 2004). The pericellular matrix is less stiff and more susceptible to compression than the further removed matrix, and is thought to influence the stress-strain environment of the chondrocyte. Heparitinase treatment reduces the modulus of the PCM, suggesting perlecan might be the main determinant of PCM mechanical properties (Wilusz, DeFrate and Guilak, 2012). Other forms of enzymatic treatment do not significantly affect mechanical properties of the PCM (Wilusz and Guilak, 2014).

The pericellular matrix is described as providing mechanical protection and mechanical transduction for the chondrocyte. The PCM protects chondrocytes during mechanical loading through an adaptive water loss from PCM proteoglycans. The stiffness of the PCM is consistent throughout the depth of articular cartilage, despite an increasing compressive modulus of the further removed matrix with depth (McLeod, Wilusz and Guilak, 2013). Susceptibility of the PCM to tissue deformation and interstitial water content allows dynamic changes in the physicochemical and osmotic environment immediately surrounding the chondrocyte.

The pericellular matrix harbours growth factors such as perlecan-bound FGF2 and CTGF/CCN2. These factors are released upon mechanical injury (Vincent *et al.*, 2002; Tang *et al.*, 2018), and are able to elicit signalling in chondrocytes upon mechanical loading (Vincent *et al.*, 2004). The mechanism of release is not currently known, but the distinct mechanical properties of the PCM might play a role in the rapid mechanical release of such factors. Perlecan knockout mice develop chondrodysplasias, with disorganised chondrocyte structure and proliferation (Arikawa-Hirasawa *et al.*, 1999), highlighting an important functional role for the PCM in cartilage.

1.1.3.2 Heparan sulfate

Heparan sulfate is a glycosaminoglycan, present on cartilage proteoglycans including betaglycan, syndican and glypican on the chondrocyte surface and perlecan in the PCM.

Cartilage heparan sulfate originates from the chondrocytes, where biosynthesis occurs in the Golgi network. Linear heparan sulfate polysaccharide backbones are attached to core proteins in the Golgi network by the sequential addition of glucuronic acid (GlcA)

and N-acetylglucosamine (GlcNAc). Elongation is catalysed by exostosin (EXT) family enzymes. This creates a polysaccharide chain of repeating disaccharide units, of which the GlcNAc can be N-deacetylated and N-sulfated by bifunctional heparan sulfate N-deacetylase/N-sulfotransferase (NDST) enzymes, and the GlcA unit epimerised to iduronic acid (IdoA) by D-glycuronyl C5-epimerase (GLCE). Further sulfation occurs at the 2, 3 and 6 carbon positions by 2-O-, 3-O- and 6-O-sulfotransferases to produce variable sulfation patterning. This sulfation patterning affects the anionic charge and protein binding properties of heparan sulfate. The sulfation pattern influences the glycosaminoglycan structure, allowing them to present distinct electrostatic and Van der Waals surfaces to proteins, which can alter protein binding ability. Deletion of heparan sulfate-targeting sulfatases in cartilage alters tissue homeostasis and growth factor signalling (Otsuki *et al.*, 2010).

Heparan sulfate is of similar structure to heparin (Figure 1.3), but they differ in their post-synthesis modifications. Both are made from chains of repeating disaccharide units consisting of a glucosamine and uronic acid, however subsequent differences in sulfation renders heparin more sulfated than heparan sulfate (~2.7 : 1.0 sulfate groups per disaccharide) (Shriver *et al.*, 2012).

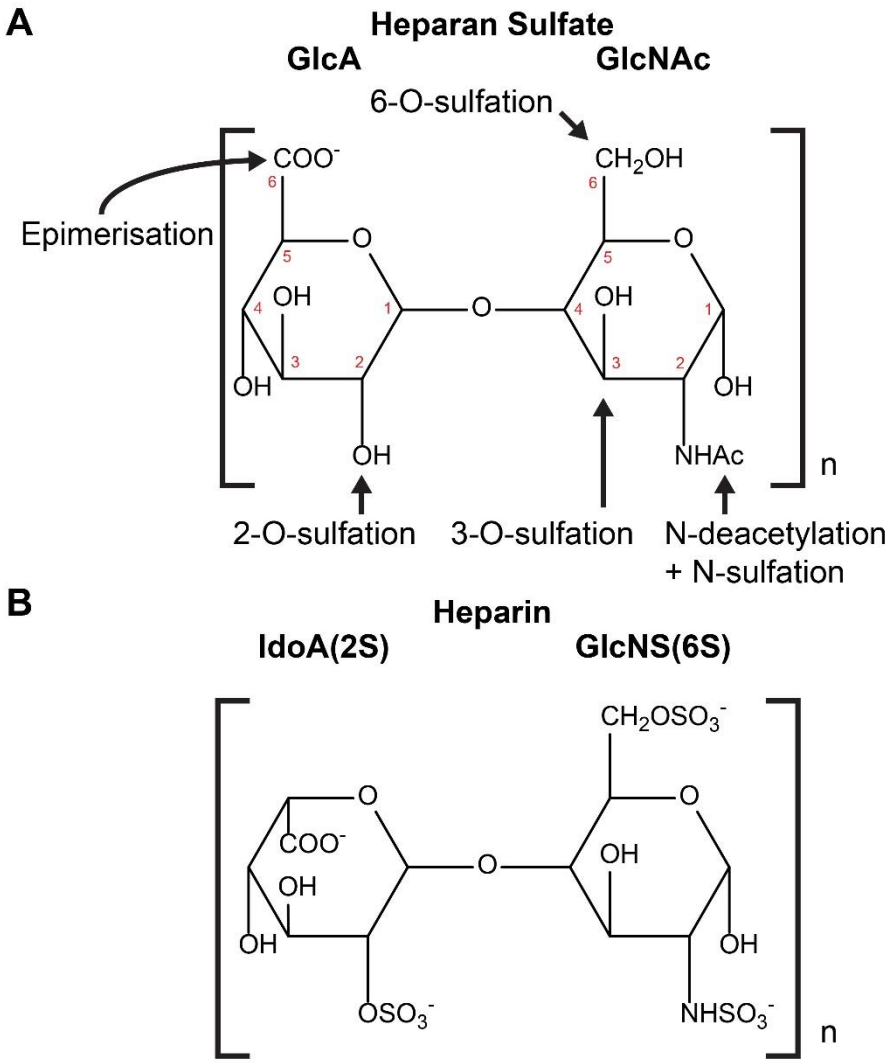

Figure 1.3 Structure of heparan sulfate and heparin disaccharide units. Common, unmodified heparan sulfate disaccharide unit of glucuronic acid (GlcA) and N-acetyl-glucosamine (GlcNAc) linked by β-1,4-glycosidic bonds, with sites labelled where epimerisation and sulfation can occur (A). Common heparin disaccharide unit of 2-O-sulfated iduronic acid (IdoA(2S)) and 6-O-sulfated N-sulfo-glucosamine (GlcNS(6S)) (B).

Heparinases selectively cleave the glycosidic bond between glucosamine residues and uronic acids via an elimination mechanism, creating a double bond at the non-reducing end of the uronic acid. The three identified heparinase enzymes are listed and compared in Table 1.2. Heparinase I cleaves highly sulfated heparin and heparan

sulfate chains, and heparinase III (heparitinase I) cleaves less sulfated heparan sulfate chains. Heparinase II cleaves domains of both high and low sulfation on heparin and heparan sulfate. In addition to heparinase III, human heparanase also degrades heparan sulfate chains, but their cleavage products are chemically distinct. Heparanase exhibits selective cleavage, which generates heparan sulfate fragments of 5–7 kDa in size, while heparinase III more extensively targets heparan sulfate.

Table 1.2 Comparison of heparin and heparan sulfate targeting enzymes

ENZYME	SYNONYMS	SUBSTRATE	RELATIVE HEPARIN ACTIVITY	RELATIVE HEPARAN SULFATE ACTIVITY	NOTES
Heparinase I	Heparin lyase I EC 4.2.2.7	Heparin	Highest	10%	β-elimination
Heparinase II	Heparin lyase II	Heparin Heparan sulfate	60%	Highest	β-elimination
Heparinase III	Heparin lyase III Heparitinase I EC 4.2.2.8	Heparan sulfate	<1%	Highest	β-elimination
Heparanase	HPSE EC.3.2.1.166	Heparan sulfate			Endohydrolysis of (1->4)-beta-D-glycosidic bonds

1.1.3.3 Chondroitin sulfate

Chondroitin sulfate is a glycosaminoglycan composed of repeating disaccharide units of N-acetylgalactosamine (GalNAc) and glucuronic acid (GlcA), polymerised by chondroitin co-polymerases (Figure 1.4). Chondroitin sulfotransferases catalyse the addition of sulfate groups to chondroitin polysaccharide chains in the Golgi of the cell. These belong to three different families that transfer sulfate groups to C-4 of GalNAc residues, to C-6 of GalNAc residues, and to C-2 of the hexuronic acid moieties. After biosynthesis, chondroitin sulfate chains attached to proteoglycans are incorporated

into the extracellular matrix, where they are subsequently vulnerable to enzymatic removal of sulfate groups by extracellular sulfatases.

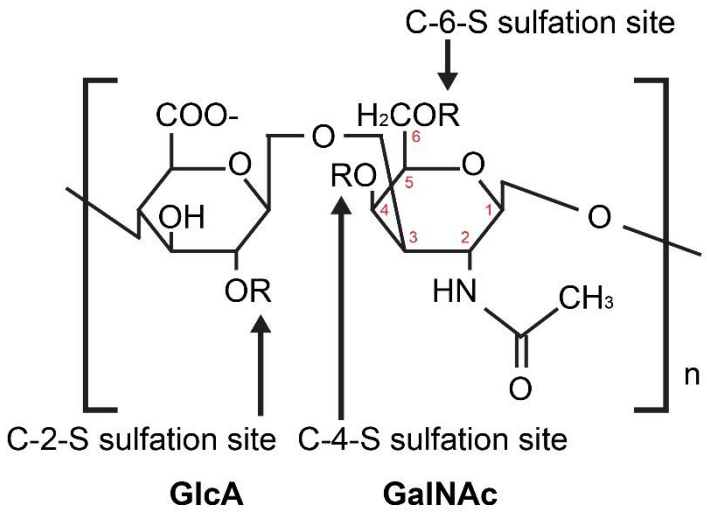

Figure 1.4 Structure of chondroitin sulfate disaccharide units. Disaccharide unit of glucuronic acid (GlcA) and N-acetyl-galactosamine (GalNAc) that repeats to form a chondroitin sulfate glycosaminoglycan chain. Site-specific sulfation (R sites) can yield chondroitin sulfate A (C-4-S sulfation), chondroitin sulfate C (C-6-S sulfation), chondroitin sulfate D (C-2-S and C-4-S sulfation) and chondroitin sulfate E (C-4-S and C-6-S sulfation).

Chondroitin sulfate chains are found in cartilage on proteoglycans such as betaglycan (TGFβR3) of the cell membrane, biglycan and decorin in the PCM and aggrecan in the further removed matrix. The majority of chondroitin sulfate in cartilage tissue is attached to aggrecan, where each core protein harbours over 100 side chains (Kiani *et al.*, 2002).

Chondroitin is sulfated to variable degrees, attributing a variable negative charge. The abundance of chondroitin sulfate in cartilage makes it the predominant contributor to the fixed charge density in cartilage. Chondroitin sulfatases are upregulated in osteoarthritis, and some evidence suggests a cartilage feedback mechanism of sulfate

rehabilitation through chondroitin sulfotransferases such as Carbohydrate sulfotransferase 11 (Chondroitin 4-Sulfotransferase 1 / *CHST11*) (Lin *et al.*, 2020). Loss of chondroitin sulfate also occurs in cartilage through aggrecanase activity, cleaving the main core protein to which chondroitin sulfate attaches.

1.2 Cartilage fixed charge density

The cartilage matrix has a high fixed charge density due to the abundance of negatively charged sulfate groups on glycosaminoglycan chains attached to the many proteoglycans in the tissue.

Fixed charge density in cartilage can be measured visually with the use of metachromatic dyes. Safranin O is an example of a metachromatic dye that produces a red stain in cartilage, correlating with the glycosaminoglycan content of proteoglycans in the tissue. A linear relation between safranin O stain optical density and cartilage glycosaminoglycan content is well established (Kiviranta *et al.*, 1985; Király *et al.*, 1996), validated against gas chromatography ($r = 0.96$, $N = 14$, 90–400 nmol/mm^3) and cation tracer ($r = 0.995$, $N = 5$, 0.1–0.2 mEq/g) methods (Nieminen *et al.*, 2002).

Fixed charge density of articular cartilage is lowest near the articular surface and increases with depth (Maroudas and Bollough, 1968; S. S. Chen *et al.*, 2001).

The largest and most abundant proteoglycan in cartilage is aggrecan, able to form large aggregates with hyaluronic acid. Aggrecan harbours keratan sulfate chains, and over 100 large (~20 kDa each) chondroitin sulfate chains that are highly sulfated and altogether comprise 90% of aggrecan mass (Roughley and Lee, 1994; Kiani *et al.*,

2002). Aggrecan is therefore a major contributor to cartilage fixed charge, through its side chains.

1.2.1 Ions in cartilage

The Gibbs-Donnan effect/equilibrium is the behaviour of charged particles near a semi-permeable membrane, which can result in uneven distribution between each membrane side, creating an electric potential called the Donnan potential. Healthy cartilage has an abundance of fixed negatively charged glycosaminoglycans in its matrix, resulting in a high fixed charge density compared to surrounding tissues. Cartilage therefore contains high concentrations of free sodium (250–350 mM), postassium (8–10 mM) and calcium (up to 20 mM) ions compared to anion concentration (60–90 mM Chloride ions) (Maroudas and Evans, 1972).

Charge density is the measure of electric charge per unit of volume of space. It is influenced by the polarity of the charge constituents, so can be positive or negative. In cartilage, its fixed charge density correlates to tissue GAG content due to the overwhelming contribution of negative charge from their sulfate groups. Fixed charge density is lower in osteoarthritic cartilage due to loss of proteoglycan, lowering GAG content. The extracellular ion concentration and osmolality can influence chondrocyte matrix production (Urban, Hall and Gehl, 1993) and matrix aggrecanase activity (Gendron *et al.*, 2007).

Proteoglycans in the matrix of cartilage are fixed to hyaluronic acid and collagen, rendering the large proteoglycans relatively immobile within the tissue. The negative charge of the GAG chains provide the tissue with a high fixed charge, countered by the presence of ions and electrolytes within the matrix. Cations in cartilage matrix

localise in pools, due to electrostatic interaction with the charged polar glycosaminoglycan chains of fixed proteoglycans. This causes an imbalance of ion concentrations between cartilage and neighbouring tissue, and a difference between free cation and anion diffusion. This osmotic imbalance causes water to be drawn into the cartilage, resulting in swelling of the tissue from the inability of fixed proteoglycan to move freely throughout the matrix in response. This is described as Donnan osmotic pressure (osmotic pressure = 0.17 MPa in 0.15 M NaCl bathing solution), which contributes to the stiffness of cartilage upon compression (due to rate of change of osmotic pressure), and also maintains the balance of the chemical potential (Freeman, 1979). This water is somewhat confined in healthy cartilage due to the strong collagen network, ultimately providing material resistance to load.

1.2.2 Extracellular sodium in cartilage

Tissue sodium concentration is important in the physiology of chondrocytes, and cartilage as a whole system. Cells express sodium/calcium exchange ion transport proteins on their plasma membrane, which extrude Ca^{2+} ions for the internalisation of Na^{+} cations and can function with reversibility in order to internally transport Ca^{2+}. The active ATP-dependent expulsion of Na^{+} from a cell through a Na^{+}/K^{+} ATPase channel allows the maintenance of low intracellular Na^{+} concentration.

Sodium is the major cation constituent of the extracellular fluid of physiological systems. The physiological concentration of sodium in the extracellular matrix of cells is between 136 mM and 150 mM for most tissues, however cartilage has an especially high sodium concentration of 250 mM, originally determined by cation tracing and

explant culture experiments, but more recently confirmed by sodium-MRI techniques (Maroudas and Freeman, 1979; Urban, Hall and Gehl, 1993; Shapiro *et al.*, 2002).

The most abundant proteoglycan in cartilage is aggrecan, which harbours over 100 chondroitin sulfate glycosaminoglycan chains per aggrecan molecule (Kiani *et al.*, 2002). Chondroitin is highly sulfated in cartilage, exhibiting a high negative charge. This suggests that the predominant contribution to holding sodium in the cartilage matrix is from chondroitin sulfate on aggrecan.

In the diet, typical intake of sodium daily is between 130–280 mmol (8–15g) in the form of sodium chloride, with a body requirement of 1–2 mmol per day, with excess intake excreted by the kidneys into the urine. There is no evidence to suggest a link between dietary sodium intake and extracellular sodium concentration of cartilage, as the main determinant of matrix sodium presence is fixed charge density.

1.2.3 Alternative cations ions in cartilage

The normal extracellular calcium concentration in cartilage is in the 10^{-3} M range (~2 mM) (Parvizi et al., 2002). Normal cell cytosol calcium concentration, not during a calcium flux, can be as low as 10^{-7} M (Matta, 2013).

Chondroitin sulfate also binds calcium. In the case of salmon nasal cartilage, chondroitin sulfate selectively binds calcium over sodium, and the sulfate groups bind calcium stronger than the carboxyl groups (Uchisawa *et al.*, 2001). However, there is a relative scarcity of extracellular calcium ions compared to sodium in the extracellular space, including that of cartilage.

Cations are noted to play a role in the response to mechanical loading of cartilage. In articular chondrocytes, a response to osmotic stress has been posed to be mediated by transient receptor potential vanilloid 4 (TRPV4) channels, a Ca^{2+}-permeable Ca^{2+}-preferred cation channel implicated in the transduction of extracellular cues through generation of intracellular Ca^{2+} transients (Darling *et al.*, 2010; O'Conor *et al.*, 2014). This TRPV4-mediated intracellular calcium response in chondrocytes can induce gene expression changes in response to osmotic and mechanical stress. A study into intracellular calcium in relation to different stages of osteoarthritis, and furthermore the differing zones of cartilage, shows a relationship between osteoarthritis severity and features of spontaneous calcium oscillations (Gong *et al.*, 2017).

1.2.4 Measuring charge in tissue

Ions in cartilage matrix can be measured either directly or inferred from the fixed charge of the tissue. Methods are listed and compared in Table 1.3.

Table 1.3 Comparison of sodium ion imaging methods

ION MEASUREMENT METHOD	TECHNIQUE	ADVANTAGES / DISADVANTAGES	RERERENCE
Fluorescent imaging	Sodium Green	Improved version of fluorescein precursor, detects 0.5-50 mm Na^+. Only detects intracellular changes, not ratiometric.	(Szmacinski and Lakowicz, 1997)
	SBFI	Available as cell-permeant and cell-impermeant. Great selectivity of sodium over potassium (~41-fold). Only available as cell-permeant.	(Meier, Kovalchuk and Rose, 2006)
	Corona Green	Available as cell-permeant and cell-impermeant. High fluorescent intensity and range of detection than Sodium Green and SBFI. Ratiometric. Less selective for sodium ions over potassium than Sodium Green. UV-light excitable.	(Meier, Kovalchuk and Rose, 2006)
	Corona Red	Positive charge targets mitochondria of cells. Only available as cell-permeant.	
	Optode nanosensors	Ratiometric, photostable, high dynamic range for intracellular concentrations. Only intracellular, minimally selective (~1.4 fold).	(Ruckh *et al.*, 2013)
Magnetic resonance	^{23}Na-MRI microimaging	Minimal tissue preparation, differentiate between free and bound ionic species. Long capture times, low resolution, requires high magnetic induction.	(Maudsley and Hilal, 1984; Reddy, Insko and Leigh, 1997; Shapiro *et al.*, 2002)
	TPPI Spectroscopy	Quantification of free and bound ionic species. No spatial information.	
Electrode sensor		Large, cannot enter tissue, cannot detect rapid local changes.	
Electrophysiology microelectrode		Small and highly sensitive, used to measure membrane conductivity and action potentials. Cannot enter hard tissue due to microelectrode fragility.	

Experimentally, tissue sodium concentration can be determined by assays such as sodium magnetic resonance imaging (MRI). One main use for standard proton MRI is the visualisation of water molecules through proton sensitivity due to the alignment of

^{1}H nuclei from H_2O with magnetic spin. This concept can be used to image other nuclei such as ^{23}Na in sodium MRI. This allows the visualisation of Na^+ ions, but with less sensitivity than for H^+ due to less abundance in tissue (Romanzetti *et al.*, 2014). Quantitative sodium MRI is possible in cartilage (Shapiro *et al.*, 2002), and is an established sensitive method for the measurement of proteoglycan loss, validated against a proteoglycan dimethylmethylene blue assay for sulfated GAG loss (Borthakur *et al.*, 2000). This allows the spatial resolution of proteoglycans within cartilage, through the inferred quantification of fixed charge density. The high fixed charge density and sodium content of cartilage owing to high GAG concentration is consistently measured and validated in the literature a plethora of sodium and charge-based techniques (Bashir, Gray and Burstein, 1996).

Clinical quantitative sodium MRI imaging is also possible in humans (Wetterling *et al.*, 2012), *in vivo*, but requires a high magnetic induction imaging system. The current gold standard for quantification of sodium via these methods is through measurement of signal-to-noise ratios, which shows a clinical decrease with age and with grade of cartilage lesions (Widhalm *et al.*, 2016). Further, the anisotropy of sodium in tissue enables the use of multiple quantum filtering in NMR spectroscopy to discern bound sodium ions from free sodium ions (Jaccard, Wimperis and Bodenhausen, 1986). Free sodium ions are detected with single quantum filtering. Time proportional phase increment spectroscopy using multiple quantum filtering is validated *in vivo* compared to agarose samples (Schepkin *et al.*, 2017).

One alternative approach for the imaging of sodium is through the use of fluorescent sodium ionophores. Examples include monensin sodium salt, SQI-Et (Na) and SQI-Pr

(Na). These are all able to bind to sodium and allow transport across the membrane, and the latter two exhibit intrinsic fluorescence for sodium visualisation. Additionally, SBFI is a commercially available ratiometric Na^+ indicator used to measure intracellular sodium. Its ratiometric quality is advantageous in many instances; a shift in fluorescence emission when changing from a free state to a bound state allows the measurement of free and bound compound with separation of emission spectrum. This can be used to calculate substrate concentration irrespective of aspects such as probe loading amount and bleaching. Other fluorescence based probes, such as CoroNa green and CoroNa red work in a similar capacity but are available in cell permeant and cell impermeant forms, to allow or exclude measurement of intracellular sodium.

1.3 Protein-salt interactions

An increase in the ionic concentration (ionic strength) of a solution can have two main effects on protein-protein interaction. Firstly, addition of low concentrations of salt to a buffer can increase solubility of proteins by salt counterion solubilisation (salting in), and addition of high concentrations of salt can cause salt-induced protein precipitation (salting out) (Arakawa and Timasheff, 1984). Secondly, counterions at high enough concentrations can compete with the ability of proteins to electrostatically interact with molecules of opposing charge, due to ionic screening. This is applicable to the electrostatic interaction between basic growth factors and negatively charged sulfated glycosaminoglycans in cartilage.

1.3.1 Salt precipitation

At low salt concentrations typically ranging from 0 to 500 mM, proteins and other polyelectrolytes can be stabilised in solution, through non-specific electrostatic

interactions. Proteins are surrounded by the salt counterions and this screening leads to a decrease in the electrostatic free energy of the protein and the increased activity of the solvent, resulting in increased overall solubility sometimes referred to as 'salting in'. The salt concentration needed for this effect is dependent on the protein. Conversely, with a very high salt concentration, water is removed from around the protein which exposes the hydrophobic patches. These hydrophobic patches interact with one another, resulting in protein aggregation. The salt threshold of precipitation or 'salting out' is dependent on size and number of hydrophobic patches.

Salting in and salting out will not be explored in detail, as the effect of ionic screening is more relevant with protein affinity chromatography. However, the 'salting in' phenomenon can be explained by the Debeye-Hückel theory and relative contributions of ions in 'salting out' are stated in the Hofmeister series.

1.3.2 Ionic screening

Electrostatic competition by ionic screening is used in some forms of affinity chromatography and ion-exchange chromatography. Aqueous ions from dissolved salt weaken the binding of the protein to the affinity column ligand, interfering with ionic interactions. The analyte protein (e.g. basic growth factor) and similarly charged ions (e.g. Na^+) of the eluent compete to bind to the oppositely charged ionic functional group on the surface of the stationary phase (e.g. sulfate/carboxylate groups of heparin). The affinity of interaction between the salt ions and the functional groups will eventually exceed that of the interaction between the protein charges and the functional groups, resulting in protein displacement by an increase in salt concentration.

Ion-exchange chromatography is explained with the following reversible equation (Acikara, 2013):

$$S\text{-}X^{-}C^{+}+M^{+} \leftrightarrow S\text{-}X^{-}M^{+}+C^{+}$$

M^{+} mobile cation, C^{+} analyte cation, X^{-} fixed anionic charge, S chromatographic support.

Affinity chromatography of charged proteins (e.g. heparin affinity chromatography) utilises the same concept, but is more complex due to multiple ionic interaction sites of the protein and stationary phase.

1.4 Osteoarthritis

Osteoarthritis (OA) is a disease estimated to affect over 250 million people worldwide (Hunter and Bierma-Zeinstra, 2019), and is a leading cause of disability and significant source of societal cost. The disease is increasing in prevalence and has no current disease modifying drugs approved for use. OA is a mechanically driven disease of synovial joints, with mechanisms of pathogenesis that remain elusive. Pathognomonic features of the OA joint include cartilage degradation, synovial hypertrophy and bone changes, including osteophyte formation and subchondral bone sclerosis.

A number of pathogenic mechanisms have been proposed for the development of OA, which can be broadly divided into those that drive proteolytic degradation of the matrix and those that supress the intrinsic repair of the tissue. However, the key underlying factor in all cases is the presence of mechanical injury.

1.4.1 Matrix changes in osteoarthritis

Significant changes occur to the matrix in osteoarthritis. Disruption of the cartilage collagen network increases matrix water content with a corresponding decrease in tissue modulus and fixed charge density (Maroudas *et al.*, 1985). Loss of proteoglycan is responsible for the reduction in fixed charge density.

Aggrecanase enzymes are responsible in early osteoarthritis for loss of proteoglycan. Aggrecan degradation products with an ARGS neoepitope are released from OA tissue into synovial fluid, with NITEGE neoepitopes (Figure 1.5) remaining in OA cartilage, indicative of aggrecanase activity (Lohmander, Neame and Sandy, 1993). ADAMTS-1, ADAMTS-4 and ADAMTS-5 aggrecanase proteins are present in cartilage, capable of degrading aggrecan. In OA, ADAMTS-5 is the primary aggrecanase responsible for proteoglycan loss (Glasson *et al.*, 2005). ADAMTS-1 is not involved in models of cartilage degradation (Little *et al.*, 2005). ADAMTS-4 is the primary aggrecanase in murine growth plates, but is not the main enzyme responsible for ARGS cleavage in human OA (Glasson *et al.*, 2004). As aggrecan (Figure 1.5) is the most abundant proteoglycan in cartilage, and 90% of each aggrecan structure is composed of negatively charged glycosaminoglycan chains, it is the major contributor of fixed charge in the tissue. Cleavage at the inter-globular domain site by aggrecanase activity, removes the chondroitin sulfate chains from the protein attached to the cartilage matrix.

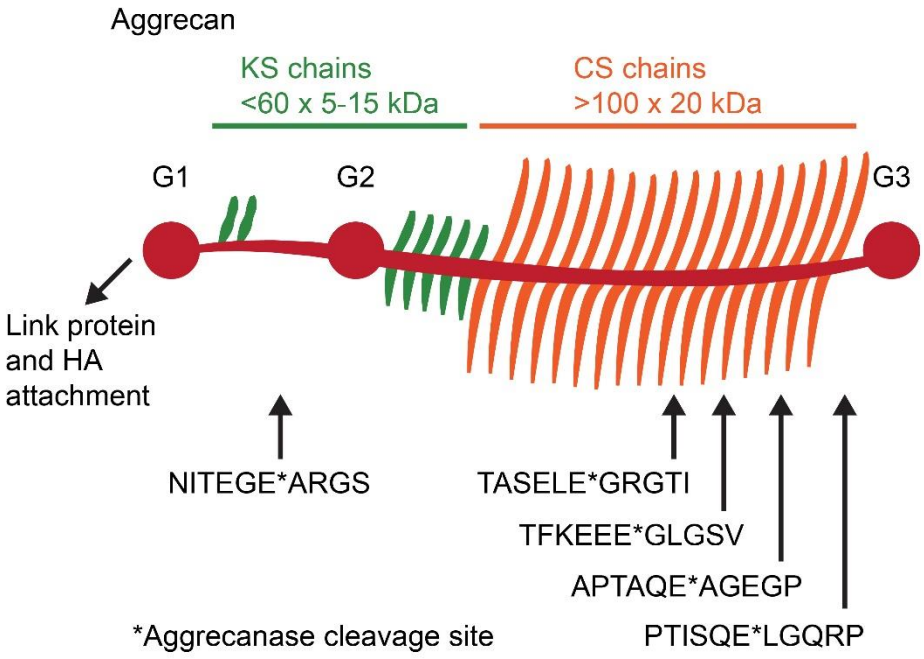

Figure 1.5 Aggrecan structure and aggrecanase cleavage. Aggrecan proteoglycan structure with core protein (red) with globular domains, with attached keratan sulfate (green) and chondroitin sulfate (orange) glycosaminoglycan chains. Aggrecanase proteolytic cleavage sites (*) between amino acids of the aggrecan core protein. Aggrecan also contains multiple MMP cleavage sites (not shown).

The pericellular matrix changes through the course of osteoarthritis. The Young's Modulus (elastic stiffness) of the cartilage matrix reduces in osteoarthritis, but the pericellular matrix maintains a lower mechanical stiffness compared to the interterritorial matrix (Wilusz, Zauscher and Guilak, 2013). Chondrocyte expression and pericellular matrix incorporation of perlecan are increased in human knee osteoarthritis samples (Chanalaris *et al.*, 2019), and in areas next to osteoarthritic cartilage defects *in vivo* (Tesche and Miosge, 2004). Despite being largely resistant to classical collagen degrading enzymes, Collagen VI has a high turnover in articular cartilage. Collagen VI turnover is enhanced in osteoarthritis, and can be present in the territorial matrix or extended pericellular zone (Sö *et al.*, 2002).

1.4.2 Sulfation patterning in osteoarthritis

Chondroitin sulfate is lost from cartilage tissue during osteoarthritis progression, due to aggrecan proteoglycan loss. However, there are also metabolic alterations in the sulfation of chondroitin in osteoarthritis (Plaas *et al.*, 1998). Overall, sulfation of chondroitin is reduced in osteoarthritic tissue due to upregulation of sulfatase enzymes. Regions of damaged cartilage have a compensatory upregulation of chondroitin 4-sulfotransferase-1 (*CHST11*) (Lin *et al.*, 2020). The *CHST11* gene has been implicated in multiple genome-wide association studies as a candidate gene for a SNP conferring susceptibility to osteoarthritis (Karlsson *et al.*, 2010; Zeggini *et al.*, 2012; Reynard and Loughlin, 2013). *CHST11* codes for a sulfotransferase that transfers a sulfate group to position 4 of the N-acetyl-galactosamine (GalNAc) residue of chondroitin during biosynthesis. Mice lacking *CHST11* exhibit chondrodysplasia, with reduced glycosaminoglycan content and altered Smad signalling in the growth plate (Klüppel *et al.*, 2005). These results highlight the importance of chondroitin sulfation in cartilage, and involvement in responding to damage in osteoarthritis.

Heparan sulfate proteoglycan synthesis is dysregulated in osteoarthritis, where expression of core protein and modification enzymes are generally increased. Perlecan expression and secretion is increased in chondrocytes from osteoarthritic patients (Tesche and Miosge, 2004), whereas expression of syndecan 4 and betaglycan are decreased (Chanalaris *et al.*, 2019). Osteoarthritic cartilage shows increased 6-O-sulfation, correlated with increased *HS6ST1* and *GLCE* that catalyse and promote 6-O-sulfation respectively (Chanalaris *et al.*, 2019).

Sulfatases Sulf-1 and Sulf-2 remove 6-O-sulfate groups from heparan sulfate, and are both overexpressed in osteoarthritic cartilage. Knockout of *Sulf1* or *Sulf2* in mice both result in accelerated GAG loss and increased severity of surgically-induced OA. Further, *Sulf* $^{-/-}$ mice have more cells positive for phosphorylated ERK1/2 and fewer positive for phosphorylated Smad1/5 in cartilage (Otsuki *et al.*, 2010). Sulfation patterning affects growth factor binding to heparan sulfate, and potentiation of their receptor binding, which could indicate changes in growth factors dynamics with osteoarthritis progression.

1.4.3 Mechanical changes in osteoarthritis

Osteoarthritis progression changes cartilage tissue and alters its ability to respond to mechanical loading. The normal cartilage response to mechanical load is discussed in Section 1.7. In normal cartilage the osmotic pressure, attributed to the high fixed charge density of the tissue, stretches the collagen network, which in turn restricts tissue water content. In early OA, proteoglycan degradation decreases fixed charge density of the tissue and disruption of the collagen network increases its ECM water content (Maroudas, 1976). Decreased glycosaminoglycan and increased water content both correlate with a decrease in compressive modulus (less resistance to compression) (Setton, Elliott and Mow, 1999); this decrease in compressive modulus occurs in OA tissue due to a decrease in fixed charge density and increase in porosity (Mow, Ratcliffe and Poole, 1992). Increased water content, in turn, produces a less stiff but more permeable tissue (Armstrong and Mow, 1982; Mow, Ratcliffe and Poole, 1992). Due to increased water content and decreased compressive modulus, OA cartilage exudes more water upon compression than healthy cartilage.

Perlecan content in the PCM is greater in more severely osteoarthritic regions of articular cartilage (Tesche and Miosge, 2004). The PCM of early osteoarthritic cartilage exhibits a 30% decrease in Young's modulus compared with macroscopically normal cartilage, rendering it more susceptible to strain (Wilusz, Zauscher and Guilak, 2013). Perlecan is responsible for the reduced compressive modulus in the PCM compared to the further removed matrix, as heparitinase treatment increases the PCM modulus without affecting other matrix regions (Wilusz, DeFrate and Guilak, 2012). The further removed matrix exhibits a 45% decrease in modulus with osteoarthritis, but it remains higher than the PCM modulus (Wilusz, Zauscher and Guilak, 2013). These distinct mechanical changes of the matrix and PCM with OA progression can affect mechanotransduction of chondrocytes in diseased tissue.

1.4.4 Models of osteoarthritis

Osteoarthritis is a disease of late onset, slow progression and difficult accurate early diagnosis. Experimental limitations of long timeframes and difficult diagnosis can be somewhat overcome with the use of animal models of osteoarthritis. Animal models mature quickly, can exhibit spontaneous onset of disease within a relatively short timeframe and have established models of artificially initiating the onset of osteoarthritis.

Osteoarthritis can be modelled in mice through surgical intervention, mechanical loading models, the spontaneous onset of OA with age or genetic modification, chemical induction and alteration of the diet or onset of obesity (Table 1.4).

Table 1.4 Animal models of osteoarthritis

OA MODEL	PROCEDURE	ADVANTAGES
SURGICAL	Destabilisation of the medial meniscus (DMM)	Reliable, reproducible, structurally similar to OA, validated for pain endpoints. Less severe.
	Anterior cruciate ligament transection (ACLT)	Severe form of surgical OA, widely used in other species.
	Partial meniscectomy (PMX)	Fast onset, without full severity of total menisectomy.
	Total meniscectomy	Fastest onset of surgical OA models.
MECHANICAL / LOADING	Overload / fracture	Mimics sudden joint injury and PTOA.
	Overuse loading	Represents susceptibility to mechanical damage over multiple compressions.
SPONTANOUS / GENETIC	Spontaneous OA	Reflects onset of OA without traumatic insult.
	Gene modification	Can reflect susceptibility to OA in spontaneous and induced models.
DIET / OBESITY		Represents dietary influences of OA, and mimics obesity (human OA risk factor)
CHEMICAL	Monoiodoacetate	Rapid onset, but less clinically representative of OA.
	Carrageenan	
	Kaolin	
	Collagenase	
	Sodium urate	

A commonly used surgical model of OA in the mouse is the destabilisation of the medial meniscus (DMM). This model involves the surgical transection of the medial meniscotibial ligament, causing instability of the joint. The damage as a result of the

DMM model is consistent with that observed in aged spontaneous mouse models of OA, and is sensitive enough to observe effects of disease intervention (Glasson *et al.*, 2005; Glasson, Blanchet and Morris, 2007). The biomechanics of the unbalanced joint subsequently leads to cartilage destruction, subchondral bone sclerosis and formation of osteophytes, typical of OA onset. OA severity can be histologically assessed by a number of scoring systems, including the recommended semi-quantitative OARSI score system (Glasson *et al.*, 2010). These systems typically assess cartilage damage, and some also assess multiple aspects of OA including bone, osteophyte and synovial changes if appropriate to the model used.

1.5 Cartilage injury responses

The response of cartilage to mechanical injury can be broadly categorised into two interconnected responses: the response of the matrix and the inflammatory response of the chondrocyte. The matrix structurally responds to mechanical injury, and can influence the chondrocyte through mechanotransduction and flow of ions, solutes and fluids. The chondrocyte can influence the matrix, after responding to mechanical and injurious stimuli, with an inflammatory response by the production of matrix components and degradative factors.

In addition to tissue and matrix damage, cartilage injury also exhibits deleterious effects on chondrocytes. Mechanical injury can directly influence chondrocyte metabolism through mechanotransduction. Further, injury and damage of the matrix can indirectly induce an inflammatory response in chondrocytes through the production of damage-associated molecular patterns (Sokolove and Lepus, 2013).

Physiological levels of cartilage loading cartilage enables nutrient transportation and enables cartilage homeostasis through induction of chondrocytes signalling. Moderate dynamic compression of cartilage abolishes cytokine-induced aggrecanase activity and chondrocyte apoptosis. However, severe and injurious loading (30% compressive load) has been shown to increase chondrocyte necrosis (C. T. Chen *et al.*, 2001) and apoptosis (D'Lima *et al.*, 2001), and does not inhibit cytokine-induced aggrecanase activity (Y. Li *et al.*, 2013). This indicates mechanical thresholds for mechanical load that distinguish between a beneficial and detrimental response of the tissue.

These responses to injury are crucial in chondrocyte homeostasis, the intrinsic tissue repair response and susceptibility to disease. Mechanical tissue injury is key aspect of osteoarthritis, as it is present in all established cases of the disease.

1.5.1 Mechanoflammation

There are two main aspects to mechanosensitive signalling in cartilage injury, which include the release of growth factors from the matrix to stimulate repair, and the induction of inflammatory signalling; a process termed mechanoflammation (Figure 1.6).

Mechanoflammation concerns the inflammatory response of the chondrocytes to mechanical injury. The initial upstream mechanism by which chondrocytes are able to sense mechanical injury is not yet known, but subsequent rapid phosphorylation and polyubiquitination of TGFβ-activated kinase 1 (TAK1) causes downstream MAPK, p38, JNK and NFκB signalling pathway activation (Ismail et al., 2017). This can induce a plethora of inflammatory genes, and ultimately lead to cartilage matrix

degradation via JNK2-mediated aggrecanase activity (Ismail *et al.*, 2015, 2016) and pain via induction of NGF (Driscoll *et al.*, 2016).

In addition to the direct effect on chondrocytes, mechanical injury also affects the cartilage matrix. Upon mechanical injury of cartilage tissue, growth factors such as FGF2 (Vincent et al., 2002) and CTGF (Tang et al., 2018) are released which have been implicated in the development of osteoarthritis. FGF2 knockout results in accelerated spontaneous osteoarthritis after 6 months, and a more severe response to DMM in a mouse model (Chia *et al.*, 2009). Conditional knockout of CTGF in cartilage leads to increased articular cartilage thickness and a less severe histological osteoarthritis score in response to murine DMM. However, the addition of CTGF to articular cartilage enhances regeneration in a full-thickness defect model (Nishida *et al.*, 2004). CTGF is implicated in connective tissue repair in other tissue, and in cartilage is known to activate TGFβ-induced SMAD signalling upon its release from the matrix in a TGFβR3-dependent manner, via initial sequestration of latent TGFβ (Tang *et al.*, 2018). These results highlight the importance of extracellular factors in the chondrocyte response to injury.

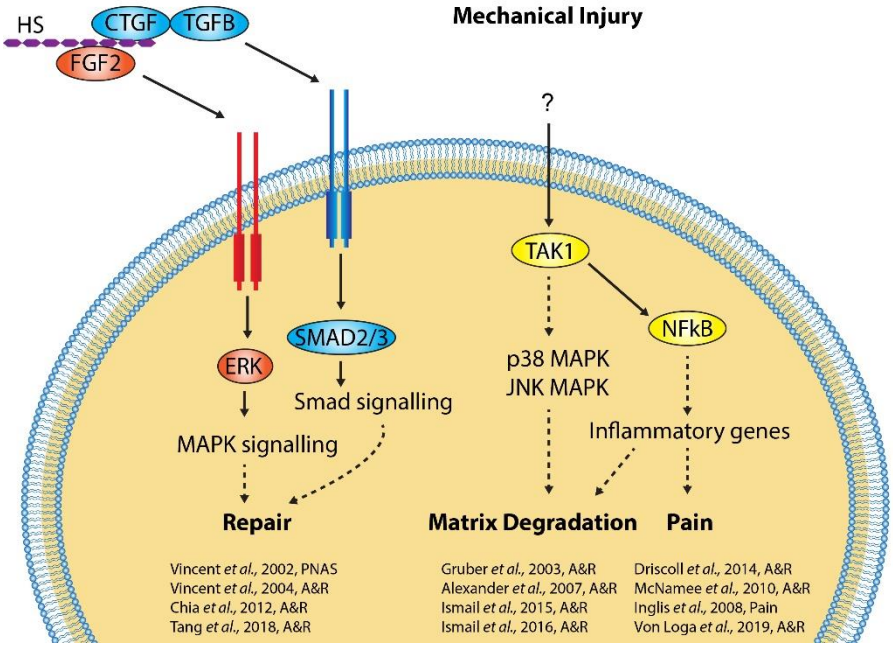

Figure 1.6 Cartilage injury-activated pathways in the chondrocyte. Pathways activated in chondrocytes upon simple cutting injury of articular cartilage. Release of matrix sequestered growth factors drives tissue repair responses. Mechanoflammation drives TAK1-dependent pathways that lead to pain and matrix degradation *in vitro* and *in vivo* via an unknown upstream event. Reproduced from (Vincent, 2019).

Antibodies that target inflammatory cytokines have failed in clinical trials for osteoarthritis, despite a range of successes in rheumatoid arthritis. TNF-α targeting antibodies (Aitken *et al.*, 2018) and antibody fragments, IL-6 receptor inhibitors and IL-1 inhibitors (Fleischmann *et al.*, 2019) have proven unsuccessful. This may be a reflection of treating a cause of disease too late, when degradation is already occurring.

When considering mechanoflammation of chondrocytes, one must distinguish between the different types of mechanical load. There are differences between the inflammatory gene profiles induced by shear stress, compressive load and upon the superficial damage of cartilage compared to full-thickness injury down to the underlying bone. However, much of the gene induction response upon cartilage injury

in *ex vivo* models is recapitulated in damaged osteoarthritis tissue (Dell'Accio *et al.*, 2008). The stratification of cell subtypes, type of strain and localisation within cartilage should also be considered when investigating the role of mechanoflammation in osteoarthritis and cartilage injury.

In the context of joint disease and arthritis, contribution of inflammation comes from multiple constituents of the joint, not just the cartilage. The synovium that encapsulates the joint fluid and the articulating surfaces of the joint can become inflamed in a range of pathologies, and can promote the infiltration of cells, ultimately producing inflammatory promoting elements. The inflammatory synovial response may be initiated by the breakdown of cartilage matrix macromolecules and chondrocyte responses; a secondary inflammation response occurs subsequent to the initial chondrocyte and mechanoflammation-mediated cartilage degradation or remodelling (Pelletier, Martel-Pelletier and Abramson, 2001). Synovial inflammation can cause the infiltration of T cells, B cells and macrophages into the synovial fluid of the joint (Nakamura *et al.*, 1999; Benito *et al.*, 2005). These are known to influence the inflammatory landscape of the joint, and possibly contribute to chondrocyte and cartilage matrix degradation. However, the cartilage itself is devoid of vasculature and resident immune cells. The principal cell in cartilage is the chondrocyte, which is able to respond inflammatory mediators and synthesise its own.

1.5.2 Cartilage tissue repair

Cartilage tissue was historically considered to be void of the ability to intrinsically repair. However, technological advancements in cartilage imaging have demonstrated clinical evidence of cartilage repair arthroscopically (Nakamura *et al.*, 2008) and by

MRI imaging (Intema *et al.*, 2011; Wiegant *et al.*, 2013; van der Woude *et al.*, 2017). Although the mechanisms of cartilage repair are not fully understood, recently developed cartilage injury models allow further investigation.

The canonical wound healing response in most tissues starts with the blood clotting cascade, allowing a transient influx of neutrophils, followed by macrophage recruitment to the site of injury and neovascularisation. This allows for subsequent remodelling of extracellular matrix, cellular proliferation and reorganisation of tissue at the end of the healing response. Despite previous dogma, the immune cell and hematopoietic cell responses in tissue repair are not always necessary; PU.1 null neonatal mice without macrophages and some other hematopoietic cell lineages maintain a highly efficient wound healing response (Martin *et al.*, 2003).

Cartilage is avascular and aneural, lacking resident immune cells and blood vessels that contribute to the typical repair response. However, cartilage is still able to exhibit some repair in response to damage. The DBA-1 mouse is a common model of cartilage repair, able to regenerate cartilage in full-thickness defects of the patellar groove (Eltawil *et al.*, 2009). Repair and matrix remodelling are described in response to injury (Redman *et al.*, 2004; Aurich *et al.*, 2006) and during osteoarthritis (Nelson *et al.*, 1998; Bay-Jensen *et al.*, 2008). Furthermore, exogenous application of growth factors, matrix proteins and tissue engineering structures/cells (Roberts *et al.*, 2001; Deng *et al.*, 2007) are able to enhance the intrinsic repair response of cartilage tissue.

The pathogenic mechanisms that contribute to the development of OA can be broadly divided into those that drive proteolytic degradation of the matrix and those that supress the intrinsic repair of the tissue. Cartilage tissue has low intrinsic repair,

especially in aged and osteoarthritic joints, which invites an opportunity to target the repair responses in the treatment and prevention of osteoarthritis.

A host of growth factors are implicated in the cartilage repair response. FGF2 is well characterised in cartilage injury, and stimulates a cartilage repair response *in vivo* as a recombinant protein (Cuevas, Burgos and Baird, 1988), when overexpressed in chondrocytes (Kaul *et al.*, 2006) and when transduced into rabbit synoviocytes (Hiraide *et al.*, 2005) or chondrocytes (Cucchiarini *et al.*, 2005). FGF18 is another fibroblast growth factor family member that induces chondrocyte proliferation and cartilage formation *in vivo* (Moore *et al.*, 2005; Reker *et al.*, 2020). Hydrogel incorporation of recombinant CTGF in a rat patellar groove subchondral defect model stimulated repair and filling of the defect within 4 weeks (Nishida *et al.*, 2004). CTGF also induces TGFβ signalling in cartilage, through its action as a latent TGFβ-binding protein. TGFβ exhibits anabolic effects in chondrocytes, stimulating ECM proteoglycan production (Bos, Verhaar and van Osch, 2006) and inducing repair in response to IL-1 damaged cartilage (Blaney Davidson *et al.*, 2006). TGFβ is highly chondrogenic, and introduction of MSCs/TGFβ3 immobilized scaffolds induces chondral defect repair in rabbits after 8 weeks (Fan *et al.*, 2010). BMP-7 (OP-1) is a growth factor extensively studied in cartilage repair; recombinant protein administration (Louwerse *et al.*, 2000; Jelic *et al.*, 2001; Kuo *et al.*, 2006) and introduction of BMP-7 transfected MSCs (Mason *et al.*, 2000) both result in stimulation and improvement of cartilage repair in pre-clinical joint defect models. BMP-2 is also able to stimulate regeneration of rabbit cartilage defects (Suzuki *et al.*, 2002), and acts as a driver of chondrogenesis *in vitro* (Jha *et al.*, 2009). These studies

demonstrate that intervention with growth factors can stimulate repair of cartilage tissue, and play a protective role against the progression of osteoarthritis.

Genome-wide association studies have linked intrinsic repair pathway components such as FGF18 and TGFβ1 to susceptibility variants in osteoarthritic populations (Tachmazidou *et al.*, 2019). TGFβ1 in synovial fluid further predicts knee OA progression (Hsueh *et al.*, 2021) and clinical response to surgical joint distraction in OA patients (Watt *et al.*, 2020); a procedure which drives regeneration of articular cartilage. A truncated recombinant form of FGF18 (sprifermin) induces the building back of articular cartilage in osteoarthritis patients (Hochberg et al., 2019; Eckstein et al., 2020). These clinical data highlight the importance of growth factor-mediated repair mechanisms in human osteoarthritis.

Cells and factors extraneous to cartilage tissue also influence cartilage repair, in addition to the intrinsic cartilage responses. There is evidence that mesenchymal stem cells (MSCs) contribute to cartilage repair through proliferation and chondrogenesis. Lineage tracing in a full-thickness mouse cartilage defect model provides evidence that the majority of cells contributing to repair are of GDF5 MSC lineage, from either the synovium, subchondral bone marrow or articular cartilage (Roelofs *et al.*, 2017). Marrow-derived MSCs proliferate and fill osteochondral defects in a rat patellar groove cartilage injury model (Anraku *et al.*, 2009). Adipose tissue-derived mesenchymal stem cells are being investigated as a source of progenitor cells for autologous chondrocyte implantation, as a form of cartilage repair (Jo *et al.*, 2014; Pers *et al.*, 2016).

1.5.3 Cartilage injury models

Ex vivo models of cartilage injury are used to study the response of articular cartilage to mechanical injury in primary tissue, without surgery. These include explantation (cartilage cut directly from the intact joint surface), re-cutting (explanted cartilage rested *in vitro* for 48 h, then re-injured by cutting), avulsion (shearing of the immature femoral head cartilage from the mouse hip epiphysis) and various forms of mechanical compression. Cartilage tissue is paucicellular (predominantly matrix, with 10% cellularity), aneural, avascular and has one resident cell type, the chondrocyte. The chondrocyte must therefore be responsible for receiving, and responding to, injurious signals transmitted through the matrix in these cartilage models.

The recutting injury model has been validated by the Vincent lab in multiple studies (Vincent *et al.*, 2002; Chong *et al.*, 2013). This model shows the release of FGF upon injury and induction of ERK signalling pathways in a manner inhibited by a neutralising anti-FGF antibody (Vincent *et al.*, 2002). The injury response in cartilage exhibits an FGF-dependent response, which induces proteins such as TIMP1, PDPN and Activin A and expression of genes such as *Tnfaip6* (TSG6) and *Mmp19*. These chondrocyte gene responses are recapitulated *in vivo*, with mouse injury models through destabilisation of the medial meniscus (DMM) of the joint, a model of osteoarthritis induced by destabilisation of mechanical load in the animal joint (Chong *et al.*, 2013). The same FGF-dependent proteins are also induced in the synovial fluid following knee injury (Watt *et al.*, 2016).

1.6 Cartilage matrix growth factors

1.6.1 Fibroblast growth factors

Fibroblast growth factors belong to a family of 22 structurally related proteins that are involved in a variety of signalling processes. Canonical FGF growth factors (FGF2–FGF10, FGF16–FGF18, FGF20, FGF22) have a high affinity for heparan sulfate and act in an autocrine/paracrine manner on cell surface receptor tyrosine kinases. These growth factors are secreted by the cell and can bind heparan sulfate in the extracellular matrix or cell surface, which also acts as a cofactor for receptor-mediated signalling. Other secreted FGFs are endocrine-mediated factors (FGF15, FGF19, FGF21, FGF23) that use klotho protein as a cofactor. Non-secreted FGFs are intracellular (FGF11–FGF14) and serve as cofactors for voltage-gated sodium channels and other molecules. The focus will be on canonical secreted FGFs, of particular interest FGF2.

Fibroblast growth factor receptors (FGFR1–4) are tyrosine kinase receptors, activated by receptor dimerisation upon ligand binding. Each of these have extracellular immunoglobulin-like domains (Ig I, Ig II, Ig III), a transmembrane domain and two intracellular kinase domains. These initiate a downstream cascade of protein phosphorylation and cellular signalling upon ligand binding (Figure 1.7).

Canonical FGFs bind FGFRs between the extracellular Ig-like II and Ig-like III receptor domains. FGF-FGFR binding is mediated by heparan sulfate binding to the Ig-like III receptor domain of FGFR and to the heparan sulfate-binding site of FGF (Schlessinger *et al.,* 2000). This forms a FGF:FGFR:HS complex which allows a conformational change to stabilise a biologically active symmetrical dimer (Schlessinger *et al.,* 2000). An alternative crystallography study of FGF1 shows a

asymmetrical 2:2:1 complex of FGF1:FGFR2:HS (Pellegrini *et al.*, 2000). Heparan sulfate chain length and level of sulfation have been implicated in modifying differential biological activity of FGF:FGFR complexes (Guimond *et al.*, 1993). Receptor dimerisation can activate the intracellular tyrosine kinase domains by phosphorylation at 7 tyrosine transphosphorylation sites (Y463, Y583, Y585, Y653, Y654, Y730, and Y766 in the case of FGFR1) (Lew *et al.*, 2009). Adaptor proteins become phosphorylated after docking at these intracellular transphosphorylation sites and activate multiple downstream signal transduction pathways; these include mitogen-activated protein kinase (MAPK), Janus kinase signal transducer (JAK/STAT), phosphatidylinositol-3-kinase and protein kinase B (PI3K/AKT) and phospholipase C (PLC) signalling (Carter, Fearon and Grose, 2015).

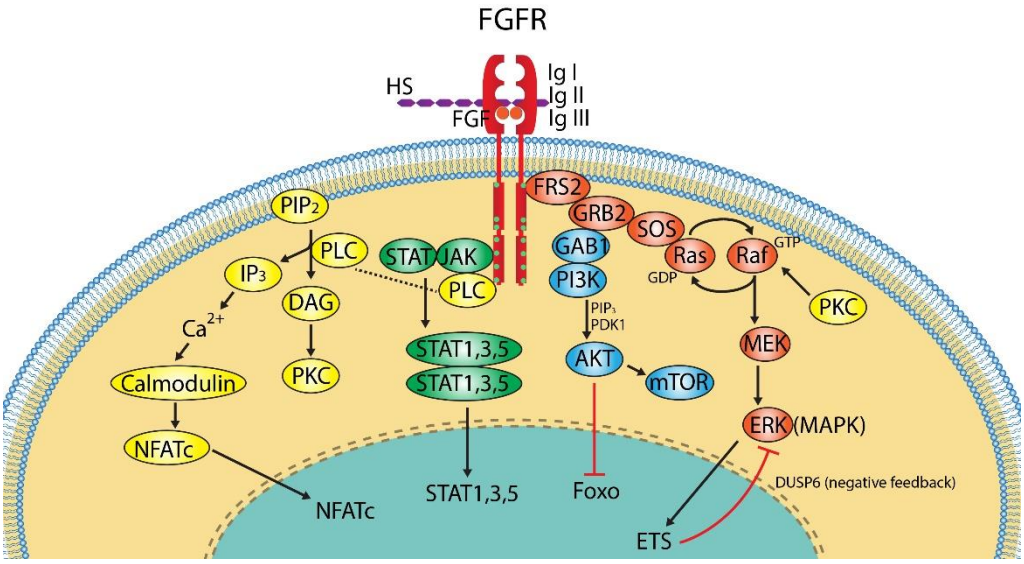

Figure 1.7 Canonical FGF:FGFR signalling. Binding of FGFs, aided by heparan sulfate as a co-factor, induces conformational change of FGFRs, allowing receptor homodimerisation and activation of the intracellular tyrosine kinase domains. This leads to transphosphorylation on FGFR tyrosine residues, which function as docking sites for adaptor proteins and activation of 4 main signalling pathways. Mitogen-activated protein kinase (MAPK) pathway (red) involves phosphorylation of FRS2 allows it to recruit adaptor protein GRB2. GRB2 recruits SOS, a guanine nucleotide exchange factor, which activates Ras GTPase. Ras activates Raf protein kinase, which phosphorylates MEK. MEK then phosphorylates MAPKs such as extracellularly regulated kinase 1/2 (ERK), which activate members of the E26 transformation-specific (ETS) transcription factor family such as ETV4, 5 and expression of negative regulators of the FGF signalling pathways such as SPRY, SEF, and DUSP6. Phosphatidylinositol-3-kinase/ Protein kinase B (PI3K/AKT) pathway (blue) involves GRB2 recruitment of the adaptor protein GAB1, which activates PI3K. PI3K phosphorylates the enzyme AKT. AKT phosphorylates TSC2 and leads to activation of RHEB GTPase, a potent activator of mTORC1. Activated AKT also phosphorylates the pro-apoptotic transcription factor FOXO1, causing it to exit the nucleus, promoting cell survival. The Phospholipase C (PLC) pathway (yellow) involves activation the enzyme PLCγ, which hydrolyses PIP2 to IP3 and DAG. PIP3 induces calcium ion release from intracellular stores and the activation of downstream signalling pathways, while DAG activates the enzyme PKC (protein kinase C). PKC phosphorylates Raf, reinforcing the MAPK pathway. The Janus kinase/signal transducer and activator of transcription (JAK/STAT) pathway (green)involves phosphorylation of JAKs which then phosphorylate and activate STATs. Phosphorylated STATs dimerise and can translocate to the nucleus to act as transcription factors.

FGFR knockout mouse studies have highlighted an important role for FGF signalling in cartilage. Knockout of *Fgfr1* in mouse articular chondrocytes (conditional *Col2a1-creER*) delays the degradation of articular cartilage in a DMM model of OA (Weng *et*

al., 2012). Comparable conditional knockout of *Fgfr3* increases progression of articular cartilage degradation within 1 month of DMM surgery (Tang *et al.*, 2016). FGFR3 is reduced in osteoarthritic monolayer chondrocytes compared to healthy human chondrocytes (Yan *et al.*, 2011), which highlights potential effects of altered receptor availability with disease progression. FGF signalling predicts clinical response to surgical joint distraction in OA patients; a procedure which drives regeneration of articular cartilage (Watt *et al.*, 2020). Further, recombinant fibroblast growth factor 18 (sprifermin) is the first structure modifying drug to demonstrate efficacy in human clinical trials by building back articular cartilage in osteoarthritis (Hochberg *et al.*, 2019; Eckstein *et al.*, 2020).

1.6.1.1 Fibroblast growth factor 2

Fibroblast growth factor 2, also known as basic fibroblast growth factor, was initially purified with FGF1 from cultured fibroblasts as a mitogenic factor (Armelin, 1973; Gospodarowicz, 1974). FGF2 is an 18 kDa protein, but has been since found as high molecular weight variants that predominantly remain localised to the nucleus (Chlebova *et al.*, 2009). The lower molecular weight (18 kDa) form is found in the cytoplasm and secreted from the cell (Davis *et al.*, 1997).

Fgf2 $^{-/-}$ mice are viable, fertile and do not exhibit obvious developmental defects. These mice exhibit decreased vascular smooth muscle contractility, reduced neuron density (Ortega *et al.*, 1998), reduced bone mineral density (Montero *et al.*, 2000) and defects in the wound healing response to cardiac (Virag *et al.*, 2007) and cutaneous injury (Ortega *et al.*, 1998).

FGF2 plays an important role in cartilage homeostasis. In articular cartilage, FGF2 is bound to heparan sulfate, on the proteoglycan perlecan, in the pericellular matrix (Vincent *et al.*, 2007). Sequestered FGF2 is released from the pericellular matrix to mediate cellular responses via FGFR-mediated signalling upon injury and mechanical loading (Vincent *et al.*, 2002, 2004). FGF2 more readily dissociates from heparan sulfate, with a dissociation half-time of minutes, than its receptor, with a binding half-time of hours (Moscatelli, 1992). This, combined with the proximity of the PCM to chondrocytes, suggests dissociation could occur rapidly enough for FGF2 to bind its receptors by laws of mass action, rather than needing enzymatic activity. However, the mechanism by which FGF2 dissociates and is released upon mechanical injury is not yet known.

There is evidence suggesting a catabolic role of FGF2 in cartilage. FGF2 administration to human cartilage upregulates MMP-13 (Yan *et al.*, 2011) and induces proteoglycan loss (Li *et al.*, 2012). FGF2 also inhibits the anabolic cartilage activity of IGF-1 and BMP-7 (OP-1) (Loeser *et al.*, 2005), and stimulates MMP-13 (Im *et al.*, 2007; Muddasani *et al.*, 2007) in human adult articular chondrocytes. On the other hand, a host of independent studies demonstrate an *in vivo* anabolic role of FGF2 in cartilage. FGF2 induces repair in rabbit models of patellar groove cartilage injury (Hiraide *et al.*, 2005) and knee articular cartilage injury (Cuevas, Burgos and Baird, 1988; Yamamoto *et al.*, 2004; Cucchiarini *et al.*, 2005; Kaul *et al.*, 2006). FGF2 also inhibits IL-1 induced *ADAMTS-4* and *ADAMTS-5* human cartilage breakdown (Sawaji *et al.*, 2008) and de-differentiates human articular chondrocytes (Schmal *et al.*, 2007), which might regulate the proliferation and differentiation balance that is needed for cartilage repair. Further, FGF2 administration suppresses OA progression in animal

models, including a rabbit ACLT model (Inoue *et al.*, 2006) and mouse DMM model (Chia *et al.*, 2009). *Fgf2* $^{-/-}$ mice develop spontaneous OA by 6 months of age, which is prevented by subcutaneous injection with recombinant human FGF2 (Chia *et al.*, 2009), indicating a protective role for FGF2 in cartilage.

FGF2 is also implicated in chondrogenic differentiation of MSCs (Solchaga *et al.*, 2005). Sequential exposure to recombinant FGF2, along with FGF9 and FGF18, enhances human MSC chondrogenic differentiation (Correa *et al.*, 2015).

1.6.2 Connective tissue growth factor

Connective Tissue Growth Factor (CTGF/CCN2) was first discovered as a fibroblast mitogenic and chemotactic factor in the conditioned medium of human umbilical vein endothelial (HUVEC) cells *in vitro* (Bradham *et al.*, 1991). Human and porcine CTGF comprise of 349 amino acid residues, the first 26 of which comprise a hydrophobic signal peptide (Bradham *et al.*, 1991; Harding, Surveyor and Brigstock, 1998). Mouse CTGF (also termed fisp-12, betaIG-M2 or CCN2) is predicted to comprise 348 residues, of which the first 25 are a hydrophobic signal peptide (Brunner *et al.*, 1991; Ryseck *et al.*, 1991). CTGF is secreted without its N-terminal signal peptide with the same number of amino acids in human, porcine and mouse species with 38 conserved cysteine residues. Its direct receptor, and therefore exact mechanism of action, is unknown.

CTGF is classified within the CCN family of proteins as CCN2 for its structural homology (Brigstock *et al.*, 2003). This family comprises of six proteins: CYR61 (CCN1), CTGF (CCN2), NOV (CCN3), WISP1 (CCN4), WISP2 (CCN5) and WISP3 (CCN6). These proteins contain an N-terminal secretory factor followed by four

structural domains with partial sequence identity to insulin-like growth factor-binding proteins, von Willebrand factor type C repeat, thrombospondin type 1 repeat, and a C-terminus with sequence similarity to the C-termini of von Willebrand factor, mucin, and slit protein. The CCN family proteins are matricellular and regulate cell adhesion, migration, proliferation, survival, and differentiation, some cases at least in part through integrin mediated mechanisms.

In cartilage, CTGF is sequestered in the PCM on the heparan sulfate proteoglycan perlecan, owing to its heparan sulfate binding affinity (Ori, Wilkinson and Fernig, 2011). CTGF stimulates human chondrocyte expression of *CTGF* and *TGFβ1* in a TGFβ-dependent manner. Similarly, TGFβ1 induces *CTGF* expression via TGFβR signalling. At the protein level, CTGF induces TGFβ-dependent SMAD2 phosphorylation. This is achieved through CTGF acting as a latent TGFβ-binding protein (LTBP) in cartilage, where it binds covalently binds by disulfide bond to the small, latent complex of TGFβ (TGFβ + LAP) prior to secretion. After secretion, CTGF binds to heparan sulfate in the cartilage matrix, sequestering the bound latent TGFβ to control its release in an injury-dependent manner. Upon cartilage injury, the complex activates chondrocytes by first engaging with TGFβR3 in a heparan sulfate/CTGF-dependent manner, allowing the TGFβ activation of SMAD phosphorylation via TGFBR1/2 canonical signalling (Tang et al., 2018) (Figure 1.8).

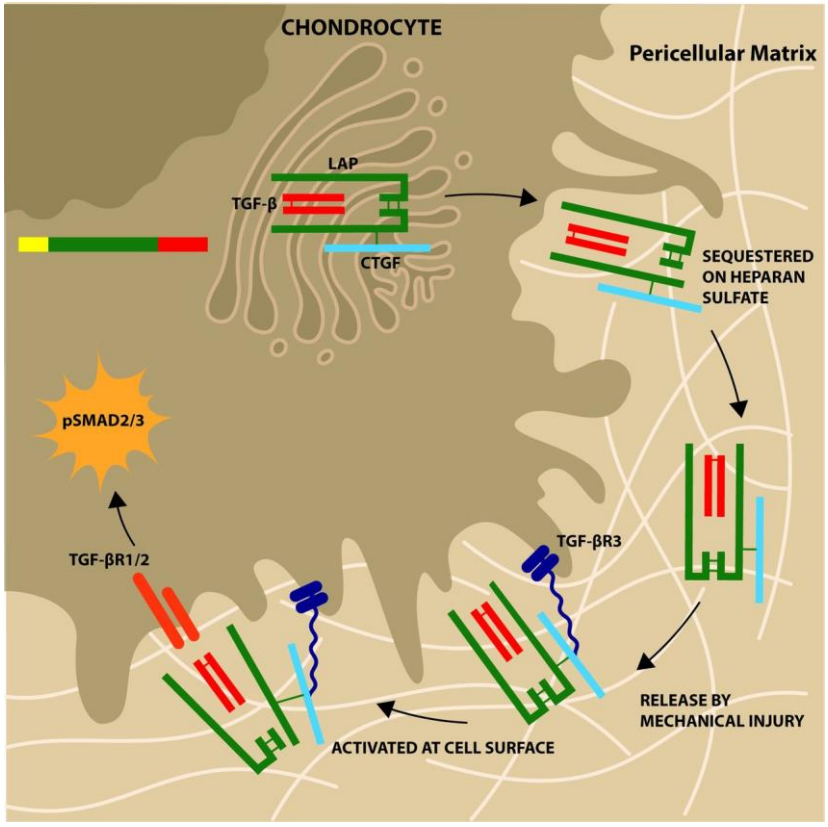

Figure 1.8 Connective tissue growth factor (CTGF/CCN2) function in cartilage. CTGF is covalently bound (disulfide bond) to latent TGFβ in the endoplasmic reticulum of the chondrocyte. It is secreted as a large latent complex and sequestered in the pericellular matrix, attached to heparan sulfate chains of perlecan (HSPG2). Mechanical compression causes release of heparan sulfate-bound factors, allowing latent complex engagement with TGFβR3 on cell surface (in a heparan sulfate/CTGF-dependent manner). This allows activation of latent complex with autocrine activation of canonical pathway of TGFβ involving SMAD2/3 phosphorylation. Reproduced from (Tang *et al.*, 2018).

CTGF overexpression in growth plate cartilage stimulates the proliferation and differentiation of growth plate chondrocytes and results in endochondral ossification. CTGF knockout impairs DNA synthesis and matrix proteoglycan production in articular cartilage chondrocytes (Nishida *et al.*, 2007). Implementation of recombinant CTGF to rat knee articular cartilage in a hydrogel allows filling of a full-thickness defect within 4 weeks (Nishida *et al.*, 2004).

CTGF is expressed in both normal and OA cartilage, and localises to the PCM (Omoto *et al.*, 2004). Knockout of *Ctgf* in mice prevents age-related osteoarthritis-like changes (Takigawa, 2013). *Ctgf* knockout also results in thickening of the cartilage and protection from surgically-induced OA by DMM (Tang *et al.*, 2018). Further research suggests this protective effect might be a compensatory mechanism of activin-mediated signalling in response to *Ctgf* knockout.

1.6.2.1 Transforming growth factor beta

The transforming growth factor beta (TGF-β) superfamily of growth factors contains over 30 members, including TGF-βs, bone morphogenetic proteins (BMPs), growth and differentiation factors (GDFs), Activins, and Nodal, which are vital for development and homeostasis across tissues.

TGFβ ligands are secreted from cells in a large complex that includes a cleaved latency-associated peptide (LAP) pro-region of the TGFβ precursor, and Latent TGFβ-Binding Proteins (LTBPs). These complexes act to control ligand activity by sequestering TGFβ in the extracellular matrix or by mediating interactions with receptors to release the mature ligand. CTGF acts as a LTBP in cartilage.

TGFβ ligands signal through a TGFβR2 homodimer that forms a complex with a TGFβR1 homodimer. TGFβ ligand binding can be enabled through the betaglycan cell surface proteoglycan TGFβR3, although TGFβR3 is not directly involved in signal transduction. BMP ligands signal through a complex of BMPR1 and BMPR2 homodimers. Canonical signalling, involving the phosphorylation of SMADs by TGFβR and BMPR serine/threonine kinases, is described in Figure 1.9. Both receptor complexes also signal through non-SMAD pathways (Derynck and Zhang, 2003).

BMPR signalling can activate TAK1-mediated JNK and p38 signalling. TGFβR signalling can activate Rac/Cdc-42, RhoA-ROCK, PI3K pathways, and TAK-1 mediated JNK, p38 and NFκB signalling.

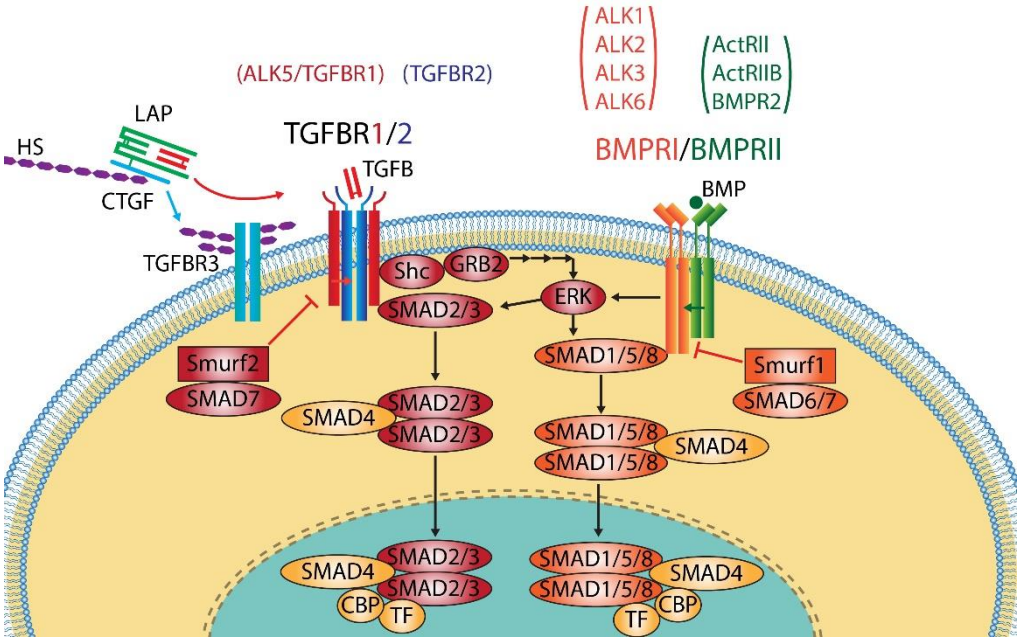

Figure 1.9 Canonical TGFβ and BMP signalling pathways. TGFβ superfamily signalling pathways of TGFβ and BMP growth factors signal via ligand-induced oligomerisation of serine/threonine receptor kinases and phosphorylation of the cytoplasmic canonical Smad signalling and other non-canonical signalling pathways. TGFβ ligands (e.g. TGFβ1, Activin, Nodal) signal bind to a TGFβ type II receptor dimer (TGFβR2), which recruits a type I receptor dimer (TGFβR1/ALK5). The heterodimer phosphorylates SMAD2 and SMAD3 molecules. BMP ligands (e.g. BMP-2, -4, -7) exert their cellular responses by binding a BMP type I receptor dimer (ALK1/ACVRL1, ALK2/ACVR1, ALK3/BMPRIA and ALK6/BMPRIB) complexed with a type II receptor dimer (BMPRII, ActRII and ActRIIB). The constitutively active type II receptor phosphorylates the type I receptor (ALK1/2/3/6) that phosphorylates R-SMAD1, 5 and 8. Activated SMADs form complexes with co-SMAD4, which then acts as a transcription factor (TF) complex to regulate gene transcriptional responses. Inhibitory SMADs (SMAD6/7) act to antagonize signal transducing SMADs. In addition to the canonical SMAD pathways, ERK/MAPK, Rho-like GTPase, PI3K/Akt, ERK/MAPK, JNK and p38 signalling pathways.

TGFβ growth factors are linked to cartilage function and osteoarthritis progression. TGFβ1 is identified in osteoarthritis genome wide association studies, where hypomorphic variants are associated with increased risk of disease (Zengini *et al.*, 2018; Tachmazidou *et al.*, 2019). Changes in TGFβ1, activin A and LTBP2 occur in the synovial fluid after surgical joint distraction in OA patients, and a greater increase in TGFβ1 predicts response to the treatment (Watt *et al.*, 2020). The TGFβ gene pathway is enriched in a surgical OA mouse model 2 weeks post-DMM (Gardiner et al., 2015); Tgfb2, Tgfb3, Ltpb1 (latent TGF-beta-binding protein 1) and Ltpb4 are upregulated, but Tgfbr1 and Tgfbr3 are downregulated. These associations highlight a mechanical responsiveness of TGFβ signalling and potential involvement in response to disease.

TGFβ is essential for driving chondrogenic differentiation *in vitro* (Yang *et al.*, 2001; Awad *et al.*, 2003; Fukumoto *et al.*, 2003; Murdoch *et al.*, 2007; Muhammad *et al.*, 2014) and plays a role in wound healing and fibrosis in other tissues (Daniels *et al.*, 2003; Bos, Verhaar and van Osch, 2006; Penn, Grobbelaar and Rolfe, 2012). Mechanical loading of mesenchymal stem cells stimulates TGFβ1 and TGFβ3 expression, and further stimulates chondrogenic differentiation (Kisiday *et al.*, 2009; Li *et al.*, 2010; Gardner *et al.*, 2017). Concentrations of TGFβ ligand are high in subchondral bone from humans with osteoarthritis and can induce MSC clustering (Zhen *et al.*, 2013).

The result of TGFβ signalling in the joint is somewhat tissue-dependent. TGFβR2 knockout in articular cartilage (*Col2ER* conditional knockout) results in an ADAMTS-5 and MMP13 dependent progression of OA development (Shen *et al.*,

2013). Conditional knockout of *Alk5* (TGFβR1 protein coding gene) in lubricin-expressing articular cartilage stem cells results in increased cartilage damage in a murine DMM model (Tan *et al.*, 2021). However, TGFβR2 knockout in nestin-positive MSCs of the subchondral bone attenuates ACLT-induced OA (Zhen *et al.*, 2013). Further, subchondral injection of anti-TGFβ reduces ACLT-induced cartilage degradation (Zhen *et al.*, 2013); this was conducted to reflect Camurati-Engelmann disease, which predisposes to osteoarthritis with a TGFβ1 activating mutation. High TGFβ activity in bone-resident MSCs might promote OA through bone remodelling, but activity in the cartilage is required for the maintenance of the chondrocyte phenotype. Therefore, alterations in physiological TGFβ signalling might influence cartilage degeneration.

1.6.3 Hepatoma-derived growth factor

Hepatoma-derived growth factor (HDGF) was first purified from the HuH-7 human hepatoma cell line (Nakamura *et al.*, 1989). Similar proteins have since been discovered, termed HDGF-related proteins (HRPs), including HDGF-like protein 1 (HDGFLP-1), HDGF related protein-2,3 and 4 (HDGFRP-2,3,4) and lens epithelium-derived growth factor (LEDGF). The HDGF-related proteins have varying abundances according to cell type, but HDGF itself is ubiquitously expressed in most tissues. The protein family shares 54-78% sequence homology of the HATH (homologous to amino terminal of HDGF) region (Abouzied *et al.*, 2004).

There are no full protein crystal structures of HDGF, mainly due to its variable disordered C-terminal region from amino acids 100–240. Published protein structures are listed in the appendix (Table 8.4). These structures image a portion of the protein

or utilise domain-swapped dimerisation, due to difficulties in crystallising unstructured portions of HDGF. The PWWP domain of HDGF confers heparin binding and DNA binding properties (Figure 1.10). Basic motifs homologous to bipartite nuclear localisation sequences have been described in the protein sequence (Kishima *et al.*, 2002). The N-terminal region of HDGF is positively charged, and the first 10 amino acids and phosphorylation of serine 165 are essential for non-classical secretion, through disulphide bridge formation and proteolytic processing (Thakar et al., 2010). This secretion occurs despite HDGF lacking a classic secretion signal peptide.

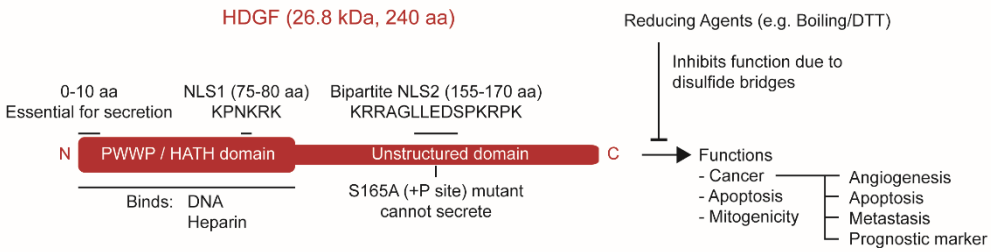

Figure 1.10 Illustrative structure and domains of HDGF. Illustrative figure of the domain structure and properties of Hepatoma-Derived Growth Factor (HDGF). The first 10 amino acids were demonstrated as essential for secretion, although do not constitute a classical secretory peptide. HDGF contains two nuclear localisation sequences (NLS1, NLS2), one 5 amino acid sequence in the PWWP/HATH domain (amino acids 1–100) and one bipartite 15 amino acid sequence in the unstructured domain (amino acids 100–240). The PWWP domain is the chromatin and heparin-binding portion of the protein.

HDGF shares 36% sequence homology with the high mobility group box 1 (HMGB1) protein (Nakamura *et al.*, 1994), with high homology in the C-terminal region. HMGB1 is classified as an alarmin (Harris and Raucci, 2006), and consequently highlighted HDGF as a candidate alarmin (Giri *et al.*, 2016); a messenger of cellular condition and stress, which feeds back to modulate cellular functions. HMGB1 signals

for tissue repair in a number of musculoskeletal tissues, and a number of studies demonstrate an increase in HMGB1 in OA tissue compared to normal control tissue (Gacaferi *et al.*, 2020). However, HDGF has not previously been investigated in the context of OA or cartilage tissue.

HDGF is a potential prognostic factor in a plethora of cancers (Bao *et al.*, 2014). Elevated HDGF levels are present in a variety of malignancies, in addition to the hepatocellular carcinoma, from which it was initially purified. Elevation of HDGF correlates with a poor prognosis in a host of cancers, in some cases independent of established clinical factors (Ren *et al.*, 2004; Uyama *et al.*, 2006; Chang *et al.*, 2007; Yamamoto *et al.*, 2007; Hu *et al.*, 2009; D. Li *et al.*, 2013; S. Z. Li *et al.*, 2013; Wang *et al.*, 2014; Zhang *et al.*, 2014). In hepatic cholangiocarcinoma, elevated HDGF can also be detected in patient serum, in addition to immunohistochemistry of the tissue (Zhang *et al.*, 2010).

HDGF is involved in repair of other tissue types, including vascular smooth muscle and lung epithelium. HDGF is highly expressed by proliferating smooth muscle cells, and exhibits a mitogenic effect when exogenously applied or overexpressed, which is partially heparin-dependent (Everett *et al.*, 2000). It is upregulated in damaged vascular walls (Everett *et al.*, 2000) and upregulated by cyclic mechanical stretch in smooth muscle, indicating a role in injury and an influence of mechanics for HDGF (Kao *et al.*, 2018). HDGF is also implicated in the hepatic fibrotic response in mice, where HDGF expression is elevated in fibrotic livers and overexpression leads to enhanced collagen deposition and TGFβ1 expression (Kao *et al.*, 2010). Mitogenic

effects of HDGF are also mediated after translocation to the nucleus (Everett, Stoops and McNamara, 2001; Kishima *et al.*, 2002; Zhou *et al.*, 2004; Bremer *et al.*, 2013).

HDGF is able to activate ERK signalling (Ooi *et al.*, 2010; Hollander *et al.*, 2012; Lu, Chen and Qiu, 2015) and induce PI3K signalling (Hollander *et al.*, 2012; Zhang *et al.*, 2019) in multiple cell lines and cell types *in vitro*, yet its mechanism of action has not been demonstrated (Figure 1.11).

HDGF is a secreted protein, which can be internalised from the extracellular space in a heparan sulfate-dependent manner (Wang *et al.*, 2011), due to its strong heparin binding affinity (Ori, Wilkinson and Fernig, 2011). The receptor for HDGF is unknown, but thought to signal *via* amino acid residues 81–100 of the HDGF PWWP domain (Abouzied *et al.*, 2005). Liquid chromatography tandem mass spectrometry has identified nucleolin as a binding partner for HDGF, from a hepatoma cell line. Nucleolin is therefore purported to be a membrane-bound receptor for HDGF, and is capable of PI3K signalling (Chen *et al.*, 2015). However, nucleolin is a nucleolar protein in non-tumour cells (Bremer *et al.*, 2013), so any binding in normal cells is likely intracellular. The HDGF extracellular receptor and HDGF signalling/internalisation is not fully understood.

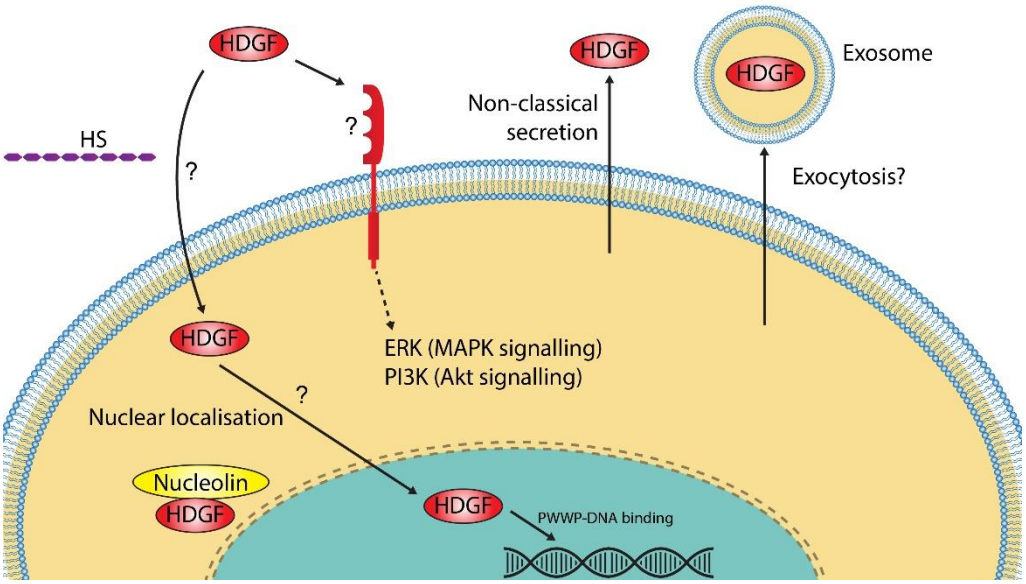

Figure 1.11 Putative actions of hepatoma-derived growth factor. Hepatoma-derived growth factor (HDGF) signalling and mechanism of action is not fully characterised, but literature suggests a mechanism of action via an unknown cell surface receptor and by heparan sulfate-mediated internalisation. HDGF can stimulate ERK (MAPK) and PI3K (Akt) signalling in a variety of cells, and can be found bound to nucleolin in a ribonucleoprotein complex. HDGF has two nuclear localisation sequences (NLS) for nuclear translocation and DNA-binding sites in its PWWP domain for chromatin interaction. A lack of secretory signal peptide suggests a non-classical secretion mechanism. When overexpressed, HDGF HATH domains are released from the cell in exosomes.

1.6.4 Other cartilage growth factors

BMPs are structurally related to the TGFβ superfamily of growth factors, and are conserved across species. Originally purified from bone, BMPs are present in a range of tissues including articular cartilage. Bone morphogenic protein 7 (BMP-7), also named osteogenic protein 1 (OP-1), is a cartilage repair growth factor, and upregulates chondrocyte metabolism without inducing uncontrolled proliferation or bone differentiation. BMP-7 stimulates cartilage-specific ECM proteins such as collagen type II, collagen type VI, hyaluronan, aggrecan and other proteoglycans. It is endogenously synthesised by the chondrocyte (Chubinskaya *et al.*, 2002), and interacts

with other growth factors and signalling response pathways. BMP-7 counteracts catabolic chondrocyte responses to IL-1 (Huch *et al.*, 1997), and reduces intrinsic production of cytokines and MMP-1 and MMP-13 *in vitro* (Chubinskaya *et al.*, 2011). Combined application of BMP-7 and IGF-1 has a synergistic effect on chondrocyte matrix synthesis and proliferation (Im *et al.*, 2003; Loeser, Pacione and Chubinskaya, 2003).

BMP-2 promotes expression of hypertrophic chondrocyte markers (Gomes *et al.*, 2002), influences late stage chondrogenesis (Gomes, Carson and Carson, 2003), and can influence MSC proliferation and matrix production. BMP-2 overexpression in the murine knee joint increases proteoglycan synthesis (Davidson *et al.*, 2007).

Insulin-like growth factor-1 (IGF-1) promotes matrix synthesis and cell proliferation in cartilage (Guenther *et al.*, 1982; McQuillan *et al.*, 1986). IGF-1 stimulates ERK (MAPK) and PI3K (Akt) pathway activation in chondrocytes, but the latter is responsible for observed proteoglycan synthesis (Starkman *et al.*, 2005). In addition to synergy with BMP-7, IGF-1 is produced by chondrocytes in response to FGF2, and by osteoblasts in response to TGFβ (Elford and Lamberts, 1990). Other studies show a counter-regulation of IGF-1 by FGF2 and TGFβ1 in chondrocytes, where FGF2 inhibits IGF-1 production, whereas TGFβ1 induces it (Shi *et al.*, 2009). Chondrocytes lose their responsiveness to IGF-1 with age and OA (Loeser *et al.*, 2000).

Platelet-derived growth factor (PDGF) has been investigated in the joint, but induces no adverse effects on cartilage or synovium in normal joints (Fortier *et al.*, 2011). However, PDGF is a potent mitogenic factor for mesenchymal stem cells (Ataliotis,

2000); its release from chondrocytes might act to prime progenitor cells for reparative chondrogenesis.

1.6.5 Heparin-binding growth factors

Heparan sulfate can bind over 400 soluble protein mediators and cell surface receptors (Ori, Wilkinson and Fernig, 2011). The ability to bind to heparin and heparan sulfate is conferred by a structurally complementary and negatively charged binding site. The negative charge of carboxyl and sulfate groups on heparin and heparan sulfate attract positively charged clefts on proteins and growth factors, allowing binding and sequestration.

FGF2 and CTGF bind the heparan sulfate proteoglycan perlecan in the pericellular matrix of cartilage (Vincent *et al.,* 2007; Tang *et al.,* 2018). Further, both growth factors induce signalling via receptors by a mechanism enhanced by heparan sulfate-receptor interaction. FGF2 binds to FGFRs in a complex with a heparan sulfate chain, where it increases affinity of FGF for its receptor (Pellegrini *et al.*, 2000; Schlessinger *et al.,* 2000; Pellegrini, 2001). CTGF binds the heparan sulfate proteoglycan betaglycan (TGFβR3) to enable TGFβ activation of TGFβR1/2 in cartilage.

IGF-1 does not directly bind to heparan sulfate, but some insulin-like growth factor-binding proteins (IGFBPs) exhibit heparin binding affinity (Ori, Wilkinson and Fernig, 2011). IGF-1 is able to bind and introduce a conformational change to IGFBP-2, exposing a glycosaminoglycan-binding domain, enabling binding of IGFBP-2 on a heparin-sepharose column and to fibroblast ECM (Arai, Busby and Clemmons, 1996). Imaging of IGF in cartilage tissue is generally localised to the chondrocyte and

periosteum (Serrat and Ion, 2017), but some IGFBPs can be imaged in the pericellular matrix (Martin *et al.*, 2002).

BMP proteins, including BMP-2 and BMP-7 exhibit heparin binding affinity (Ori, Wilkinson and Fernig, 2011) and are targeted to the extracellular matrix in a variety of tissues. However, these BMP growth factors are not described in the pericellular matrix of cartilage. Instead, cell surface proteoglycans such as syndecan-3 modulate BMP receptor signalling (Fisher *et al.*, 2006). Unlike FGF signalling, heparan sulfate does not stabilise BMP ligand-receptor binding, but does catalyse the formation of receptor complexes (Kuo, Digman and Lander, 2010).

Tracking of FGF2 labelled with gold nanoparticles shows that heparan sulfate binding sites for the growth factor are heterogenous across the pericellular matrix. It is proposed that they are able to translocate between binding sites by diffusion, dependent on binding site availability (Duchesne *et al.*, 2012). Growth factors are not trapped by binding heparan sulfate, but primarily exhibit confined motion. In this regard, the attraction of growth factors to heparan sulfate controls their bioavailability to nearby cells.

1.7 Cartilage response to mechanical load

Collagen II is the predominant type of collagen in articular cartilage, and the covalent cross-links between alpha chains and collagen molecules maintain a cohesive fibrous network, providing high tensile stiffness and strength to the tissue (Mow, Ratcliffe and Poole, 1992). Cartilage also responds to mechanical load with its swelling pressure, which consists of a physicochemical response via osmotic pressure and an electrostatic

repulsive force exerted by closely spaced (1–1.5 nm) negatively charged groups of proteoglycans in the matrix.

Articular cartilage can be modelled as biphasic, as a hydrated tissue with a mixture of porous solids that are permeable and elastic (proteoglycans, collagens and chondrocyte cells), with a movable interstitial fluid (water and dissolved ions) (Mow *et al.*, 1980; Guilak and Mow, 2000). Mechanical compression and deformation of the tissue influences both phases of cartilage. Cartilage can also be modelled as triphasic, as an extension to the original model, considering the negatively charged proteoglycans fixed to the solid matrix and ions present in the interstitial fluid (Lai, Hou and Mow, 1991). Both the water and the dissolved ions and solutes in the fluid phase are affected by mechanical compression, and have been extensively studied for decades with respect to fluid flow, molecular transport (e.g. cartilage nutrition, growth factor transport) and ion fluxes (DiDomenico, Lintz and Bonassar, 2018).

The response of articular cartilage to load is different across the depths of the tissue, owing to depth-dependent changes in matrix properties in normal cartilage. In healthy cartilage, water content decreases with increasing depth from the superficial surface (Maroudas, 1976; Shapiro *et al.*, 2001; Yang and Momot, 2016). Fixed charge density increases with depth (Maroudas and Freeman, 1979; S. S. Chen *et al.*, 2001). The compressive modulus (resistance to compression upon load) increases with depth (Schinagl *et al.*, 1997; S. S. Chen *et al.*, 2001; Yang and Momot, 2016). Overall collagen organisation increases with depth. The most superficial layer is highly organised, as are the middle-deeper layers, but the region below the superficial layer exhibits disorganised collagen (Nieminen *et al.*, 2001).

Mechanical loading on cartilage has both transient effects and long term influences on tissue homeostasis. Immediately, the release of factors from the matrix, the induction of signalling cascades in chondrocytes and physical stress on the tissue compose a rapid response. Mechanical loading is also able to modulate the TGFβ-induced chondrogenesis and matrix production of mesenchymal stem cells in the joint (Kisiday *et al.*, 2009; Li *et al.*, 2010; Gardner *et al.*, 2017). Subsequently, with continuous loading comes alterations in chondrocyte metabolism and extracellular matrix remodelling of the tissue (Jørgensen, Kjær and Heinemeier, 2017).

1.7.1 Chondrocyte mechanotransduction

Mechanical load in cartilage is propagated through the matrix to the chondrocyte cells through mechanotransduction. Individual chondrocytes express mechanically sensitive proteins and structures on the cell surface, or linked to the surrounding matrix, that are able to respond to physical stresses.

The involvement of ion channels in the chondrocyte response to mechanical stimulus is demonstrated in 3D cultures and cartilage explants with the use of generic types of ion channel inhibitors. Upon compression, ion channel inhibitors differentially influenced protein and sulfated GAG synthesis, indicating the role of ion channels in mechanically induced protein changes (Mouw, Imler and Levenston, 2007). Furthermore, mechanically sensitive ion channels have been discovered in other tissues such as the TRPV4 channel (Transient Receptor Potential Vanilloid 4), PIEZO1 and PIEZO2 channels (Coste *et al.*, 2010), which have since been implicated in chondrocyte mechanical sensing.

Sub-nanoscale mechanical stimulation of cultured porcine chondrocytes with atomic force microscopy induces intracellular Ca^{2+} signalling and electric currents. This calcium signalling is inhibited by GsMTx4 peptide, able to block PIEZO function, and by siRNA targeting PIEZO1 and PIEZO2, directly implicating these ion channel proteins in articular cartilage mechanotransduction at a cellular level (Lee *et al.*, 2014).

TRPV4 is a membrane ion channel expressed in chondrocytes and mediates intracellular Ca^{2+} signalling transients. Mechanical dynamic loading of agarose-embedded chondrocytes stimulates gene expression and biosynthetic responses that are attenuated with inhibition of TRPV4 (O'Conor *et al.*, 2014). Deletion of *Trpv4* abrogates these mechanically-sensitive Ca^{2+} transients and causes degradation of cartilage with age in mice (Clark *et al.*, 2010). However, chondrocyte-specific loss of TRPV4 does not affect disease progression after DMM, and inducible knockout of TRPV4 in adult mice reduces age-associated OA severity. These results highlight a role of TRPV4 in physiological chondrocyte mechanotransduction, rather than pathological injurious loading and destabilisation.

Integrins are expressed on the surface of many cell types, involved in facilitating extracellular matrix adhesion and propagating cellular signals. Chondrocytes express α1β1, α2β1, α3β1, α4β1, α5β1, α6β1, α10β1, αvβ1, αvβ3 and αvβ5 integrins, with some differentially and exclusively expressed by chondrocytes in osteoarthritic tissue (Salter *et al.*, 1992; Loeser, 2014). Mechanical stimulation of chondrocytes in the presence of integrin inhibition initially demonstrated the involvement of integrins in mechanotransduction (Wright *et al.*, 1997).

The primary cilium is a cellular organelle, present on virtually all cells that do not possess motile cilia, including the chondrocyte. A mutant mouse model harbouring a mutation in the intraflagellar transport component IFT88, an essential protein of primary cilia, did not show the mechanically-induced upregulation of aggrecan mRNA and sulfated GAG secretion (Wann *et al.*, 2012). This first highlighted the role of the chondrocyte primary cilium in propagating mechanotransduction pathways, downstream of ATP release. Further, post-natal deletion of the primary cilium causes development of spontaneous OA at 34 weeks, severe OA response to DMM 12 weeks after joint destabilisation and reduced cartilage thickness. These data highlight a role for the primary cilium in mechanosensitive regulation of cartilage.

1.7.2 Fluid flow

Upon cartilage compression, water is forced out of the extracellular matrix. Cyclical loading of cartilage increases the quantity of water exuded from the tissue, with a decrease in ionic concentration upon each iteration.

Permeability of the cartilage tissue influences fluid flow. The surface of cartilage is less permeable than the initial layer beneath the surface, which is the most permeable. Permeability then decreases with depth of articular cartilage (Maroudas and Bollough, 1968). Fixed charge density follows an opposite trend to permeability, increasing with articular cartilage depth (Maroudas and Bollough, 1968; S. S. Chen *et al.*, 2001).

1.7.3 Ion fluxes

Fluid flow does not significantly contribute to the rate of movement of small solutes in articular cartilage (O'Hara, Urban and Maroudas, 1990). Small solutes are more influenced by diffusion, and in the case of charged ions by electrostatic forces. The

extracellular matrix of cartilage contains an abundance of cations as counterions to the negative fixed charge density of the tissue. Matrix sodium cation concentration is measured between 250–350 mM in articular cartilage (Bashir, Gray and Burstein, 1996; Shapiro *et al.*, 2002).

Extracellular ion changes in cartilage have been investigated in the context of solute diffusion, fluid flow for cartilage nutrition and fluxes upon mechanical compression. The total extracellular ion concentration is dependent on the fixed charge density, which provides the basis for counterion equilibrium. The region below the cartilage surface (0–500 μm) has a lower fixed charge and decreased compressive modulus compared with deeper regions which is correlated to, but not fully explained by, fixed charge density (S. S. Chen *et al.*, 2001).

Ion fluxes can occur intracellularly (e.g. signalling responses of intracellular ion stores), trans-membranously (e.g. ion channel transport and neuronal propagation of action potentials via salutatory conduction) and extracellularly where ions can interact with constituents of the extracellular matrix.

Mechanotransduction of the chondrocyte mediates intracellular ion fluxes in cartilage. Membrane-based structures such as the primary cilium (Wann *et al.*, 2012) and the Ca^{2+}-permeable osmomechano-sensitive cation channel TRPV4 (O'Conor *et al.*, 2014) allow intracellular Ca^{2+} ion signalling in the chondrocyte in response to mechanical load, altering matrix protein metabolism. These responses of cartilage to mechanical load are discussed in Chapter 1.6.

1.8 Research aims

1. **Investigate the release of heparin-binding growth factors from the cartilage pericellular matrix upon injury**
    a. Validate HDGF as a heparin-binding growth factor of the pericellular matrix
    b. Interrogate the mechanism of growth factor release
2. **Explore the potential role of matrix-bound sodium in cartilage injury and growth factor release**
    a. In healthy and diseased tissue
    b. Validate sodium dynamics via direct visualisation
3. **Investigate the effect of HDGF deletion on the mouse joint**
    a. Assess morphology, cartilage thickness, and differences upon surgical induction of osteoarthritis
    b. Measure gene expression profiles in response to a hip avulsion cartilage injury model
    c. Assess functional cells of the joint with HDGF stimulation

2 Materials and Methods

This chapter details methodologies used throughout this work. Methodologies or details pertaining to experiments within a particular chapter are included therein.

2.1 Tissue culture

Dulbecco's modified Eagle's medium (DMEM) (Lonza, Verviers, Belgium) with 4.5 g/L of glucose and 584 mg/L L-glutamine was supplemented with 1% (100 U/ml) Penicillin and Streptomycin (Lonza, Verviers, Belgium). Serum DMEM (SF-DMEM) was supplemented with 10% FBS (heat-inactivated; Gibco, Massachusetts, USA).

Tissue culture incubations were maintained at 37 °C and 5% CO_2 unless otherwise specified.

All tissue culture experiments were carried out under sterile conditions inside a class II laminar flow cabinet.

2.1.1 Cartilage explantation

Trotters from 3–6 month old pigs were obtained from an abattoir (Cheale Meats Limited, Essex, UK) within 12 h of slaughter. Trotters were disinfected in 1% virkon solution for 20 min prior to dissection. Skin and dewclaws were removed using a 22-blade scalpel (sterile scalpels, all from Swann Morton, Sheffield, UK). The metacarpophalangeal (MCP) joint was opened under sterile conditions. The articular surface was washed with 10 ml PBS 3 times to remove synovial fluid. Cartilage was then dissected from the articular surfaces at the bone-cartilage interface using a 15-blade scalpel; in some cases, uniform biopsies were taken by 4 mm diameter puncture

of cartilage to the subchondral bone with a biopsy punch (Stiefel, Brentford, UK) and dissecting through cartilage along the bone-interface with a 15-blade scalpel.

2.1.2 Chondrocyte isolation

Porcine MCP cartilage explants were dissected into a 50 ml Falcon tube containing a 20 ml solution of 10 % FBS DMEM with 1 mg/ml collagenase A (Roche Pharmaceuticals, Hertfordshire, UK). Cartilage was digested overnight (16 h), with shaking (180 rpm) at 37 °C and 5% CO_2. The digest was passed through a 70 µm cell strainer and centrifuged at 235x g for 5 min. The cell pellet was resuspended in 20 ml SF-DMEM and centrifuged at 235x g for 5 min, 3 times.

Cells were counted and plated at $2x10^6$ cells/well of a 6-well plate in 2 ml 10 % FBS DMEM for gene expression experiments, or $1x10^6$ cells/well of a 12-well plate in 1 ml 10 % FBS DMEM for protein analysis experiments. Cells were left to adhere to the bottom of the plate overnight.

2.1.3 Chondron isolation

Chondron isolation was developed by Lee *et al.* (Lee *et al.*, 1997). Porcine MCP cartilage was dissected into 10% FBS DMEM and rested for 16 h at 37 ℃ with 5% CO_2. Cartilage was washed in PBS, then digested in 10% FBS DMEM containing 0.3% collagenase and 0.2% dispase at 37 ℃ and 5% CO_2 with 180 rpm shaking for 2 h. Chondrons were filtered using a 70 µl nylon filter and centrifuged at 528x g for 15 min. Chondrons were resuspended in 5 ml 10% FBS DMEM and 200 µl was plated per 16 mm borosilicate glass coverslip (Thermo Fisher, Massachusetts, USA) for imaging.

2.1.4 Adipose tissue derived mesenchymal stem cells

Adipose tissue-derived mesenchymal stem cell (MSC) experiments were conducted in collaboration with Felipe Dias de Oliveira and Hayat Muhammad at the Kennedy Institute of Rheumatology.

MSCs were isolated from the epididymal fat pad of 6 week old Wild Type C57BL/6J mice (adipose tissue-derived MSCs) by adhesion to plastic. Epididymal fat pads were collected into serum-free αMEM MSC medium (αMEM Glutamax, 1% penicillin-streptomycin) (Gibco, Massachusetts, USA) and digested with 4 mg/ml Collagenase A for 45 min at 37 °C on a tube shaker (120 rpm). The fat pad digest was filtered through a 70 µm cell strainer and centrifuged (235x g, 10 min). Supernatant was discarded and cells resuspended in αMEM containing fetal bovine serum (αMEM Glutamax, 1% penicillin-streptomycin, 20% FBS). After homogenisation, cells were cultured on 10 cm culture dishes overnight. Medium was discarded and the plate washed 5 times with PBS to remove non-adherent cells (passage zero - P0). Cells were cultured in growth medium and sub-cultured (culture passage) when the plate reached 90% confluency. Medium was changed every two days. Cells were plated at $5x10^3$ cells/cm^2 on a 6-well plate with 1 ml of MSCs growth medium for 24 h prior to 8 h serum starvation. Cells were then stimulated as per experimental conditions.

2.2 Cartilage Injury

2.2.1 Explantation Injury

Dissected cartilage was immediately cultured in SF-DMEM after injurious explantation. 0 h time points were immediately snap-frozen in liquid nitrogen and stored at -80 °C.

In human cartilage experiments, individual explants were rested or recut in 250 µl serum-free medium, then weighed after removal of superficial water to normalise conditioned medium volume to cartilage wet weight. Samples were diluted to normalise 10 mg cartilage per 250 µl medium prior to analysis.

2.2.2 Recut Injury

Dissected cartilage was washed in SF- DMEM, then cultured in SF- DMEM for 24–48 h to rest from the initial injury response to explantation. Cartilage was washed in SF- DMEM after rest and replenished with fresh serum-free medium. Recutting injury was performed with a 15-blade scalpel, cutting 4 mm cartilage biopsies into four pieces while in culture medium. Rested cartilage had medium replenished with no injury performed. Recut and rested cartilage were respectively incubated in serum-free medium, then conditioned medium supernatant was collected after 15 min, unless other times specified, and stored at -20 °C prior to use or protein analysis.

In porcine cartilage experiments, five uniform biopsies were pooled per sample, then rested or recut in 200 µl serum-free medium.

2.2.3 Mechanical loading

Osteochondral cubes 1 cm^3 in size were dissected from the porcine knee medial tibial plateau, then vacuum-sealed and placed in a custom-made compression cell. A single compression/relaxation cycle was performed. The cartilage specimen was placed in the centre of the cell and compressed to 28% of the original cartilage thickness using a screw-driven plunger entering the cell from the top. Compression was released by returning the screw-driven plunger into its original position.

Imaging and spectroscopy was conducted for sodium nuclei (described in Section 4.2.8) firstly when uncompressed, then after 28% deformation compressive load to the cartilage surface, and finally after relaxation with no compression.

2.3 RNA extraction

2.3.1 Chondrocytes

Cells were cultured in a 6 well plate with 2 million cells per well. Medium was removed, plate put on ice and 1 ml TRIzol was added to cells. TRIzol cells were collected and vortexed for 10 min at room temperature. TRIzol samples were centrifuged at 16000 g for 10 min. Supernatant was removed and mixed with 100 µl 1-Bromo-3-chloropropane (BCP) (Sigma-Aldrich, Missouri, USA), then incubated at room temperature for 5 min. Sample was centrifuged at 16000 g for 15 min at 4 °C then an equal volume of 70% ethanol was added. RNA was extracted from the mixed solution using QIAGEN RNeasy Mini Kit columns as per manufacturer protocol (QIAGEN, Hilden, Germany), including DNase treatment, into 30 µl RNAse-free H_2O.

2.3.2 Tissue explants

Snap-frozen tissue was pulverised into a fine powder using a metal pestle and mortar in liquid nitrogen. Homogenised tissue was added to RLT buffer (QIAGEN, Hilden, Germany) containing 10% β-mercaptoethanol. Twice the volume of H_2O was added, then >6.6 mAU/ml proteinase K was added and incubated at 55 °C for 10 min. Supernatant was then added to half volume of 70% ethanol. RNA was extracted from the mixed solution using RNeasy Mini Kit (QIAGEN, Hilden, Germany) columns for large tissue volumes (porcine tissue) or RNeasy Micro Kit (QIAGEN, Hilden,

Germany) columns for small tissue volumes (murine hips) as per manufacturer protocol including DNase treatment.

2.4 Real-time polymerase chain reaction (RT-PCR)

2.4.1 Reverse Transcription

Extracted RNA was quantified using Nanodrop One spectrophotometer measuring wavelength absorbance at 260 nm. RNA purity was validated by wavelength ratio of 260:280 nm (A260/280 ~2.0). Reverse transcription with Applied Biosystems High Capacity reverse transcription cDNA kit was performed on the same amount of RNA per 20 µl volume sample within experiments, with 500 ng per sample unless otherwise stated. 13.2 µl of RNA in H_2O was mixed with 2 µl RT buffer, 0.8 µl 25x dNTPs, 2 µl 10x random primers, 1 µl reverse transcriptase and 1 µl RNase inhibitor (Thermo-Fisher, Massachusetts, USA). Reverse transcription was run on a benchtop thermocycler at 25 °C for 10 min, 37 °C for 2 h, 85 °C for 5 min and 4 °C until samples were stored at -20 °C.

2.4.2 Primer Design

Primers were designed using NCBI Primer-BLAST against mRNA sequences validated against Ensembl gene entries. Primers were designed to be exon spanning and to yield 50–250 bp size PCR products. *In silico* PCR was performed using PremierBiosoft NetPrimer to choose primer candidates by predicting hairpin formation, self-dimerisation and cross-dimerisation. Primers were optimised at 60 °C by amplification with genomic cDNA, run on a DNA agarose gel to ensure a single band at the correct PCR product size and run on a standard curve using an Applied

Biosystems ViiA7 PCR system (Thermo-Fisher, Massachusetts, USA). Primers were selected for use with 100±5% amplification efficiency and a single melt curve peak.

2.4.3 Manual quantitative RT-PCR

A total volume of 10 µl per well in a 384 well plate consisted of 2.5 ng cDNA in a volume of 4.2 µl H_2O added to 5 µl SYBR Green Master Mix, 0.4 µl of 10 mM forward primer and 0.4 µl of 10 mM reverse primer. Quantitative PCR was run on an Applied Biosystems ViiA7 PCR system for 20 s at 95 °C, followed by 40 cycles between 95 °C for 1 s and 60 °C for 20 s. Melt curves were achieved with 15 s at 95 °C, 1 min at 60 °C, then 15 s at 95 °C.

2.4.4 Taqman gene array microfluidic cards

Gene expression arrays of injured mouse hip avulsion cartilage were run on custom TaqMan low-density array (TLDA) cards (Thermo-Fisher, Massachusetts, USA). 50 µl TaqMan master mix and 30 µl nuclease-free H_2O was added to 20 µl samples of 250 ng cDNA. Each 100 µl sample was added per well and amplified for 48 genes on an Applied Biosystems ViiA7 PCR system. BMPR2 was utilised as a housekeeper, based on consistency with 18S in samples.

2.4.5 Relative gene expression quantification

Relative gene expression was calculated using the ΔΔCt method with 18S as the control gene for porcine experiments (±0.5 Ct for each sample) and with *Bmpr2* as the control gene for TLDA card experiments (±0.5 Ct for each sample). Results were displayed as relative quantification of fold change to control.

2.5 Protein analysis

2.5.1 Protein extraction

Whole protein extraction was performed using tissue-dissociative RIPA lysis buffer. Cartilage biopsies were placed in 500 µl RIPA buffer at 4 °C with shaking, then lysate was collected after 1 h. Matrix protein extraction was performed using 2.5 M NaCl high-salt buffer. Cartilage biopsies were placed in 500 µl 2.5 NaCl at 4 °C, then supernatant was collected after 15 min.

For chondrocytes, cell culture medium was removed and replaced with 400 µl ice cold RIPA for cells in a 12 well plate. Cells were left in RIPA on ice for 30 min, then cells were scraped and collected, centrifuged at 16000x g at 4 °C for 5 min, then 350 µl supernatant was collected and stored at -20 °C.

2.5.2 Western blot

Samples were mixed with 4x Laemmli buffer for non-reduced gels, or 4x Laemmli buffer containing 1:1000 β-mercaptoethanol for reduced gels to run by sodium dodecyl sulfate polyacrylamide gel electrophoresis (SDS-PAGE). Non-reduced samples were run on a hand-cast tris-glycine gel or pre-cast NuPAGE 3-8% tris-acetate protein gel (Invitrogen, California, USA). Reduced samples were run on a hand-cast tris-glycine gel or pre-cast NuPAGE 4-12% bis-tris protein gel. Proteins on the gel were transferred to a polyvinylidene fluoride (PVDF) membrane, then gels were stained in Coomassie blue and membranes were stained in ponceau red to ensure efficient protein transfer. Membranes were blocked in 5% milk (or 5% BSA for phospho-proteins) solution. Membranes were incubated with primary antibodies against proteins of interest. Secondary antibodies were HRP-conjugated and bands

were visualised by enhanced chemiluminescence (ECL) (GE Healthcare, Illinois, USA). Protein band exposure was detected by camera capture using G:Box imager (Syngene, Cambridge, UK) or exposed onto photo-sensitive X-ray film (GE Healthcare, Illinois, USA) processed in a dark room developer.

2.5.3 FGF2 ELISA

MSD V-PLEX human bFGF (FGF2) enzyme-linked immunosorbent assay (ELISA) (MesoScaleDiscovery, Maryland, USA) was used to quantify FGF2 protein concentrations. Samples were normalised by diluting to 10 mg dry weight per 250 µl sample volume. Samples were then diluted 1:2 in kit diluent 7 buffer and 40 µl loaded per MSD plate well. MSD plate was measured using an MSD QuickPlex SQ 120 plate reader, with Discovery Workbench 3.0 software, against an FGF2 recombinant protein standard.

2.5.4 Immunohistochemistry

Human OA tissue was acquired from arthroplasty surgery and cryo-prepared as per Section 2.6.3. Sections were air dried and fixed with 10% neutral buffered formalin for 5 min, then ice cold acetone for 10 min at 4 °C. Tissue was treated with 0.1 U chondroitinase ABC for 30 min at 37 °C, then blocked with 1% goat serum and 5% BSA in PBS for 1 h at room temperature. Anti-HDGF and anti-perlecan primary antibodies were applied overnight at 4 °C, and secondary antibodies were applied for 1 h at 25 °C. Slides were mounted with coverslips using Prolong Gold DAPI mount and sealed.

Chondrons were isolated and seeded onto coverslips as per Section 2.1.3. Coverslips fixed with ice cold methanol for 10 min at 4 °C, treated with 10 mU/ml chondroitinase

ABC for 50 min at 37 °C and blocked with 5% goat serum and 1% BSA in PBS for 1 h at 25 °C, with PBS washes between steps. Anti-perlecan and anti-collagen VI primary antibodies were applied overnight at 4 °C, and secondary antibodies were applied for 1 h at 25 °C. Coverslips were mounted with Prolong Gold DAPI mount and sealed.

Confocal imaging was captured on an Olympus FV1200 IX83 Confocal System microscope.

2.5.5 Heparin affinity chromatography

A HiTrap heparin HP affinity column (GE Healthcare, Illinois, USA) with 1 ml total column volume was washed with 10 ml buffer at a rate of 1 ml/min prior to use. Buffer contained distilled H_2O with 10 mM sodium phosphate (pH 7). Elution buffer was a gradient mixture of washing buffer and washing buffer containing 2.5 M NaCl.

Samples were filtered through a 20 µm pore syringe filter and injected via an AKTA FPLC with UPC-900 and P-920 (GE Healthcare, Illinois, USA) to load onto the column at a rate of 1 ml/min. Flow-through (non-heparin-binding proteins) was collected in 1 ml fractions. Column was washed again with 10 ml buffer, then either eluted with a gradient of 0–2.5 M NaCl across 10 fractions of 1 ml volume each, or in a single 1 ml fraction of 2.5 M, at a flow rate of 1 ml/min. Fraction positions, UV absorbance (protein A280), temperature compensated conductivity (NaCl) and pump output (expected NaCl) were recorded throughout the process. Elution fractions were dialysed in 100x volume PBS for 24 h at 4 °C using a Float-A-Lyzer G2 Dialysis Device with 3.5–5 kDa molecular weight cut-off and stored at -20 °C.

2.6 Histology

Paraffin embedded tissue was processed and embedded by the histology department at the Kennedy Institute of Rheumatology. Tissue processing was carried out using a Tissue Tek VIP (Sakura, Alphen aan den Rijn, Netherlands) automated machine.

2.6.1 Paraffin embedding

Formalin-fixed tissues were processed in formal saline for 1 h 30 min at 40 °C, 70% ethanol for 1 h 30 min at 40 °C, 5 times 100 % ethanol for 1 h 30 min at 40 °C, 3 times Xylene for 1 h 30 min at 40 °C and 4 times paraffin for 1 h 30 min at 63 °C. Tissue was embedded in paraffin blocks and serially sectioned with 5 µm intervals.

2.6.2 Safranin O

Slides were processed for 20 s in water, 30 s in Harris haematoxylin, 1 min wash in water, 20 s in acid alcohol (70 % ethanol plus 10 ml hydrochloric acid per litre), 1 min wash in water, 1 min in blueing water (600 ml water with 1.6 ml ammonia), 6 min in fast green, 15 s in 1 % acetic acid, 1 min wash in water, 2 min in Safranin O, 1 min wash in water, 1 min in ethanol 3 times, 1 min in xylene 3 times and mounted in DPX.

2.6.3 Cryosectioning

Tissue samples were snap-frozen in liquid nitrogen and set in optimal cutting temperature compound (OCT) on dry ice for 30 min. Samples were stored in OCT at -80 °C. OCT blocks were sectioned with 5 µm intervals and dried onto a microscope slide for 1 h at 25 °C for subsequent staining.

2.7 Knockout mouse generation

Heterozygous mouse embryos with constitutive whole-body knockout of *Hdgf* were acquired from the University of Bremen (Gallitzendoerfer *et al.*, 2008), and bred to produce homozygous breeding pairs at the Kennedy Institute of Rheumatology. Herein, homozygous knockout mice are referred to as *Hdgf* $^{-/-}$ mice. Briefly, *Hdgf* exons 2–6 in embryonic stem cells were replaced with eGFP, a *HindIII* site and *LoxP*-flanked HPRT (for positive selection with HAT-containing medium) by homologous recombination. Positively selected targeted clones were screened by PCR and reconfirmed by Southern blot analysis after digestion with *HindIII* and hybridisation with a 5' external probe. These cells were injected into C57BL6/N blastocysts (Charles River, Sulzfeld, Germany). Genotyping was performed using HDGF sense primer 5'-GGTTGACAGGTCAGAAATGGTT-3' with wildtype antisense primer 5'-CTTGGTATTTGTTGGCTGTTGA-3' or knockout antisense primer 5'-GTCGTCCTTGAAGAAGATGGTG-3', where PCR resulted in fragments of 554 bp for the wildtype and 835 bp for the mutant fragment.

2.8 Animal husbandry

Animals were housed in the Kennedy Institute of Rheumatology unit of the University of Oxford in approved animal-care facilities. Animals were fed a certified mouse diet (RM1 diet; Special Diet Services, Devon, UK) and water *ad libitum*.

2.8.1 Surgery

Surgeries were performed by a trained technician, Jadwiga Zarebska. At 10 weeks of age, mice were anaesthetised by inhalation of isofluorane (Vetpharma, Leeds, UK) at 4% for induction and 2% for maintenance with continuous 1.5–2 L/min oxygen flow.

Prior to surgery, once anaesthesia levels were achieved, animals were injected subcutaneously with 0.3 mg/mL buprenorphine (Vetergesic Alstoe Animal Health, UK). Destabilisation of the medial meniscus was performed as previously described (Glasson *et al.*, 2005), detailed in Section 5.2.1.2. Post-surgery, animals were placed in an incubator of ambient temperature at 30 °C and recovered within 5–10 min. Once fully recovered, animals were transferred to their cages.

2.9 Statistics

Data were analysed using GraphPad Prism 8.0.

Statistical tests and adjustments are specified with results of experiments. Statistical significance was reported based on p value format in Table 2.1.

Table 2.1 P value symbol assignment of statistical significance

SYMBOL	**P VALUE**
ns	$P > 0.05$
*	$P \leq 0.05$
**	$P \leq 0.01$
***	$P \leq 0.001$
****	$P \leq 0.0001$

3 HDGF Release upon Cartilage Injury

3.1 Introduction

Growth factors are naturally occurring proteins that are typically capable of either stimulating cell proliferation, repair responses or cellular differentiation. In cartilage, a host of anabolic growth factors contribute to modulating protease activity, ECM and proteoglycan synthesis, stimulating chondrocyte proliferation and triggering a repair response (Fortier *et al.*, 2011). The Vincent laboratory has previously investigated cartilage growth factors of the extracellular matrix and their role in the response to injury. FGF2 is released rapidly upon cartilage injury, after which it stimulates activation of ERK in chondrocytes (Vincent *et al.*, 2002). The source of this released FGF2 is the pericellular matrix of cartilage, where it is bound to the heparan sulfate proteoglycan perlecan (Vincent *et al.*, 2007). Further work from the Vincent laboratory identified CTGF as another growth factor bound to perlecan in the PCM, which acts as a latent TGFβ-binding protein. Once the latent complex is released upon injury, it engages with cell surface TGFβR3, allowing TGFβ to activate its signalling pathway (Tang *et al.*, 2018). The pericellular matrix of cartilage is distinct in composition to the further removed matrix, and is highly mechanosensitive (Wilusz, Sanchez-Adams and Guilak, 2014). Proteomic analysis of freshly isolated PCM from human and porcine articular cartilage identified a host of pericellular matrix proteins (Tang *et al.*, 2018), of which four are widely considered growth factors: FGF2, CTGF, HDGF and CYR61. All four are known to exhibit affinity for heparin (Ori, Wilkinson and Fernig, 2011). The functional role of HDGF and CYR61 in cartilage injury is not yet known, and HDGF has never previously been characterised or explored in the context of cartilage.

In this chapter, the presence of HDGF in cartilage is validated and its ability to bind to heparin and to heparan sulfate in cartilage is explored.

Chapter Aim

Investigate the release of heparin-binding growth factors from the cartilage pericellular matrix upon injury

Hypotheses

- HDGF is released upon injury in the same capacity as CTGF and FGF2
- HDGF is bound to perlecan in the pericellular matrix of cartilage
- Heparin-bound pericellular matrix growth factors are released by a common mechanism

3.2 Methods

3.2.1 Cartilage injury

3.2.1.1 Recutting model

Resting and recutting of cartilage was performed on porcine MCP joint cartilage, and on human knee arthroplasty articular cartilage biopsy samples of osteoarthritis patients, as per method section 2.2.2.

Five porcine biopsies per sample, or one human biopsy per sample, were collected with a 4 mm biopsy punch and rested in serum free DMEM (SF-DMEM) for 48 h. After resting, biopsies were injured by cutting twice, in 250 µl SF-DMEM in a 48 well plate. Recut conditioned medium was collected at specified time points post-injury, along with rested (uninjured) controls. Human cartilage explants were weighed afterwards for wet weight normalisation of protein loading between experimental samples.

3.2.1.2 Explantation model

Porcine articular cartilage was explanted from the MCP joint, into SF-DMEM medium as per Section 2.2.1. Explanted cartilage was further injured where specified, by cutting cartilage pieces twice with a 15-blade scalpel. Explantation injury conditioned medium collected at specified times was analysed by Western blot.

3.2.2 Chondrocyte ablation and treatment

Porcine MCP cartilage explants of 4 mm diameter were dissected and rested in SF-DMEM for 24 h prior to treatment. Explants were washed in SF-DMEM and pre-treated in various conditions before another SF-DMEM wash, then rested or recut in 250 µl SF-DMEM. Rested conditioned medium and recut conditioned medium were

collected after 30 min. Conditioned medium was assessed for released protein by Western blot.

Normal cartilage was pre-treated in SF-DMEM for 30 min. Dead cartilage was snap-frozen in liquid nitrogen then reconstituted at 37 ℃, freeze-thaw was repeated three times total then washed in SF-DMEM for 30 min. Cartilage at 4 ℃ was pre-treated in SF-DMEM at 37 ℃ for 15 min then transferred to 4 ℃ for a subsequent 15 min, then washed in 4 ℃ SF-DMEM. MMP inhibited cartilage was pre-treated with 10 µM Batimastat (AbCam, Cambridge, UK) for 30 min in SF-DMEM. Protease inhibited cartilage was pre-treated with 1x cOmplete EDTA-Free Protease Inhibitor Cocktail (Roche, Basel, Switzerland) as per manufacturer instructions for 30 min in SF-DMEM.

3.2.3 Red blood cell assay

10 ml human blood was received fresh from a consenting donor with ethical approval (KIR-HC-066) in a BD Vacutainer EDTA 18 mg (Fisher Scientific, Waltham, USA). Whole blood was centrifuged at 800x g for 5 min without brake, then supernatant and buffy coat were removed and discarded. Red blood cells were pelleted, resuspended in 5 ml PBS and 400 µl of 1:10 diluted cell suspension was added to porcine chondrons, isolated as per Section 2.1.3.

3.2.4 Immunohistochemistry

Human OA tissue was prepared and cryosectioned as per Section 2.6.3, and immunohistochemistry performed as per Section 2.5.4 with Prolong Gold DAPI mount, anti-HDGF (AbCam, Cambridge, UK) and anti-perlecan (Merck, Darmstadt, Germany).

Porcine chondrons were isolated as per Section 2.1.3 and immunostained as per Section 2.5.4 with Prolong Gold DAPI mount and anti-collagen VI (AbCam, Cambridge, UK).

3.2.5 Heparitinase treatment

Cartilage biopsies were dissected as per Section 2.1.1, rested in SF-DMEM for 48 h. Five uniform biopsies were pooled per sample.

Heparitinase I (heparinase III / heparin lyase III) (Sigma Aldrich, Missouri, USA) was reconstituted in heparitinase buffer (20 mM Tris-HCl,

pH 7.5, 0.1 mg/ml BSA and 4 mM $CaCl_2$) and immediately added to samples in SF-DMEM. Samples were incubated with heparitinase at 37 °C and 5% CO_2 with 0 mU, 0.1 mU or 1 mU for 4 h, or were incubated with 0.1 mU/ml for 0.5 h, 2 h, 4 h or 24 h. Conditioned medium was collected and analysed by Western blot.

3.2.6 Heparin column chromatography

Recut injury conditioned medium was generated as per Section 2.2.2, with 1 g of porcine cartilage injured per 1 ml of SF-DMEM. 5 ml of recut injury conditioned medium was loaded onto a heparin column, as per Section 2.5.5, and eluted with a single 1 ml fraction of 2.5 M NaCl high salt buffer. Recut injury conditioned medium starting material, flowthrough material and high salt elution material were analysed by Western blot.

3.3 Results

This chapter sought to characterise the properties of HDGF in cartilage tissue and the cartilage injury response. HDGF was released rapidly from cartilage upon injury, the same as other known heparin-binding growth factors of the pericellular matrix; CTGF and FGF2. CYR61 was not detectable in these experiments, and therefore further work focused on HDGF, CTGF and FGF2.

Structural data, homology analysis and experimental data indicate that the HDGF protein exhibits heparin binding affinity and is able to bind to heparan sulfate. The identification of HDGF by proteomic analysis of the chondrocyte PCM indicates it may be present on heparan sulfate proteoglycans within the PCM, such as perlecan. This was shown by heparitinase treatment of cartilage tissue to assess HDGF release and attempted by immunofluorescence and confocal imaging in cartilage and chondrocytes.

Furthermore, in this chapter, potential mechanisms by which HDGF and other pericellular growth factor proteins could be released from the cartilage tissue upon injury were tested. It was confirmed that HDGF is released rapidly upon injury by cartilage explantation from the joint, as well as *ex vivo* recut injury after resting in culture. It was also demonstrated that heparitinase enzyme treatment of cartilage is able to liberate HDGF from cartilage, releasing it into the supernatant, indicating the growth factor is bound to heparan sulfate in the matrix. This behaviour is shared by other known pericellular matrix growth factors, and their conserved mechanism of release by injury was demonstrated to be independent of cell viability, temperature, matrix metalloproteinase activity and proteinase activity.

3.3.1 HDGF is released upon cartilage injury

To ensure equal tissue was taken for each experimental sample, uniform explants of 4 mm diameter were collected from various surfaces of the MCP joint of the porcine trotter and assessed for variation by weight.

Mean dry weight of explants did not statistically significantly differ between biological replicates sourced from different porcine trotters, as determined between group means by one-way ANOVA ($F=1.827$, $p=0.1826$) (Figure 3.1). Ranges for individual sample sources were 0.0004 g (14% of mean), 0.0007 g (22% of mean) and 0.0012 g (39 % of mean). Biopsies were pooled for use in experiments to minimise variation and error, but this weight variation introduces a limitation to the detection of differences of small magnitude.

Pooling the 5 smallest biopsies, and comparing to 5 largest biopsies, from the trotter with greatest range in Figure 3.1 would give a maximal weight difference of 20.9% (33.6 - 27.8 = Δ5.8 g). Experiments conducted with this methodology showed consistent differences much greater than 20.9%, and interpretations of data consider this maximal error.

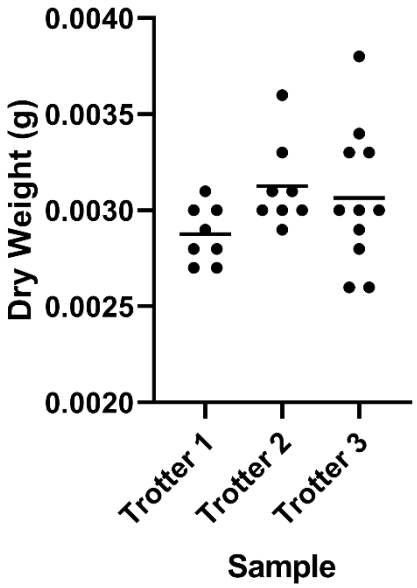

Figure 3.1 Dry weight of explants from three independent porcine trotters. Mean explant weight of air dried 4 mm diameter porcine metacarpophalangeal cartilage biopsies. One-way ANOVA (F=1.827, p=0.1826) (n=3 biological replicates).

To assess whether HDGF was released upon injury, porcine articular cartilage explants were cultured following dissection for 48 h in serum-free medium. At this point, explants were replenished with fresh medium and either rested or recut (cut twice, into a total of four pieces). Conditioned medium from this injury was immunoblotted for HDGF. HDGF protein was detected in the conditioned medium of recut cartilage after 5 minutes (Figure 3.2). There was no difference between the protein released within the first 5 minutes and the first 30 minutes (Figure 3.2) indicating that the majority of protein was released within the first 5 minutes. A single band was detected for HDGF that migrated at the same molecular weight under reduced and non-reduced conditions (40 kDa). This band also corresponded to the molecular weight of recombinant human HDGF protein.

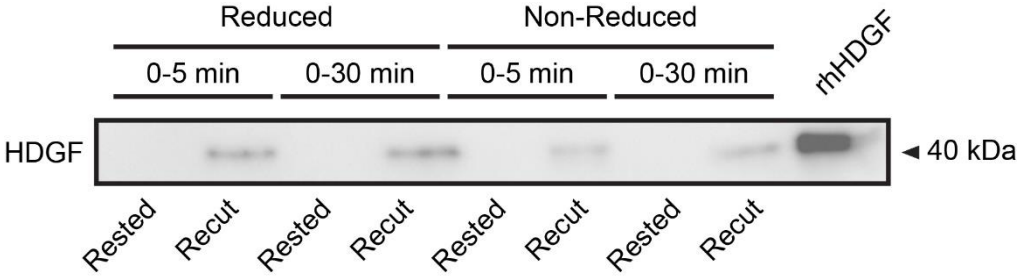

Figure 3.2 HDGF release by recut injury. Porcine articular cartilage explants were rested or injured by recutting, after 5 or 30 minutes the conditioned medium was immunoblotted for HDGF under reduced (beta-mercaptoethanol) or non-reduced conditions against 10 ng recombinant HDGF protein (rhHDGF). Representative blot.

The release of HDGF from cartilage upon injury was also assessed by explantation injury (the initial injury upon dissection, prior to culture). Some explants were also further cut into four pieces at the time of explantation to assess growth factor release with grade of injury. Assessment of the explantation injury conditioned medium by Western blot confirmed the rapid release of HDGF protein by the explantation-damaged cartilage (Figure 3.3). The protein was predominantly released within the first 5 minutes of explantation, whereas minimal protein was found in the conditioned medium of subsequent time points (5–30 min and 30–60 min). Additional recutting of the explanted cartilage increased the amount of HDGF released.

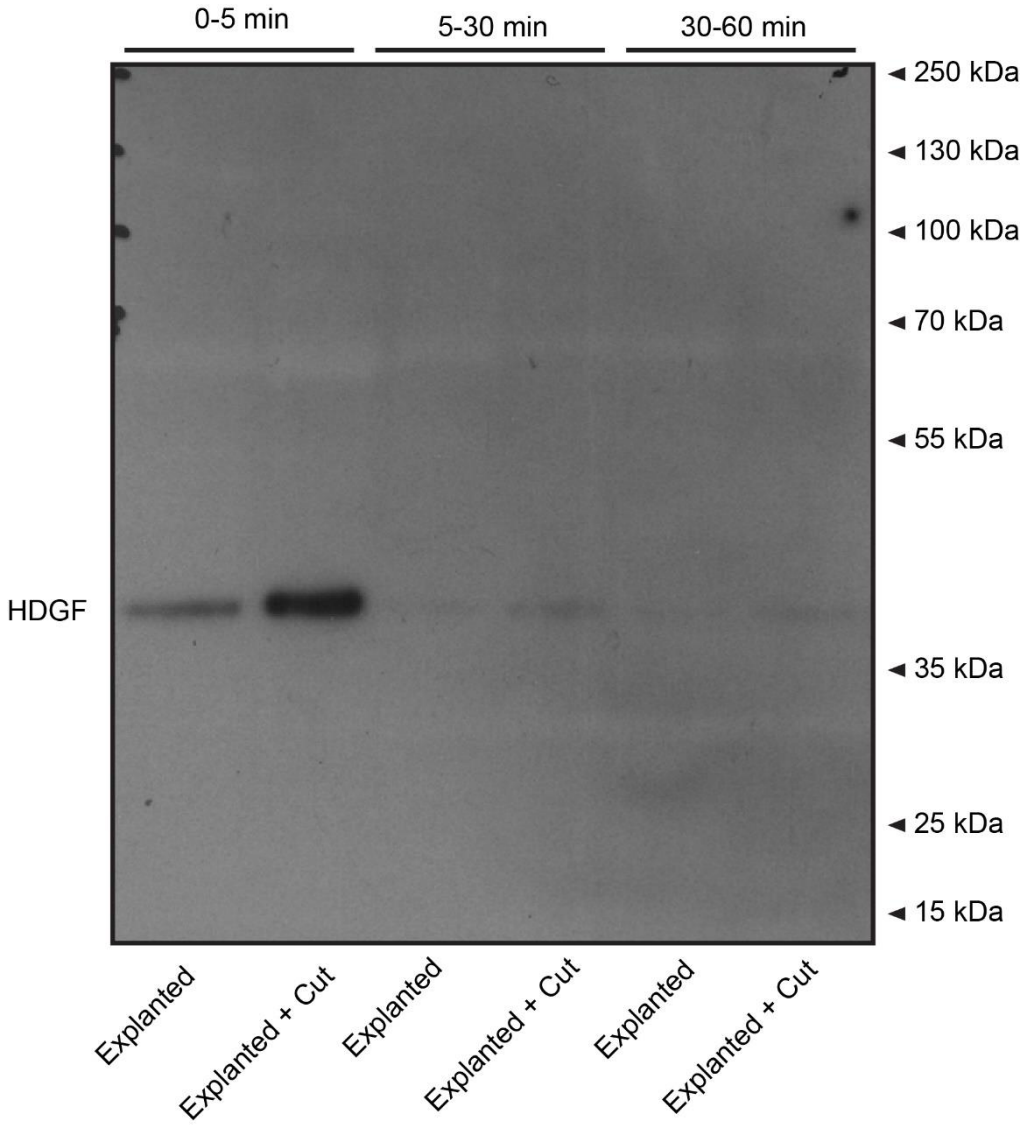

Figure 3.3 HDGF release by explantation injury. Porcine articular cartilage was explanted into serum-free DMEM, or explanted then further injured by cutting in serum-free DMEM, then conditioned medium was collected after 5, 30 and 60 minute time points and immunoblotted for HDGF. Representative blot.

To verify the specificity of the antibody used, conditioned medium (0–30 min) was generated from wildtype and *Hdgf* $^{-/-}$ avulsed mouse hips. The anti-HDGF antibody detected a band at 40 kDa in wildtype conditioned medium that was not present in *Hdgf* $^{-/-}$ conditioned medium (Figure 3.4). Both wildtype and *Hdgf* $^{-/-}$ injury conditioned medium released CTGF and FGF2 during this period.

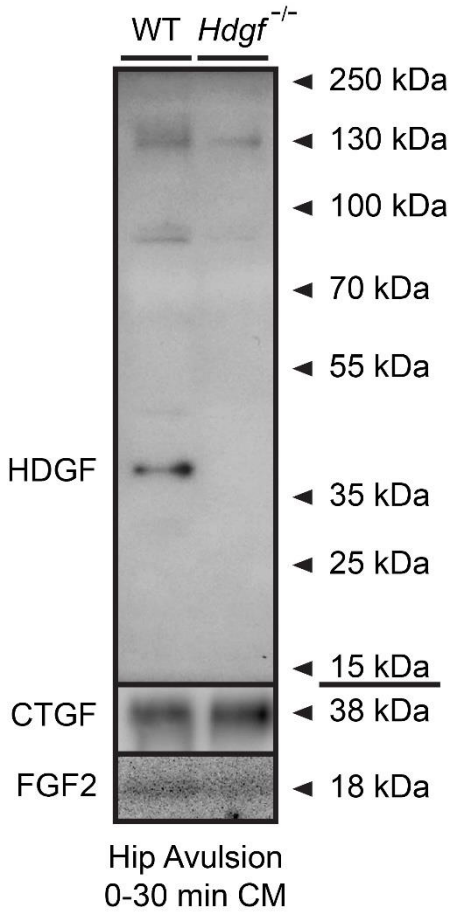

Figure 3.4 Mouse hip avulsion injury in *Hdgf*$^{-/-}$ mice releases CTGF and FGF2, but not HDGF. Hips from wildtype (WT) and *Hdgf* $^{-/-}$ mice were avulsed into serum-free DMEM (0–30 min), recut once, and conditioned medium was immunoblotted for HDGF, CTGF and FGF2 protein. Representative blot.

To confirm this response was consistent in human cartilage tissue, human injury conditioned medium from macroscopically normal osteoarthritic samples was immunoblotted for HDGF, CTGF and FGF2. All growth factors were released upon recutting human articular cartilage within 30 minutes of injury (Figure 3.5), indicating a conserved release between species and likely relevance of this injury response to human physiology.

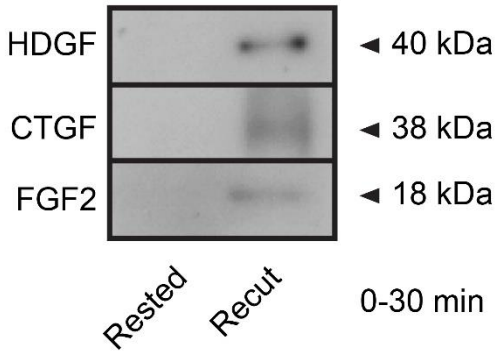

Figure 3.5 Growth factors HDGF, CTGF and FGF2 are released upon injury from human cartilage. Conditioned medium (0–30 min) from rested and recut human osteoarthritic cartilage (macroscopically normal) was immunoblotted for HDGF, CTGF and FGF2. Representative blot.

3.3.2 HDGF mRNA is not regulated upon injury

Although the release of HDGF was not likely to be a consequence of new protein synthesis, the regulation of *HDGF* mRNA was assessed after explantation.

HDGF showed no significant regulation throughout the 24 h period after explantation (Figure 3.6). Known injury-responsive inflammatory genes *COX2* and *IL6* showed significant mRNA upregulation during the 24 h period post-explantation, as shown previously by the Vincent laboratory (Chong *et al.*, 2013). *COX2* mRNA was significantly upregulated in porcine cartilage by explantation ($F(4,19)=13.89$, $p<0.0001$). Multiple comparisons testing showed significant *COX2* upregulation at 1 h and 4 h after explantation, with a mean peak 4.452 times above baseline at 4 h, subsequently returning to and remaining at baseline levels 12 h after explantation. *IL6* mRNA was significantly regulated by explantation over 24 h ($F(4,22)=4.517$, $p=0.0081$). *IL6* expression increased after 1 h and was significantly upregulated 4 h after explantation, remaining 4–5 times above baseline levels for the 24 h period, at 12 h and 24 h.

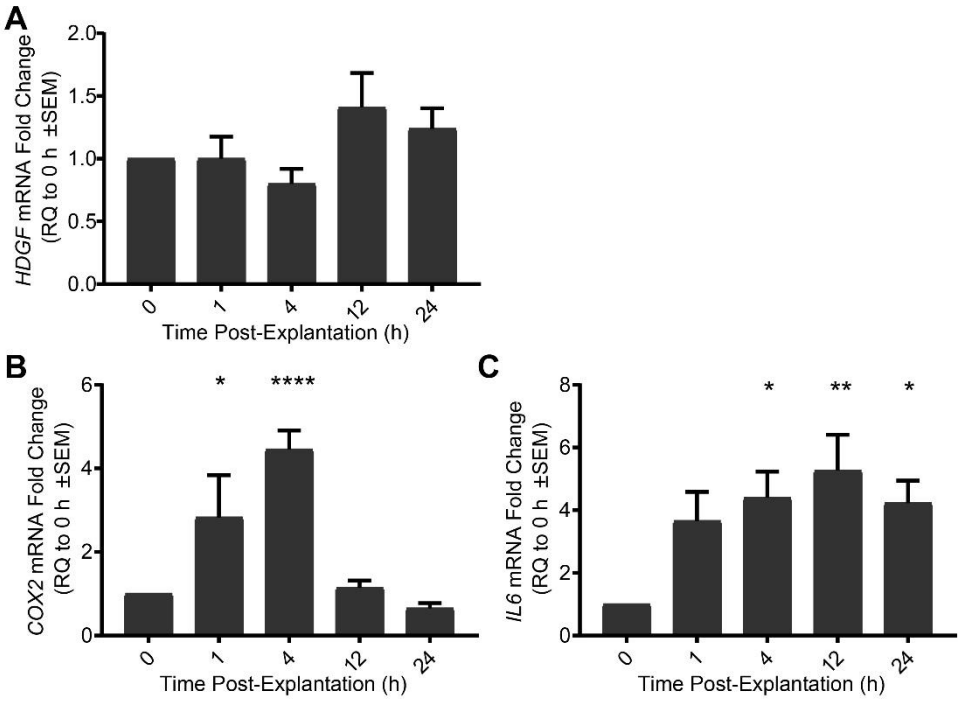

Figure 3.6 *HDGF* mRNA is not regulated in porcine cartilage 24 h after explantation. Cartilage was explanted from the porcine metacarpophalangeal joint and assessed for changes in *HDGF* (A), *COX2* (B) and *IL6* (C) mRNA. Relative quantification (RQ) is displayed as fold change compared to 0h baseline for each gene and normalised to 18S mRNA (n=6). ANOVA with Dunnett's multiple comparisons to 0 h (ns=non-significant, *p≤0.05, **p≤0.01, ****p≤0.0001).

3.3.3 Cartilage releases growth factors irrespective of chondrocyte viability

In order to determine whether the release of HDGF upon injury was dependent on cellular viability, the cellular regulation of HDGF was assessed after explantation and the release of HDGF was assessed with concurrent inhibition of cellular processes.

Dead cartilage, in which chondrocytes were killed by freeze-thawing, maintained the ability to release growth factors HDGF, CTGF and FGF2 upon recutting injury, similar to live cartilage (Figure 3.7). Dead cartilage rested without recutting injury exhibited some constitutive release of growth factors HDGF and FGF2, but less than the amount released upon recutting injury.

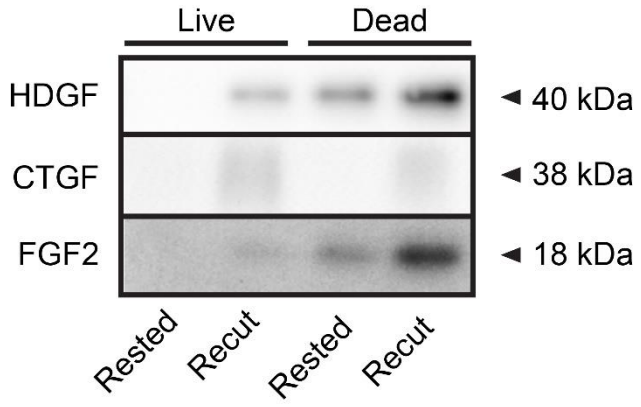

Figure 3.7 Growth factors are released from live and dead cartilage upon recutting injury. Conditioned medium (0-30 min) from rested or recut live or dead (freeze-thawed three times) cartilage were immunoblotted for HDGF, CTGF and FGF2. Representative blot.

3.3.4 Release of growth factors upon injury is temperature and protease independent

Cartilage recutting injury was performed at low temperature (4 °C), after pre-treatment with a broad-spectrum MMP inhibitor (Batimastat) or after pre-treatment with a protease inhibitor cocktail. None of these conditions affected the release of HDGF, CTGF or FGF2 compared with the normal recutting injury response at 37 °C (Figure 3.8).

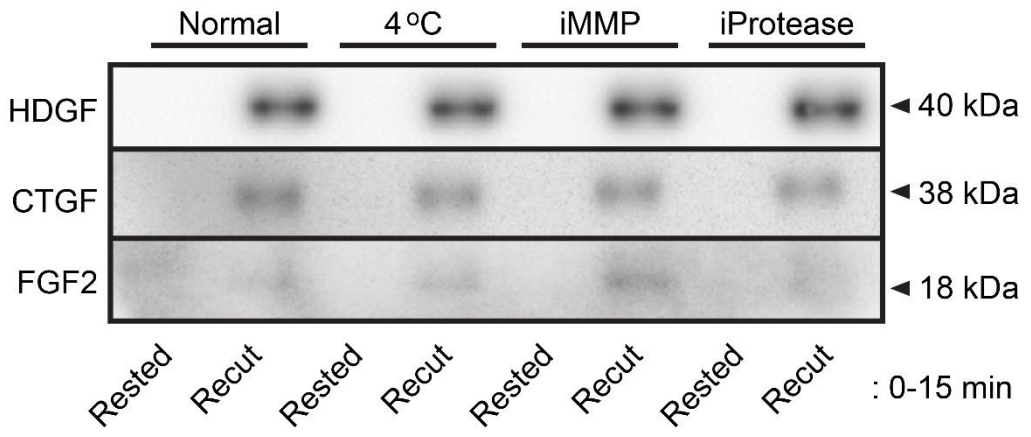

Figure 3.8 Growth factors are released by recutting injury, independent of temperature, MMP activity and protease activity. Porcine articular cartilage explants were pre-treated with 10 μM batimastat (MMP inhibitor), with protease inhibitor cocktail, or were incubated at 4°C (low temperature) or 37°C (normal) prior to resting or injury by recutting. Conditioned medium collected after 15 minutes was immunoblotted HDGF, CTGF and FGF2. Representative blot.

3.3.5 Imaging HDGF in cartilage

Human osteoarthritic cartilage from arthroplasty of the knee joint was cryosectioned and immunohistochemically imaged for the pericellular matrix proteoglycan perlecan and the growth factor HDGF. Confocal microscopy was used to visualise perlecan in the pericellular matrix, surrounding the chondrocyte cells (Figure 3.9). HDGF was not detectable in the pericellular matrix, but colocalised with DAPI staining of the nucleus, with some perinuclear staining in the cytoplasm.

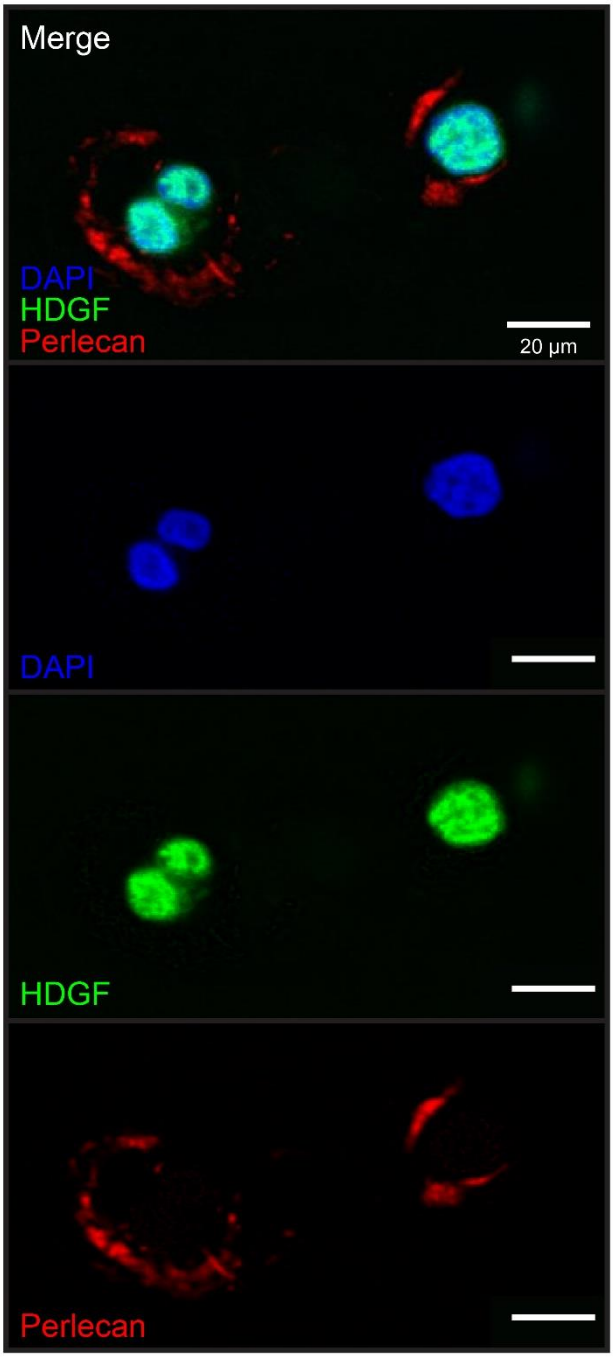

Figure 3.9 Confocal microscopy of HDGF and perlecan in human osteoarthritic tissue chondrons. Two chondrons imaged from human osteoarthritic cartilage, immunostained with DAPI (blue), for HDGF (green) and for perlecan (red). Merged image (top). Representative image. Scale 20 µm.

Cells positive for HDGF staining were present throughout the depths of osteoarthritic cartilage tissue. Perlecan signal was sparse in the regions just below the articular

surface, but was present around most cells visible by DAPI staining in the remaining depths of the tissue (Figure 3.10).

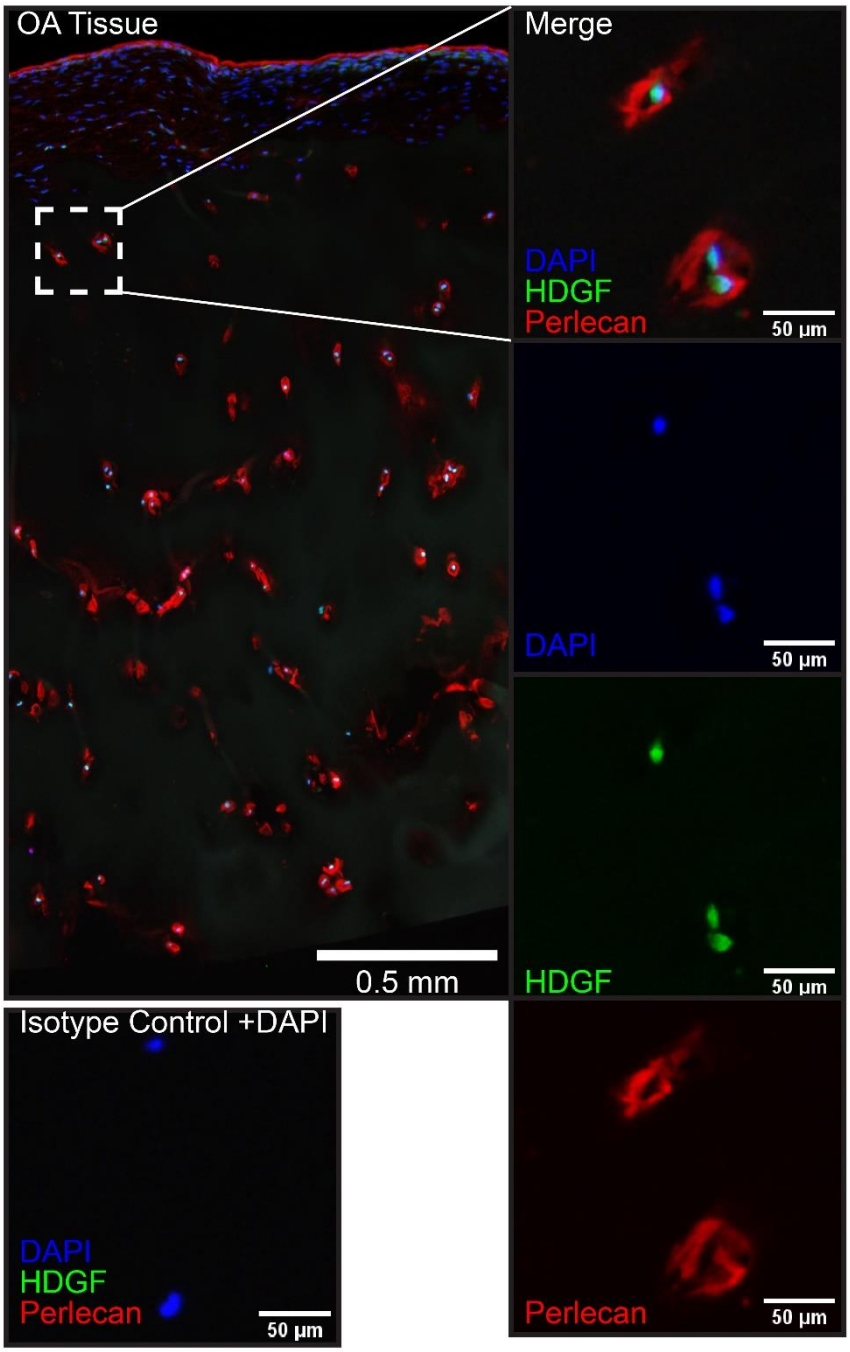

Figure 3.10 Human osteoarthritic whole tissue confocal of HDGF and perlecan. Whole tissue section imaged from human osteoarthritic cartilage, immunostained with DAPI (blue), for HDGF (green) and for perlecan (red). Merged image (OA Tissue & Merge). Isotype control with DAPI stain. Representative image. Scale 0.5 mm (OA Tissue), 50 µm (insets).

An alternative model for imaging proteins within the pericellular matrix is the isolation of chondrons from the tissue, composed of the chondrocyte cells with surrounding pericellular matrix.

Porcine MCP articular cartilage was digested with a combination of collagenase and dispase for 2 h, yielding cultured chondrocytes that maintained a pericellular matrix surrounding the cell, observable by red blood cell exclusion assay (Figure 3.11). Red blood cells settled on the coverslip surface, but were excluded from areas occupied by a cell or by its pericellular matrix. An area of exclusion was observed around chondrocyte cells plated after 2 h digestion with collagenase and dispase, indicating an intact pericellular matrix.

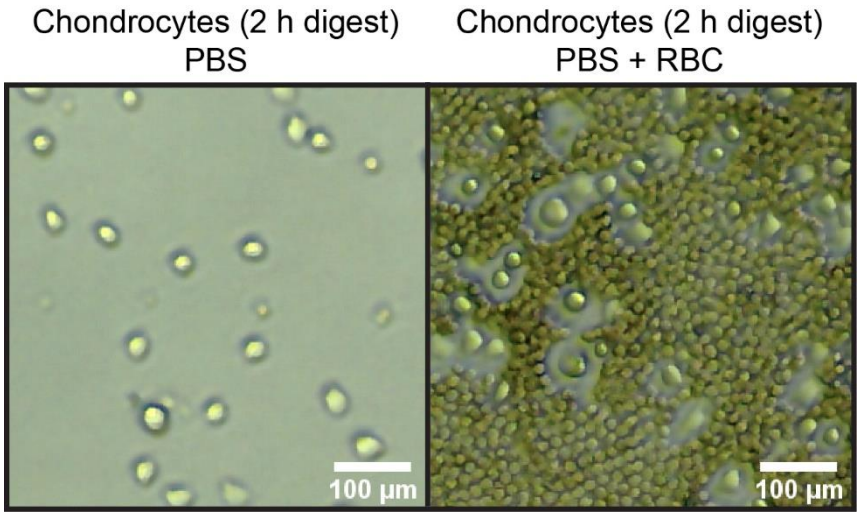

Figure 3.11 Red blood cell exclusion assay validation of chondron isolation with 2 h collagenase and dispase. Porcine cartilage tissue was digested with collagenase and dispase for 2 h, cultured, then imaged with brightfield microscopy after replenishment with PBS, or PBS containing red blood cells (PBS + RBC). Representative image.

Isolated chondrons were antibody labelled for the pericellular matrix proteins collagen VI and perlecan, to visualise the distinct pericellular matrix region around the cell.

Collagen VI was visible by immunohistochemistry, but perlecan signal was not present (Figure 3.12, Figure 3.13). The lack of distinct perlecan and collagen VI localisation in the chondrons rendered them of insufficient quality to perform immunohistochemistry for HDGF protein.

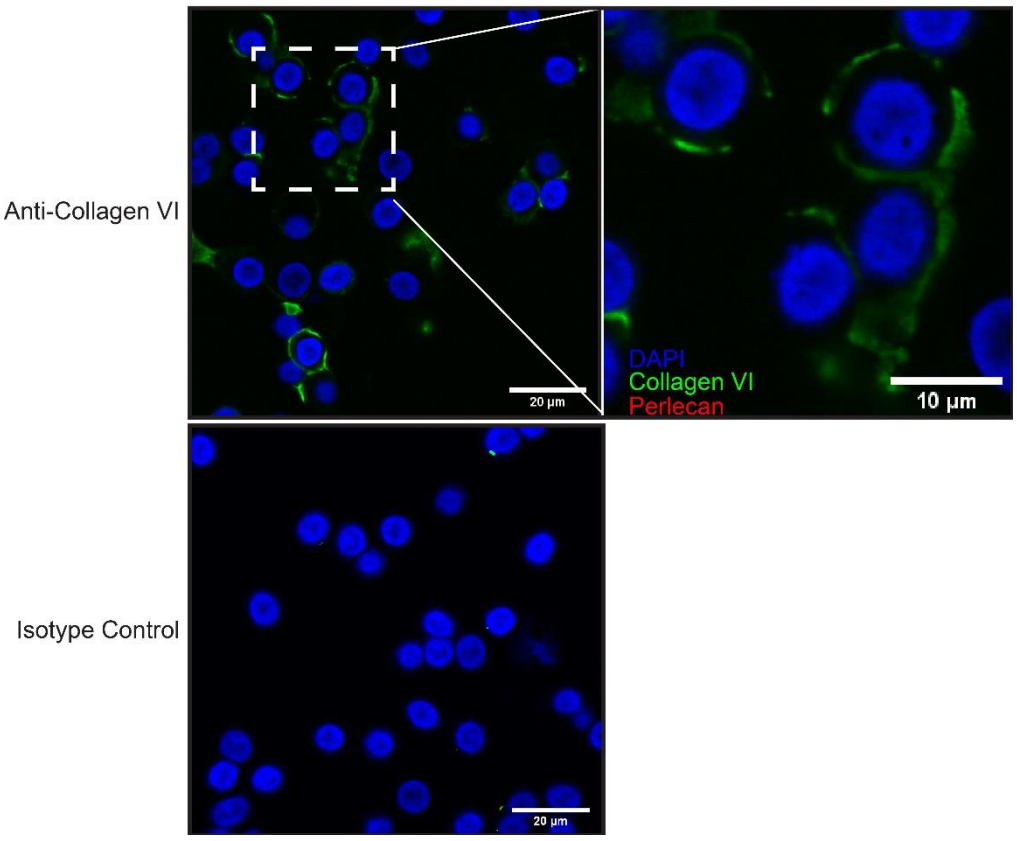

Figure 3.12 Porcine pericellular matrix confocal imaging. Nucleus staining with DAPI (blue), collagen VI staining (green) and unsuccessful perlecan staining (red) of primary porcine isolated chondrons. Representative image. Overview scale 10 µm (left), inset scale 10 µm (right).

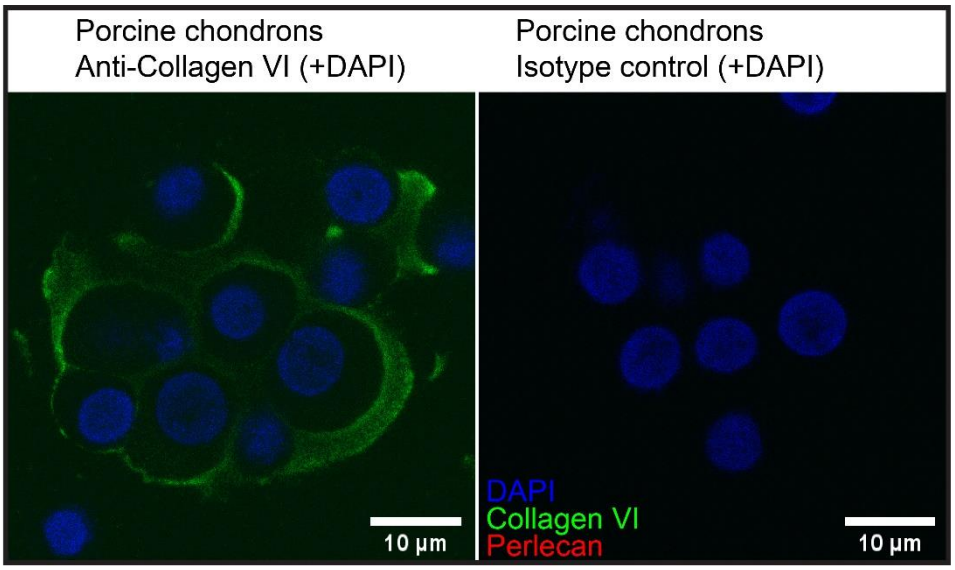

Figure 3.13 Porcine pericellular matrix confocal imaging. Nucleus staining with DAPI (blue), collagen VI staining (green) and unsuccessful perlecan staining (red) of primary porcine isolated chondrons. Representative image. Scale 10 µm.

3.3.6 Heparitinase treatment liberates HDGF from cartilage explants

Rested cartilage was treated with heparitinase I for 4 h at concentrations of 0.1 mU/ml and 1 mU/ml in SF-DMEM or left untreated in SF-DMEM with enzyme buffer. Supernatant of heparitinase treated cartilage was assessed for the growth factor HDGF, as well as the known heparan sulfate-binding proteins CTGF and FGF2.

CTGF was released constitutively from the cartilage tissue over the 4 h period, but heparitinase released of HDGF, CTGF and FGF2 in a dose dependent manner (Figure 3.14).

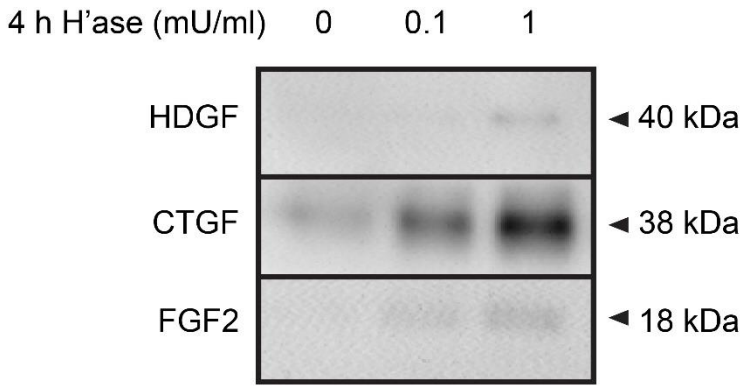

Figure 3.14 Heparitinase treatment of cartilage releases growth factors HDGF, CTGF and FGF2. Conditioned medium of rested porcine articular cartilage, after 4 h culture in serum-free DMEM containing buffer (0 mU/ml), 0.1 mU/ml or 1 mU/ml heparitinase I (H'ase) enzyme, was immunoblotted for released HDGF, CTGF and FGF2 protein. Representative blot.

Rested cartilage was also treated with heparitinase over a time course to demonstrate time-dependent enzymatic release. HDGF was released into the conditioned medium by 0.1 mU/ml heparitinase within 30 minutes, and cartilage continued to release more HDGF over a course of 4 h with enzyme treatment (Figure 3.15). After 24 h, both the untreated and heparitinase treated cartilage samples showed released HDGF indicating a longer term constitutive release of HDGF over prolonged culture, independent of enzyme activity.

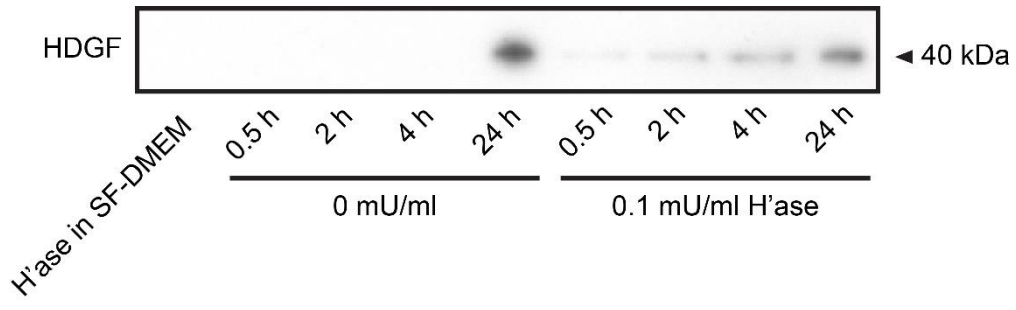

Figure 3.15 Heparitinase treatment of porcine cartilage releases HDGF with time. Conditioned medium of porcine cartilage cultured in serum-free DMEM containing buffer (0 mU/ml) or 0.1 mU/ml heparitinase I was immunoblotted for HDGF released over a 24 h enzymatic treatment period. Representative blot.

3.3.7 Pericellular matrix growth factors bind to heparin-sepharose and are eluted with salt

Having demonstrated the release of growth factors HDGF, CTGF and FGF2 upon cleavage of heparan sulfate in cartilage tissue, their interactions with heparan sulfate were confirmed using heparin as an analogous form of glycosaminoglycan.

Conditioned medium from porcine cartilage, 30 minutes after recutting injury, was run through a heparin affinity chromatography column. Growth factors immobilised to heparin-sepharose were eluted with 2.5 M sodium chloride (NaCl). HDGF, CTGF and FGF2 were detected in the recut conditioned medium, but were all depleted from the sample once run through a heparin affinity column, indicating binding to heparin in the column. The growth factors HDGF, CTGF and FGF2 were displaced from the heparin column with a single elution of 2.5 M NaCl, confirming their interaction with heparin within the affinity column (Figure 3.16).

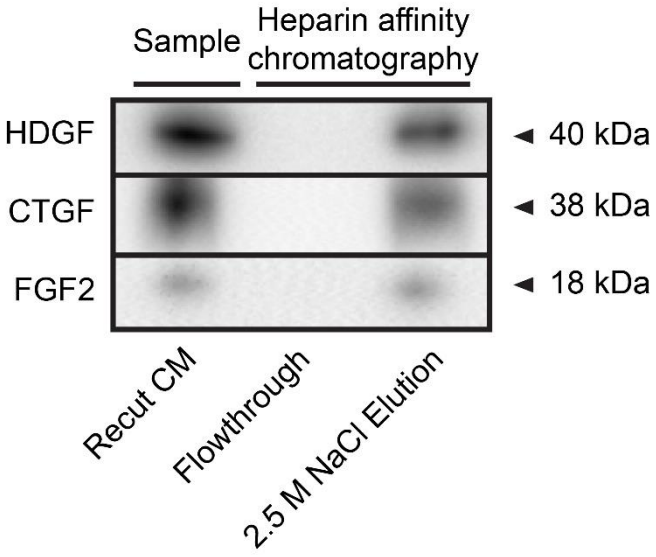

Figure 3.16 Growth factors HDGF, CTGF and FGF2 bind heparin and can be eluted by NaCl. Porcine articular cartilage was injured by recutting, and after 30 minutes the conditioned medium (Recut CM) was collected. Recut conditioned medium was loaded onto a heparin affinity column, flowthrough was collected after wash with low-salt elution buffer, elution was collected after wash with high salt (2.5 M NaCl elution). Recut conditioned medium starting material, flowthrough and elution were immunoblotted for HDGF, CTGF and FGF2. Representative blot.

3.4 Discussion

HDGF has not previously been investigated in the context of cartilage. These data demonstrate a reproducible release of HDGF protein rapidly upon injury, detectable by Western blot. Cartilage that was explanted from the articular joint surface released HDGF protein rapidly within 5 minutes, releasing more protein with subsequent immediate injury within this first 5 minute period. Rested cartilage also released HDGF upon recutting injury, which is characteristic of the growth factors CTGF (Tang *et al.*, 2018) and FGF2 (Vincent *et al.*, 2002).

The specificity of the anti-HDGF antibody used to the protein of interest was validated within this chapter. The detection of a single band (40 kDa) by electrophoresis in porcine and human tissue (Figure 3.3, Figure 3.5), the absence of this band in *Hdgf* $^{-/-}$ mouse compared to wildtype (Figure 3.4), and the detection of this band in independent studies validate its use for HDGF protein. In porcine and human tissue, the 40 kDa HDGF protein band is the only signal detectable in injury conditioned medium, indicating the absence of non-specific binding (Figure 3.3, Figure 3.5). HDGF protein consists of 240 amino acids, with a predicted molecular mass of 26.3 kDa in mouse (26.8 kDa in human). However, rHDGF-His runs at 40 kDa on SDS-PAGE while giving a predicted molecular mass of 27.1 kDa by MALDI-TOF imaging in independent studies (Abouzied *et al.*, 2004). This indicates the discrepancy between predicted and immunoblot-based molecular weights might be explained either by post-translational modifications or by abnormal running behaviour of these proteins on SDS-PAGE.

Despite confirmed antibody specificity, a limitation of Western blotting as a protein detection method is the limited dynamic range of detection. This renders it a semi-quantitative technique. For example, the detection of small changes in protein levels is limited with Western blotting. However, large differences in protein levels between conditioned medium from injured and uninjured cartilage means that growth factor release is within detectable range of this technique. Further, Western blot semi-quantification of human FGF2 released upon injury is validated against quantitative ELISA in Section 4.3.3. Finally, rested or recut conditioned medium did not contain any endogenous protein that constitutively released at constant levels, thus limiting the possibility of using an internal housekeeping loading control. Where possible, later Western blot experiments utilised housekeeper controls (Section 4.3.1). The uniformity of explants partially accounts for this, but internal loading controls would further contribute to confirming that the protein changes between samples were due to observable experimental results, rather than sample loading. The spiking of media samples with a molecule that could be detected as a loading control would help account for loading and transfer irregularities in future experiments, however this was not considered at the time. Total protein staining of blots should be used in future experiments to confirm consistent release of protein between recut injury samples, and between rested samples, respectively; this cannot be used to compare the rested and recut samples, as injury releases more total protein than resting.

Limitations in the recutting method are addressed by the assessment of cartilage explant weight. In order to standardise for cartilage tissue volume, explants were dissected with uniform surface area and paired from equivalent regions of the joint. Individual explant weight variation was validated, showing an average weight range

variation of 25% (Figure 3.1). Pooling of explants from equivalent regions reduces this variation, but variation error is considered when interpreting data; conclusions can be made with strong, reproducible trends that are consistently detectable by Western blot, but subtle or inconsistent trends cannot be interpreted. This limitation is not applicable in experiments that do not quantify between samples, such as the heparin column experiment (Figure 3.16), which uses the same starting material for each output sample. Also, later experiments use explant weight as a method of normalisation for sample loading (Section 4.3.3).

Despite efforts to visualise HDGF in the PCM, and its colocalisation to the heparan sulfate proteoglycan perlecan, the successful isolation of chondrons with distinct collagen VI and perlecan in the PCM was not achieved. Chondron isolation by cartilage digestion with dispase and collagenase relies on the distinct properties of the pericellular matrix and its resistance to enzymatic degradation. The resistance of collagen VI to bacterial collagenase digestion allows selective degradation of the further removed matrix, leaving the chondron predominantly intact. However, enzymatically isolated chondrons do exhibit subtle differences when compared to chondrons in situ. Fibronectin and specific chondroitin sulfate epitopes (e.g. 7D4 CS epitope) are lost upon isolation (Lee *et al.*, 1997). Enzymatically isolated chondrons share similar structural characteristics with mechanically isolated chondrons from osteoarthritic tissue, but with a reduction in the size of the pericellular matrix and less mechanical integrity (Knight *et al.*, 2001). These harsh effects on the pericellular matrix disrupt cell–matrix and matrix–matrix interactions and might displace growth factors bound to perlecan. With culture, isolated chondrons are able to remodel their

pericellular environment, and therefore replenish their pericellular environment over time.

In human osteoarthritic tissue, perlecan was visualised in conjunction with HDGF protein, but the growth factor was only localised to the nucleus. Other studies have demonstrated the internalisation of extracellular HDGF heparin-binding HATH domain after binding to matrix or cell surface heparan sulfate (Wang *et al.*, 2011), presence of extracellular HDGF in vesicles (Nüße *et al.*, 2017) and detected it in a microarray of digested pericellular matrix (Tang *et al.*, 2018). Nuclear and cytoplasmic HDGF has also been visualised in a plethora of cell types. In this respect, it is plausible that the matrix portion of HDGF in cultured cells and prepared tissue is less than the intracellular portion. The release of residual HDGF in rested dead cartilage (Figure 3.7) and from whole tissue lysis after matrix protein dissociation (Figure 4.5, Figure 4.13) indicate an intracellular portion of growth factor in addition to a matrix fraction. The release of HDGF upon explantation (Figure 3.3) might account for why tissue sections, undergoing injurious dissection before fixation for visualisation, do not readily show matrix-bound HDGF — it is released from the matrix by the initial insult, subsequently released from the tissue and taken up by the cell. Despite this, both CTGF and FGF2 have been visualised in the pericellular matrix of cartilage, colocalised with perlecan (Vincent *et al.*, 2007; Tang *et al.*, 2018). One explanation for HDGF being more easily depleted from the matrix could be a lower binding affinity for heparin / heparan sulfate; a weaker interaction with heparan sulfate in the PCM could cause a lower threshold for release, more readily releasing HDGF upon acute injury such as the injurious dissection used in the protocol for visualisation.

The binding of HDGF to heparan sulfate in cartilage was confirmed with the use of enzymatic cleavage of heparan sulfate chains. Heparitinase I (heparinise III) treatment at 1 mU/ml for 4 h released HDGF, CTGF and HDGF from cartilage, indicating that these growth factors are bound to heparan sulfate in cartilage tissue. Heparan sulfate proteoglycans in cartilage can be on the cell surface, within the PCM or in the TM and ITM (Table 1.1). While this growth factor release with heparitinase does not rule out the possibility of the growth factors residing on cell surface or TM/ITM heparan sulfate proteoglycan, the established preferential colocalisation of FGF2 and CTGF with perlecan in the PCM, and identification of HDGF in addition to FGF2 and CTGF in a microarray of the pericellular matrix, indicate a release from the PCM. The use of an inhibitor of heparitinase in conjunction with the treatment enzyme could reinforce this release as being directly due to enzymatic effects, rather than an off-target consequence. However, direct inhibitors of heparitinase I (heparinase III) are not available. Persulfonated GAGs can be used as competitive inhibitors of heparitinases, but show lower efficacy inhibiting heparinise III (heparitinase I) compared to heparinase I, due to the targeting of heparinase I to regions of higher sulfation (Aich *et al.*, 2011). In this respect, inhibition could be achieved with heparan sulfate saturation, or the experiment could be repeated using heparanase, for which inhibitors are available. Other studies confirm that HDGF binds to heparan sulfate, but not chondroitin sulfate, using murine HDGF with surface plasmon resonance (Dietz *et al.*, 2002).

Confirming the binding of HDGF, CTGF and FGF2 to heparin reinforces the hypothesis that these growth factors are bound to heparan sulfate in cartilage. Each growth factor was eluted from a heparin affinity column with a high NaCl

concentration of 2.5 M to ensure competition of the electrostatic interactions holding growth factors to heparin. This confirms independent studies predicting and demonstrating heparin affinity of each of these growth factors (Ori, Wilkinson and Fernig, 2011; Chiu *et al.*, 2014). The relative binding affinities of these three growth factors for heparin was not explored in this experiment, as a single concentration elution was employed, but this is investigated later on in Section 5.3.5. The use of heparin affinity chromatography to explore affinity for growth factor binding to heparan sulfate in cartilage has two main limitations. Firstly, heparan sulfate in cartilage has variable sulfation patterning and fewer sulfate groups compared to heparin, which determines the binding dynamics. Secondly, the *in vitro* setting of a buffered heparin column is of different constitution than cartilage and is void of other matrix interactions that could affect growth factor binding. However, using growth factors extracted with cartilage injury on the column overcomes some artificial limitations of the system; the proteins binding to heparin in the column are sourced from primary cartilage tissue, and therefore should possess any modifications specific to endogenous cartilage growth factors.

In summary, HDGF was explored in cartilage for the first time, where it can be both extracted from the matrix and imaged in the nucleus. The growth factors HDGF, CTGF and FGF2 were confirmed to bind heparan sulfate in the cartilage matrix, and be released from cartilage upon injury, and from heparin by NaCl. The release upon cartilage injury was rapid and independent of cellular viability. This suggested a biophysical response of the matrix might be responsible for their release upon injury, possibly involving sodium.

4 Sodium Mobilisation as a Mechanism for Release of Heparan Sulfate-Bound Growth Factors upon Cartilage Injury

4.1 Introduction

The commonality of HDGF, CTGF and FGF2 binding to heparan sulfate in cartilage, and being rapidly released upon mechanical injury, suggested a conserved mechanism of release between growth factors that was independent of cellular-dependent processes. This chapter details the exploration of tissue sodium, a highly abundant cation in the cartilage extracellular matrix, as a mechanism by which growth factors could be released from heparan sulfate in cartilage.

Three distinct properties of cartilage support the hypothesis that release of heparan sulfate-bound growth factors upon cartilage injury is due to a shift in the matrix sodium concentration. Specifically, articular cartilage has a high fixed charge density and high extracellular sodium concentration; a high fixed charge density in the territorial matrix, indicated by chondroitin sulfate (2B6, on aggrecan) (Figure 4.1), but not in the PCM, suggests the possibility of a gradient being able to modulate sodium concentration in the PCM through mobilising stores in the territorial matrix. The third indication is that all three growth factors bind to heparan sulfate by ionic interaction that can be overcome with NaCl (Figure 3.16). These aspects suggest the feasibility of tissue sodium recapitulating the process of growth factor elution *in situ*.

A cartilage model of matrix sodium depletion was used in this chapter to assess sodium dependence of growth factor release, achieved through proteoglycan loss via IL-1 treatment. This IL-1 depleted cartilage serves as a model for investigating growth

factor release by injury in a sodium-depleted cartilage environment. IL-1 stimulation of cartilage induces aggrecanase activity within the tissue via TRAF-g/TAK-1/MKK-4 and JNK-2 signalling (Ismail *et al.*, 2015). This aggrecanase, secreted by chondrocytes, cleaves aggrecan fragments with attached chondroitin sulfate chains — the predominant source of sodium sequestration and cartilage fixed charge density — to ultimately degrade the matrix and reduce the sodium counterion content in the tissue.

Furthermore, sodium dynamics were investigated through the use of a sodium-sensitive kinase as a proxy for matrix sodium changes that could be detected by the chondrocyte cell. SGK1 is reported as a salt-sensing kinase, and therefore was investigated for sodium-dependent changes at the protein and mRNA level in cartilage (Kleinewietfeld *et al.*, 2013; Wu *et al.*, 2013). Microarray and quantitative PCR analysis of $CD4^+$ T cells shows significant upregulation of *Sgk1* upon treatment with 40 mM NaCl (Wu *et al.*, 2013), while NaCl stimulation of T_H17 cells increases SGK1 protein (Kleinewietfeld *et al.*, 2013). If conserved in cartilage, *Sgk1* could act as a proxy or biomarker for sodium changes in the extracellular environment, sensed by the chondrocyte cell. Moreover, direct visualisation of sodium dynamics was conducted upon mechanical strain or compression of the tissue. Firstly, a fluorescent crown-ether structured cation dye with sodium selectivity was utilised, and secondly sodium MRI and spectroscopy techniques were deployed in cartilage tissue under load, to simulate mechanical insult.

Further, manipulation of the sodium content and fixed charge density of cartilage was employed in an *ex vivo* porcine injury model to demonstrate the effects of sodium on

growth factor release, via exogenous addition and endogenous depletion of sodium. This depletion of sodium is also translated into the disease context of osteoarthritis, where loss of fixed charge density through proteoglycan degradation is an established and clinically measurable aspect of disease progression (Shapiro *et al.*, 2002; Goldring and Goldring, 2016). The fixed charge density, as a proxy for sodium content, of human osteoarthritic cartilage was also investigated in relation to growth factor release to assess the implications of this putative mechanism in disease pathogenesis.

Chapter Aim

Explore the potential role of matrix-bound sodium in cartilage injury and growth factor release

Hypotheses

- Heparin-bound pericellular matrix growth factors are released by a sodium-dependent mechanism
- The mechanism of growth factor release is altered in osteoarthritic cartilage
- Sodium dynamics can be visualised in cartilage with respect to mechanical

4.2 Methods

4.2.1 Cartilage injury

4.2.1.1 Recutting model

Resting and recutting of cartilage was performed on cartilage from the porcine MCP joint, as per method section 2.2.2.

Five porcine biopsies per sample, or one human biopsy per sample, were collected with a 4 mm biopsy punch, rested in serum-free DMEM (SF-DMEM) for 48 h then injured (cut twice with a 15 blade scalpel) or rested (uninjured) in 250 µl SF-DMEM in a 48 well plate. Biopsies were stimulated with exogenous NaCl (Section 4.2.2) or depleted of matrix sodium (Section 4.2.3), then injured by cutting. Recut conditioned medium was collected at specified time points post-injury, with rested (uninjured) controls.

4.2.1.2 Explantation model

Human osteoarthritic articular cartilage was explanted from the knee joint of arthroplasty samples into SF-DMEM medium as per Section 2.2.1, using a 4 mm biopsy punch. Explanted cartilage biopsies were immediately further injured by cutting twice with a 15-blade scalpel. Injury conditioned medium was collected after 15 min. Remaining matrix protein was subsequently extracted using 2.5 M NaCl, and subsequent remaining whole tissue protein was extracted using RIPA buffer, as per Section 2.5.1. Injury conditioned medium, NaCl matrix extracts and RIPA tissue protein content were analysed by Western blot and ELISA, normalised to wet weight (diluted to 10 mg cartilage per 250 µl medium).

4.2.2 Sodium addition

Recutting injury experiments were performed as per Section 3.2.1.1, for samples in SF-DMEM containing physiological NaCl (0.137 M), and supraphysiological NaCl levels with exogenous NaCl added (2x, 274 mM; 4x, 548 mM; 6x, 822 mM total NaCl). Injury conditioned medium with exogenous NaCl was collected after 15 min and analysed by Western blot.

4.2.3 IL-1 dependent sodium depletion

Per biological replicate, 20 cartilage explants were collected from the porcine MCP joint with a 4 mm biopsy punch at the bone-cartilage interface. Explants were washed with SF-DMEM, then rested in 5 ml SF-DMEM for 48 h. 10 explants from each trotter were treated with 50 ng/ml IL-1 in 1 ml SF-DMEM and the other 10 explants were left untreated in SF-DMEM. Conditioned medium was collected entirely every 24 h and explants were replenished with fresh medium (± 50 ng/ml IL-1) over a course of 7 days. After 7 days of treatment, explants were washed in SF-DMEM then 5 explants were placed together in 300 µl of fresh SF-DMEM in a 48 well plate. 5 of the IL-1 treated explants were injured (recut) together, and 5 of the treated explants were left uninjured (rested), as per Section 4.2.1.1. The same was done for untreated explants. Rested and recut conditioned medium was collected after 15 min. Explants were then stored in formalin for histological analysis.

4.2.4 DMMB assay

Porcine conditioned medium from each 24 h period of the 7 day IL-1 treatment was diluted 1:20 with SF-DMEM, then 40 µl of diluted sample was added to a 96 well plate. A serial dilution of chondroitin sulfate glycosaminglycan was used as a standard

(10–60 µg/ml). 250 µl DMMB dye, with an absorbance of 0.4 A at 535 nm, was added to 40 µl of diluted sample and to 40 µl of chondroitin sulfate standard samples. Absorbance was measured at 595 nm with a reference measurement at 655 nm. Data that fit on the linear portion of the standard curve were scaled ($\times 20\ dilution, \div 10\ explants$) to give µg glycosaminoglycan released per explant per ml conditioned medium.

Injured human osteoarthritis biopsy explants were weighed, then fully digested with 50 µg/ml proteinase K (QIAGEN, Hilden, Germany) at 55 °C in 1 ml K_2PO_4 buffer for 16 h and assessed for GAG content by DMMB assay as described above. Samples were diluted to fit within the serial dilution of chondroitin sulfate glycosaminglycan used as a standard (10–60 µg/ml), then values were scaled based on sample wet weight to give a µg/ml/mg value.

4.2.5 Histology

IL-1 treated explants were embedded in paraffin and stained with Safranin O as per section 2.6.2. Safranin O stained explants were imaged with brightfield microscopy using an Olympus BX61 microscope.

4.2.6 Osteoarthritis disease scoring

Human osteoarthritis cartilage was macroscopically inspected visually for severity of disease in areas biopsies were taken from, scored by a modified disease score and established Outerbridge Classification score (Table 4.1).

Table 4.1 Disease scoring of osteoarthritic cartilage

MODIFIED DISEASE SCORE	**OUTERBRIDGE SCORE** (NOYES AND STABLER, 1989)
1 – White, deep cartilage	**0** – Visually normal
2 – Adjacent to red patch **3 –** Adjacent to scratched patch	**I** – Cartilage with softening and swelling
4 – adjacent to abrasion **5 –** Red cartilage	**II** – Partial-thickness defect with superficial fissuring
6 – Scratched cartilage **7 –** Abraded cartilage **8 –** Abraded, red cartilage	**III** – Deep fissuring
9 – Area of minimal cartilage **10 – A**djacent to full erosion to subchondral bone	**IV** – Exposed subchondral bone

4.2.7 CoroNa imaging

CoroNa imaging was conducted in collaboration with Peter Winlove and Jessica Mansfield at the University of Exeter.

Bovine knee osteochondral plugs were dissected using a saw. 1.5 mm osteochondral strips of bone with intact cartilage were cut using two razorblades. Osteochondral strips were incubated in 10 μM corona green dye in PBS at 4 °C for 1 h. Osteochondral strips were confined in a loading cell apparatus (Figure 4.20A), submerged in medium containing corona dye. Compression was applied perpendicular to the articular cartilage surface manually using a micrometer, and compression was measured with a load cell adjacent to the cut surface of underlying bone. Fluorescence intensity was captured by z-stack two-photon microscopy, at 488 nm, at each interval of compression applied. Fluorescence intensity was measured in ImageJ with use of cellular structural landmarks to maintain the depth of plane of focus in the analysis.

4.2.8 Sodium MRI imaging

Sodium MRI imaging was conducted in collaboration with Galina Pavlovskaya and Christopher Philp at the Sir Peter Mansfield Imaging Centre, University of Nottingham. Imaging and spectroscopy was conducted for sodium nuclei in porcine articular cartilage before, during and after 28% deformation compressive load, as described in Section 2.2.3.

NMR and MRI were performed on a 9.4 T Bruker Avance III Microimaging system (Bruker, Germany). Single-channel 25 mm ^{23}Na and ^{1}H commercial microimaging coils (Bruker, Germany), and a dual tuned ^{1}H/^{23}Na microimaging coil (Bruker, Germany) were used. Coils were tuned to the resonance frequency of 400.18 MHz for protons and 105.86 MHz for sodium, for ^{1}H and ^{23}Na porcine cartilage measurements. The length of the ^{1}H $\pi/2$ pulse was 32 μs at 150 W, the dwell time was set to 40 μs, and the resonance offset was set at the maximum of the proton peak height associated with water phase in each experiment or a series of consecutive experiments. One dimensional (1D) proton spectrum recorded for the cartilage specimen during compression/relaxation cycle did not reveal any significant changes in the spectrum indicating that no structural changes were induced by the loading cycle. The length of the ^{23}Na $\pi/2$ hard pulse was 48 μs at 200 W, the dwell time was set to 80 μs, and the resonance offset was set at the maximum of the sodium peak height in each experiment or a series of consecutive experiments as only one peak was observed. 1D sodium spectra of a given cartilage specimen did not change during loading cycle also suggesting that structural integrity of the cartilage was preserved during the time-course of the loading cycle.

TopSpin 3.2 (Bruker, Germany) home-written 23Na MRS triple quantum filtered protocol (Jaccard, Wimperis and Bodenhausen, 1986; Navon *et al.*, 2001) was used to characterise time evolution of stored sodium in the skin. 23 triple quantum evolution delays τ were used to determine a delay τ_{max} where a maximum of triple quantum signal occurred. This τ_{max} delay was used in the design of the triple quantum filter used in the visualisation of bound sodium in the cartilage during the loading cycle. 960 transients were collected for each τ delay, with a recycle delay of 0.2 s, thus bringing the total time for the entire series to be within 2 h.

Two-dimensional triple quantum-filtered with time proportional phase incrementation (TQ-TPPI) (Jaccard, Wimperis and Bodenhausen, 1986; Schepkin, 2016) incorporated into home written code for TopSpin 3.2 (Bruker, Germany) was used to determine fractions of sodium in free and bound states during compression/relaxation cycle. Spectral width in the direct dimension was set to 5 KHz, the indirect dimension was incremented using 512 50 μs time increments, recycle delay was 0.1 s, allowing for a spectrum collection in under 2 min. Data were processed with TopSpin3.2 with 20 Hz broadening in both dimensions and manual phasing of two-dimensional spectra in both dimensions. Fractions of free and bound sodium were produced by analysing central traces extracted at zero frequency in the direct dimension using build-in Multipeak fitting routine in IgorPro8.2 (Wavemetrics, USA). Normalised intensities of Lorentzian distributions obtained during spectra deconvolution were used as fractions of stored and free sodium observed in cartilage samples during loading cycle.

^{23}Na MRI Localisation of free sodium was performed with TopSpin 3.2 (Bruker, Germany) using a home written non-selective Gradient Echo (GE) MRI protocol. The

width of the π/2 pulse was 54 μs, the recycle delay was 0.2 s, the spectral width was 25 kHz. Images were collected into 64 × 64 matrices with the phase encoding time of 0.66 ms, and with maximum phase and read gradients set to 14% and 9%, respectively, resulting in a field of view, FOV = (30 × 28) mm^2. 512 transients were accumulated resulting in image collection within 1.8 h. Images were reconstructed in Prospa 3.2 (Magritek, Germany) by zero filling to 256 × 256 matrices, sinc-squared apodisation performed in both dimensions with consecutive magnitude two-dimensional Fourier transformation. The plane resolution in processed images was approximately (0.117 × 0.109) mm^2.

Visualisation of bound sodium was performed using TopSpin 3.2 (Bruker, Germany) home written code where triple quantum filter was applied before localisation of bound sodium with the gradient echo. The evolution time in the filter was set to the τ_{max} value identified in the triple quantum filtered ^{23}Na MRS. The width of the π/2 pulse was 49 μs with the width of π pulse in the triple quantum filter set to 98 μs, the triple quantum filtered evolution time τ was set to 0.7ms, the recycle delay was 0.2 s and spectral width was 50 kHz. Images were collected in 172 × 16 matrices with phase encoding time of 0.32 ms, and with maximum phase and read gradients set to 9% and 13.8%, respectively, resulting in FOV = (16 × 22) mm^2. 960 transients were accumulated resulting in image collection under 1.8h. The images were reconstructed in Prospa 3.2 (Magritek, Germany) by zero filling to 256 × 256 matrices, sinc-squared apodisation performed in both dimensions with consecutive magnitude two-dimensional Fourier transformation. The plane resolution in processed images was (0.062 × 0.086) mm^2.

Sodium concentrations were measured by sodium spectroscopy, expressed in terms of signal-to-noise ratios (SNRs), to reflect relative sodium levels. Intensity images were converted to SNR images using the following expression (Wetterling *et al.*, 2012; Anisimov *et al.*, 2021):

$$SNR_j = \frac{S_j - \overline{N_S}}{\sigma(N_S)}$$

Where S_j is the signal intensity measured in voxel *j*, $\overline{N_S}$ is the mean signal measured in the region of interest representing noise chosen as a square region with 6400 pixels from a region in the image containing no signal from the cartilage, and $\sigma(N_s)$ is the respective standard deviation of the noise mean. Multiple quantum filtering was utilised to distinguish between, visualise and characterise free and bound sodium fraction changes in the cartilage tissue during compression/relaxation cycle.

4.3 Results

Chondroitinase treated human cartilage was fluorescently imaged for the pericellular matrix component collagen VI, and co-stained for collagen II and the chondroitin sulfate neoepitope 2B6 of aggrecan (Figure 4.1). Type II collagen and chondroitin sulfate staining was excluded from the pericellular matrix, but present in the territorial matrix. Collagen VI was consistently present in the region surrounding the chondrocytes, localised by nuclear staining. This suggests a fixed charge density difference between the territorial matrix and PCM, considering chondroitin sulfate as the predominant contributor of fixed charge in the matrix.

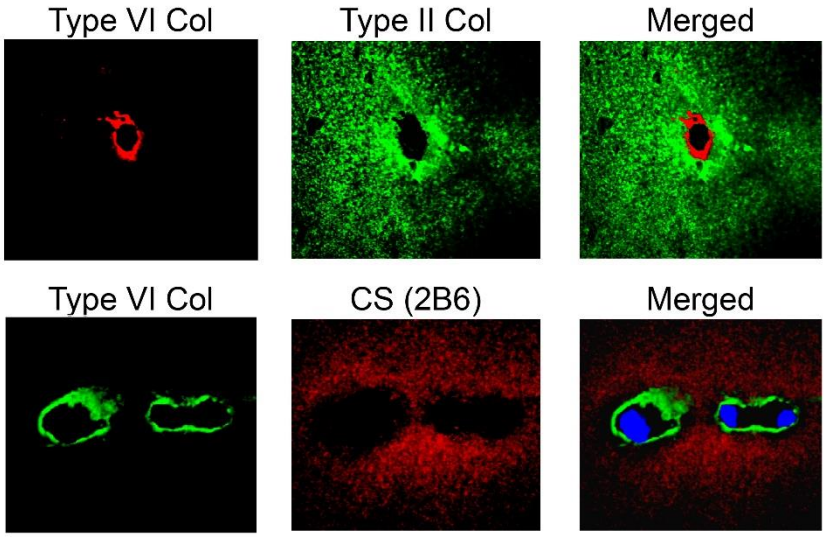

Figure 4.1 Confocal imaging of PCM collagen VI and TM collagen II and aggrecan chondroitin sulfate. (McLean, Personal Source).

4.3.1 Exogenous sodium releases growth factors

To explore a proposed role of sodium in the mechanical injury response of cartilage, exogenous NaCl was added to cartilage to determine the ability of sodium to release endogenous growth factors from tissue. This was also performed on dead cartilage, in order to determine the biophysical effects of NaCl, independent of the cell.

Uniform 4 mm diameter cartilage biopsies dissected from the porcine MCP joint were rested in serum-free medium prior to stimulation with exogenous NaCl. Supraphysiological concentrations of NaCl were supplemented to serum-free medium to make 1x, 2x, 4x and 6x NaCl solutions (137 mM, 274 mM, 548 mM and 822 mM total NaCl, respectively). Recutting injury was performed on explants, or they were rested without injury, whilst in physiological or supraphysiological NaCl medium. Injury/rested NaCl conditioned medium was collected after 15 minutes and assessed for growth factors released by NaCl.

Live porcine cartilage explants exhibited the same injurious response of releasing growth factor upon recutting injury as seen previously (Figure 3.2, Figure 4.2). Addition of exogenous sodium to live cartilage caused release of heparin-binding matrix growth factors, and this release was further enhanced with simultaneous recutting injury in a concentration-dependent manner, for both HDGF and CTGF. Culture of rested cartilage explants with supraphysiological NaCl in the absence of recutting injury also released detectable amounts of HDGF and CTGF growth factor. This was also NaCl concentration-dependent, but caused less release than when combined with recutting injury.

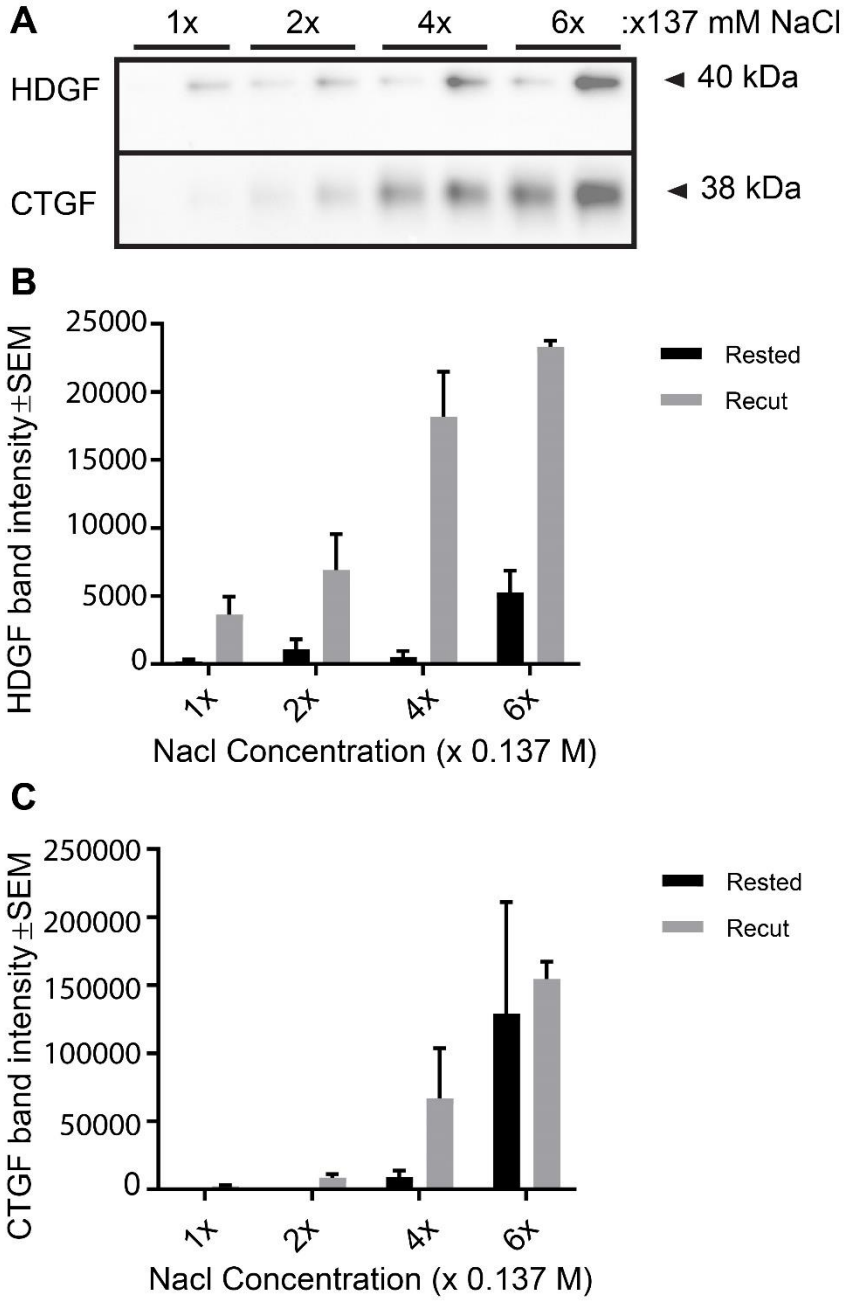

Figure 4.2 Sodium addition releases growth factors from cartilage. Porcine articular cartilage explants were rested or injured by recutting in serum-free DMEM with physiological NaCl (0.137 mM) or supraphysiological NaCl concentrations (2–6 fold). After 15 minutes conditioned medium was immunoblotted for (A) and quantified for HDGF (B) and CTGF (C) (n=3).

An equivalent experiment was conducted on dead cartilage explants, after freeze-thaw to kill the chondrocytes. A greater range difference in release between physiological and supraphysiological NaCl concentrations was observed in dead cartilage (Figure

4.3) compared with live cartilage (Figure 4.2), but absolute amounts were not directly compared. Dead cartilage exhibited the same trend as live cartilage, where supraphysiological NaCl released growth factors from cartilage and simultaneous recutting injury induced further release of more growth factor. These observed data indicate an ability of exogenous NaCl to release heparin-binding growth factors from cartilage devoid of cellular activity, at comparable amounts and further inducible by injury.

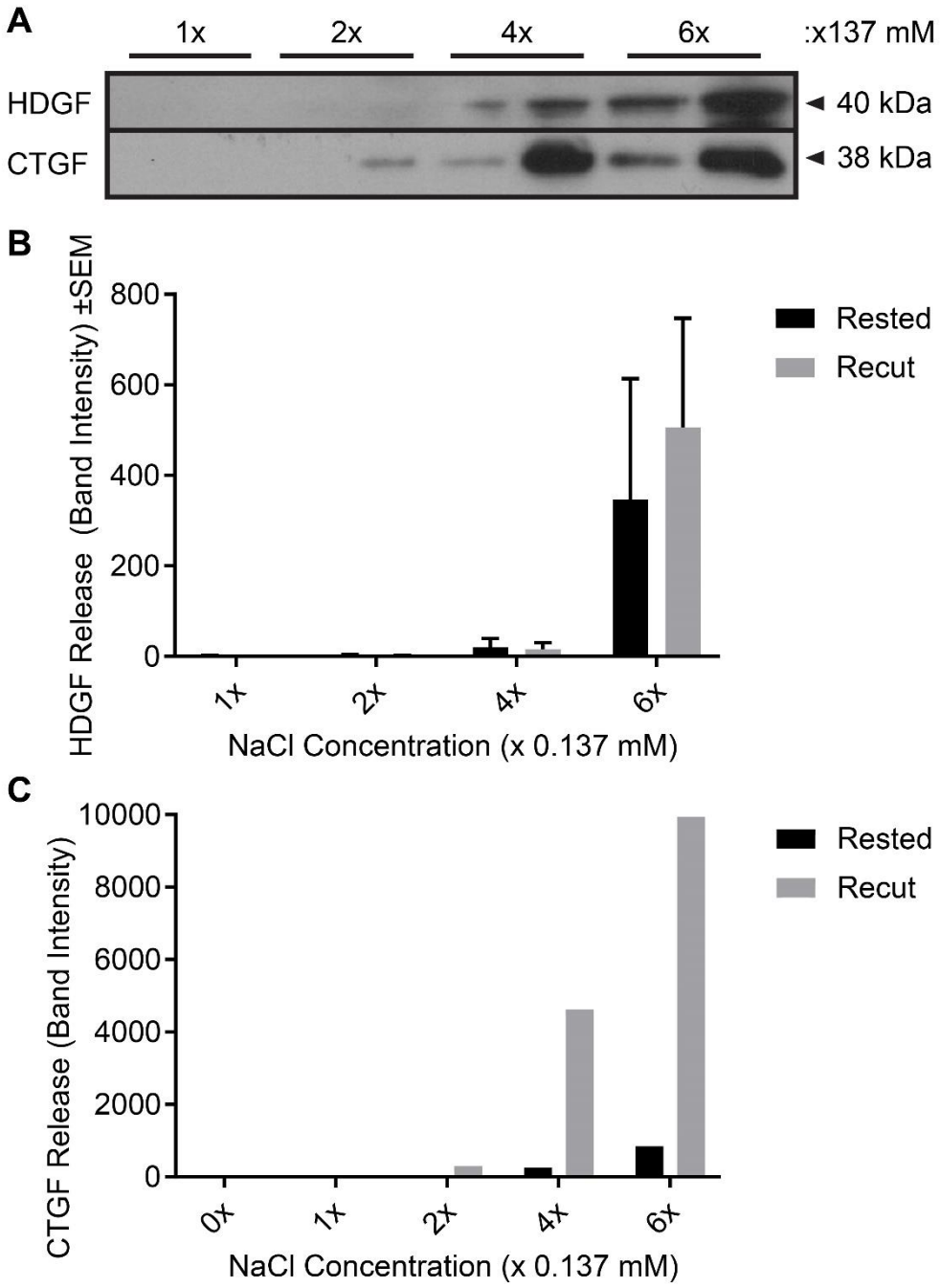

Figure 4.3 Sodium addition releases growth factors from dead cartilage. Dead porcine articular cartilage explants, killed by three freeze-thaw cycles, were rested or injured by recutting in serum-free DMEM with physiological NaCl (0.137 mM) or supraphysiological NaCl concentrations (2–6 fold). After 15 minutes conditioned medium was immunoblotted (A) and quantified for HDGF (B) and CTGF (C) (n=3,1).

4.3.2 Reduced fixed charge density reduces growth factor release

Further to demonstrating that the addition of exogenous sodium induces the release of heparin-binding growth factors from cartilage, the converse was explored; depletion of sodium from cartilage was investigated to assess whether this would inhibit, or reduce the amount of, growth factor released upon injury.

Uniformly sized, 4 mm diameter, rested cartilage biopsies were treated with 50 ng/ml interleukin-1 (IL-1) for 7 days in order to induce aggrecanase activity and deplete cartilage of aggrecan proteoglycan content. This would deplete the ability of cartilage to bind and retain sodium counterions due to loss of charged chondroitin sulfate on aggrecan. DMMB assay of conditioned medium from each 24 h treatment period quantified the sulfated GAG released from the tissue, and showed IL-1 induced release of chondroitin sulfate from the cartilage (Figure 4.4A). The increased release of chondroitin sulfate GAG by IL-1 compared to that from untreated cartilage occurred consistently until day 7. The magnitude of GAG release also exhibited a cyclical 3 day pattern, with maximal GAG loss on day 1 and day 4, while decreasing over the following 2 days. After 7 days of IL-1 treatment, the cartilage tissue was no longer releasing more glycosaminoglycan than control cartilage. Staining with Safranin O, a metachromatic dye indicating fixed charge density of the tissue, at day 7 showed a loss of staining representative of proteoglycan loss (Figure 4.4B). Day 7 cartilage explants were subjected to recutting injury or further resting without injury, after which growth factor release was measured in conditioned medium. Recutting injury of proteoglycan-depleted cartilage consistently released less growth factor than recut untreated cartilage (Figure 4.4C, D). HDGF and CTGF exhibited an approximately 60%

reduction in growth factor released from depleted cartilage upon injury, and FGF2 was released more than 80% less in depleted cartilage rendering it comparable to levels released from rested (uninjured) cartilage (Figure 4.4D).

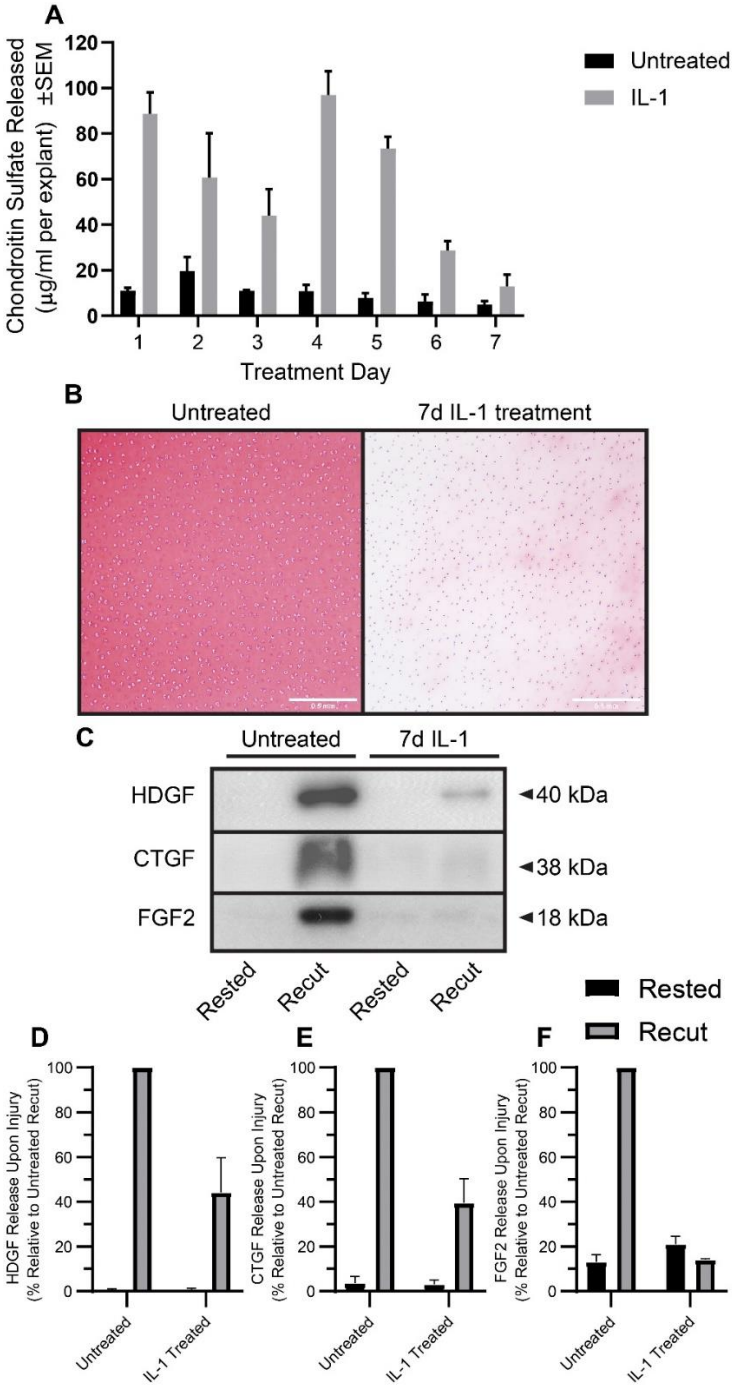

Figure 4.4 Full charge depletion reduces growth factor release upon cartilage injury. Porcine articular cartilage was biopsied and rested for 24 h in serum-free medium, then treated with 50 ng/ml IL-1 for 7 days to deplete proteoglycan (sodium depletion). Chondroitin sulfate GAG release was measured in daily conditioned medium over the treatment period by DMMB assay (A). Explants were stained with Safranin O for fixed charge density after 7 days (B). Explants were then either rested or recut (injury) in fresh serum-free medium. After 30 minutes, conditioned medium was immunoblotted (C) for growth factors HDGF, CTGF and FGF2 which were quantified (D–F) (n=6).

In order to demonstrate the reduction in growth factor released upon injury was due to an injury-dependent mechanism, rather than a consequence of IL-1 treatment increasing cartilage growth factor content, matrix extractable protein, total tissue protein (Figure 4.5), and regulation of gene expression (Figure 4.7) were measured.

IL-1 treatment of cartilage for 7 days did not affect the presence of HDGF, CTGF or FGF2 in the cartilage matrix, extracted with 2.5 M NaCl matrix extraction buffer, when measured by Western blotting (NaCl, Figure 4.5A). Changes in matrix protein were not detectable by immunoblotting, but quantitative FGF2 ELISA detected statistically significantly more FGF2 in matrix extracted samples from IL-1 treated explants than untreated explants ($t(4)=3.047$, $p=0.0381$) (Figure 4.5B).

IL-1 treatment resulted in no difference in total growth factor content of HDGF and CTGF by immunoblotting, or in FGF2 by immunoblotting or ELISA, measured in whole cartilage tissue after digestion with a dissociative tissue lysis buffer (RIPA, Figure 4.5). The decrease in growth factor release in fully depleted cartilage compared to normal cartilage in Figure 4.4 was therefore not due to any overall decrease in matrix or tissue growth factor content.

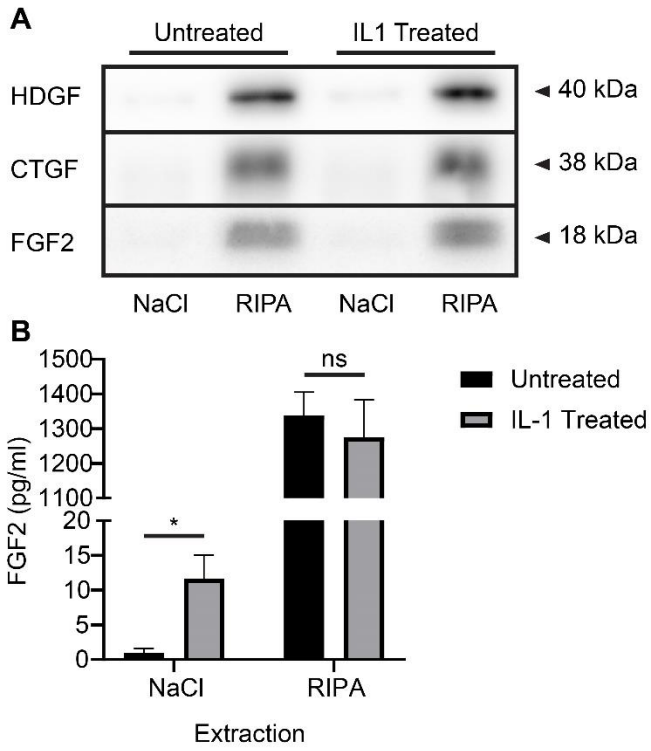

Figure 4.5 NaCl and RIPA extraction of 7 day untreated and IL-1 treated explants. Immunobloting of growth factors extracted from the matrix (NaCl) and from the whole cartilage tissue (RIPA) after proteoglycan depletion (A), representative blot. FGF2 ELISA from equivalent samples (B) (n=3). Unpaired t-test (ns=non-significant, *p≤0.05).

In addition to protein at the culmination of IL-1 treatment in Figure 4.5, the regulation of *HDGF*, *CTGF* and *FGF2* mRNA over each of the 7 days of IL-1 treatment was measured by quantitative PCR (Figure 4.6).

HDGF was modestly significantly upregulated after 4 days of treatment with IL-1 ($t(4)=5.891$, $p=0.004152$), however was not significantly upregulated any of the remaining time during 7 days of treatment with IL-1 (Figure 4.6A). *CTGF* mRNA was significantly upregulated during the 7 day treatment period on treatment days 1, 3 and 5, with non-significant upregulation compared to untreated explants in the interim days. *CTGF* mRNA had reduced to levels comparable to the untreated control by day 7, at the point of proteoglycan depletion (Figure 4.6B). *FGF2* mRNA was significantly

downregulated in IL-1 treated explants compared to untreated on day 7, due to an increase of untreated *FGF2* levels compared to baseline and slight decrease in treated samples (Figure 4.6C).

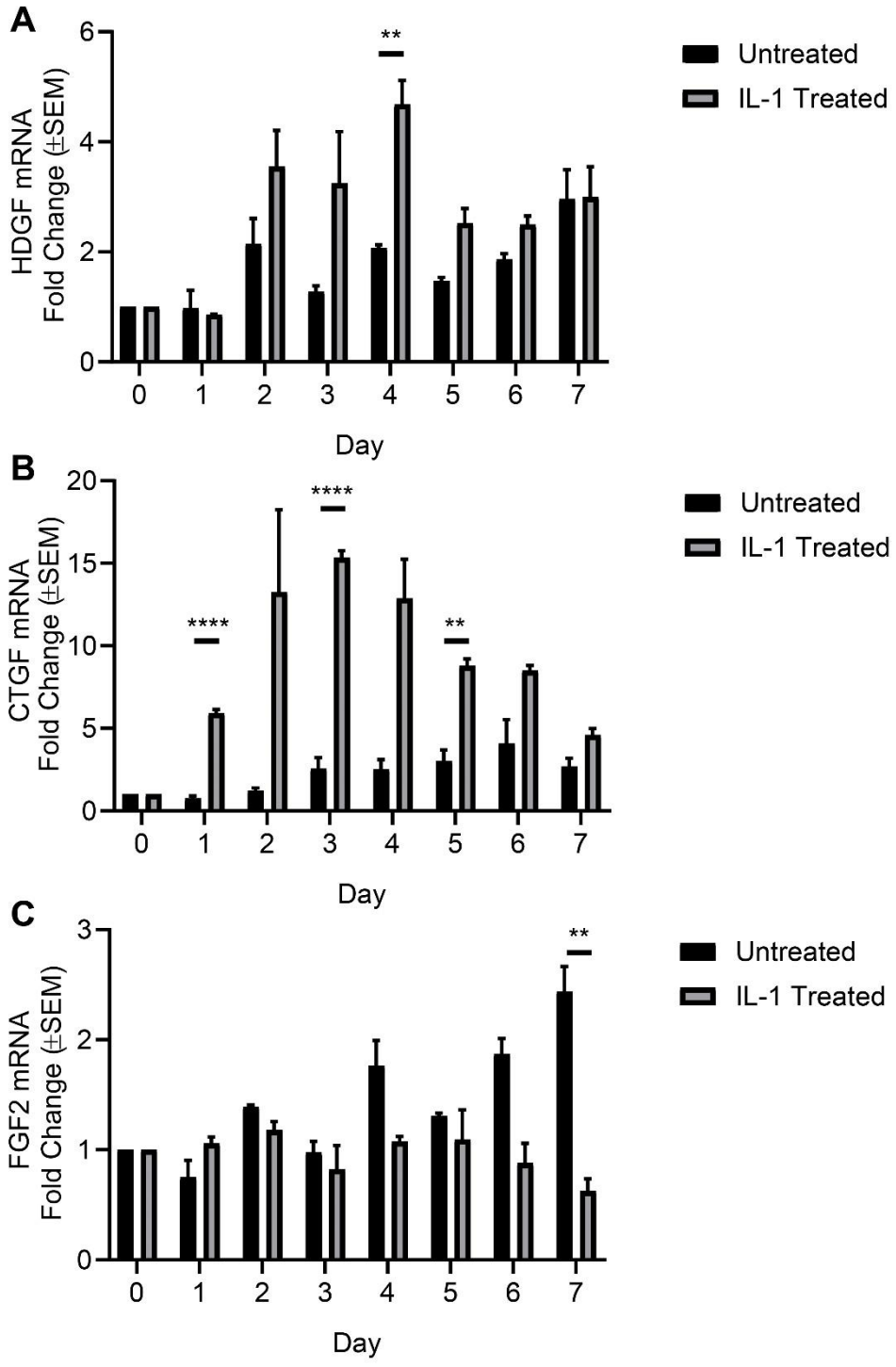

Figure 4.6 Growth factor mRNA regulation throughout 7 days of IL-1 treatment for proteoglycan depletion. Quantitative PCR of porcine cartilage explants each day of the 7 day IL-1 treatment for proteoglycan depletion, for *HDGF* (A), *CTGF* (B) and *FGF2* (C) mRNA fold change relative to day 0. 18S housekeeper (n=3). Multiple t-tests were conducted, corrected for multiple comparisons using the Holm-Sidak method (**p≤0.01, ****p≤0.0001).

Further, I confirmed that *HDGF* gene expression is not regulated by IL-1 treatment in porcine chondrocyte cells over a 24 h period. Porcine chondrocytes isolated from cartilage of the MCP joint were treated with 20 ng/ml IL-1 for up to 24 h. Quantitative PCR of *HDGF* showed no significant regulation over a 24 h period compared with untreated chondrocytes. In contrast, the known inflammatory-mediated genes *COX2* and *IL6* increased over the course of 24 h IL-1 treatment. *COX2* was significantly upregulated 51-fold compared to untreated cells at 24 h ($p < 0.0001$); over 300-fold compared to baseline. *IL6* was significantly upregulated in IL-1 treated cells compared to untreated control cells at 1 h, 2 h, 12 h and 24 h ($p<0.05$), exhibiting a 76-fold increase over untreated cells at 24 h; a 914-fold increase from baseline. *HDGF* gene expression is not regulated by IL-1 treatment in porcine chondrocytes within 24 h.

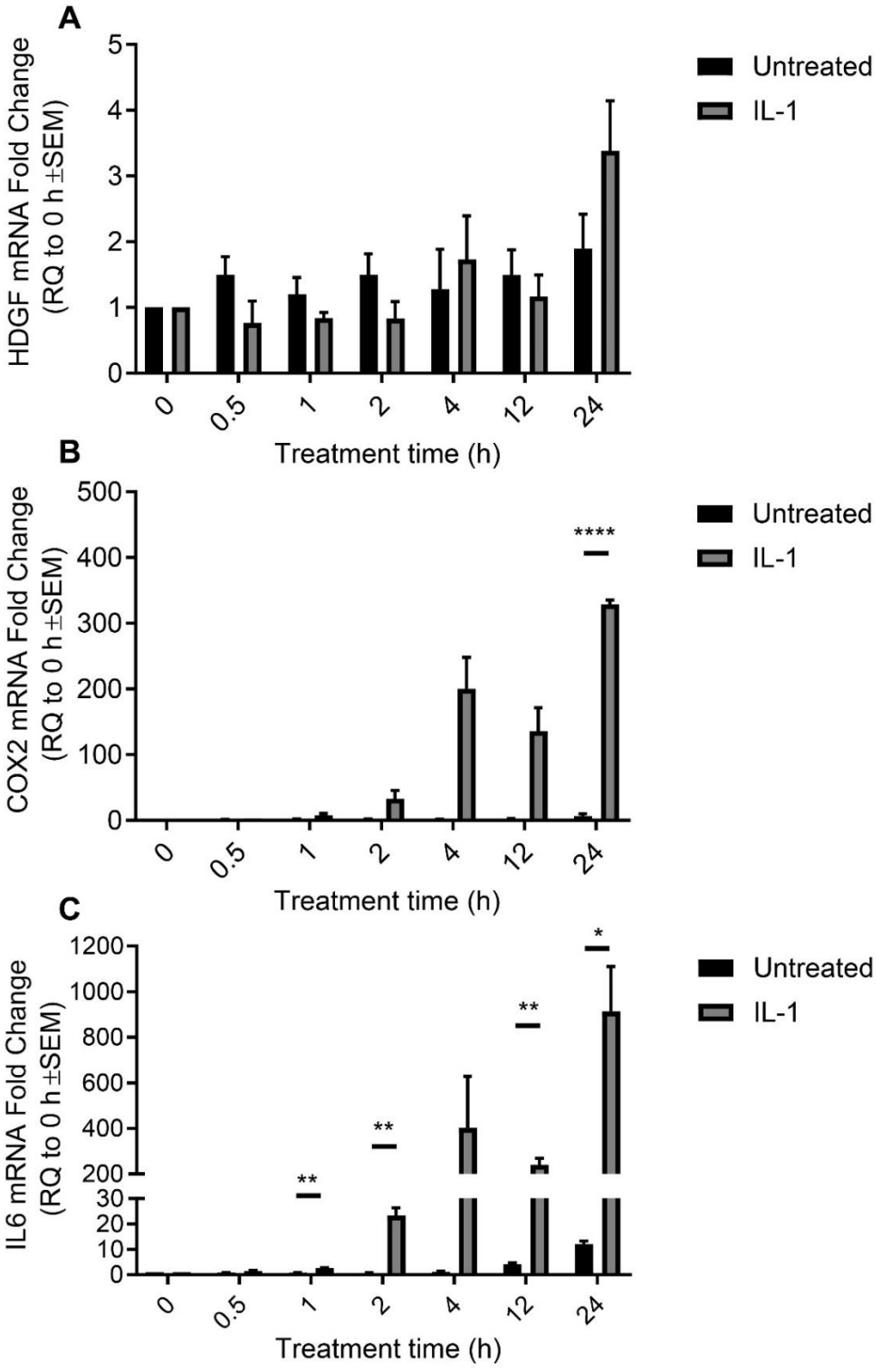

Figure 4.7 Porcine chondrocyte mRNA regulation by IL-1. *HDGF* (A), *COX2* (B) and *IL6* (C) mRNA regulation in primary cultured porcine chondrocytes, over 24 h of treatment with 20 ng/ml IL-1, fold change relative to 0 h. 18S housekeeper. Multiple t-tests were performed and corrected for multiplicity (n=3) (*p≤0.05, **p≤0.01, ****p≤0.0001).

IL-1 depletion of cartilage was also attempted over a treatment period of 4 days, but yielded only partial depletion of the tissue. The GAG released from the tissue by IL-1 was greater than that released from untreated cartilage throughout the 4 day treatment and peaked during the first day and the fourth day (Figure 4.8). This was consistent with data from the 7 day treatment (Figure 4.4). Safranin O staining after day 4 of treatment showed a slight reduction in red staining, indicating partial depletion of proteoglycan from the cartilage and partial reduction of tissue fixed charge density. Partial depletion of proteoglycan in porcine cartilage resulted in variable effects on growth factor release upon recutting injury (Figure 4.8C, D). Of three biologically paired samples that were recut, one released modestly more HDGF but less CTGF, one released more of both growth factors, and the final replicate released less of each growth factor (Figure 4.8D). In this respect, there was no consistent effect on the release of growth factors upon recutting injury when cartilage was only partially depleted of proteoglycan.

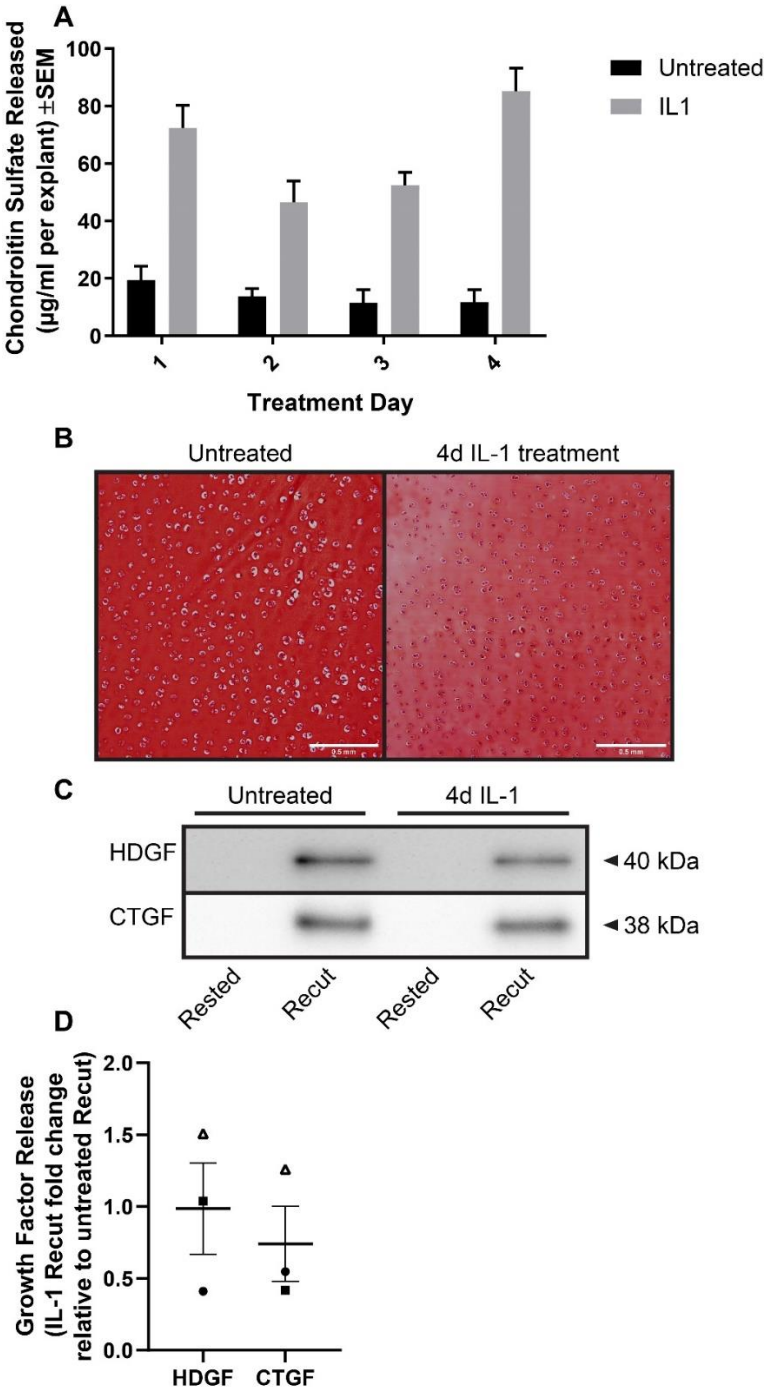

Figure 4.8 Partial charge depletion variably affects growth factor release upon cartilage injury. Porcine articular cartilage was biopsied and rested for 24 h in serum-free medium, then treated with 50 ng/ml IL-1 for 4 days, resulting in only partial depletion of proteoglycan. Chondroitin sulfate GAG release was measured in daily conditioned medium over the treatment period by DMMB assay (A). Explants were stained with Safranin O for fixed charge density after 4 days, showing minimal reduction in stain intensity (B) (representative image). Explants were then either rested or recut (injury) in fresh serum-free medium. After 30 minutes, conditioned medium was immunoblotted (C) for growth factors HDGF and CTGF which were quantified (n=3).

4.3.3 Fixed charge density and growth factor release are lost in osteoarthritis progression

The implication of a sodium-dependent mechanism of growth factor release upon injury, and proteoglycan depletion, was investigated in the context of osteoarthritis using human osteoarthritic articular cartilage samples.

Normal human cartilage from a healthy donor was stained for proteoglycan content by Safranin O stain, compared to cartilage from an osteoarthritic patient (Outerbridge Grade II). Osteoarthritic cartilage showed depleted proteoglycan staining, reflective of a reduced fixed charge density, compared to healthy tissue (Figure 4.9).

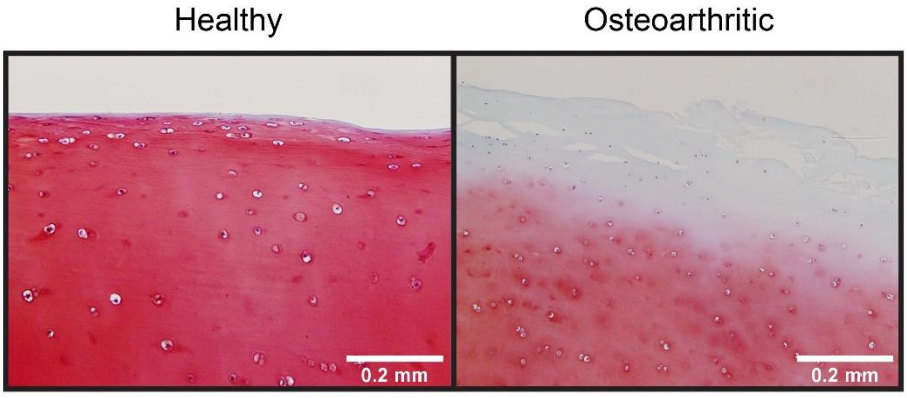

Figure 4.9 Human cartilage loss of proteoglycan by Safranin O stain with osteoarthritis progression. Brightfield microscopy of normal cartilage (healthy, non-osteoarthritic post-mortem sample) and osteoarthritic cartilage (osteoarthritic, Outerbridge Grade II) from human tibial plateau, stained with safranin O metachromatic dye. Representative images. Scale bar 0.2 mm.

Human osteoarthritic cartilage was macroscopically graded for severity of disease by modified Outerbridge classification (Grade 0; normal cartilage, Grade 1; cartilage with softening and swelling, Grade 2; partial-thickness defect with superficial fissuring, Grade 3; deep fissuring, Grade 4; exposed subchondral bone) and by a modified

disease score (Table 4.1). Articular cartilage biopsies were taken from respective areas (Figure 4.10).

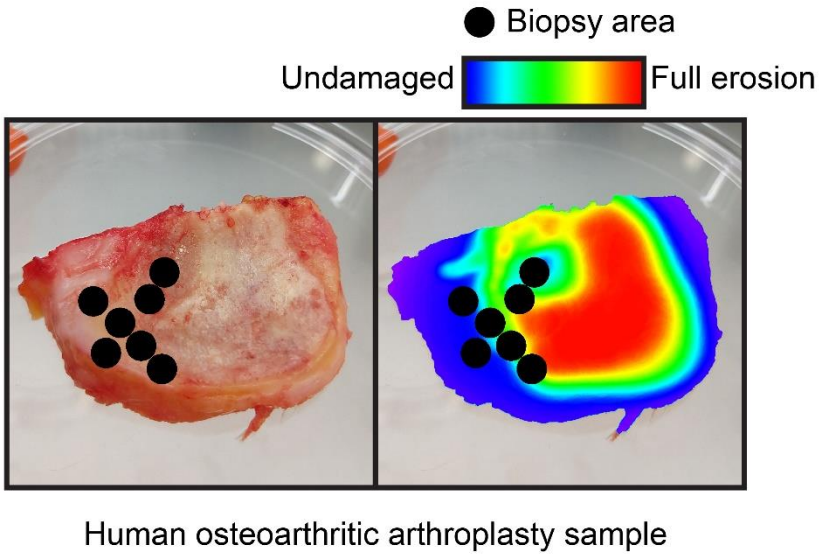

Figure 4.10 Macroscopic grading and biopsy dissection of human osteoarthritic articular cartilage. Qualitative visual representation of human cartilage arthroplasty sample condition and areas of cartilage biopsy collection. Cartilage condition of biopsies were subsequently macroscopically scored using the Outerbridge Score.

The fixed charge density was determined by DMMB assay of GAG content, after cartilage biopsy digestion with proteinase K. Four osteoarthritic cartilage donors showed an inverse correlation between GAG content and disease severity, controlled for biopsy weight (Figure 4.11A). Grading of disease severity by the established Outerbridge Classification also showed a trend for decreasing GAG content by weight, with increasing disease severity (Figure 4.11B). In this respect, areas of severely osteoarthritic cartilage showed lower fixed charge density by weight-controlled measurement GAG content compared to relatively undamaged, or less diseased, areas.

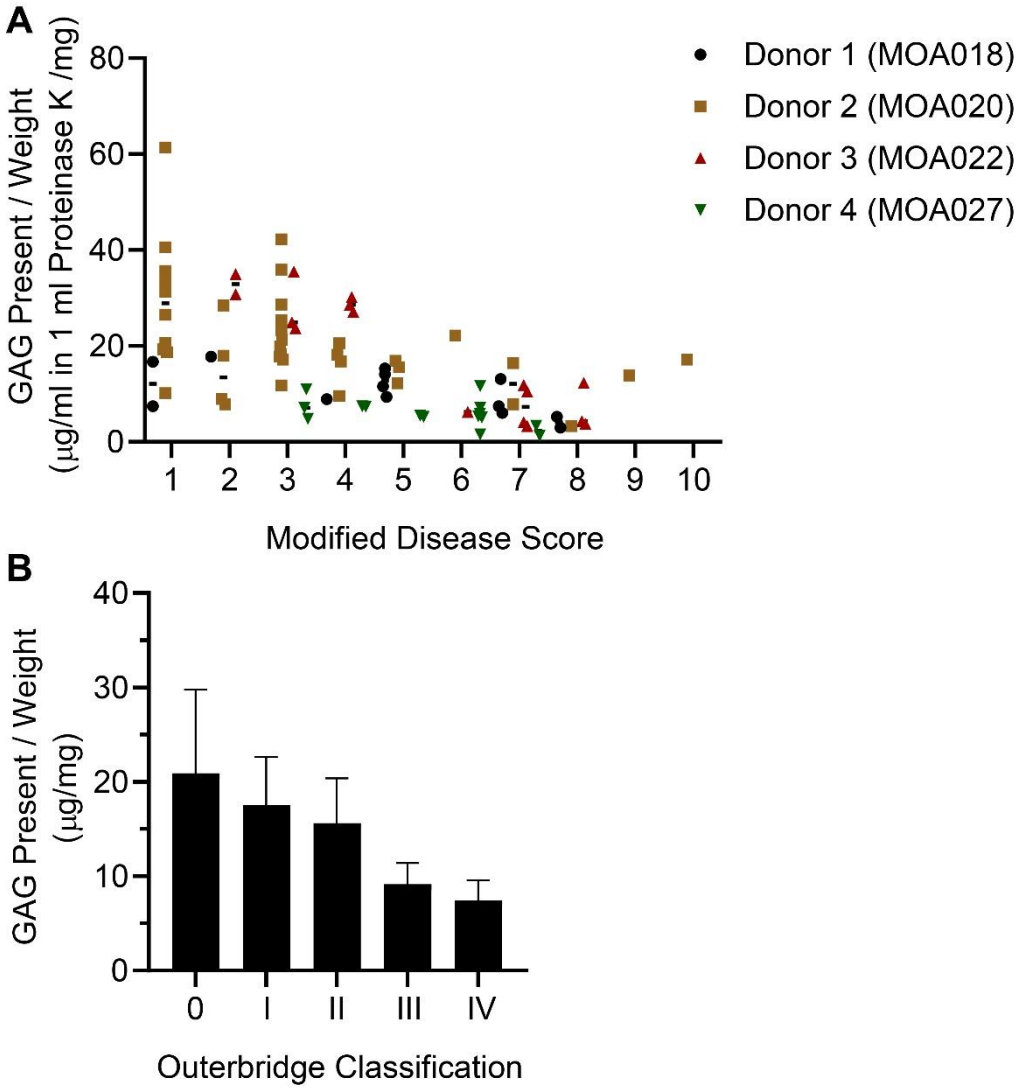

Figure 4.11 Fixed charge density inversely correlates with severity of disease in osteoarthritic cartilage samples. Human osteoarthritic cartilage samples were fully digested with proteinase K and assessed for GAG content, a proxy for fixed charge density, by DMMB assay. GAG content of individual biopsies of varying disease severity from 4 donors (A). GAG content when alternatively classified by established Outerbridge classification of disease severity (B).

Human osteoarthritic cartilage biopsies from relatively undamaged regions (Outerbridge 0–I) and severely diseased areas (Outerbridge III–IV) were injured by cutting, immediately after explantation, and assessed for growth factor released after 15 minutes relative to biopsy wet weight (normalised 10 mg cartilage per 250 µl SF-DMEM). Biopsies from severely diseased areas of human cartilage released significantly less HDGF, CTGF and FGF2 upon injury, compared to undamaged areas

by immunoblotting (Figure 4.12A–D). Quantitative ELISA analysis of FGF2 released from human osteoarthritic cartilage also showed significantly less FGF2 released upon injury from severely diseases areas compared to relatively undamaged areas (Figure 4.12E). FGF2 release did not strongly correlate with GAG content within individual biopsies.

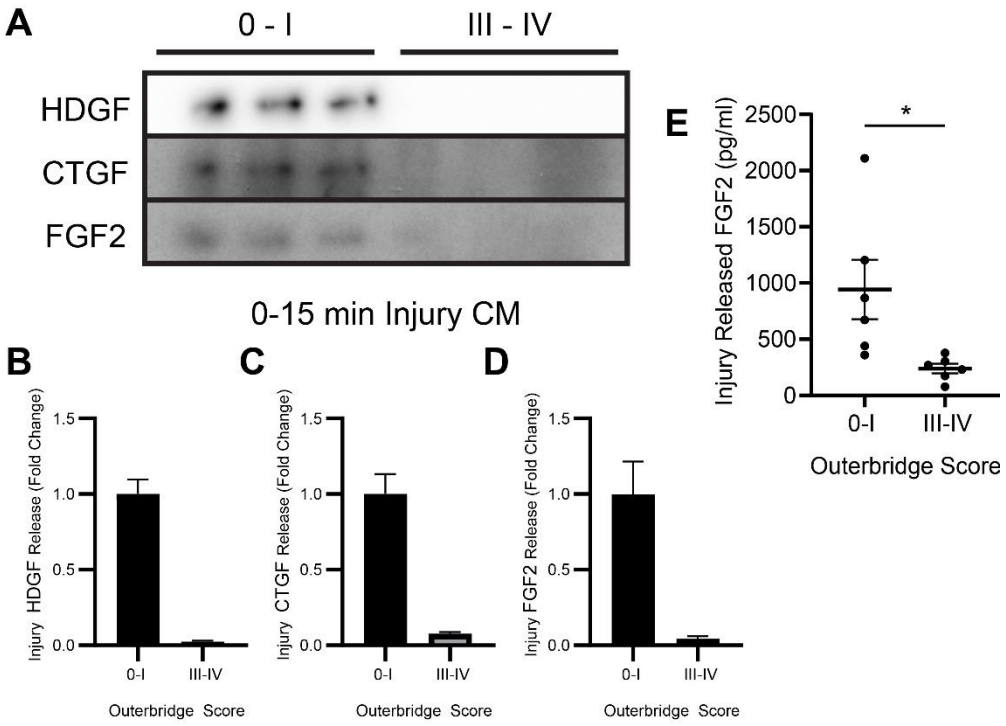

Figure 4.12 Severely diseased regions of osteoarthritic cartilage release less growth factor upon injury compared with undamaged regions. Human cartilage biopsies were taken from regions with varying osteoarthritic severity, assessed by Outerbridge Classification. Biopsies from undamaged (0–I) and severely diseased (III–IV) areas were injured in serum-free medium. After 15 minutes, conditioned medium was immunoblotted for HDGF, CTGF and FGF2 (A), quantified in B-D (n=3), or assessed by FGF2 ELISA (E) for growth factor release (n=6). Samples normalised 10 mg wet weight cartilage per 250 µl serum-free DMEM. Unpaired T-test (*p≤0.05).

In order to ensure differences in growth factor release were not due to discrepancies in overall growth factor content, the total matrix protein extractable, and the subsequent total protein extractable from the whole cartilage tissue, was compared between relatively undamaged and severely diseased biopsies, controlled for weight.

Explanted cartilage biopsies from undamaged regions contained less matrix growth factor, extractable by 2.5 M NaCl, than equivalent severely diseased biopsies (NaCl, Figure 4.13A–E). Subsequent whole tissue extraction of remaining protein showed regions of differing disease severity contained equivalent amounts of growth factors HDGF, CTGF and FGF2 (RIPA, Figure 4.13A).

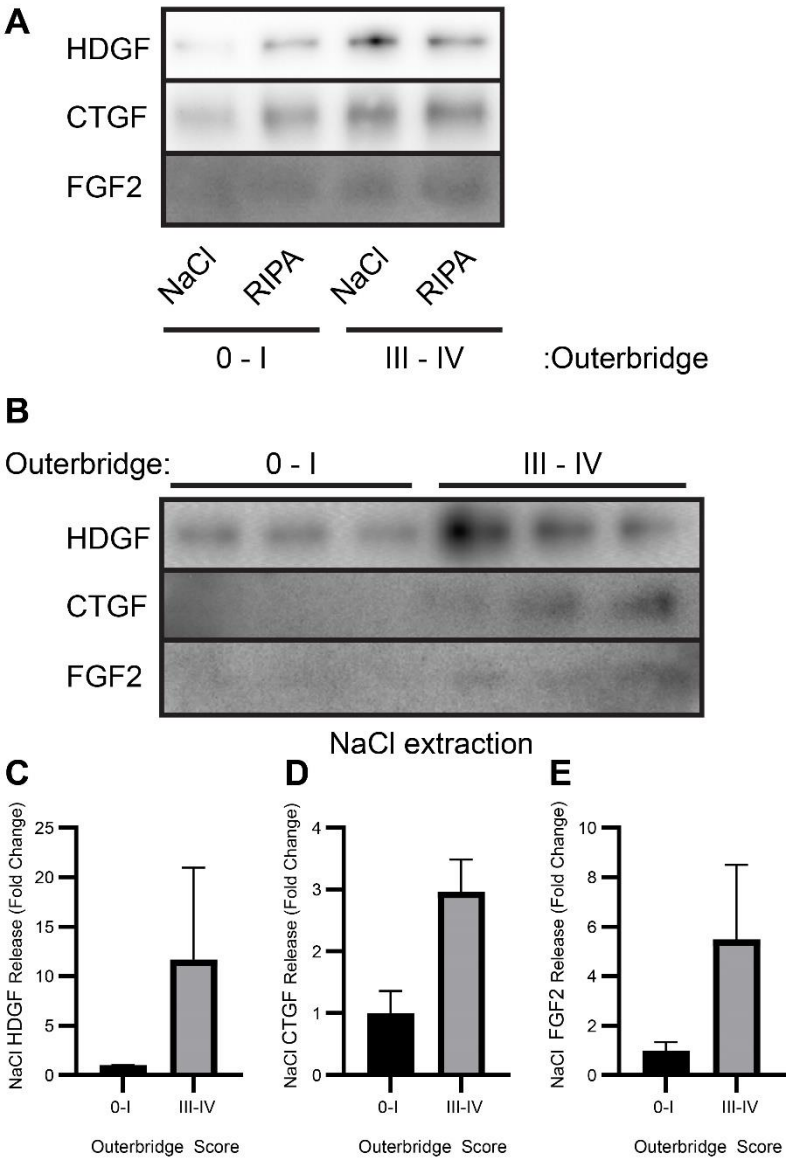

Figure 4.13 Severely diseased regions of osteoarthritic cartilage contain more matrix and whole tissue growth factor than undamaged regions. Representative immunoblot of matrix extracted protein (NaCl – 2.5 M matrix extraction NaCl buffer) (A, NaCl) and subsequent total tissue protein content (RIPA – dissociative tissue lysis buffer) (A, RIPA) from undamaged (0–1 Outerbridge) and severely diseased (III–IV) dissected human osteoarthritic cartilage biopsies. Matrix extracts were immunoblotted (B) and quantified for HDGF, CTGF and FGF2 growth factor (C-E). Representative blots, n=4).

4.3.4 SGK1 sodium-sensitivity

Methods of sodium detection were explored in cartilage tissue, to provide direct evidence of matrix sodium dynamics capable of releasing heparin bound growth factors.

Serum glucocorticoid kinase 1 (SGK1) was investigated as a potential biomarker for sodium sensing in chondrocytes and porcine cartilage. In order to assess the putative salt-sensing properties of SGK1, porcine cartilage was explanted from the MCP and snap frozen for a 0 h time point, or transferred into SF-DMEM for further time points. *SGK1* mRNA levels were evaluated by qPCR relative to 18S. *SGK1* mRNA was significantly regulated after explantation ($F(4,24) = 15.86$, $p<0.0001$). Post hoc comparisons using Dunnett's multiple comparisons test indicated a significant increase in *SGK1* mRNA 1 h after explantation compared to 0 h baseline (M=2.282, SEM=0.3203). The mRNA levels of *SGK1* were returning by 4 h, yielding no significant difference to baseline. At 12 h and 24 h, *SGK1* exhibited reduction to below baseline levels, not of statistical significance.

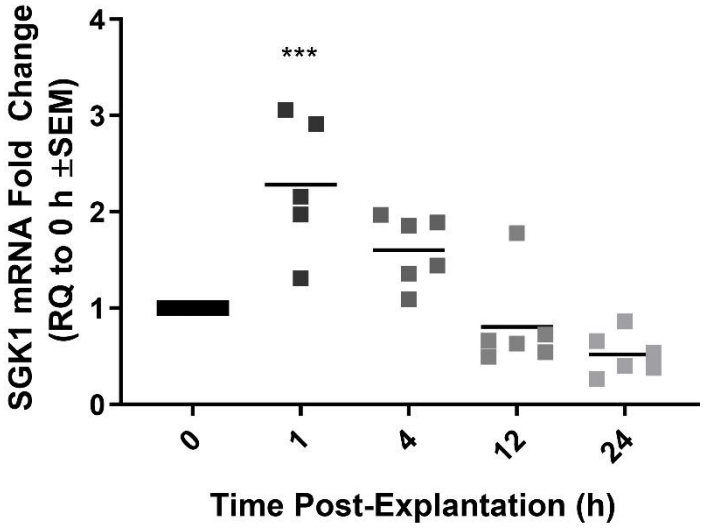

Figure 4.14 *SGK1* mRNA regulation in porcine cartilage after explantation. Quantitative PCR controlled to 18S mRNA (n=6). One-way ANOVA with Dunnett's multiple comparisons to 0 h (*** = $p<0.001$).

The upregulation of *SGK1* in cartilage upon injurious explantation might be a result of sodium dynamics upon injury. To test whether the upregulation of *SGK1* mRNA after explantation was due to sensing of sodium by the cells, chondrocytes were stimulated

with additional NaCl (150 mM in addition to physiological 137 mM) and assessed for *SGK1* regulation.

Chondrocytes were stimulated with 150 mM additional NaCl for 2 minutes, then cultured in medium containing physiological NaCl. Then, mRNA expression was measured after 1 h and 4 h; these two time points showed upregulation of *SGK1* expression upon injurious explantation (Figure 4.14). Quantitative PCR, relative to 18S mRNA levels, showed no regulation of *SGK1* by transient 2 minute stimulation of chondrocytes with 150 mM additional NaCl after 1 h or 4 h. *COX2* mRNA was evaluated as a negative control, also showing no regulation by transient NaCl stimulation after 1 h or 4 h.

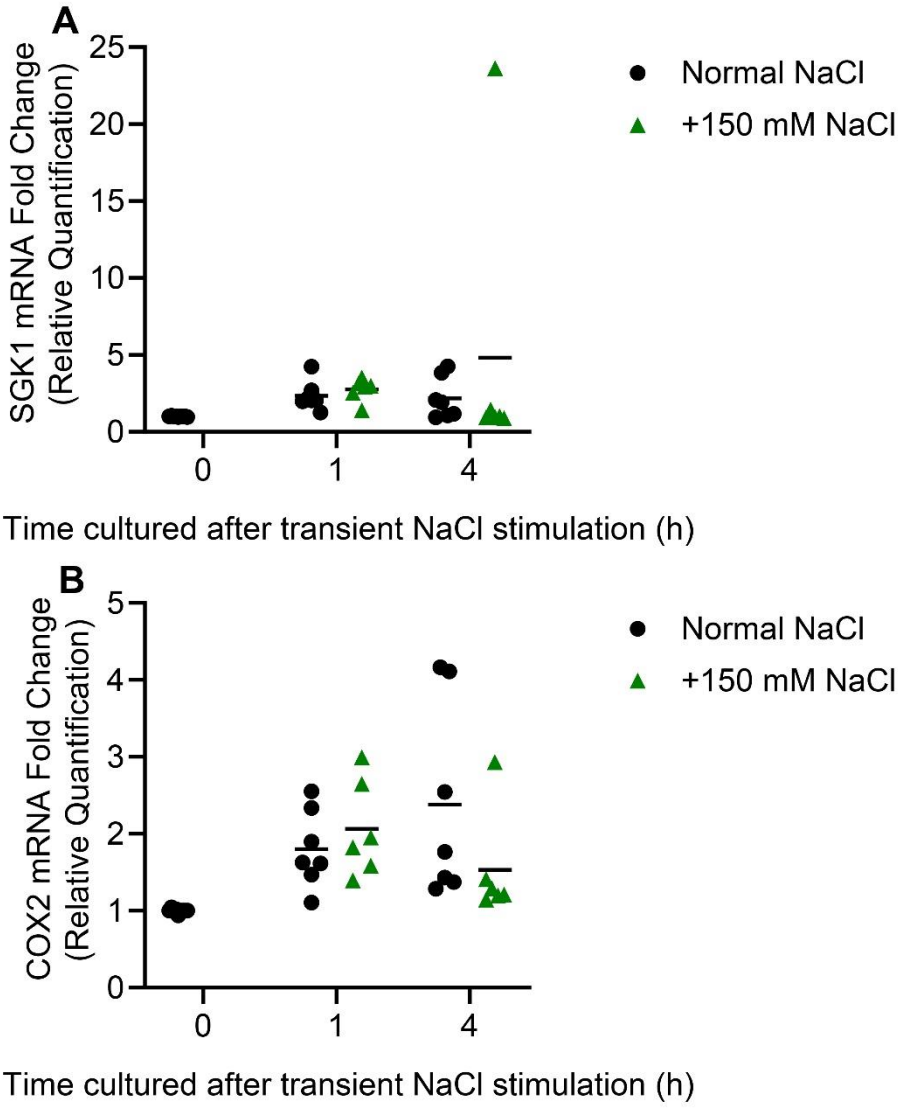

Figure 4.15 *SGK1* and *COX2* mRNA in porcine chondrocytes transiently stimulated with NaCl. Primary porcine chondrocytes, isolated by collagenase digestion, serum-starved after culture in DMEM were stimulated with an additional 150 mM NaCl for 2 minutes, then mRNA was extracted and quantified by qPCR after 0, 1 or 4 h for *SGK1* (A) and *COX2* (B) (n=7).

To further explore the putative salt-sensing kinase properties of SGK1 in chondrocytes, its protein activity was measured upon injurious explantation and NaCl stimulation by phosphorylation immunoblotting.

Porcine cartilage was explanted from the MCP joint and cellular protein content was assessed by Western blot of dissociated tissue lysate. SGK1 protein was

phosphorylated at the Threonine 256 (pThr256) site *in situ*, immediately upon explantation. Levels of phosphorylation did not change up to 60 minutes after explantation.

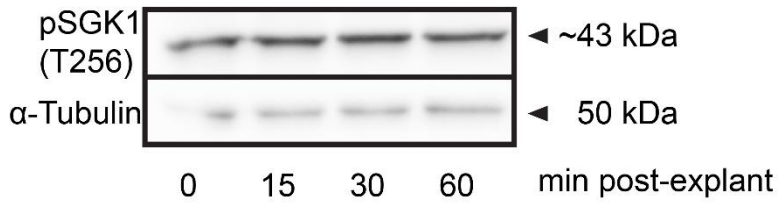

Figure 4.16 Phosphorylated SGK1 in porcine cartilage after explantation. Protein was extracted with RIPA lysis buffer from porcine articular cartilage explants 0, 15, 30 or 60 minutes after explantation into serum-free DMEM, and immunoblotted for phosphorylated SGK1 protein (T256) against an α-Tubulin housekeeper. Representative blot.

Porcine articular cartilage, rested after dissection, was stimulated with 40 mM additional NaCl for 15, 30 or 60 minutes. Phosphorylation at the Thr256 site remained constant, relative to a beta-actin loading control (Figure 4.17).

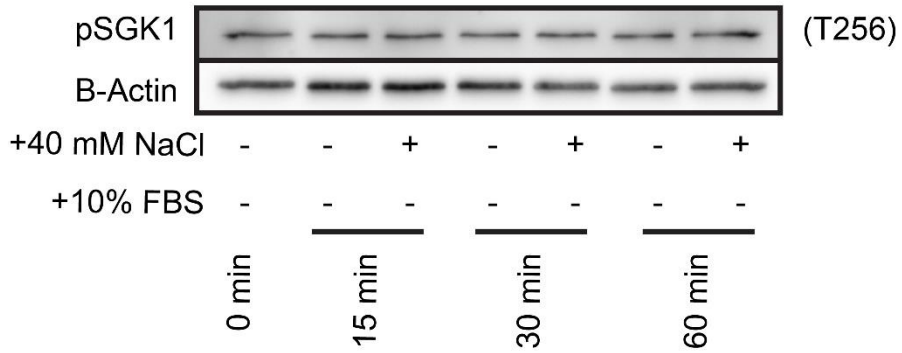

Figure 4.17 Phosphorylated SGK1 (Thr256 site) in porcine cartilage stimulated with NaCl. Protein was extracted with RIPA lysis buffer from porcine articular cartilage explants 0, 15, 30 or 60 minutes after stimulation with 40 mM additional NaCl in serum-free DMEM, and immunoblotted for phosphorylated SGK1 protein (T256) against a β-Actin housekeeper. Representative blot.

An additional phosphorylation site of SGK1 was investigated for regulation in response to sodium. Porcine explants were stimulated with 50 mM or 100 mM

additional NaCl in culture medium (originally containing physiological concentration of 137 mM NaCl). SGK1 was constitutively phosphorylated at the Ser422 site, and remained unchanged upon 50 mM and 100 mM NaCl stimulation for 15 minutes and 30 minutes (Figure 4.18).

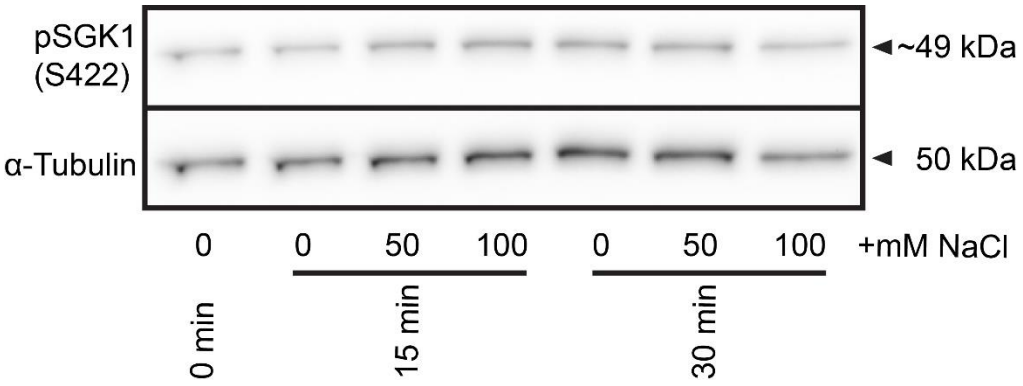

Figure 4.18 Phosphorylated SGK1 (Ser422 site) in porcine cartilage stimulated with NaCl. Protein was extracted with RIPA lysis buffer from porcine articular cartilage explants 0, 15 or 30 minutes after stimulation with 50 or 100 mM additional NaCl in serum-free DMEM, and immunoblotted for phosphorylated SGK1 protein (S422) against an α-Tubulin housekeeper. Representative blot.

Despite an upregulation of *SGK1* mRNA 1 h after explantation from the MCP joint, this was not demonstrated with exogenous sodium stimulation of chondrocytes. SGK1 protein was constitutively phosphorylated at sites Thr256 and Ser422 in porcine articular cartilage, but this phosphorylation was not regulated by injurious explantation or exogenous sodium stimulation.

4.3.5 Fluorescent sodium imaging with CoroNa green

As an alternative approach to finding a cellular biomarker for sodium sensing within cartilage, a sodium-sensitive fluorescent dye was utilised to directly measure extracellular sodium within the cartilage tissue. This was conducted in collaboration with Dr Jessica Mansfield and Professor Charles Peter Winlove at the University of Exeter.

A cell impermeant CoroNa green dye was optimised so that incubation time and dye concentration rendered changes in sodium detectable in culture medium, and the dye permeated the cartilage fully with no further dependence on time for dye incubation. Sodium concentrations, achieved by manipulation of NaCl content in PBS solution, were detectable within the physiological (137 mM NaCl) and supraphysiological range in medium with 10 µM CoroNa green dye (Figure 4.19).

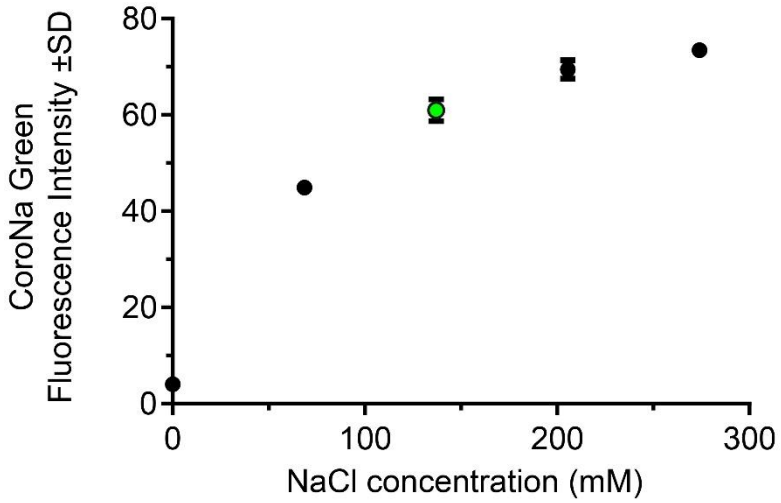

Figure 4.19 CoroNa green dye can detect physiological and supraphysiological sodium levels in solution. Fluorescent signal intensity of 10 µM CoroNa green dye (488 nm) in PBS solution with adjusted NaCl content (0 mM; 0x, 68.5 mM; 0.5x, 137 mM; 1x, 205.5 mM; 1.5x, 274 mM; 2x) compared to physiological content (green), measured by multiphoton microscopy.

Thick 2 mm sections of bovine articular cartilage, overlying bone, were visualised by multiphoton microscopy in a confined compression rig, saturated and submerged in 10 µM CoroNa green dye (Figure 4.20A). Intervals of increasing strain were measured by change in potential difference of a load cell, while relative sodium concentration was determined by measuring average fluorescent intensity in an area between consistent cellular landmarks of multiphoton microscopy images (Figure 4.20C). Increasing the strain on cartilage samples increased the sodium signal from two of six

samples (sample 1, 5); all other samples showed a modest reduction of sodium overall (Figure 4.20B).

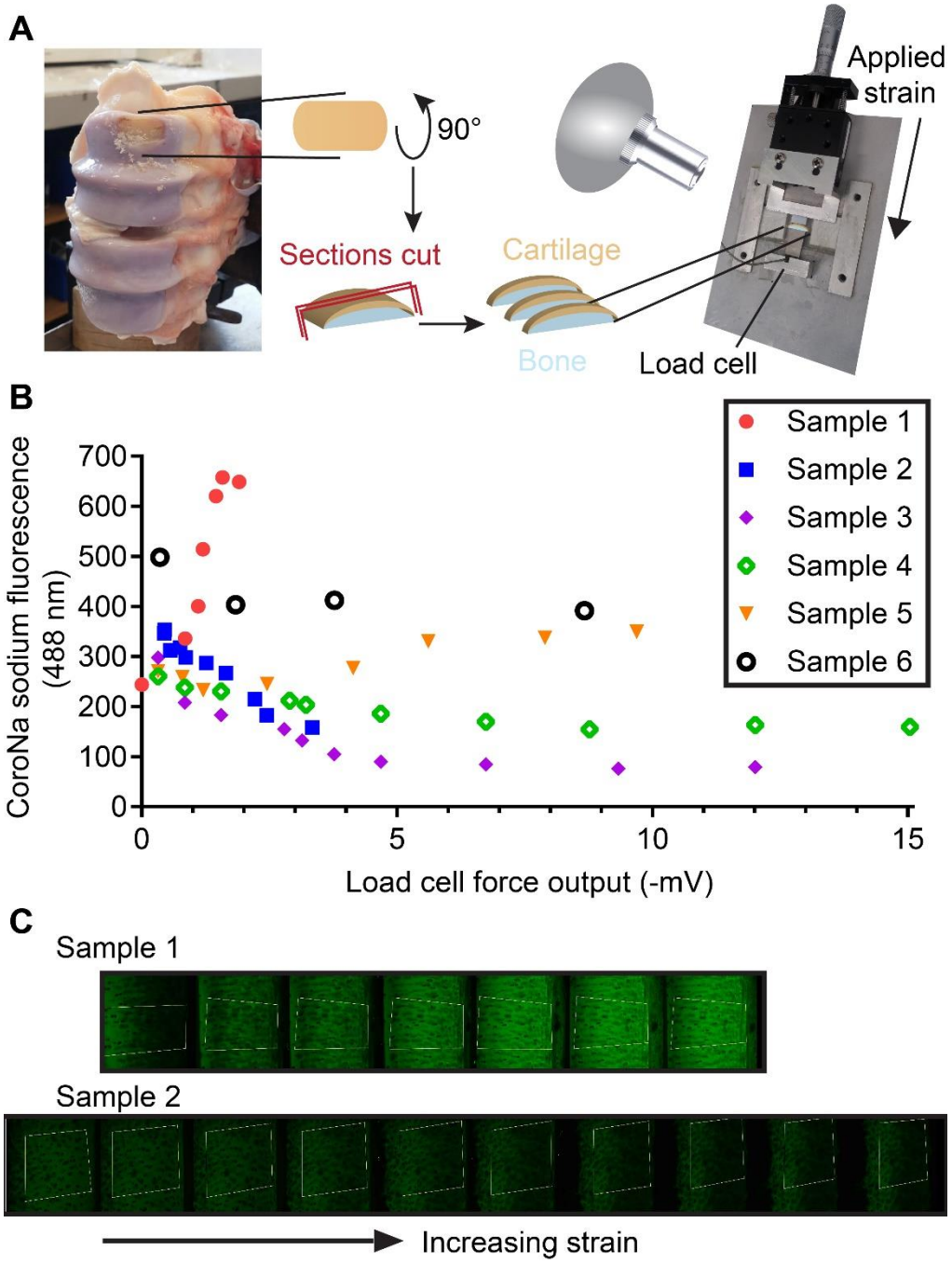

Figure 4.20 CoroNa green dye does not robustly detect sodium changes in cartilage upon compression. Bovine condyle samples of bone with overlying cartilage were prepared, sectioned at 2 mm intervals, and loaded onto a compression rig for multiphoton microscopy (A). CoroNa green sodium signal of samples, relative to measured force applied to cartilage by load cell, measured by multiphoton microscopy (B). Multiphoton images of sodium fluorescent intensity at increasing strain intervals (C), with measurement region in yellow from cell landmarks.

CoroNa green dye was not able to distinguish a robust trend of sodium dynamics upon compressive strain to articular cartilage. Alternative analyses were conducted with differing measurement regions, specific measurement of the pericellular matrix region and normalisation to the decrease in area caused by tissue compression, however results similarly did not show any robust trends.

4.3.6 Sodium ^{23}Na-MRI imaging in cartilage

An inability of methods to distinguish between sodium in a free state and in a bound state poses difficulties for observing sodium dynamics as a mechanism of responding to mechanical injury. Sodium MRI and spectroscopy techniques were utilised to overcome this limitation of other methods; multiple quantum filtering can determine sodium behaviour relative to macromolecules, discerning between free and interacting sodium. Sodium MRI imaging was conducted in collaboration with Dr Christopher Philp and Associate Professor Galina Pavlovskaya at the Sir Peter Mansfield Imaging Centre, University of Nottingham.

Free and bound sodium fractions were imaged by sodium magnetic resonance imaging (^{23}Na-MRI) and quantified by sodium triple-quantum time proportional phase incrementation (TQ-TPPI) magnetic resonance spectroscopy (MRS) in porcine articular cartilage before, during and after compressive load. In all images sodium signal was detected within the articular cartilage, but not subchondral bone (Figure 4.21B). Multiple quantum filtering discerned bound sodium ions from the free fraction of sodium, demonstrating that at resting state the total amount of sodium in the tissue was 51% free and 48% bound by mean average. Upon compression (28% strain), free sodium significantly increased by 46% (Uncompressed=0.52, Compressed=0.75,

p=0.0052), with a reciprocal change in bound sodium ($F(2,9)=9.709$, $p=0.0057$) (Figure 4.21C). Upon relaxation of the tissue, the total free and bound sodium fractions partially recovered towards uncompressed levels, indicating a dynamic and reversible flux of sodium after compression. The region of highest free sodium intensity in the tissue, when uncompressed, was located in the middle zone. Upon compression, free sodium signal shifted towards the superficial zone (Figure 4.21B). Regional variations of sodium flux were observed within the tissue upon compression, with an increase in free sodium upon compression of confined cartilage just below the superficial zone.

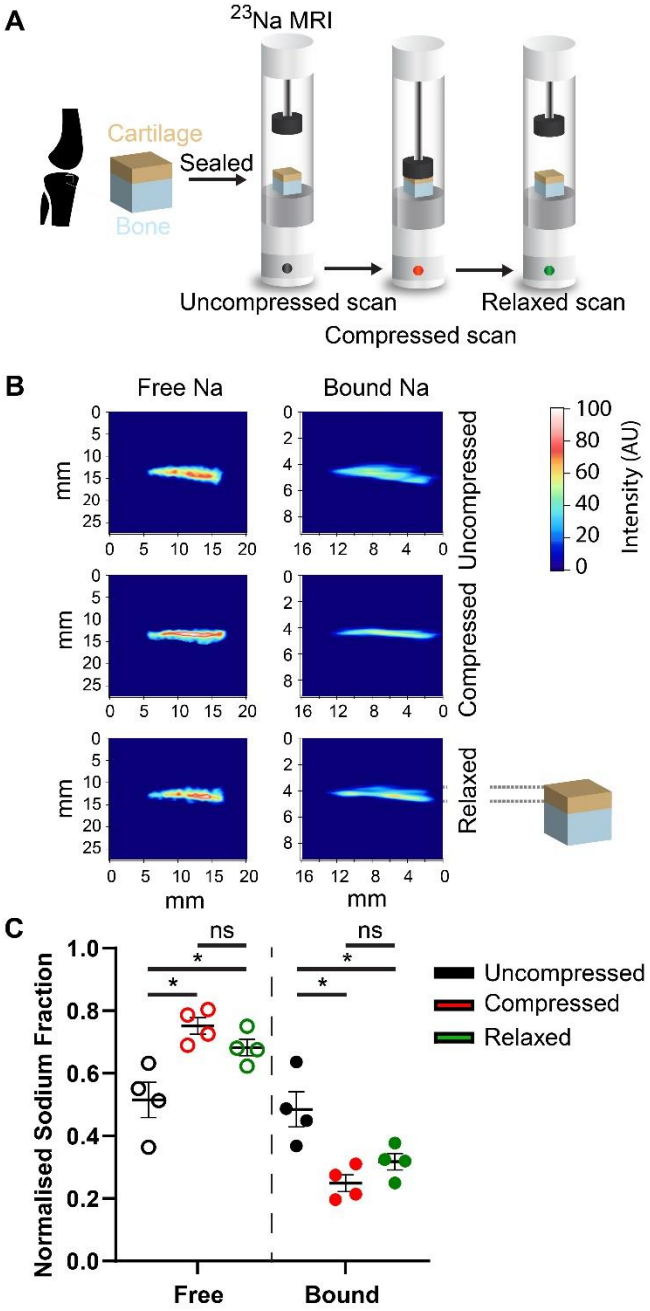

Figure 4.21 ^{23}Na-MRI imaging and spectroscopy of loaded articular cartilage. (A) Schematic of how osteochondral plugs were taken from the medial tibial plateau and vacuum-sealed for 23Na MRI microimaging under uncompressed, compressed and relaxed conditions. (B) Porcine osteochondral plugs were scanned with a Bruker 9.4T Ultra-high field microimaging system for free sodium and bound sodium (MQF filtering). Cartilage was then mechanically loaded with compression of 28% deformation and scanned (compressed). Cartilage was then relaxed with no mechanical load and scanned (relaxed). Scan orientation was with cartilage surface facing upwards, with a single compression uniformly perpendicular to the cartilage surface. Representative scans shown. (C) Relative free and bound sodium fractions of total sodium were quantified with spectroscopy before, during and after compression (n=4). One-way ANOVA with Tukey multiple comparisons (*p≤0.05, **p≤0.01).

4.4 Discussion

This chapter investigated the potential role of extracellular matrix sodium in the release of growth factors from heparan sulfate in the pericellular matrix of cartilage. HDGF shared commonalities with other heparin-binding growth factor molecules of the cartilage PCM: shared rapid release upon injury, release from heparan sulfate in cartilage (Figure 3.14, Figure 3.15) and identification in the PCM by microarray (Tang *et al.*, 2018). This indicated a possible shared mechanism of release upon injury. As injurious release of these growth factors was independent of cellular processes (Figure 3.8, Figure 3.7), and occurred in dead cartilage, this chapter tested a biophysical hypothesis. This was formed based on three factors: NaCl is able to electrostatically compete for the binding interactions of these PCM growth factors with heparin, cartilage tissue has a high extracellular concentration of sodium, and the PCM is devoid of chondroitin sulfate, the major contributor of sodium sequestration in cartilage, by immunohistochemistry. These factors could allow for a flux of free sodium in the cartilage matrix upon injury of the tissue, elicited by the mechanically compressive component of injury. This would free sodium from abundant bound stores on chondroitin sulfate in the TM, causing a local relative increase in free sodium in isotonic areas of the extracellular matrix (i.e. the PCM). At sufficient levels, sodium could electrostatically displace growth factors bound to heparan sulfate.

There are undoubtedly structural differences between the PCM and adjacent TM of the cartilage matrix. Results from our lab show the distinct colocalisation of type VI collagen with the PCM, and the exclusion of type II collagen and aggrecan (visualised by CS stub after chondroitinase treatment) from the PCM, specifically found in the TM (Figure 4.1). This might suggest a high fixed charge density in the TM relative to

the PCM, as the hundreds of chondroitin sulfate chains on aggrecan molecules confer the predominant fixed charge density of cartilage tissue, whereas the cell surface and PCM proteoglycans have less sulfated glycosaminoglycan chains (Maroudas, 1972). Hyaluronic acid, the attachment glycosaminoglycan for aggrecan, can be found attached to the cell surface (Scrimgeour *et al.*, 2017), but link protein attachment sites for aggrecan are abundant in the further removed matrix (Poole *et al.*, 1982). Aggrecanase nor chondroitinase treatment alter the elastic modulus of the PCM, despite reducing further removed extracellular matrix moduli (Wilusz and Guilak, 2014). This indicates either a resistance of the PCM to enzymatic degradation, or relatively low levels of aggrecan and chondroitin sulfate in the PCM. However, others have imaged chondroitin-6-sulfate in the chondron (Wang, El Haj and Kuiper, 2008), and safranin O staining shows intense staining around the PCM, indicating a high fixed charge density (Stockwell, 1970; Korhonen *et al.*, 2011; Ojanen *et al.*, 2018). However, brightfield macro-scale microscopy of metachromatic dyes might not be sufficient to distinguish the thin pericellular matrix. $CaCl_2$ x-ray microprobe analysis, shows increased fixed charge density in the outer rim of the pericellular matrix (Maroudas, 1972), suggesting this might be further removed than the pericellular matrix itself. More recently the introduction of chondroitin sulfate and biomimetic proteoglycans (similar charge density and water uptake as natural proteoglycans, but do not have the same sites for enzymatic degradation) shows selective diffusion to the pericellular matrix within cartilage. This is reversed in severely osteoarthritic tissue (when ECM fixed charge density is lost) where the chondroitin sulfate and biomimetic proteoglycans are found enhanced outside of the PCM, in favour of the territorial and interterritorial matrix (Phillips *et al.*, 2019). This would indicate a higher fixed charge

density in the PCM. The concurrent exclusion of type II collagen from the PCM in Figure 4.1 is corroborated with collagen II-targeted nanoparticle introduction to articular cartilage, where the collagen VI-rich PCM does not immobilise the nanoparticles (Rothenfluh *et al.*, 2008). Further, collagenase digestion of cartilage tissue completely degrades the further removed extracellular matrix but leaves the chondron intact (Guilak *et al.*, 1999), corroborating collagen II exclusion from the PCM.

Manipulation of sodium in cartilage tissue was achieved in two ways; exogenous sodium was added to cultured *ex vivo* cartilage tissue, or the bound sodium, sequestered in the matrix by chondroitin sulfate, was depleted by IL-1 induction of aggrecanase. Addition of exogenous sodium caused dose dependent release of heparin-binding growth factors from cartilage, comparable to that released by injury, and was able to augment the amount released with simultaneous recutting injury (Figure 4.2). This occurred in dead and live tissue, reinforcing the biophysical nature of this mechanism, independent of cellular activities. These data are consistent with the knowledge that NaCl can elute growth factors on a heparin column (Figure 3.16). The data were also in keeping with a matrix dependent mechanism of release, independent of cellular activity, as NaCl was able to release growth factors from dead cartilage (Figure 4.3).

Studies report heparin-binding affinities of HDGF and FGF2 based on heparin column affinity chromatography, corresponding to NaCl elution concentrations of approximately 0.75 M and 1.39 M respectively (Chiu *et al.*, 2014). However, exogenous NaCl was able to release these growth factors at concentrations below this

in cartilage. Affinity for heparan sulfate in cartilage could be lower *in vivo*, as heparan sulfate GAGs are less sulfated than heparin, due to different post-translational modifications, and therefore have lower electrostatic binding attraction (Handel *et al.*, 2005; Olczyk, Mencner and Komosinska-Vassev, 2015). As the normal extracellular sodium concentration is greater than 240 mM in human articular cartilage (Urban, Hall and Gehl, 1993; Shapiro *et al.*, 2002), this might be sufficient to provide enough free sodium for growth factor displacement. Relative binding affinities of the growth factors were explored in the next chapter.

Bashir, Gray and Burstein (1996) measured NMR tissue sodium concentrations of control and IL-1 degraded articular cartilage (11 days) at 280 mM and 166 mM, respectively, directly confirming the ability of IL-1 to deplete tissue sodium. Depletion of sodium from cartilage in Section 4.3.2 reduced the amount of HDGF, CTGF and FGF2 growth factors released from cartilage upon recutting injury. This agrees with the hypothesis that the injurious release of heparan sulfate bound growth factors from the PCM is sodium-dependent, however there are limitations to the model of depletion. The effects of IL-1 treatment other than on sodium sequestration were examined by monitoring content and regulation of the growth factors during the treatment period. Between IL-1 treated and untreated samples, *HDGF* and *CTGF* mRNA were not downregulated by treatment, although *FGF2* was downregulated at day 7. Also, all three growth factors were at comparable protein levels after depletion, except FGF2 which, despite mRNA downregulation, was increased in the matrix when measured by ELISA. In this respect, the reduction in growth factor release was not a consequence of growth factor downregulation in the tissue. Although this does not account for other possible complex and off-target signalling effects of IL-1, the strong reduction of

growth factor release upon injury in depleted explants points to sodium sequestered in the matrix as the mechanism of release.

These models of sodium release do not distinguish whether there is a sodium threshold needed to release the particular growth factors, or whether they are released in a dose dependent manner. If released at a threshold, one would expect partial depletion of proteoglycan to have a differential effect on the release of growth factors upon injury based on their affinity or electrostatic threshold. However, partial depletion with IL-1 did not show any distinct trends of growth factor release upon injury. The partial depletion shown by safranin O in Figure 4.8B might not have been great enough to reduce the fixed charge density below this threshold. Another approach to investigating thresholds of sodium-mediated release would be to test growth factor release with different magnitudes of injury. Postulating that the mechanical aspect of injury mediates sodium dependent release of growth factors, one could mechanically load cartilage at different thresholds and find the load at which each growth factor is released from the tissue.

Other physiological aspects of the tissue might also contribute to growth factor release. Evans and Quinn (2005) show a correlation of large (500+ kDa) solute diffusivities with explant GAG density and fluid volume in statically compressed cartilage explants; their diffusivity decreases with tissue compression. Other studies show fluid transport does not significantly affect the rate of small solutes (e.g. sodium iodide), as diffusion coefficients are the dominant factor for small solutes (O'Hara, Urban and Maroudas, 1990). Diffusion occurs across a concentration gradient (δC) and is defined

by Fick's law of diffusive flux (J), with diffusion coefficient (D m^2/s), solute concentration (C) and path distance (x):

$$J = D\frac{\delta C}{\delta x}$$

The other solute transport force is convection, which is also highly dependent on tissue structure, loading conditions and fluid flow. Solute diffusivity decreases with increasing solute size, rendering convection the dominant influence for large solutes (e.g. growth factors) (O'Hara, Urban and Maroudas, 1990; Jackson and Gu, 2009). The Peclet number (Pe) can define convection in cartilage; Pe < 1 favours diffusion, whereas Pe > 1 favours convection. Pe is based on characteristic fluid velocity (U), diffusion distance (L), and diffusivity of solute (D) (Deen, 1998):

$$Pe = UL/D$$

Finally, hydraulic permeability affects fluid flow and is a measure of volumetric flow rate (Q, m^3/s), pressure difference across the sample (Δp), permeation area (A) and sample thickness (h). Hydraulic permeability is related to water content (increases in OA, allowing more water expulsion upon compression), fixed charge density (decreases in OA, due to proteoglycan loss), ion diffusivities and water:matrix frictional coefficient in the tissue (Maroudas and Freeman, 1979). Upon cartilage compression, fluid flows away from loaded regions to unloaded regions and is expelled from the tissue (Linn and Sokoloff, 1965). Whilst fluid flow would not contribute to sodium flux, it might contribute to the release of heparan sulfate bound growth factors from cartilage. However, the significant increase in water expulsion and fluid flow with osteoarthritis progression was not accompanied by an increase in growth factor

release. It is possible the high matrix sodium concentration in non-osteoarthritic tissue, locally increased upon compression, competes with the binding of growth factors to heparan sulfate, allowing fluid flow to carry the large growth factor molecules. Despite an increase in water and fluid flow in osteoarthritic tissue, the growth factor binding potential to heparan sulfate remain strong.

The IL-1 model of sodium depletion is somewhat recapitulated in the pathological context of osteoarthritis. During osteoarthritis progression, aggrecan loss occurs at early stages, depleting the cartilage tissue of proteoglycan. This can be observed histologically by metachromatic staining (Figure 4.9), and more recently can be observed clinically using a host of MRI-based techniques (Widhalm *et al.*, 2016). This loss of proteoglycan, corroborated with osteoarthritic cartilage digests by DMMB assay, showed severity of osteoarthritis inversely correlated with GAG content (Figure 4.11). Further, when samples were stratified by undamaged or severely diseased criteria, it was shown that severely diseased cartilage released less growth factor than undamaged regions with less disease (Figure 4.12). This release was not a consequence of differing growth factor content between samples, as despite releasing less of each of these growth factors upon injury, the severely osteoarthritic tissue consistently contained more protein extractable from the matrix by 2.5 M NaCl (Figure 4.13). Furthermore, the subsequent protein extractable from the whole tissue, by dissociative lysis buffer, was comparable between samples of differing disease severity. These data are in agreement with independent studies, including CTGF visualisation by Nishida *et al*. (2004), detecting CTGF protein throughout cartilage of normal, early OA, moderate OA and severe OA patients (Omoto *et al.*, 2004). Overall, these data indicate that matrix growth factor content increases with OA progression, but the ability of the

cartilage to release them upon injury from the PCM diminishes. Further, evidence suggests aggrecanase activity and loss of fixed charge density may precede structural damage and MMP-activity (Little et al., 2009), indicating this concurrent loss of growth factor availability might occur prior to structural damage, at a key early temporal window in osteoarthritis progression. However, early disease tissue retained the ability to release growth factor upon injury (Figure 4.12), suggesting the loss of growth factor release may only occur in late disease. This proposed mechanism of growth factor release upon cartilage injury, due to aggrecan-dependent sodium flux, is therefore lost in osteoarthritis and the bioavailability of these growth factors likely has severe implications on cartilage repair.

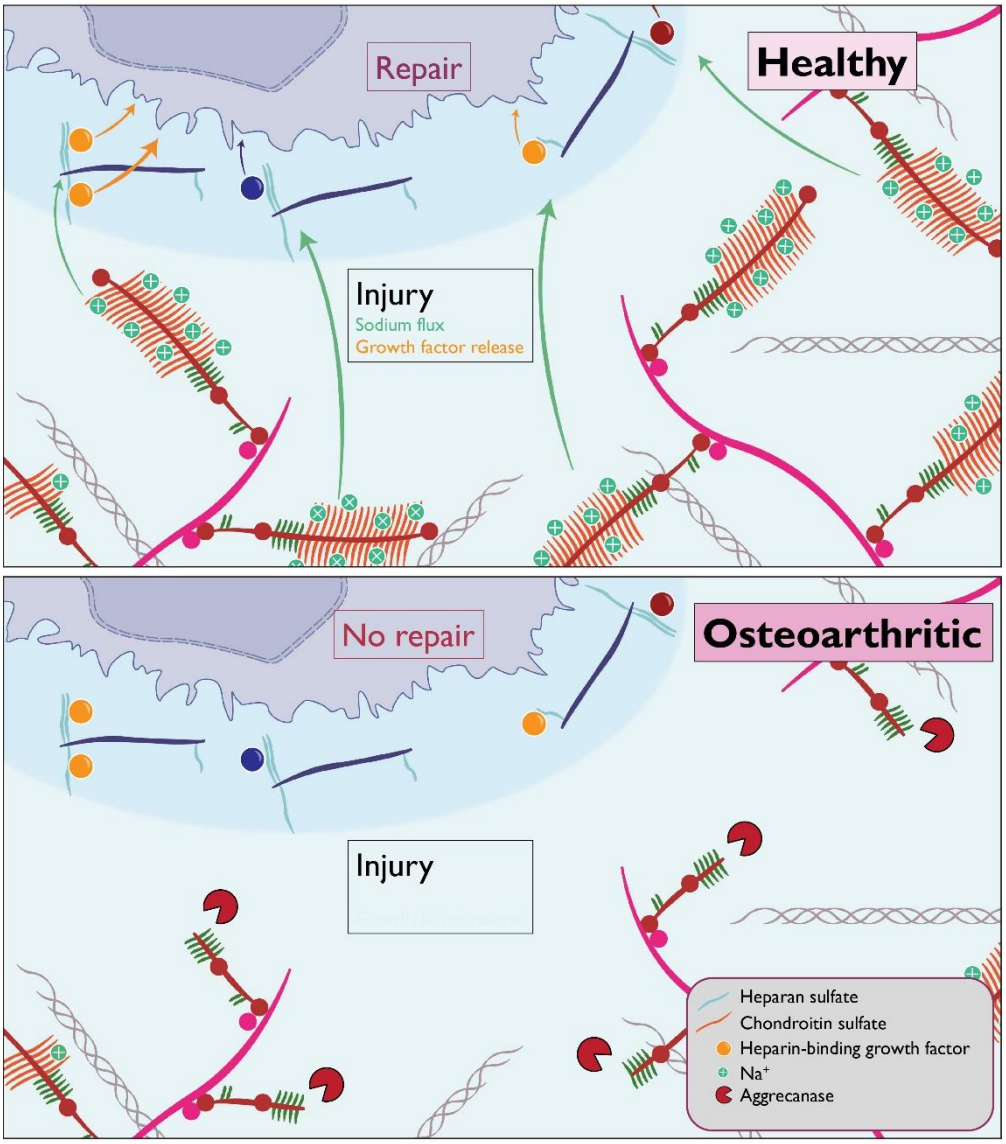

Figure 4.22 Proposed injury response mechanism of sodium flux and growth factor release in normal and osteoarthritic cartilage. Severely osteoarthritic cartilage with reduced fixed charge cannot exhibit a sodium flux upon injury, causing a loss of ability to release heparan sulfate bound PCM growth factors.

Independent studies have modelled cation fluxes and showed marked differences between healthy and pathological cartilage. With osteoarthritis progression, cation flux lowered within the whole cartilage sample, especially in the upper surface (Manzano *et al.*, 2015). This is in keeping with a sodium flux towards the upper regions, which is lost in osteoarthritis, being a driver of growth factor release. Progression of osteoarthritis is also accompanied by loss of the collagen network, which leads to water

intake and swelling (Venn and Maroudas, 1977). This further highlights a potential contribution of fluid flow to the release of these factors upon injury.

Having demonstrated the release growth factors upon injury is dependent on sodium, matrix sodium was directly visualised within the cartilage.

Firstly, it was tested whether SGK1 could act as a biomarker for extracellular sodium changes within the tissue. SGK1 is established as a salt-sensing kinase in $CD4^+$ T cells, showing significant upregulation of *SGK1* upon treatment with 40 mM NaCl (Wu et al., 2013), and in T_H17 cells where NaCl stimulation increased SGK1 protein (Kleinewietfeld et al., 2013). *SGK1* mRNA expression was upregulated 1 h after injurious explantation. It was speculated this upregulation might be due to a sensing of sodium upon injury. This was tested by transient exogenous sodium stimulation. *SGK1* gene expression and SGK1 protein, tested against multiple activating phosphorylation sites, were not regulated by NaCl stimulation. It is plausible the NaCl addition did not recapitulate the sodium concentration or temporal aspects of an injury induced sodium flux. An additional 150 mM NaCl was added transiently for 2 minutes to cartilage explants to ensure tissue penetration, and an additional 40 mM to isolated chondrocytes to recapitulate the NaCl concentrations of Kleinewietfeld *et al.*, 2013. Longer, non-transient stimulations with NaCl were also conducted but showed no effect on *SGK1* (data not shown). A physiological matrix sodium flux might occur much quicker, could be highly concentrated at a local region of cartilage, and might not be sensed by the cell in the same way as upon exogenous addition of NaCl. Further, it was not feasible to measure *SGK1* mRNA and SGK1 protein at all time points with

high temporal resolution, and therefore the detection methodology might miss a rapid increase of *SGK1* at a different time point.

Visualisation of sodium was attempted with a fluorescent dye; a plethora of options have been developed and optimised, including SBFI, Sodium Green, CoroNa Green and CoroNa Red. The sodium selective fluorescent cationic dye CoroNa Green was utilised, selected for its brighter intensity, exhibiting larger changes in fluorescence after binding of sodium as compared to SBFI and Sodium Green. It is also available in a cell-impermeant form, allowing the measurement of matrix sodium without intracellular contribution. Additionally, CoroNa green exhibits a wide dynamic range of fluorescence, unlike SBFI which saturates at 100 mM and is not suitable for measuring extracellular sodium (Ruckh *et al.*, 2013). The dye was used to measure matrix sodium in bovine cartilage upon compression, to simulate the compressive aspect of mechanical injury. Despite optimisation to detect changes in sodium from physiological to supraphysiological levels (Figure 4.19), it did not reproducibly show a sodium flux (Figure 4.20). One difficulty encountered was the change in position and shape of the cartilage tissue upon compression; bulging of strained cartilage in the plane of the microscope objective altered the field of view, and in some cases caused portions of the imaged area to become deeper or shallower than the plane of focus. Of importance, imaging deeper into the tissue, although possible by multiphoton microscopy, decreases signal intensity detectable due to dye obstruction by tissue depth. This was partly overcome by acquiring z-stack images, and post-hoc analysis of sodium content based on cellular landmarks, to ensure equivalent depths of tissue were being measured, but bulging could explain the steady but subtle decline in sodium intensity in those heavily strained samples not exhibiting increases in sodium intensity

(Figure 4.20B). A consideration of sodium dyes is the selectivity of sodium over other cations; CoroNa green is less selective for sodium over potassium than Sodium Green (Table 1.3). Although the hypothesis tested states sodium as a driver for growth factor displacement, feasibly this could be achieved by other cations in the extracellular space. However, the established abundance of sodium in the ECM of tissues and cartilage suggest sodium would be the greater contributor of all physiological ions. Finally, one possible limitation regarding the use of a dye reporter for sodium is the relationship between the dye binding sodium in a 'free' and 'bound' state. The effect of the dye on bound sodium populations (i.e. interacting with charged proteoglycan structures in the matrix), nor the selectivity of binding free ions over bound species, are clearly established; this is less relevant in intracellular contexts without macromolecular structures to sequester pools of bound sodium ions.

Many of the aforementioned limitations in sodium imaging were overcome with the use of sodium MRI and spectroscopy to image whole cartilage explants. This imaging technique is not dependent on dye or contrast agent concentration, does not have limitations with changes in depth or plane of tissue imaging, and importantly can distinguish between free and bound sodium fractions with multiple-quantum filtering (MQF). The quadrupolar nature of a sodium nucleus allows capture of changes in sodium molecular dynamics when freely moving sodium ions come into contact with molecular surfaces and slow down. This slowing down can be captured by sodium multiple-quantum coherence filtering technique that leaves out MR signals produced by sodium ions undergoing fast isotropic motion, therefore filtering out signal from free sodium ions. This was first demonstrated in a phantom model of living tissues, using Ficoll to simulate proteoglycan moieties of the matrix, and BSA to simulate

proteins that do not contribute to charge, chemical ion exchange or sodium binding (Whang *et al.*, 1994). Addition of Ficoll (proxy for binding sites) increases double quantum filtered signal (bound sodium) and decreases single quantum filtered signal, whereas addition of BSA does not increase double quantum filtered signal or diminish the single quantum filtered signal, highlighting the potential of multiple quantum filtering to distinguish between free and bound sodium compartments. Previous studies demonstrate that sensitivity of multiple quantum filtering techniques is apt for detecting motional anisotropies in biological systems (Shinar *et al.*, 1993; Mouaddab *et al.*, 2007; Yang and Momot, 2016). ^{23}Na-MRI reproducibly measured an increase in free sodium with a simultaneous decrease in bound sodium upon cartilage compression (Figure 4.21C), indicative of a mechanically dependent sodium flux. This was visualised by MRI, distinguishing bound sodium by applying a MQ filter before localisation, confirming a shift in free sodium most evident just below the surface layer. Others have demonstrated that the fixed charge density reduces the compressibility of cartilage, consistent with the notion that the region just below the surface is both lower in FCD and more likely to compress upon load (S. S. Chen *et al.*, 2001). This region might selectively lose water, causing a local increase in free sodium and this drives growth factor release when compression is applied, in keeping with confined models of fluid flow with variable fixed charge density (Yao and Gu, 2004; Manzano et al., 2015). At this stage, it is difficult to ascertain whether this mechanism and sodium flux is simply due to a change in ambient sodium concentration or whether fluid flow is part of the release mechanism.

In normal cartilage tissue, the area of observed sodium flux just below the surface has reduced fixed charge density (Maroudas and Freeman, 1979; S. S. Chen *et al.*, 2001),

increased permeability (Maroudas and Bollough, 1968), and is more likely to compress upon load (Schinagl *et al.*, 1997; S. S. Chen *et al.*, 2001; Yang and Momot, 2016). It is also where the tissue exhibits high cation fluxes (Manzano *et al.*, 2015). The proposed hypothesis is that fluid flow away from more readily compressed regions to unloaded regions (Linn and Sokoloff, 1965) results in local concentration of free sodium in compressed areas, able to displace growth factors from the PCM. Fluid flow is also high in osteoarthritic tissue which loses its fixed charge density, has a lower compressive modulus (more susceptible to compression) and becomes more permeable (Armstrong and Mow, 1982; Mow, Ratcliffe and Poole, 1992; DiDomenico, Lintz and Bonassar, 2018). This allows growth factor release upon mechanical injury in early disease, which is lost in severe disease when sodium is no longer present in the tissue due to proteoglycan loss. The increased susceptibility of the PCM to mechanical load (Wilusz, Zauscher and Guilak, 2013) and altered proteoglycan content compared to the further removed matrix might also play a role in regional sodium flux.

In conclusion, these data demonstrate a sodium-dependent mechanism of growth factor release upon cartilage injury, which can be visualised as a regional mobilisation of free sodium upon mechanical compression. This mechanism is lost in osteoarthritis, highlighting potential implications for these growth factors in disease pathogenesis. Functional relevance of CTGF and FGF2 in osteoarthritis have been explored in other studies, but HDGF remains unexplored in this context. The next chapter investigates the unknown function of HDGF in cartilage and osteoarthritis, to understand functional implications of this sodium dependent release mechanism.

5 Function of HDGF in Cartilage

5.1 Introduction

The release of growth factors by an aggrecan dependent sodium flux upon cartilage injury, that is lost in osteoarthritis, has major implications for the understanding, treatment and prevention of the disease. CTGF and FGF2 have both previously been explored in cartilage, implicating them in chondrogenesis (Handorf and Li, 2011; Correa *et al.*, 2015), homeostasis (Otsuki *et al.*, 2010), cartilage repair (Nishida *et al.*, 2004; Yamamoto *et al.*, 2004; Cucchiarini *et al.*, 2005) and disease progression (Chia *et al.*, 2009; Tang *et al.*, 2018). However, little is known about the role of HDGF in cartilage. This chapter aims to investigate the possible functions of HDGF in the knee joint and articular cartilage, and to assess whether this novel growth factor might play a role in osteoarthritis pathogenesis.

A constitutive knockout *Hdgf* $^{-/-}$ mouse strain originally developed by Professor Franken, University of Bonn (Gallitzendoerfer *et al.*, 2008), was used as a model to test HDGF dependence in cartilage injury and osteoarthritis. *Hdgf* $^{-/-}$ mice express *Hdgf* with exons 2–6 deleted, targeted by homologous recombination into embryonic stem cells. The original strain of mice are viable with no apparent morphological abnormalities, with no difference in weight up to 6 weeks of age. Further, cultured dermal fibroblasts from the *Hdgf*-deficient mice show no altered proliferation or TNFα-induced apoptosis compared to wildtype fibroblast cells (Gallitzendoerfer *et al.*, 2008). Despite being morphologically and skeletally normal at birth, assessed by alizarin red and alcian blue skeletal staining on postnatal day (P) 10, there plausibly could be more minute changes at the joint level. As the *Hdgf* $^{-/-}$ mice have not been

challenged with injury models or assessed over longer periods of time, little is known about how loss of HDGF affects the response of cartilage to injury, the development or progression of OA, and the effects of ageing. As previously shown, HDGF is released from human cartilage (Figure 3.5) and mouse cartilage (Figure 3.4) in the same manner. Furthermore, human cartilage seems to lose its propensity to release HDGF with the development of osteoarthritis (Figure 4.12). This highlighted a potential role of HDGF in the joint, which could be investigated using models of cartilage injury and OA in *Hdgf* $^{-/-}$ mice.

Researchers have not previously investigated the role of HDGF in the context of cartilage. Despite demonstrable effects of HDGF's role in other tissues, the mechanism of action remains elusive and its receptor unknown.

This chapter investigated morphological changes in *Hdgf* $^{-/-}$ mice over time, including body weight, cartilage thickness, and disease progression in a surgical model of osteoarthritis. In addition, gene expression changes were assessed upon cartilage injury using a hip avulsion injury model. Finally, the functional potential of heparin-binding growth factors was investigated in adipose-derived mesenchymal stem cells (MSCs), capable of chondrogenic differentiation and a potential autologous method of osteoarthritis therapy.

Chapter Aim

Investigate the effect of HDGF on the mouse joint

Hypotheses

- Constitutive knockout of *Hdgf* in mice affects joint morphology and osteoarthritis susceptibility
- Constitutive knockout of *Hdgf* in mice alters differential gene expression upon cartilage injury
- Heparin-binding growth factors stimulate progenitor cells of the joint

5.2 Methods

5.2.1 Cartilage injury

5.2.1.1 Hip avulsion model

Mice at 5–6 weeks of age were culled by CO_2 asphyxiation and confirmatory cervical dislocation. Mice were skinned from the midriff downwards; the leg was extended and the quadriceps muscle cut to the point of the femoral artery to expose the hip joint. Ligaments were cut to expose the femoral head. Sterile forceps were used to squeeze the sides of the femoral head to release the articular cartilage from the bone epiphysis.

For 0 h time-points, hips were placed in 50 µl RNAlater solution, frozen on dry ice and stored at -80 °C. Hips collected for time point experiments were washed in serum-free DMEM (SF-DMEM) then placed into a 96-well round bottom plate well containing 100 µl of SF-DMEM. Hip cartilage was then injured by cutting once with a 10-blade scalpel (Swann-Morton, Sheffield, UK), then cultured in an incubator at 37 °C, 5% CO_2 for 4 or 24 h. Hips were then transferred to 50 µl RNAlater solution, frozen on dry ice and stored at -80 °C. Two hips were pooled per sample for RNA isolation as per section 2.3.2.

5.2.1.2 Destabilisation of the medial meniscus

Destabilisation of the medial meniscus (DMM) was performed on 10 week old mice by Jadwiga Zarebska as previously described (Glasson *et al.*, 2005), depicted in Figure 5.1. After the full effect of anaesthesia was achieved, the right hindlimb was shaved and the animal transferred to a sterile surface under a dissection microscope for surgery. The limb was sterilised with iodine before a 5–8mm incision was made using a sterile 15-blade scalpel (Swann-Morten, Sheffield, UK) on the midline starting at the

superior end of the patella. Using a 3 mm size 15 ophthalmic scalpel (MSP, Puerto Rico), a medial para-patellar incision was made to cut through the fascia protecting the joint capsule. This incision could potentially lead to some mild bleeding, which was halted by applying pressure on the wound using sterile cotton swabs. The meniscotibial ligament, which connects the meniscal horn to the tibial plateau, was visually identified and cut using the same scalpel. Successful transection of the meniscotibial ligament was confirmed visually, before closing the joint capsule using absorbable 6/0 Vicryl sutures (Ethicon, Belgium). The wound was subsequently closed using two to three stitches with 5/0 Ethilon sutures (Ethicon, Belgium).

Sham surgeries used the same procedure as DMM, however, after visualisation of the meniscotibial ligament, there was no transection and instead the wound was closed again.

Mice were sacrificed for histological analysis of the joint 8 weeks or 12 weeks post-surgery.

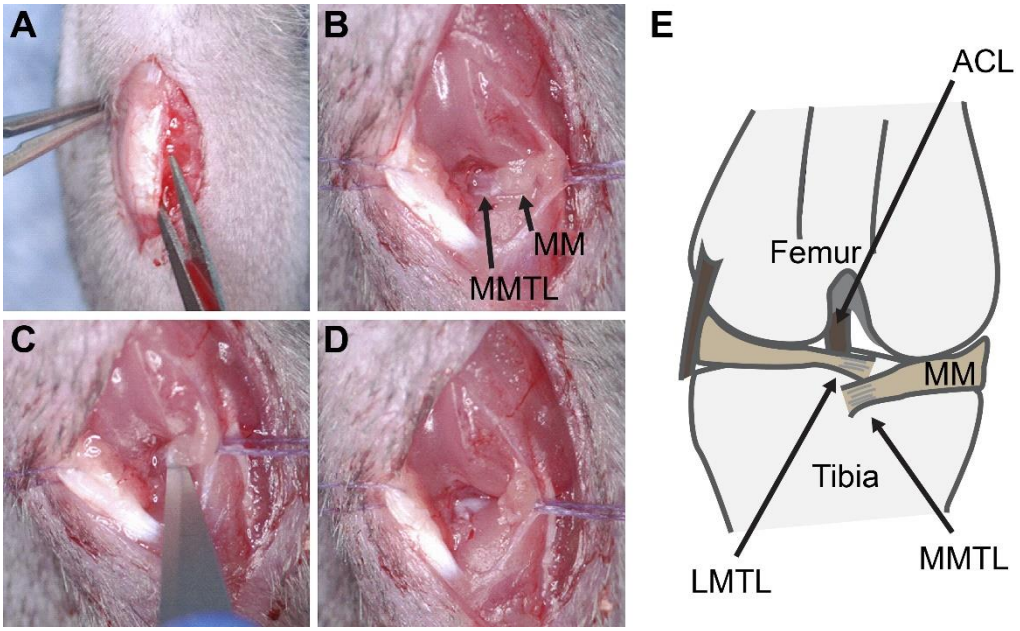

Figure 5.1 Destabilisation of the medial meniscus surgery. Opening of the right mouse knee joint capsule (A). Identification of the medial meniscus (MM) and medial meniscotibial ligament (MMTL) (B). Transection of the meniscotibial ligament (C). Confirmation of destabilisation of the medial meniscus (D). Schematic of the normal right knee joint (E). Anterior (cranial) cruciate ligament (ACL), lateral meniscotibial ligament (LMTL). Reproduced with permission from (Glasson, Blanchet and Morris, 2007).

5.2.2 Histology

5.2.2.1 DMM staining

Whole mouse knees were collected by cutting the muscles and bones distal to the tibia and proximal to the femur. The joints were carefully dissected of any remaining muscle and then fixed in 10% neutral buffered formalin (CellPath, Newtown, UK) for 24 h. Knees were decalcified for seven days in 20% formic acid plus 10% formalin. Joints were then processed using a Tissue-Tek VIP (Sakura, California, USA). The processing sequence was in the following order: formalin changed once, 70% alcohol, 100% alcohol changed five times, xylene changed three times, molten paraffin wax changed four times. Knees were embedded in paraffin wax, as per section 2.6.1, with the patella facing the bottom of the mould. Coronal sections of 4 µm were cut using

an Accu-Cut SRM 200 microtome (Sakura, Torrance, California, USA), at 80 µm intervals throughout the knee before Safranin O staining as per section 2.6.2.

5.2.2.2 Histological OA scoring

Histological scoring followed a modified OARSI scoring system and was consistently performed by two scorers who were blinded throughout the scoring process. Two independent assessors scored the coronal knee sections using a semi-quantitative scoring system for each section, as described in Table 5.1. For every joint, at least six sections were assessed in their medial and lateral compartments as well as the tibial and femoral surface, resulting in four scores per section (sub-subscores). The summed score resulted in one final score per section (subscore). The three sections with the highest subscores were added to generate the final score for each joint. If scores between assessors differed, a third independent assessor was included to reach a consensus upon review.

Table 5.1 Modified OARSI histological osteoarthritis scoring system

Grade	**Observation**
0	Normal
0.5	Loss of proteoglycan (Safranin O) without structural change
1	Superficial fibrillation without loss of cartilage
2	Loss of superficial cartilage
3	Cartilage delamination at the tidemark
5	Loss of tissue extending into the calcified cartilage
6	Loss of tissue extending into subchondral bone

5.2.2.3 Cartilage thickness

Mouse knees from 18 week old mice were prepared as in section 5.2.2.1, resulting in coronal sections stained with Safranin O as per section 2.6.2. Three consecutive 80 µm interval sections were selected from the middle of the joint based on anatomical reference of the medial meniscus. Cartilage thickness was measured from the top of

the articular surface to the beginning of the subchondral bone. Average measurements were taken as the mean of three point measurements across the articular cartilage, perpendicular to the articular surface. Maximal cartilage thickness was measured at the thickest region of cartilage, excluding the peripheries of the plateau. Images were captured on the Olympus BX71 microscope and section images were measured using ImageJ software (Schneider, Rasband and Eliceiri, 2012).

5.2.3 TaqMan microfluidic cards

RNA from hip avulsion cartilage of wildtype and *Hdgf*$^{-/-}$ mice was extracted from 2 hips of one mouse, pooled for one sample, as per Section 2.3.2. RNA was reverse transcribed from a volume of 200 ng as per Section 2.4.1. Cartilage cDNA was run on custom TaqMan low density array fluidic gene cards with primers for genes listed in Table 5.2, as per Section 2.4.4. 0 h, 4 h and 24 h post-injury samples for wildtype and *Hdgf* $^{-/-}$spanned two separate cards with 36 overlapping genes, and used BMPR2 as a housekeeper based on the 18S profile (Figure 5.2).

Table 5.2 Microfluidic array gene list

Gene	**Assay ID**	**0 h Samples**	**4 h Samples**	**24 h Samples**
Adamts1	Mm00477355_m1	✓	✓	✓
Adamts5	Mm00478620_m1	✓	✓	✓
Adamts4	Mm00556068_m1	✓	✓	✓
Pmepa1	Mm00452229_m1	✓	✓	✓
Cd68	Mm03047340_m1	✓	✓	✓
Lrp1	Mm00464608_m1	✓	✓	✓
Ctgf	Mm01192932_g1	✓	✓	✓
Fgf2	Mm00433287_m1	✓	✓	✓
Inhba	Mm00434339_m1	✓	✓	✓
Ngf	Mm00443039_m1	✓	✓	✓
Timp1	Mm00441818_m1	✓	✓	✓
Tac1	Mm01166996_m1	✓	✓	✓
Tnfrsf12a	Mm00489103_m1	✓	✓	✓

Fgfr1	Mm00438930_m1	✓	✓	✓
Fgfr2	Mm00438941_m1	✓	✓	✓
Fgfr3	Mm00433294_m1	✓	✓	✓
Bmpr2	Mm00432134_m1	✓	✓	✓
Mmp19	Mm00491300_m1	✓	✓	✓
Trpv4	Mm01203726_m1	✓	✓	✓
Il6	Mm00446190_m1	✓	✓	✓
Il1a	Mm00439620_m1	✓	✓	✓
Il1b	Mm00434228_m1	✓	✓	✓
Ccr2	Mm01216173_m1	✓	✓	✓
Arg1	Mm00475988_m1	✓	✓	✓
Npy	Mm03048253_m1	✓	✓	✓
Has1	Mm03048195_m1	✓	✓	✓
Mmp13	Mm00439491_m1	✓	✓	✓
Mmp3	Mm00440295_m1	✓	✓	✓
Ptgs2	Mm00478374_m1	✓	✓	✓
Ltbp2	Mm01307379_m1	✓	✓	✓
Tnfaip6	Mm00493736_m1	✓	✓	✓
Bdkrb1	Mm04207315_s1	✓	✓	✓
Bdkrb2	Mm00437788_s1	✓	✓	✓
Tgfbr1	Mm00436964_m1	✓	✓	✓
Tgfbr2	Mm00436977_m1	✓	✓	✓
Tgfbr3	Mm00803538_m1	✓	✓	✓
Fgf18	Mm00433286_m1	✓	✓	✓
GAPDH	Hs99999905_m1	✓	✓	✓
Fgfr4	Mm01341852_m1	✓	✓	✓
Agtr2	Mm01341373_m1	✓	✓	✓
Tgfb1	Mm01178820_m1	✓	✓	✓
Tgfb2	Mm00436955_m1	✓	✓	✓
Tgfb3	Mm00436960_m1	✓	✓	✓
Ltbp1	Mm00498234_m1	✓	✓	✓
Cyp26a1	Mm00514486_m1	✓	✓	✓
Cyp26b1	Mm00558507_m1	✓	✓	✓
Cyp26c1	Mm03412454_m1	✓	✓	✓
Aldh1a2	Mm00501306_m1	✓	✓	✓
Adamts15	Mm01176187_m1	✓	✓	✗
Has2	Mm00515089_m1	✓	✓	✗
18S	Hs99999901_s1	✓	✓	✗
Il33	Mm00505403_m1	✓	✓	✗
Sost	Mm04208528_m1	✓	✓	✗
Tnc	Mm00495662_m1	✓	✓	✗
Tnn	Mm01284101_m1	✓	✓	✗
Fmod	Mm00491215_m1	✓	✓	✗

Ccl2	Mm00441242_m1	✓	✓	✗
Wnt16	Mm00446420_m1	✓	✓	✗
Tgfbi	Mm01337605_m1	✓	✓	✗
Tspan2	Mm00510514_m1	✓	✓	✗

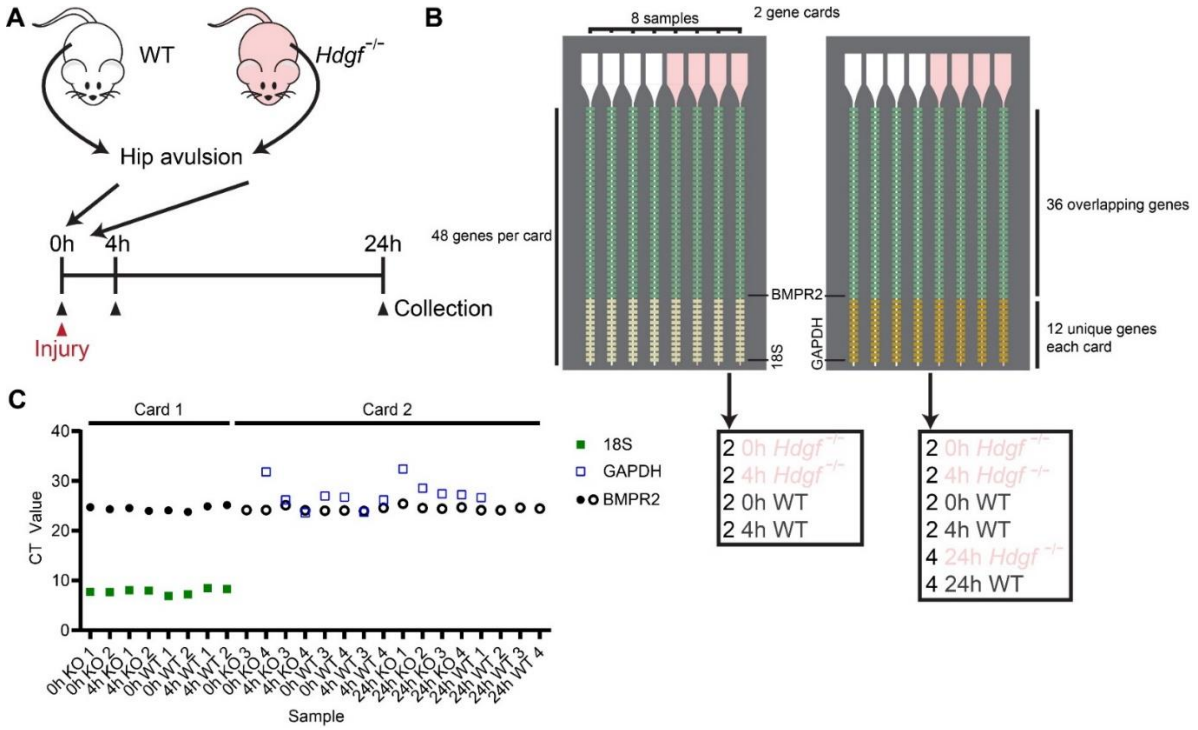

Figure 5.2 GAPDH is an inconsistent housekeeper, whereas 18S and BMPR2 are consistent housekeepers in mouse hip avulsion. Hip avulsion experiment schematic (A) Hips from wildtype and *Hdgf* $^{-/-}$ were avulsed and injured, then mRNA extracted for TaqMan gene array after 0, 4 or 24 h. TaqMan gene array cards (B). CT values of potential housekeeper genes (C). GAPDH was inconsistent across samples, and 18S was consistent but not present on both array cards; BMPR2 was consistent with 18S, so used as housekeeper. Two custom array cards were used for mRNA analysis, with 36 overlapping genes for n=4 samples.

5.2.4 Heparin column chromatography

Injury conditioned medium was generated by explanting and further injuring cartilage as per section 2.2.1. 30 min post-injury, the injury conditioned medium from 5 g cartilage tissue was collected in 10 ml SF-DMEM. 10 ml conditioned medium was filtered with a 20 µM filter syringe and used for heparin affinity chromatography as per section 2.5.5. Heparin-binding proteins were eluted with a NaCl gradient between 0–2.5 M NaCl into 1 ml fractions. Injury conditioned medium starting material, flowthrough material and elution gradient fractions were collected and analysed by Western blot. Flowthrough and elution fractions containing heparin-binding proteins were dialysed in dH_2O using Float-A-Lyzer G2 Dialysis Devices (3.5–5 kDa MW cutoff). Elution fractions were pooled as specified, based on growth factor content by elution. Starting material, flowthrough material and elution fractions were diluted 1:1 in serum-free αMEM and used to stimulate adipose-tissue derived MSCs.

5.2.5 Adipose tissue-derived mesenchymal stem cell stimulation

Adipose tissue dissection and derivation of MSCs was performed as described in Section 2.1.4. Cells were counted after serum-starvation, then stimulated with various conditions. Cells from each condition were counted after 48 h by brightfield microscopy, using image capture and ImageJ software.

In Figure 5.9, cells were stimulated with starting material, flow through material and pooled elution fractions from heparin affinity chromatography of injury conditioned medium, described in Section 5.2.4.

In Figure 5.10, cells were stimulated using 1 ml of SF-αMEM containing a combination of reagents listed in Table 5.3, as specified by experimental conditions.

Table 5.3 Adipose tissue-derived mesenchymal stem cell stimulation conditions

Stimulus	**Concentration**	**Source**
Injury conditioned medium (Section 2.2.1)	1 g porcine cartilage tissue per 1 ml	Cartilage explantation with further cutting injury
FGFR inhibitor (SB402451)	250 nM	GSK, London, UK
TGFβR inhibitor (SB431542)	10 µM	Bio-Techne, Minnesota, USA
Recombinant human FGF2 (bFGF)	20 µg/ml	Peprotech, New Jersey, USA
Recombinant human TGFβ3	10 ng/ml	Bio-Techne, Minnesota, USA

5.3 Results

5.3.1 Phenotype of the *Hdgf* $^{-/-}$ knockout joint

Hdgf $^{-/-}$ and wildtype mice were monitored for physiological differences during biological development. *Hdgf* $^{-/-}$ mice were not overtly morphologically or skeletally different to wildtype mice at birth. Homozygous *Hdgf* $^{-/-}$ knockout mice were used as breeding pairs, bred from *Hdgf* $^{+/-}$ heterozygous mice received as embryos.

Overall body weight of *Hdgf* $^{-/-}$ mice bred in-house were statistically significantly different to in-house wildtype C57BL6/J mice by two-way ANOVA ($F(2,109)=100.5$, $p<0.0001$). *Hdgf* knockout mice exhibited a significantly greater body weight measured at 6 weeks ($p=0.0014$), 10 weeks ($p<0.0001$) and 18 weeks ($p<0.0001$) (Figure 5.3). Heavy *Hdgf* $^{-/-}$ mice had noticeable amounts of subcutaneous fat on the body and upon dissection.

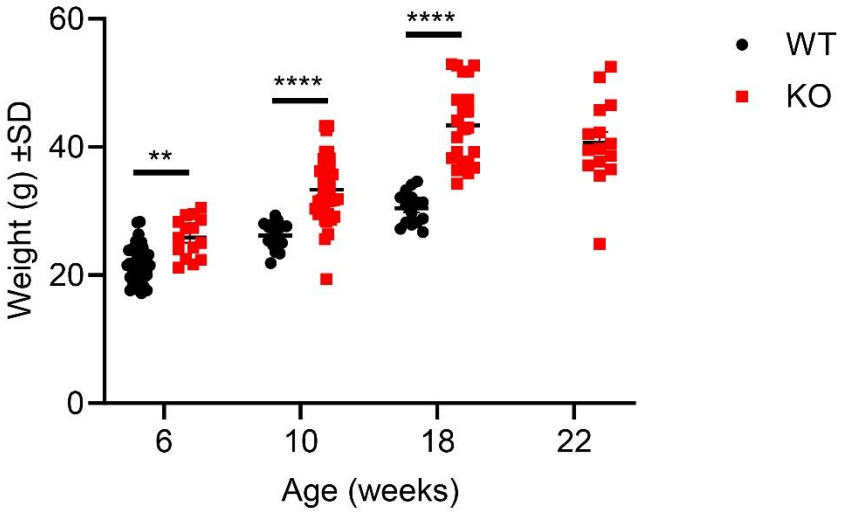

Figure 5.3 HDGF knockout mice gain more body weight than in-house C57BL6/J wildtype mice over time. Body weight of *Hdgf* $^{-/-}$ C57BL6/N mice and wildtype C57BL6/J mice 6 weeks, 10 weeks and 18 weeks after birth, with additional *Hdgf* $^{-/-}$ mouse body weight measurement at 22 weeks. Two-way ANOVA with Sidak correction for multiple comparisons (**$p\leq0.01$, ****$p\leq0.0001$).

In addition to increased body weight, histological analysis of knee joints revealed large cystic regions in the bone marrow of *Hdgf* $^{-/-}$ mice at 18 weeks and 22 weeks, which were not present in wildtype mice (Figure 5.4). These regions were circular, well corticated with bone marrow lining and exhibited a similar appearance to adipose deposits. Other histological artefacts adjacent to calcified bone regions and of indistinct border were not considered cysts. Small cysts (≤ 70 µm) were present in 94% of all *Hdgf* $^{-/-}$ mice processed for histology (Figure 5.4 red arrowheads), and 80 % of wildtype mice. Large cysts (> 70 µm) were found in 66% of *Hdgf* $^{-/-}$ mice, but were not present in wildtype mice (Figure 5.4 black arrowheads).

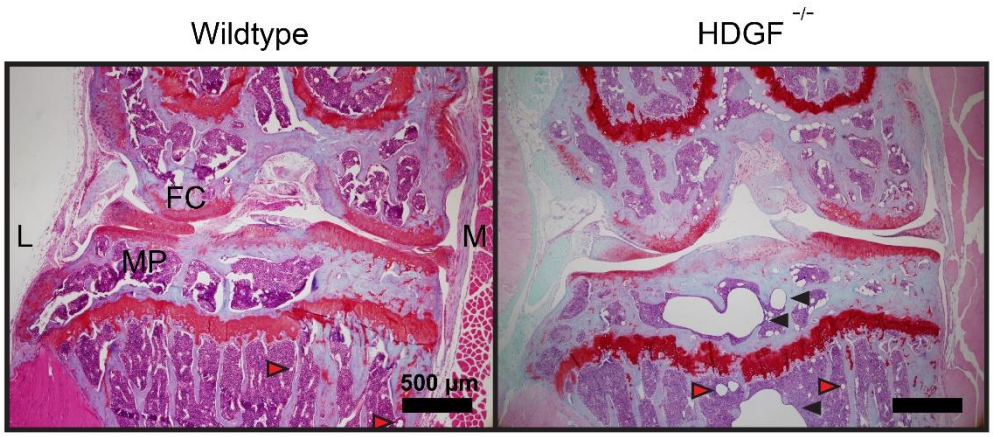

Figure 5.4 *Hdgf* $^{-/-}$ mice have cystic lesions in the bone marrow not present in wildtype mice. 18 week old mouse representative images of wildtype (C57BL6/J) and *Hdgf* $^{-/-}$ (C57BL6/N) mouse knee joint histology. Representative images with small (red) and large (black) cysts marked by arrowheads, lateral (L), medial (M), femoral condyle (FC), medial plateau (MP), scale 500 µm.

Cartilage thickness was measured in 18 week old *Hdgf* $^{-/-}$ knockout mice and compared to that of wildtype C57BL6/J mice. *Hdgf* $^{-/-}$ mice had thinner lateral and medial tibial cartilage than wildtype (Figure 5.5). Differences were more pronounced on the lateral plateau. Both wildtype and *Hdgf* $^{-/-}$ mice had thicker cartilage on their medial plateau (WT 113.3 µm ±10.9 SD, *Hdgf* $^{-/-}$ 104.8 µm ±10.3 SD) compared to lateral sides (WT

96.6 µm ±7.5 SD, *Hdgf* $^{-/-}$ 65.6 µm ±12.0 SD). *Hdgf* $^{-/-}$ mice exhibited a greater difference between lateral and medial thickness (Δ 39.2 µm, 37.4%) than in wildtype mice (Δ 16.7 µm, 14.7%).

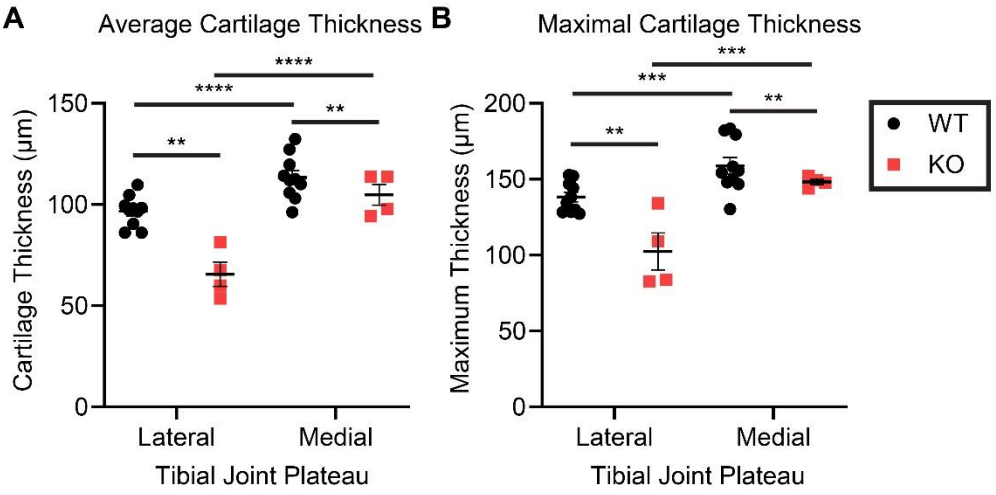

Figure 5.5 *Hdgf* $^{-/-}$ C57BL6/N mice have thinner average cartilage and maximal cartilage measurements at 18 weeks than wildtype C57BL6/J mice at 22 weeks. Histological measurement of tibial plateau cartilage by Safranin O stain brightfield microscopy in wildtype (WT) and *Hdgf* $^{-/-}$ (KO) mice (n=10,4). Two-Way ANOVA with Sidak multiple comparisons test (**p≤0.01, ***p≤0.001, ****p≤0.0001).

5.3.2 HDGF in a surgical model of osteoarthritis

Hdgf $^{-/-}$ mice were challenged with a surgical model of osteoarthritis (DMM) to investigate the effect of HDGF on disease progression and severity.

Hdgf $^{-/-}$ mice and wildtype mice underwent destabilisation of the medial meniscus (DMM) surgery at 10 weeks of age. Some mice were sham operated, performing all aspects of the surgery except medial meniscus destabilisation, as a negative control. Osteoarthritis severity was assessed by histology and OARSI scoring either 8 weeks or 12 weeks post-surgery (Figure 5.6).

Significant differences were observed 8 weeks after DMM surgery ($F(3,31)=12.75$, $p<0.0001$) between mean modified OARSI scores of sham and DMM, and between DMM scores of wildtype and *Hdgf* $^{-/-}$ mice by one-way ANOVA. DMM operated mice had statistically significantly higher mean scores than respective sham mice in wildtype (WT DMM,Sham; Mean=15,5; n=13,5; p=0.0276) and *Hdgf* $^{-/-}$ (*Hdgf* $^{-/-}$ DMM,Sham; Mean=24,10; n=12,6; p=0.0006) groups. *Hdgf* $^{-/-}$ mice 8 weeks post-DMM exhibited a significantly higher mean modified OARSI score than the wildtype DMM (WT,*Hdgf* $^{-/-}$; Mean=15,24; n=13,12 p=0.008) (Figure 5.6C).

Statistically significant differences were also observed 12 weeks after DMM surgery ($F(3,28)=8.939$, $p=0.0003$) between mean modified OARSI scores of sham mice and DMM mice. DMM operated scores remained statistically significantly higher than respective sham mice in wildtype (WT DMM,Sham; Mean=24,11; n=11,6; p=0.0292) and *Hdgf* $^{-/-}$ (*Hdgf* $^{-/-}$ DMM,Sham; Mean=29,10; n=9,6; p=0.0015) groups. However, DMM operated wildtype and *Hdgf* $^{-/-}$ scores were not significantly different 12 weeks post-DMM (WT,*Hdgf* $^{-/-}$; Mean=24,29; n=11,9; p=0.4777) (Figure 5.6D).

Osteoarthritis severity increased for both genotypes between 8 weeks and 12 weeks post-surgery. *Hdgf* $^{-/-}$ sham mice maintained a mean OARSI score of 10, both 8 weeks and 12 weeks post-surgery. Wildtype sham scores increased from 5 to 11 between 8 weeks and 12 weeks post-DMM. *Hdgf* $^{-/-}$ mice exhibited more severe OA early after DMM surgery, after 8 weeks, but this difference diminished by 12 weeks post-surgery.

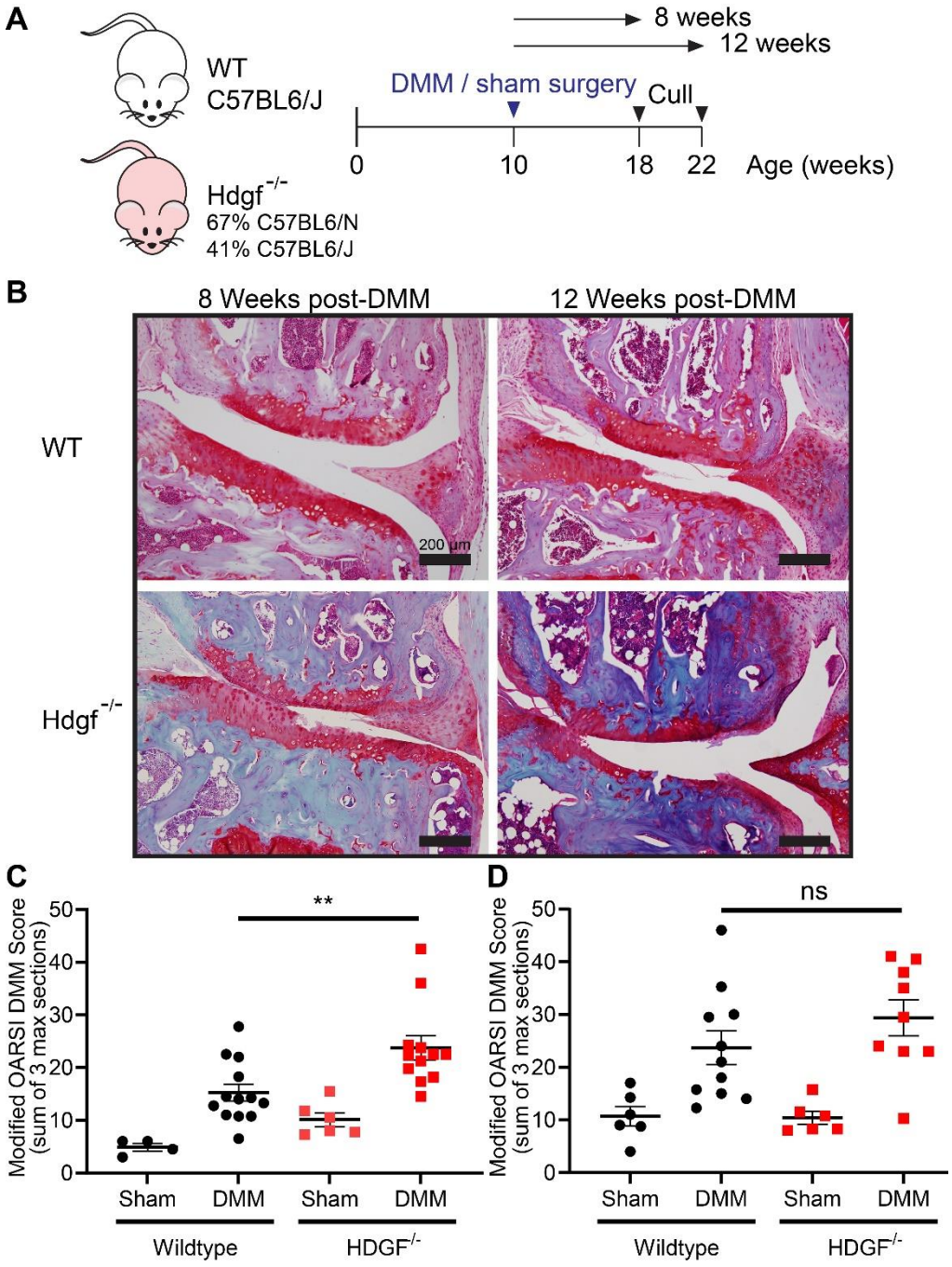

Figure 5.6 *Hdgf* knockout mice develop severe OA early after DMM surgery. Destabilisation of the medial meniscus (OA model) surgery was conducted in 10 week old wildtype and *Hdgf* $^{-/-}$ mice, culled 8 weeks or 12 weeks post-surgery for histological analysis (A). Representative Safranin O stained images of Wildtype (WT) and *Hdgf* $^{-/-}$ mouse medial joint sections (cartilage, red) (B). Modified OARSI scores (mean ± SEM) of sham (n=6) and DMM-operated (n=13) mice of wildtype and *Hdgf* $^{-/-}$ genotype, 8 weeks post-surgery (C) and 12 weeks post-surgery (D). One-Way ANOVA with Tukey Test post-hoc comparisons; DMM comparative statistics displayed (ns=non-significant, **p≤0.01).

5.3.3 Genetic substrain influence on mouse weight

Observational differences in the *Hdgf* $^{-/-}$ mouse joint prompted investigation into the background genetic composition of the mice. Microsatellite analysis of 128 SNPs confirmed substrain differences between the *Hdgf* $^{-/-}$ mice and in-house wildtype strain used as a comparator. *Hdgf* $^{-/-}$ mice were on average 69.0% homologous to a C57BL6/J-OlaHsd substrain, 66.9% homologous to a C57BL6/N-Crl substrain, whilst only 41.2% homologous to in-house C57BL6/J wildtype comparator mice. This indicates genetic discrepancy that could confound differences observed in experiments from Section 5.3.1 and Section 5.3.2.

Hdgf $^{-/-}$ C57BL6/N mice were backcrossed with C57BL6/J mice for two generations, resulting in a 75% convergence to C57BL6/J genetic background, prior to gene expression experiments. With an initial 41.2% C57BL6/J background, the expected result would be 89.7% similarity. This partial backcross offered a reasonable amount of genetic similarity within a feasible timeframe, but at least nine crossbreeding generations are needed for a full backcross.

$$Genetic\ Background\ \% = 100 - (\frac{\%\ similarity}{2^{Backcrosses}})$$

Partially backcrossing *Hdgf* $^{-/-}$ mice onto the C57BL6/J substrain decreased mean body weight at 6 weeks of age from 25.60 g (±3.10 SD) to 24.15 g (±3.54 SD) (ns, p=0.318). However, these mice remained significantly heavier than wildtype mice (*, p=0.0325). Substrain differences might account for some difference in body weight, but partial backcrossing did not significantly reverse weight differences of *Hdgf* knockout.

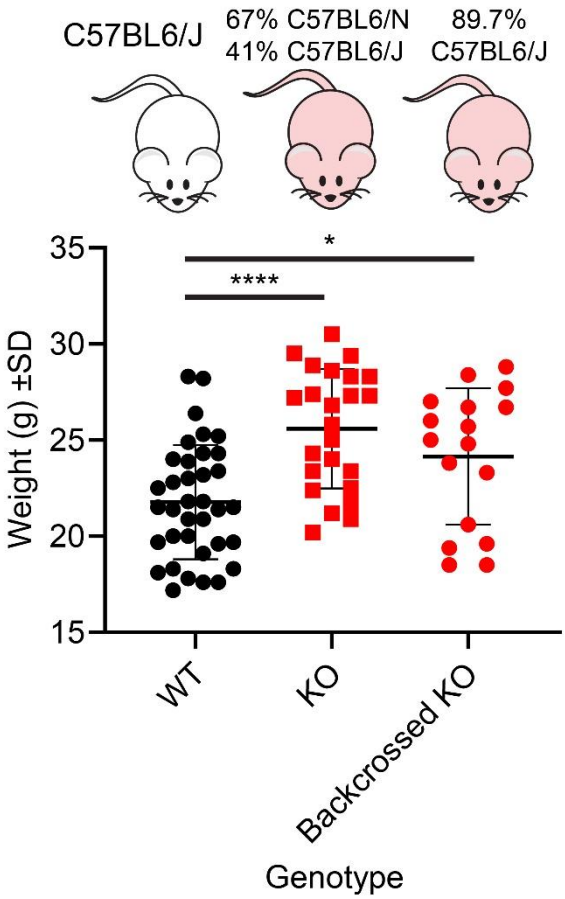

Figure 5.7 Body weight differences between *Hdgf* $^{-/-}$ and wildtype mice diminish when backcrossed onto a C57BL6/J background. Body weight of wildtype C57BL6/J (WT), *Hdgf* $^{-/-}$ C57BL6/N (KO) and 2-generation backcrossed *Hdgf* $^{-/-}$ C57BL6/J mice (Backcrossed KO) at 6 weeks. Mean and standard deviation, One-Way ANOVA with Tukey Test post-hoc comparisons (*p≤0.05, ****p≤0.0001).

5.3.4 Altered gene regulation in *Hdgf* knockout mice upon cartilage injury

At 6 weeks of age, articular cartilage was avulsed from the hips of wildtype and *Hdgf* $^{-/-}$ mice. Cartilage was injured (cut once) and mRNA was extracted immediately, or following culture (in SF-DMEM) for 4 h or 24 h after injury. A total of 60 genes were measured by microfluidic TaqMan gene expression array, listed in Table 8.5. Due to differences in custom gene card configuration (Figure 5.2), 36 genes were investigated with sufficient sample size of n=4.

Gene expression of wildtype and Hdgf $^{-/-}$ mice 4 h and 24 h after hip avulsion with injury was compared to respective 0 h baseline gene expression. 35 genes were significantly regulated over time by hip avulsion injury (Table 5.4 - Injury). Of the genes regulated by injury, 3 genes showed an overall significant difference between wildtype and *Hdgf* $^{-/-}$ genotypes (Table 5.4 - Genotype).

Table 5.4 Genes significantly regulated by hip avulsion injury in wildtype and *Hdgf* $^{-/-}$ mice compared to respective 0h baseline expression

	Wildtype Fold Change to 0h		HDGF$^{-/-}$ Fold Change to 0h		ANOVA Significance	
Gene	**4h** Avulsion	**24h** Avulsion	**4h** Avulsion	**24h** Avulsion	**Injury**	**Genotype**
Ngf	122.45 ±31.73 SD	62.21 ±12.99 SD	89.19 ±29.87 SD	40.14 ±11.93 SD	****	*
Inhba	99.57 ±34.68 SD	12.5 ±2.97 SD	135.28 ±135.28 SD	14.13 ±14.13 SD	****	
Tnfaip6	85.6 ±52.39 SD	1.22 ±0.1 SD	111.8 ±35.28 SD	1.16 ±0.33 SD	****	
Ptgs2	39.05 ±11.27 SD	13.88 ±3.71 SD	46.36 ±14.85 SD	9.77 ±2.4 SD	****	
Tnfrsf12a	21.57 ±3.44 SD	3.86 ±0.99 SD	25.66 ±7.53 SD	4.93 ±0.95 SD	****	
Bdkrb1	17.36 ±4.92 SD	1.95 ±0.67 SD	22.23 ±5.14 SD	2.23 ±1.34 SD	****	
Has1	14.93 ±4.04 SD	0.81 ±0.33 SD	39.75 ±5.54 SD	1.48 ±0.3 SD	****	****
Il6	13.46 ±14.35 SD	2.59 ±2.91 SD	35.17 ±12.99 SD	5.61 ±14.21 SD	**	
Npy	8.51 ±1.29 SD	8.92 ±4.91 SD	10.56 ±4.29 SD	7.63 ±4.23 SD	***	
Bdkrb2	6.77 ±3.17 SD	3.58 ±1.62 SD	11.89 ±5.67 SD	6.12 ±1.95 SD	****	*
Timp1	6.61 ±2.07 SD	12.69 ±1.65 SD	7.65 ±1.71 SD	13.42 ±5.39 SD	****	
Il1b	6.6 ±8.75 SD	1.79 ±5.09 SD	7.28 ±3.63 SD	3.24 ±2.87 SD	*	
Adamts1	5.17 ±0.74 SD	0.96 ±0.39 SD	5.05 ±1.41 SD	0.75 ±0.15 SD	****	
Tgfb2	4.87 ±2.47 SD	2.24 ±0.76 SD	2.67 ±1.64 SD	1.23 ±0.34 SD	**	
Fgf2	4.84 ±0.82 SD	1.5 ±0.34 SD	8.64 ±5.24 SD	3.05 ±0.63 SD	***	
Arg1	3.98 ±14.22 SD	14.37 ±11.07 SD	9.29 ±8.35 SD	95.35 ±88.77 SD	*	
Ctgf	3.07 ±0.51 SD	2.37 ±0.39 SD	3.43 ±0.37 SD	2.87 ±0.48 SD	****	
Pmepa1	2.05 ±0.61 SD	0.81 ±0.1 SD	2.86 ±0.66 SD	0.97 ±0.11 SD	****	
Fgf18	2.04 ±0.85 SD	0.16 ±0.06 SD	4.21 ±2.25 SD	0.18 ±0.07 SD	***	
Ltbp1	1.97 ±0.66 SD	3.42 ±0.97 SD	1.41 ±0.64 SD	1.48 ±0.76 SD	*	
Mmp3	1.66 ±1 SD	11.22 ±12.53 SD	4.75 ±2.39 SD	8.8 ±5.54 SD	*	
Mmp19	1.27 ±0.55 SD	0.35 ±0.25 SD	1.63 ±0.44 SD	0.53 ±0.61 SD	**	
Fgfr1	1.22 ±0.15 SD	0.92 ±0.26 SD	1.05 ±0.21 SD	0.86 ±0.05 SD	*	
Cyp26b1	0.78 ±0.2 SD	0.32 ±0.06 SD	0.9 ±0.47 SD	0.32 ±0.12 SD	***	
Lrp1	0.73 ±0.1 SD	0.79 ±0.04 SD	0.87 ±0.12 SD	0.99 ±0.11 SD	*	
Tgfbr2	0.62 ±0.3 SD	0.37 ±0.06 SD	0.82 ±0.29 SD	0.56 ±0.09 SD	*	
Tgfbr1	0.59 ±0.1 SD	0.46 ±0.17 SD	0.87 ±0.26 SD	0.65 ±0.12 SD	**	
Ltbp2	0.59 ±0.3 SD	2.22 ±0.59 SD	0.18 ±0.72 SD	2.45 ±0.32 SD	****	
Fgfr3	0.58 ±0.17 SD	0.66 ±0.09 SD	0.6 ±0.37 SD	0.76 ±0.16 SD	*	
Fgfr4	0.57 ±0.3 SD	0.27 ±0.14 SD	0.75 ±0.26 SD	0.25 ±0.21 SD	***	
Tgfb3	0.54 ±0.27 SD	0.35 ±0.11 SD	0.48 ±0.32 SD	0.25 ±0.06 SD	****	
Fgfr2	0.47 ±0.11 SD	0.53 ±0.08 SD	0.49 ±0.22 SD	0.55 ±0.08 SD	**	
Tgfbr3	0.45 ±0.17 SD	0.58 ±0.2 SD	0.42 ±0.18 SD	0.55 ±0.19 SD	*	
Agtr2	0.43 ±0.34 SD	0.29 ±0.07 SD	0.31 ±0.4 SD	0.19 ±0.06 SD	***	
Ccr2	0.24 ±0.18 SD	0.05 ±0.09 SD	0.15 ±0.13 SD	0.05 ±0.07 SD	**	

Fold change relative to 0h baseline gene expression of respective genotype, only significant genes are displayed (red ≥20% upregulation, blue ≥20% downregulation, regardless of significance), statistical significance analysed by Two-Way ANOVA with Tukey Test post-hoc comparisons.

Has1 ($F(1,18)=54.55$, $p<0.0001$), *Bdkrb2* ($F(1,18)=4.752$), $p=0.428$) and *Ngf* ($F(1,18)=5.570$, $p=5.570$) genes showed significant differential expression by genotype in *Hdgf* $^{-/-}$ mouse hip avulsion compared with wildtype mice (Figure 5.8).

Has1 expression (Figure 5.8A) was significantly upregulated 4 h after hip avulsion injury in wildtype mice ($M=14.93$, $p<0.001$) and *Hdgf* $^{-/-}$ mice ($M=39.75$, $p<0.0001$), but relative expression in *Hdgf* $^{-/-}$ mice was significantly greater at 4 h ($M=39.75$, $p<0.0001$) compared to wildtype. Both wildtype and *Hdgf* $^{-/-}$ expression of *Has1* returned to baseline by 24 h, but *Hdgf* $^{-/-}$ mice exhibited a significantly greater 4 h response to injury.

Bdkrb2 expression (Figure 5.8B) was not significantly upregulated in wildtype mice at 4 h ($M=6.77$, $p=0.0955$) or 24 h ($M=3.58$, $p=0.7963$), but was significantly upregulated in *Hdgf* $^{-/-}$ mice 4 h after avulsion injury ($M=11.89$, $p=0.0005$). The injury response of *Bdkrb2* mRNA was significantly greater in *Hdgf* $^{-/-}$ mice than wildtype mice.

Ngf expression (Figure 5.8C) in wildtype mice was significantly upregulated at 4 h ($M=122.45$, $p<0.0001$) and 24 h ($M=62.21$, $p=0.0031$). *Hdgf* $^{-/-}$ mice exhibited a significant increase 4 h after avulsion injury ($M=89.19$, $p<0.0001$), but not at 24 h ($M=40.14$, $p=0.0856$). Post-hoc comparisons did not identify significant differences between equivalent time points of wildtype and *Hdgf* $^{-/-}$ mice, but the overall response of *Ngf* to injury was significantly less than wildtype.

No significance by genotype was found in genes downregulated upon hip avulsion injury.

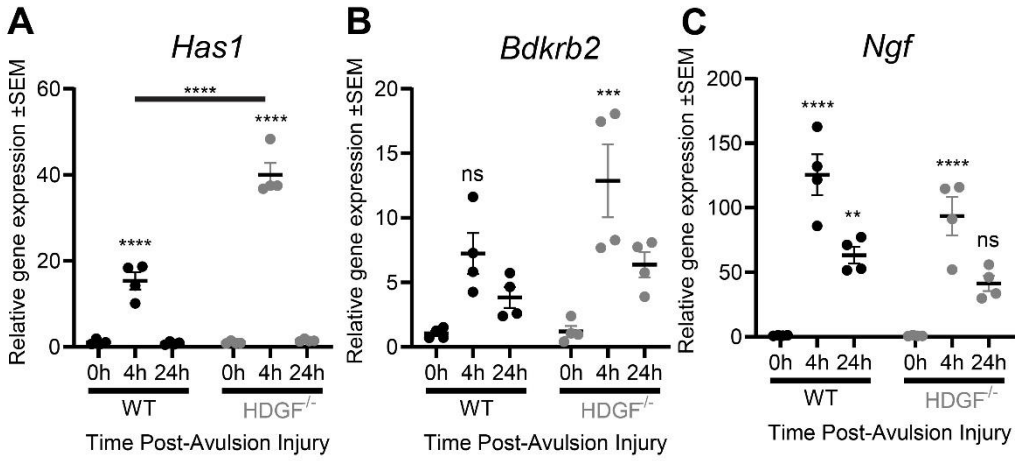

Figure 5.8 Significantly altered gene expression in *Hdgf* $^{-/-}$ mice compared to wildtype mice after hip avulsion cartilage injury. Relative quantification of cartilage *Has1* (A), *Bdkrb2* (B) and *Ngf* (C) mRNA by qPCR relative to 0h baseline gene expression of respective genotypes, 4 h and 24 h after hip avulsion injury. Genes significantly regulated upon injury and between genotypes. Mean (n=4) ± standard error. Statistical analysis by Two-Way ANOVA with Tukey Test post-hoc comparisons. Asterisk without connecting bracket denotes comparison with 0 h, banded asterisk specifies comparators (ns=non-significant, **p≤0.01, ***p≤0.001, ****p≤0.0001).

Fgf2 showed a significant difference in 0 h baseline expression, exhibiting a 0.55 fold change in *Hdgf* $^{-/-}$ compared to wildtype cartilage ($t(6)=2.702$, $p=0.0355$). This was the only gene with significant baseline differences.

5.3.5 Heparin-binding proteins from injury CM have proliferative effects on mesenchymal stem cells

Postulating a functional effect of HDGF on other aspects and cell types of the joint, heparin-binding proteins were purified to stimulate MSCs, capable of chondrogenesis. Further, signalling responses other than the immediate chondrocyte gene expression response to injury were investigated using recombinant HDGF protein on primary chondrocytes.

Growth factors released from cartilage upon injury were previously assessed for their heparin binding affinity in Chapter 3; HDGF, CTGF and FGF2 were successfully

eluted from a heparin-sepharose chromatography column, demonstrating that they bind heparin (Figure 3.16). A heparin chromatography experiment was performed, but over a gradient of NaCl elution, to elute fractions into discrete fractions based on NaCl concentration — corresponding to their relative heparin binding affinities. These heparin binding-growth factor fractions were dialysed and reconstituted to equivalent concentrations in serum-free medium, then used to stimulate adipose tissue-derived MSCs.

Injury conditioned medium was run through a heparin affinity column. Growth factors HDGF, CTGF and FGF2 bound to the column, as all three were not detectable in the flowthrough (Figure 5.9A). UV protein detection (A280) detected protein eluting from the heparin column predominantly in fraction 8 and 10, corresponding to approximately 0.63 and 1.17 M NaCl. There were also small peaks of protein detection in fractions 11–13 (1.56–2.5 M NaCl) (Figure 5.9B). Fractions containing growth factors were combined based on Western blot detection, then used to stimulate adipose tissue-derived MSCs (Figure 5.9C). Cells stimulated with recut conditioned medium exhibited a significant 1.7 fold increase ($p=0.0321$) in cell count over 48 h compared to non-treated, cultured cells ($F(7,16)=4.141$, $P=0.0088$). Stimulation with flowthrough, devoid of heparin-binding proteins, did not greatly increase proliferation over standard growth rates. Cells stimulated with fraction D (1.09–2.34 M NaCl elution) exhibited 1.6 fold increased proliferation compared to untreated cells, almost comparable to the increase caused by stimulation with recut conditioned medium, albeit non-significant ($p=0.0802$). No other fractions tested elicited an observable change in proliferation compared to untreated cells.

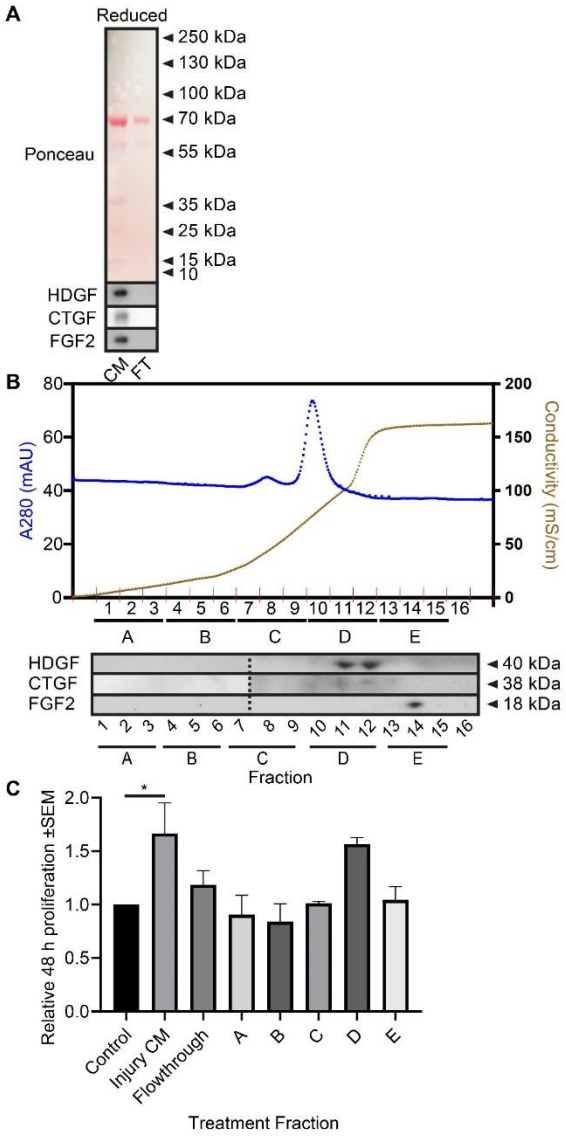

Figure 5.9 Heparin-binding proteins induce proliferation in adipose tissue-derived mesenchymal stem cells. Ponceau stain and immunoblot of HDGF, CTGF and FGF2 in injury conditioned medium (CM) and heparin column flowthrough (FT) under reduced conditions (A). NaCl elution curve (brown) and A280 protein elution (blue), with elution fractions (numbers) immunoblotted for HDGF, CTGF and FGF2 (B). Adipose tissue-derived mesenchymal stem cell proliferation over 48 h stimulation with serum-free αMEM (control) injury conditioned medium (Injury CM), column flowthrough or pooled heparin column elutions (letters) relative to control growth medium (C). Statistical significance was determined by one-way ANOVA with Dunnett's multiple comparisons (n=3) (*$p \leq 0.05$).

To test whether the proliferative effect of injury conditioned medium on adipose tissue-derived MSCs in Figure 5.9 was due to CTGF or FGF2, recombinant protein and receptor inhibitors were used in combination with injury conditioned medium

stimulation. No HDGF inhibitor is currently developed to inhibit HDGF-mediated proliferation.

Adipose tissue derived mesenchymal stem cells were cultured, serum starved, then counted to generate 0 h cell count. Cells were recounted after being stimulated for 48 h using a combination of: injury conditioned medium, FGFR inhibitor (SB402451), TGFβR inhibitor (SB431542), recombinant human FGF2 and recombinant human TGFβ3. Injury conditioned medium stimulated a significant 2.7-fold increase in cell count compared to control (SF-αMEM stimulated) proliferation over 48 h. Proliferation induced by injury conditioned medium was partly reduced by TGFβR1 inhibition, which stimulated a significant 1.8-fold increase in cell count compared to control 48 h proliferation. FGFR inhibition did not affect cell count when in combination with TGFβR1 inhibition. Stimulation with recombinant FGF2 and TGFβ3 did not significantly increase proliferation over 48 h. Inhibition of FGFR and TGFβR1 did not affect baseline proliferation rates of cells not stimulated with injury conditioned medium.

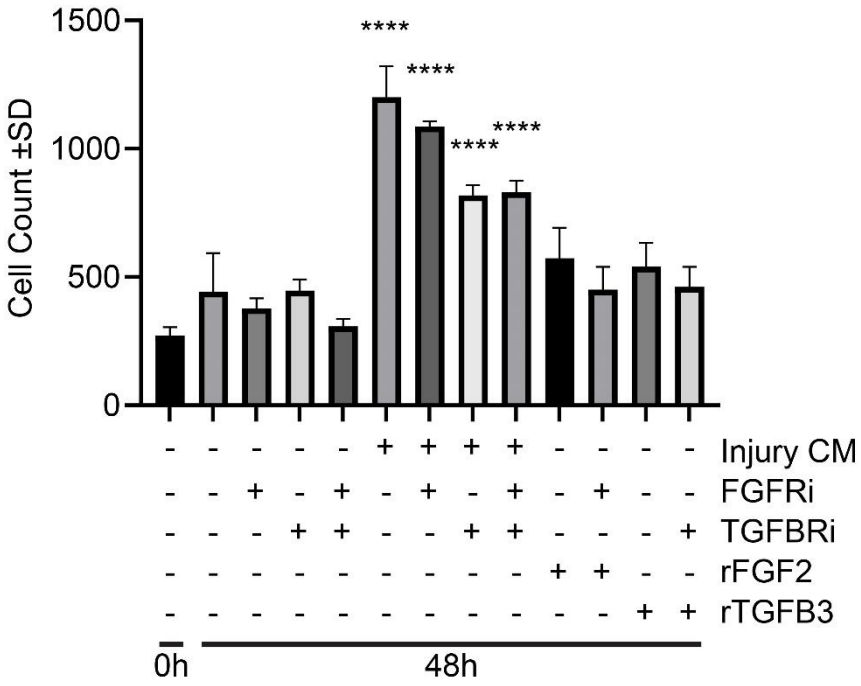

Figure 5.10 Adipose tissue derived mesenchymal stem cell proliferation in response to injury conditioned medium with FGFR and TGFβR1 inhibition. Primary mouse adipose-derived mesenchymal stem cells were cultured in α-MEM (control) for 48 h, stimulated with a combination of porcine recutting injury conditioned medium (Injury CM), receptor inhibitors (FGFRi and TGFβRi) and recombinant growth factors (rFGF2 and rTGFβ3). Number of cells per well was counted by brightfield microscopy (n=3). One-way ANOVA with Dunnett correction for multiple comparisons. All statistical comparisons against 48 h control (****$p \leq 0.0001$).

Recombinant HDGF protein was also used to stimulate cells, to investigate a putative signalling role of HDGF. Cultured primary porcine chondrocytes were serum starved and stimulated with serum-free medium containing 20 ng/ml FGF2 as a positive control, or 10, 50 or 100 ng/ml rHDGF. ERK protein phosphorylation was assessed by Western blot after 20 minutes of stimulation. FGF2 stimulation resulted in increased phosphorylated ERK1/2 after 20 minutes. Stimulation with rHDGF did not affect ERK phosphorylation.

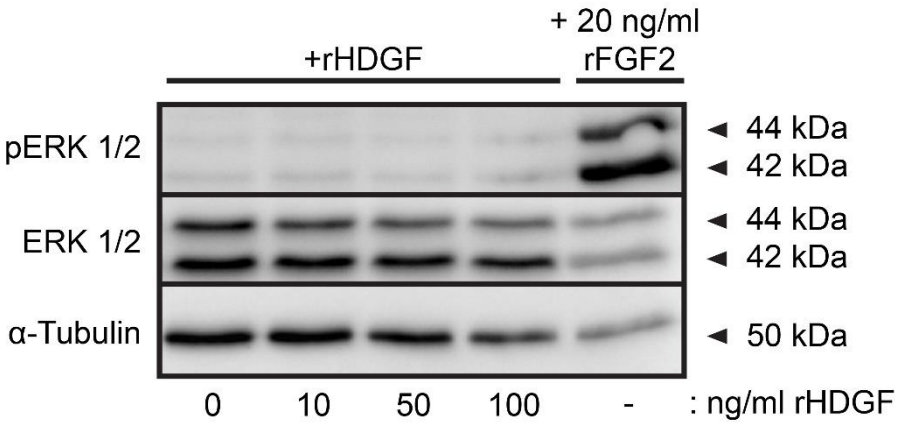

Figure 5.11 20 minute rHDGF stimulation does not activate ERK in primary chondrocytes. Serum-starved porcine chondrocytes stimulated with serum-free medium or serum-free medium containing HDGF (10, 50, 100 ng/ml) or FGF2 (20 ng/ml), immunoblotted for ERK1/2 and phosphorylated ERK1/2 (activated). α-tubulin was used as a housekeeper. Representative blot.

5.4 Discussion

A whole body constitutive knockout mouse, with exons 2–6 of *Hdgf* deleted, was used to investigate the role of HDGF in adult joint homeostasis and response to surgically induced osteoarthritis (DMM). After the commencement of these experiments, it was apparent the *Hdgf* $^{-/-}$ mice were of a different genetic background substrain. This was not initially apparent, as both in-house wildtype mice and *Hdgf* $^{-/-}$ mice were of a C57BL6 background strain. Microsatellite analysis indicated the mice, used in phenotypic and osteoarthritis model experiments, shared 41.2% C57BL/6J background (66.9% C57BL6/N). The *Hdgf* $^{-/-}$ mice were further backcrossed for two generations onto the C57BL6/J wildtype background (89.7% expected similarity) using in-house mice for the experiment investigating gene expression changes upon cartilage injury. Albeit not fully homogeneous, this generated a littermate control for use in the gene expression experiment. This substrain level difference is a confounder for the interpretation of these results. There are established metabolic differences between C57BL6/J and C57BL/6N mouse substrains which might partly explain the increased weight observed in *Hdgf* $^{-/-}$ mice (Figure 5.3). Differences in glucose intolerance, glucose levels and weight gain on a high fat diet are documented between C57BL6/J and C57BL6/N mice in other studies (Fontaine and Davis, 2016). These differences are prevalent but somewhat inconsistent in the literature, possibly due to differences in vendor sourcing. However, these could account for the partial correction in body weight observed in these mice after partial backcross to the C57BL6/J substrain (Figure 5.7). It is critical to understand the exact background substrain of the knockout mouse and its comparator for accurately interpretation of the experimental data; this was achieved upon realisation with microsatellite analysis and partial

backcrossing. Mice are considered fully backcrossed after at least nine generations, resulting in 99.8% similarity, but a partial backcross was conducted to achieve reasonable similarity (89.7%) within a feasible timeframe. *Hdgf* $^{-/-}$ mouse bodyweight was greater than wildtype mice at all ages measured, from 6 weeks of age. This suggests HDGF might play a role in metabolism, but a full backcross of HDGF mice to wildtype comparator substrain would need to be conducted, to compare bodyweight differences. All experiments were conducted in *Hdgf* $^{-/-}$ mice prior to partial backcrossing, except re-weighing (Section 5.3.3) and gene expression experiments (Section 5.3.4) which were after a two-generation backcross.

Large cyst regions were observable by histology in 66% of *Hdgf* $^{-/-}$ mouse joints that were not present in wildtype mice, despite small (≤ 70 μm) cysts presenting in both *Hdgf* $^{-/-}$ and wildtype mice. These cysts were not thought to be histological artefacts, as they maintained a well corticated perimeter of bone marrow, distinct from the calcified regions. This indicates a possible phenotype of the *Hdgf* $^{-/-}$ mouse, however the difference in substrain remains a confounding variable. The increased bodyweight and visual inspection of the *Hdgf* $^{-/-}$ mice indicated increased subcutaneous adiposity, which might also be conserved within the bone marrow if these cystic regions are lipid. Whether the cysts are lipid-filled could be determined by histological staining with Oil Red O which stains lipoproteins on paraffin sections. Further, the presence of these large cysts should be confirmed in fully backcrossed mice, however this was not feasible due to time constraints. If they maintain their presence in fully backcrossed *Hdgf* $^{-/-}$ C57BL6/J mice, a metabolic screening could be conducted including ECHO-MRI, DEXA screening, IPGTT glucose tolerance and insulin blood tests and food intake studies. Expanded marrow adipose tissue is often a consequence of impaired

hematopoesis and osteogenesis, such as with age or pathological conditions such as osteoporosis (Nuttall *et al.*, 2014).

Genetic contributions in obesity are recognised and are polygenic; numerous genes, each carrying a small individual risk. However, body weight is also affected by food intake and energy expenditure. Interaction of the brain with peripheral tissues such as the gut, the liver, the endocrine pancreas, adipose tissue and others can affect eating and autonomic activity, or energy metabolism. Due to the multifactorial nature of obesity, there are a plethora of ways in which HDGF — especially in a constitutive whole body knockout system — could affect body weight.

Average and maximal cartilage thickness measurements were thinner in *Hdgf* $^{-/-}$ mice compared to wildtype for both the medial and lateral tibial plateaus. Further, the thickness difference between thinner lateral cartilage and the medial cartilage thickness was more pronounced in *Hdgf* $^{-/-}$ mice than wildtype. Wildtype comparator mice were 22 weeks of age, compared to 18 week *Hdgf* $^{-/-}$ mice, however cartilage does not change in thickness between 18–22 weeks of age in C57BL/6 wildtype mice (Botter *et al.*, 2008; Coveney *et al.*, 2020). *Hdgf* $^{-/-}$ mice were also of different substrain genetic background; these data therefore indicate a potential phenotype, which should be confirmed in genetically homogeneous mice of the same age. Increased medial cartilage thickness, compared to lateral cartilage, is conserved across species (Malda *et al.*, 2013). Wildtype mouse cartilage thickness measurements were consistent with other studies of similar age mice (Botter *et al.*, 2008; Coveney *et al.*, 2020). Across species with differing body weights, cartilage thickness correlates with body mass and is allometrically scaled to organism size (Malda *et al.*, 2013), however this does not

necessarily hold true for body weight of individual animals. Human cartilage thickness in non-obese individuals correlates with weight, however this relationship is lost as fat mass increases (Blazek *et al.*, 2014). BMI is negatively associated with cartilage volume and thickness in older adults; this relationship is lost when independently adjusting for serum leptin, which maintains a greater negative relationship, suggesting thickness reduction in obesity is correlated with leptin (Ding *et al.*, 2007; Stannus *et al.*, 2015). Cartilage thickness also has a significant mechanical component; cartilage thinning occurs after joint unloading or immobilisation in mice and rats (Maldonado *et al.*, 2013; Nomura *et al.*, 2017). As HDGF is released upon injury (Figure 3.2), corresponding with loading-induced sodium flux (Figure 4.21), HDGF signalling in response to mechanical load might contribute to a homeostatic mechanism of maintaining cartilage thickness. Mechanical dependency of cartilage thickness could be tested in *Hdgf* $^{-/-}$ and wildtype mice after joint immobilisation. This could be achieved by measuring thickness of cartilage in wildtype and *Hdgf* $^{-/-}$ mice before and after double neurectomy (sciatic and femoral neurectomy). To remove confounding developmental phenotypes that may arise from deleting HDGF in early development, Cre recombinase can be conjugated to a modified oestrogen receptor, therefore activating deletion only following administration of tamoxifen (Cre-ER^{T2}). This can be targeted within a tissue by placing CreER^{T2} under the promoter of a cell specific gene, such as *Col2a1* (collagen II protein chain coding gene) (Davidson *et al.*, 2014) or *Acan* (aggrecan protein coding gene) (Henry *et al.*, 2009).

The DMM model of OA was chosen for its established reproducibility, with mild to moderate disease progression on the medial femoral and tibial plateaus. The surgical expertise for this model are well established within our laboratory, and DMM has been

shown to exhibit less variation in results with technique familiarity over time than other surgical models, such as the anterior cruciate ligament transection (ACLT) model (Glasson, Blanchet and Morris, 2007). All DMM operated mice were male, to control for known sex differences (Ma *et al.*, 2007; Loga *et al.*, 2020). Further, histological OA scoring was conducted blind to eliminate bias. *Hdgf* $^{-/-}$ mice exhibited statistically significantly greater OA severity at 8 weeks following surgery, but not 12 weeks post-surgery, compared with wildtype control mice. These data suggest that HDGF might be chondroprotective. This experiment is being repeated with genetically homogenous mice and being powered appropriately to detect a difference of means based on DMM data in Figure 5.6. The confounding effects for previous experiments must be considered when interpreting these DMM results; a full backcross must be conducted to eliminate any effect of background strain differences. Randomised co-housing of wildtype and knockout mice could also be introduced to methodology to eliminate subconscious bias during operation. Co-housing would also control for differences in mouse behaviour, which can affect activity level, food intake and pain-hiding behaviour (Kim *et al.*, 2013), and control for gut microbiota differences which has been shown to influence OA progression (Schott *et al.*, 2018).

Obesity is a major risk factor for OA, and although it may at least partly be attributable to increased body weight, the mechanistic link between these conditions is not fully understood. Studies suggest that the high-fat diet associated with obesity contributes to OA, rather than body weight, as extremely obese (*ob/ob* leptin-impaired and *db/db* leptin receptor-impaired) mice on a low-fat diet do not develop OA (Griffin *et al.*, 2009). High fat diet-induced models of obesity increase the incidence of osteoarthritis, to a greater extent than can simply be explained by increased joint loading (Griffin *et*

al., 2012). All mice in Chapter 5 were fed the same standard chow, albeit *ad libitum*, so dietary fat content was controlled for. This does not account for differences in food volume intake. However, no abnormal eating habits or differences in food depletion were visually observed. Metabolic factors are also linked to OA severity, including differences in leptin, resistin and adiponectin (Wu *et al.*, 2015). Mice transgenically expressing the *C.elegans* gene *fat-1* (ω-3 fatty acid desaturase protein that dehydrogenates ω-6 fatty acids to ω-3 fatty acids) develop less severe OA after DMM and less synovial inflammation, independent of body weight (Kimmerling *et al.*, 2020). This demonstrates the potential role of inherent genetic metabolic differences in influencing OA susceptibility. Further, lipodystrophy mice devoid of adipose tissue (adiponectin-Cre driving a diphtheria toxin transgene through deletion of an upstream floxed stop codon) are protected from spontaneous and DMM-induced OA at similar weights (Collins *et al.*, 2021). This protection is irrespective of diet and is reversible by adipose tissue transplantation, implicating signalling from fat tissue in susceptibility to OA in mice. Taken together, these papers suggest that diet may be important, but requires adipocytes for its response. *Hdgf* $^{-/-}$ mice with higher body weight were visually observed to have more subcutaneous fat. If the cyst regions in *Hdgf* $^{-/-}$ mouse bone marrow are fat deposits, this might also contribute to the overall burden of adipose tissue contributing to adipokine-dependent responses. The relative systemic and local contributions of fat are not fully understood, but both local adipose deposits such as the infrapatellar fat pad and systemic contributors such as subcutaneous and visceral fat could accelerate OA through pro-inflammatory cytokine stimulation (Chang *et al.*, 2018). This suggests the bone marrow cyst regions, if adipose deposits, could potentially influence OA severity in the *Hdgf* $^{-/-}$ mice. Obesity

is also associated with microbiome changes, which potentially increase susceptibility to OA. Dietary supplementation of with oligofructose, to restore the obesity-induced loss of *Bifidobactera*, protects obese mice from DMM-induced OA, and does not impact joint degeneration in non-obese mice (Schott *et al.*, 2018). This highlights another potential mechanism by which obesity might influence OA susceptibility.

Cartilage thinning in *Hdgf* $^{-/-}$ mice might also contribute to their increased severity of OA. Cartilage thickness is increased in *Ctgf* $^{-/-}$ mice, which coincides with a protection from spontaneous and surgically induced OA (Tang *et al.*, 2018). Disuse of the joint results in cartilage thinning in canine models, with a reduction in proteoglycan staining (Palmoski, Perricone and Brandt, 1979) and hyaluronan (Haapala *et al.*, 1996) in the tissue, which is mechanically induced and ultimately results in biomechanical changes in the cartilage matrix (Vincent and Wann, 2018). Further, other studies show obese subjects exhibit lower tibial cartilage thickness, lower proteoglycan content and greater tibiofemoral cartilage compressive strain with loading, measured by MRI (Collins *et al.*, 2018). This highlights a potential link between adipose tissue and cartilage thinning, independent of the normal mechanoadaptation response. Regardless, thinning of the articular cartilage will likely increase susceptibility to surgically induced destabilisation of the joint.

Other studies have investigated gene expression changes between normal and osteoarthritic cartilage (Aigner *et al.*, 2006; Karlsson *et al.*, 2010), between undamaged and damaged osteoarthritic cartilage (Sato *et al.*, 2006; Geyer *et al.*, 2009; Snelling *et al.*, 2014; Dunn *et al.*, 2016), after injurious animal model induction of OA (Appleton *et al.*, 2007; Wei *et al.*, 2010; Bateman *et al.*, 2013; Loeser *et al.*, 2013; Gardiner *et*

al., 2015), and after *ex vivo* mechanical injury (Lee *et al.*, 2005; Dell'Accio *et al.*, 2008; Zhu *et al.*, 2017) or compressive load (Burton-Wurster *et al.*, 2005; McCulloch *et al.*, 2018). These studies influenced the choice of injury-responsive genes investigated in wildtype and *Hdgf* $^{-/-}$ mice with cartilage hip avulsion injury. The hip avulsion injury model avulses the femoral head through the epiphysis, and can be regarded as an *ex vivo* cartilage injury model. In this respect, any gene changes in non-chondrocyte cells from the synovium, synovial fluid and subchondral bone that are measured in a whole joint analysis are not included in the hip avulsion model. This is beneficial for understanding selective transcriptional changes of the chondrocyte, but does not allow the capture of influence of *Hdgf* on surrounding tissues.

Expression changes upon cartilage injury were investigated for 36 genes with n=4 sample size in this chapter. This sample size was felt to be appropriate, as previous studies using similar numbers were able to distinguish wildtype and knockout tissue responses after injury (Chong *et al.*, 2013; Tang *et al.*, 2018). Of 35 genes statistically significantly regulated upon hip avulsion injury, three showed significant genotype effect by two-way ANOVA analysis. The expression of the three genes *Has2*, *Bdkrb2* and *Ngf* were all upregulated upon injury, and showed a modest alteration of magnitude of the response in the *Hdgf* $^{-/-}$ genotype. *Hdgf* knockout did not abrogate the injury response of any of these genes. Increasing the number of biological replicates might have increased the number of genes significantly regulated by genotype, but there were no clear trends in the data worthy of further investigation. *Has1* encodes the Hyaluronan Synthase 1 protein, important in synthesis of the matrix glycosaminoglycan hyaluronic acid in response to injury. *Bdkrb2* encodes the protein Bradykinin Receptor B2 (BDKRB2), which is a receptor for bradykinin; a pain-related

inflammatory mediator. *Bdrk2* polymorphisms have been implicated in altered *Bdkrb2* gene expression and osteoarthritis susceptibility (Chen *et al.*, 2012, 2017). *Ngf* encodes the neurotrophic protein Nerve Growth Factor (NGF), which can be induced by TGFβ (Blaney Davidson *et al.*, 2015) and FGF2 (Driscoll *et al.*, 2014) in articular cartilage and is clinically and pre-clinically implicated in osteoarthritis pain (Lane *et al.*, 2010; McNamee *et al.*, 2010; Von Loga *et al.*, 2019). These modest gene changes upon injury in cartilage after whole body constitutive *Hdgf* knockout indicate that HDGF might not play a critical functional role in the immediate chondrocyte injury response. This does not exclude the possibility of a role for HDGF in the joint, as this experiment measured gene expression solely in chondrocytes. HDGF release from cartilage might elicit gene changes in surrounding tissues. Injury of the whole joint, for example by DMM, with subsequent RNA extraction from the whole joint might uncover HDGF dependent changes in other cell types. Further, the genes investigated (Table 8.5) were based on previous literature of injury-dependent and DMM-regulated genes that have been refined to focus on an interest in FGF2, TGFβ and pain signalling. The gene panel is therefore a biased selection of genes. An agnostic approach would allow unbiased capture of potential HDGF signalling changes upon injury in the cartilage. This could be achieved with RNA-Seq transcriptomic analysis of cartilage or joint injury.

Adipose tissue-derived mesenchymal stem cells are an easily accessible source of multipotent stem cells that are capable of induced chondrogenesis (Cao *et al.*, 2015; Liao *et al.*, 2015). Clinical trials are ongoing to establish their potential use as a source for autologous chondrocyte implantation therapy in osteoarthritis patients (Jo *et al.*, 2014; Pers *et al.*, 2016). Despite *Hdgf* deletion exhibiting minimal effects on the injury responsive gene profile of mouse cartilage, heparin affinity purification of a broad

fraction containing HDGF elicited proliferation in adipose tissue-derived mesenchymal stem cells (Figure 5.9). This fraction also contained CTGF, and potentially a host of other heparin-binding proteins; the proliferation therefore cannot be definitively attributed to HDGF in this experiment. However, it demonstrates a functional role of injury-released heparin-binding proteins in the joint, and potentially identifies a novel role for HDGF in cartilage progenitor cells.

Subsequent affinity purification of eluted fractions from the heparin column could be performed to attain protein homogeneity. This could be used to show whether the proliferative effect in Figure 5.9 can be attributed to HDGF. This could also be determined with use of injury conditioned medium from *Hdgf* $^{-/-}$ mouse cartilage to stimulate adipose tissue derived mesenchymal stem cells. One would expect a proliferation effect from wildtype mouse injury conditioned medium that is abrogated with the use of *Hdgf* $^{-/-}$ injury conditioned medium, if HDGF is responsible for this proliferative effect. Stimulating cells with injury conditioned medium in the presence of an HDGF inhibitor would show to what extent the proliferation is dependent on HDGF. This was conducted with FGF and TGFβ inhibitors in Figure 5.10, however inhibitors for HDGF have not yet been developed and no receptor has been identified. FGF2 signals via an FGFR homodimer, and CTGF acts as a latent TGFβ-binding protein, allowing TGFβR mediated signalling in cartilage. Recombinant FGF2 and TGFβ3 did not stimulate proliferation of adipose tissue-derived MSCs over a period of 48 h, suggesting FGF2 and CTGF mediated signalling is not directly responsible for the proliferative response of injury conditioned medium. Further, FGFR inhibition did not affect proliferation from injury conditioned medium, but TGFβR1 inhibition did partly reduce the proliferative response. This suggests the proliferative mechanism

from injury-released factors in cartilage is partly reliant on TGFβR signalling for its maximal effect. It is possible that TGFβ signalling potentiates the effects of HDGF. HDGF dependence could be tested if the method of signalling was known, however, its receptor and chondrocyte signalling mechanism is currently unknown. The effect of HDGF on the chondrogenic differentiation of these cells could also be investigated, by measuring gene expression changes of chondrogenic genes *Col1a2* and *Acan*.

Stimulation of these cells with recombinant HDGF protein would elucidate the putative proliferative role of HDGF. HDGF is not commercially available in a guaranteed biologically active form; many forms of HDGF are truncated or contain genetically engineered tags for long-term stability or purification. Recombinant HDGF was tested for biological effects, but ERK activation in primary chondrocytes was not detectable (Figure 5.11), despite other studies demonstrating ERK activation in a variety of cell types with recombinant HDGF (Ooi *et al.*, 2010; Lu, Chen and Qiu, 2015). This informed approach of testing a single pathway constituent was not successful, so a higher throughput assay should be considered using HDGF-stimulated cell lysates. Antibody arrays, such as multi-spot membrane assays would give wider scope for investigating putative activity in the first instance, which can then be validated by Western blot or ELISA. One advantage of using HDGF from cartilage injury conditioned medium as a stimulant is that the protein will be in its native, endogenous form and include any function-dependent post-translational modifications.

Biologically active recombinant protein would also enable the analysis of interactions between these growth factors. For example, FGF2 and TGFβ1 counter-regulate IGF-1

in chondrocytes, by downregulation and upregulation, respectively. In combination, FGF2 exerts a stronger influence until 5 days after stimulation, after which TGFβ1 overrides the inhibition of IGF-1 by FGF2 (Shi *et al.*, 2009). Such systematic approaches could be used for HDGF, CTGF (TGFβ1) and FGF2 stimulation to recapitulate the injury response. This would highlight possible concentration-dependent, time-dependent and interaction effects, as well as influences on other growth factors.

The binding of HDGF, CTGF and FGF2 to heparin was previously demonstrated in Section 3.3.7 using a single 2.5 M NaCl elution from a heparin affinity column (Figure 3.16). In the current chapter, Figure 5.9 shows a gradient NaCl elution from a heparin affinity column, which eluted these growth factors based on relative heparin binding affinities. Exact heparin binding affinities cannot be determined due to elution into wide binned fractions, but relative heparin affinities were indicated as CTGF < HDGF < FGF2. CTGF eluted between 1.09–2.34 M NaCl, HDGF between 1.41–2.34 M NaCl and FGF2 at a concentration above 2.34 M NaCl. FGF2 exhibits a higher heparin binding affinity than HDGF in independent heparin affinity chromatography studies, with elutions of 1.39 M and 0.75 M respectively (Chiu *et al.*, 2014). CTGF heparin binding has not been directly compared to HDGF or FGF2 in other studies, but the low-mass form of CTGF (10 kDa) is eluted at 0.8 M from a heparin column in other studies (Brigstock *et al.*, 1997; Ball *et al.*, 2003). As previously discussed in Chapter 4.4, the differential binding affinities for heparin might affect the threshold at which these growth factors are released by a sodium flux in cartilage tissue. The growth factors with less affinity for heparan sulfate would need less sodium ion competition to be released from their electrostatic interaction in the PCM. This could contribute to

a fine-tuning of growth factor release based on the extent of mechanical insult, or mechanical injury, to the tissue. This might also play a role in the cross-talk between growth factor pathways, if mild cases of mechanical insult reach a threshold that selectively releases weaker-binding growth factors over more tightly bound growth factors.

In summary, *Hdgf* $^{-/-}$ mice exhibited increased body weight, thinning of cartilage, cyst regions in the bone marrow of the joint and increased early severity of disease in a DMM model of OA. These indicate HDGF might be chondroprotective. There were no notable HDGF-dependent changes in the gene expression profile of cartilage upon injury, but the heparin-binding proteins released upon injury, which include HDGF, are able to elicit a proliferative effect on adipose-derived mesenchymal stem cells. This work needs to be considered within the context of an impure strain background, and the contributions of metabolic factors. However, these data will influence the further investigation of gene regulation agnostically in the joint, a suitable DMM study and the direct role of HDGF in cells of the joint.

6 Discussion

The work of this thesis builds on previous discoveries of the Vincent laboratory on growth factors in the pericellular matrix. FGF2 and CTGF are bound to perlecan in the pericellular matrix and released upon injury (Vincent *et al.*, 2002, 2007; Tang *et al.*, 2018). Proteomic analysis of the pericellular matrix identified four growth factors: FGF2, CTGF, HDGF and CYR61 (Tang *et al.*, 2018), all of which are predicted to bind heparin and heparan sulfate (Ori, Wilkinson and Fernig, 2011). In this study, three of these growth factors, HDGF, CTGF and FGF2 were validated for their release by mechanical injury of articular cartilage (Figure 3.5). HDGF, a lesser known heparan sulfate-binding growth factor, was characterised here for the first time in cartilage. They were all released rapidly in a cell-independent manner from heparan sulfate bound stores upon injury (Chapter 3).

Residence within the PCM and heparan sulfate binding affinity of these growth factors prompted search for a common mechanism of release (Chapter 4.2.7). Three distinct properties of cartilage led to the hypothesis that release upon injury is due to a shift in the sodium concentration. Specifically, articular cartilage has a high fixed charge density and high extracellular sodium concentration (Maroudas and Freeman, 1979; Shapiro *et al.*, 2000, 2002). Secondly, a high fixed charge density in the TM indicated by chondroitin sulfate staining (2B6 epitope on aggrecan) (Figure 4.1), but not in the PCM, suggested a fixed charge gradient being able to modulate sodium concentration in the PCM through mobilising stores in the territorial matrix. The third indication was that all three growth factors bound to heparan sulfate by ionic interaction that could be overcome with NaCl (Figure 3.16, Figure 5.9). I hypothesised that tissue sodium

coming from the territorial matrix would recapitulate the electrostatic elution of these growth factors, as observed on a heparin column, *in situ* in cartilage tissue. A sodium dependent release of growth factors was demonstrated through exogenous NaCl releasing the factors from cartilage (Figure 4.2, Figure 4.3), and depletion of NaCl abrogating release of the factors from cartilage upon injury (Figure 4.4). In osteoarthritis, severe loss of proteoglycan also leads to an inability to release growth factors upon injury. Growth factors are still present in the OA tissue, consistent with the upregulation of PCM perlecan in OA (Tesche and Miosge, 2004; Chanalaris *et al.*, 2019) which provides heparan sulfate binding sites, and matrix extraction of growth factors by NaCl in OA tissue, again adding support to a mechanism of release other than simply cellular regulation. Sodium imaging was able to confirm a shift in free sodium compared with bound sodium within the tissue upon compressive loading (Figure 4.21). Moreover, these experiments suggested that free sodium concentration upon loading was most evident just below the surface layer, which corresponds to areas of cartilage more susceptible to compressive strain, fluid exudation and matrix disorganisation in normal cartilage tissue.

HDGF, a novel factor unexplored in the context of cartilage, was functionally investigated in chapter 5. With the caveat of confounding background strain differences, *Hdgf* $^{-/-}$ mice exhibited increased body weight (Figure 5.3), the presence of adipose-like cyst regions in the bone marrow of the joint (Figure 5.4), decreased mouse cartilage thickness (Figure 5.5), and increased early progression of surgically induced OA (Figure 5.6). This phenotype did not affect a panel of immediate injury-induced genes in cartilage, as only modest differences were found between *Hdgf* $^{-/-}$ and wildtype mice after hip avulsion injury (Section 5.3.4). This suggested that HDGF

signalling was not responsible for this investigated portion of the injury response in chondrocytes, but does not rule out a HDGF-dependent injury response in other genes or cell types. However, there was a suggestion that HDGF may influence proliferation of adipose-derived mesenchymal stem cells, as the heparin-binding fraction of injury conditioned medium containing HDGF induced proliferation (Figure 5.9). The proliferation induced by injury conditioned medium was not directly attributable to FGF2 or CTGF (TGFβ) signalling, as receptor inhibition did not abrogate the proliferative response and recombinant protein stimulation did not induce proliferation in these cells (Figure 5.10). This suggested that HDGF was the dominant growth factor promoting this mesenchymal stem cell proliferation response, which should be confirmed by purification of the fraction to homogeneity of HDGF. These data highlight the potential for a HDGF-mediated response in the wider context of the joint, which is being further explored.

This work demonstrates a release of HDGF, CTGF and FGF2 upon injury, and provides evidence attributing this to a flux in sodium. However, a link between the release of these factors and a functional response was somewhat outside the scope of this work, although partly explored in Section 5.3.4 and Section 5.3.5 for HDGF. Previously, the function of injury released growth factors has been investigated *in vivo* for CTGF (Tang *et al.*, 2018) and FGF2 (Vincent *et al.*, 2002, 2007). Collectively, these results point to a role for these growth factors in important chondroprotective pathways. How these molecules interact with one another in the injury response, to promote cartilage repair, is an ongoing interest of the group.

Whether this sodium-dependent response occurs consistently throughout depth of the tissue is not fully understood. However, work from our laboratory group demonstrated SMAD2 phosphorylation, indicative of CTGF (TGFβ) activation, in the sub-superficial zone of cartilage (between 50 and 300 μm from the articular surface) after cyclic compression, which was not present in non-compressed explants. This corresponded with the region of lowest tissue stiffness, measured by scanning acoustic microscopy (low wavespeed), and appeared to match the region of sodium flux observed by ^{23}Na-MRI imaging in Figure 4.21. Interestingly, proteomic analysis comparing distinct layers of the tissue showed that the growth factors were present throughout the depths of tissue (Keppie *et al.*, 2021). Instead of regulating the distribution of growth factor, which in the case of HDGF we have reason to believe is fairly uniform throughout the cartilage, differences in stiffness lead to spatial variation in free sodium concentration upon loading. This controls growth factor activity through regulating its localised release. These data provide a functional link between the sodium flux, growth factor release and regional cellular activation, dependent on matrix stiffness.

This novel mechanism of action for growth factor release upon cartilage injury has wider implications in the maintenance of cartilage health and approaches to osteoarthritis therapy. FGF2 and TGFβ have chondroregulatory roles *in vivo* (Chia *et al.*, 2009; Tang *et al.*, 2018), and polymorphisms within both pathways have been identified in osteoarthritis GWAS studies (Zengini *et al.*, 2018; Tachmazidou *et al.*, 2019). The loss of ability to release them appropriately after injury is likely to be a contributing factor to pathogenesis mechanisms in osteoarthritis. CTGF is able to mediate TGFβ signalling in cartilage (Tang *et al.*, 2018), which is a strong driver of

chondrogenesis progenitor cells (Fukumoto *et al.*, 2003; Muhammad *et al.*, 2014), and FGF2 is able to prime mesenchymal stem cells for chondrogenesis (Solchaga *et al.*, 2005; Handorf and Li, 2011; Correa *et al.*, 2015), so their contribution may be a powerful drive for stem cell-mediated repair. The importance of intrinsic growth factors is supported by the ability of a truncated version of recombinant human FGF18 (sprifermin) to cause reparative extracellular matrix remodelling in OA articular cartilage (Reker *et al.*, 2020). Further, sprifermin is the first example of a structure modifying osteoarthritis drug, increasing cartilage thickness and reducing cartilage loss in a phase II clinical trial for OA (Hochberg *et al.*, 2019; Eckstein *et al.*, 2020). This validates the targeting of intrinsic repair and response mechanisms of cartilage through growth factors as a treatment for OA, as opposed to inhibiting degradative processes.

Tissue engineering approaches are another potential avenue for osteoarthritis therapy. This work has uncovered the mechanism by which growth factors are released in normal cartilage, and by which their bioavailability is reduced under diseased conditions. A strategy to restore the normal injury response in cartilage by correcting the fixed charge density could be considered, to restore matrix sodium needed for a sufficient ion flux. When incorporating polymers into cartilage, one must consider the limitations of cartilage delivery, stable incorporation in the tissue and half-life. This is especially pertinent in cartilage, which has a dense matrix that can repel negatively charged elements, and is full of enzymes that can degrade organic products. One approach to restore the fixed charge of cartilage tissue could be to incorporate more aggrecan into the tissue. Aggrecan core protein is over 250 kDa, with over 100 additional sulfated glycosaminoglycan side chains of approximately 20 kDa (Kiani *et*

al., 2002). The large size of aggrecan and significant anionic charge in such a large molecule might raise issues with incorporation into the tissue. Furthermore, aggrecanase activity is increased in osteoarthritic cartilage, and might pose a problem for this therapeutic strategy; this could be overcome with genetic engineering of aggrecan-binding sites to render the protein resistant to degradation. One alternative approach would be to incorporate the sulfated glycosaminoglycans of aggrecan, such as chondroitin sulfate, into cartilage without the large core protein. Many studies have examined the oral effectiveness of chondroitin sulfate and other glycosaminoglycan supplementation. However, there is conflicting evidence on whether oral glycosaminoglycan supplemetation such as chondroitin sulfate or glucosamine has any effect on OA symptoms and progression, with meta-analyses producing contradictory results (McAlindon *et al.*, 2000; Richy *et al.*, 2003; Towheed *et al.*, 2005). Oral use of nutraceutical glycosaminoglycans in such a holistic or generic way does not allow for direct incorporation in cartilage, and introduces the potential for enzymatic degradation in the gut before any putative beneficial effect. A tissue engineering approach, introducing negatively charged glycosaminoglycans directly to the cartilage tissue, would ensure incorporation of fixed charge to the cartilage. This would target the ability for cartilage to exhibit a sodium flux, due to the sequestration of sodium by glycosaminoglycans. Negatively charged polysaccharide sequences can be synthesised to mimic the chondroitin sulfate that contributes to the fixed charge density of cartilage (Eller *et al.*, 2013). The negatively charged polymers could be attached to cartilage matrix through use of a modified amino acid sequence with a binding site to structural matrix components (Figure 6.1). Aggrecan degradation is thought to precede collagen and structural degradation (Little *et al.*, 2009), so would be an appropriate

target structure for glycosaminoglycan attachment in early disease. Negatively charged polysaccharide sequences with binding sites for collagen II could restore charge to all but the most severe regions of osteoarthritis tissue, and collagen II shares >95% protein homology (NCBI HomoloGene:55607) between bovine, murine and human forms allowing for translation and ease of experimentation in multiple species. This could be achieved using a WYRGRL peptide sequence, which is validated as an intra-articular targeting peptide with high specificity and collagen II selectivity (Rothenfluh *et al.*, 2008). The WYRGRL sequence has been validated for polypropylene sulphide nanoparticle introduction to cartilage *in vivo*, and excludes incorporation to the pericellular matrix region (Rothenfluh *et al.*, 2008). This would maintain the differential charge between the TM and PCM proposed in the sodium dependent hypothesis, based on Figure 4.1. Two aspects need optimisation for this approach: incorporation of the negatively charged polysaccharide chains into cartilage, and ability of the chains to cause growth factor release by flux of sequestered counterions. With regard to function after linkage, the WYRGRL sequence maintains its collagen binding function in cartilage with larger attachments such as fluorophores and contrast agents (Hu *et al.*, 2015; Yi *et al.*, 2019). Also, disaccharide chains such as chondroitin sulfate have a molecular diameter of 1.2 nm, in a semi-flexible coil, which is significantly smaller than the 38 nm nanoparticle incorporation by Rothenfluh *et al.* (2008), suggesting the attachment size should not be a limiting factor. *In vitro* validation could be performed in a simple system using a hydrogel approach, before introduction to cartilage, in a standardised collagen II synthetic matrix. However, *in vivo* validation, or use in *ex vivo* cartilage, will have the endogenous enzymes and degradative mechanisms present that might contribute to degradation of the

incorporated anionic polymer. An appropriate *ex vivo* model for fixed charge reincorporation would be the aggrecanase depleted cartilage model in Figure 4.4. Once incorporated into cartilage, compression and injury could test the ability of the cartilage to exhibit an increased sodium flux, and release PCM growth factors bound to heparan sulfate from the tissue.

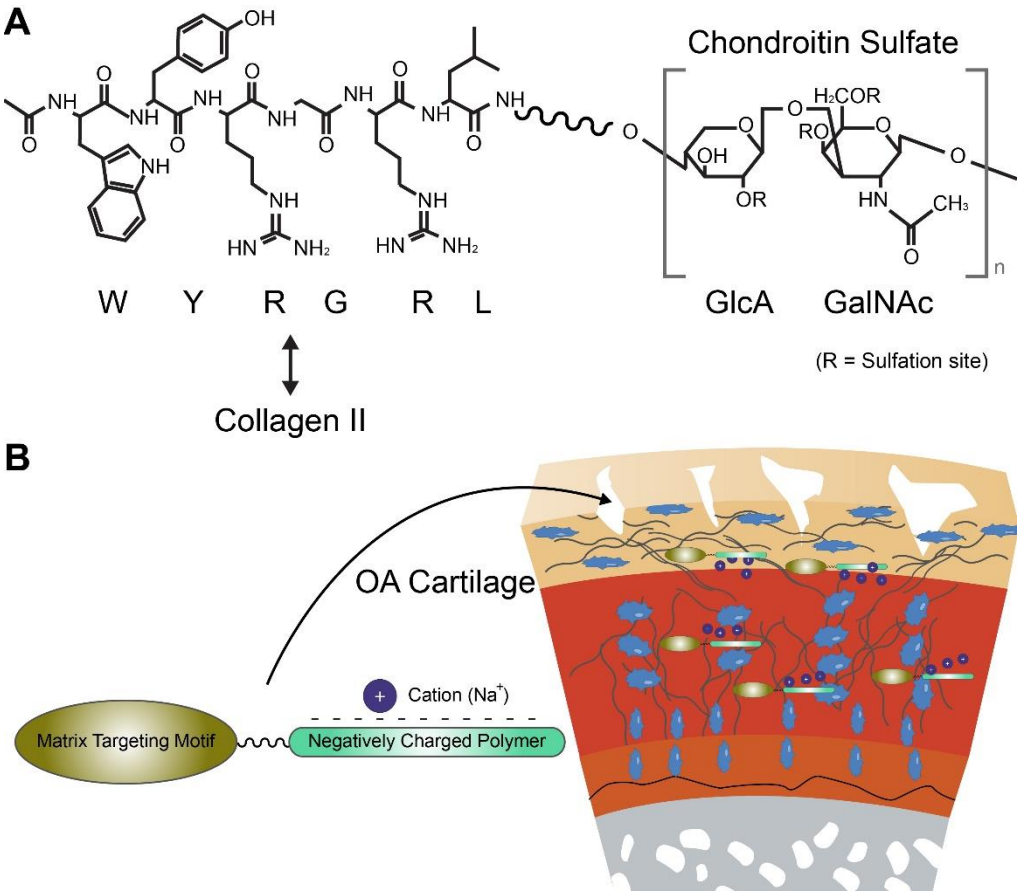

Figure 6.1 Example of theoretical negative polymer incorporation into osteoarthritic articular cartilage. (A) WYRGRL motif represents a cartilage matrix-binding element. Chondroitin sulfate represents an example of a negatively charged polymer chain capable of sequestering cations, where R = possible functional sulfation site. (B) Incorporation of a negatively charged matrix-targeting construct into osteoarthritic cartilage to restore tissue counter-cation content.

Alternatively, the growth factors themselves could be administered directly to the joint. Late stage OA cartilage contains equivalent levels, or higher levels, of heparin-binding PCM growth factors than undamaged tissue, but has lost its ability to release

them. This suggests the aforementioned approach of introducing fixed charge back into the tissue might be a suitable approach to restore the bioavailability, rather than adding excess soluble growth factor where there is no regional or temporal control of tissue response. Other limitations in direct growth factor and drug administration to cartilage are due to limited drug delivery into the tissue; biological barriers of the dense, charged cartilage matrix stop penetration, and drugs exhibit a short half-life in the tissue. However, others have developed methods to improve the cartilage penetrating ability and retention of growth factors administered to cartilage through the use of nanocarriers, such as by PEGylated cationic dendrimer conjugation to IGF-1 (Geiger *et al.*, 2018). These approaches might also aid the incorporation of growth factors into areas of the matrix, such as the PCM, where they are able to elicit a cellular effect mediated by the mechanotransduction of load through the cartilage. Similarly, many studies have used heparin hydrogels to tune and sustain the release of contained growth factors into various tissues (Seif-Naraghi *et al.*, 2012). These gels can be added as a scaffold to defective cartilage and utilise the stabilising effect of heparin and heparan sulfate on growth factors to maintain delivery to the tissue.

Recombinant FGF2 addition has shown promising effects in pre-clinical models, where it is able to protect surgically induced OA by DMM in by subcutaneous injection in FGF2 $^{-/-}$ mice (Chia *et al.*, 2009). Heparin-binding growth factors from injury conditioned medium showed a proliferative effect on joint-derived cells that might be HDGF-mediated (Figure 5.9), and is partly influenced by interaction between TGFβ-mediated signalling synergising a factor other than TGFβ (Figure 5.10). In this respect, a combinatorial growth factor treatment might elicit effects that recapitulate processes of healthy physiological cartilage.

This body of work has focused on articular cartilage to explore the sodium dependent mechanism of injurious growth factor release. However, this process might be conserved among other tissues. This work proposes that the presence of chondroitin sulfate, as a structure for sodium sequestration, is beneficial to articular cartilage by enabling the electrostatic release of growth factors upon injury. Chondroitin sulfate proteoglycans are also present at high levels in the central nervous system, where they inhibit repair and become more abundant following injury in the spinal cord. Chondroitinase ABC digestion of chondroitin sulfate proteoglycan aids spinal cord injury and allows neurite extension in glial scar models (Silver and Miller, 2004; Bartus *et al.*, 2014), which is partly reduced by laminin inhibition (McKeon, Höke and Silver, 1995). These suggest neurite outgrowth might depend on a balance of growth-promoting factors associated with laminin and growth-inhibiting factors associated with chondroitin sulfate upon injury. Articular cartilage is aneural, and therefore does not rely on neural outgrowth for repair, explaining how a chondroitin sulfate-mediated sodium release of growth factors upon injury can be beneficial in articular cartilage but not in the spinal cord or neural tissues. Further, chondroitin sulfate itself can directly bind other growth factors in the central nervous system, which might play a major role in tissue injury in other settings. Extracellular matrix sodium concentration immediately outside the cell in rat spinal cord has been measured at 156 mM Na^+ (Forsythe and Redman, 1988); this might restrict the ability of sodium to release factors by the same mechanism as in cartilage, but extracellular concentrations might vary in further removed matrix regions. Some studies pose a direct role of sodium in neuronal injury, as sodium permeation through cellular channels detrimentally increases upon compressive spinal cord injury. Replacement of sodium ions with

equivalent $NMDG^+$, impermeable to sodium channels, protected against compressive spinal cord injury. These results suggest a potential extracellular sodium flux upon compressive injury in another tissue.

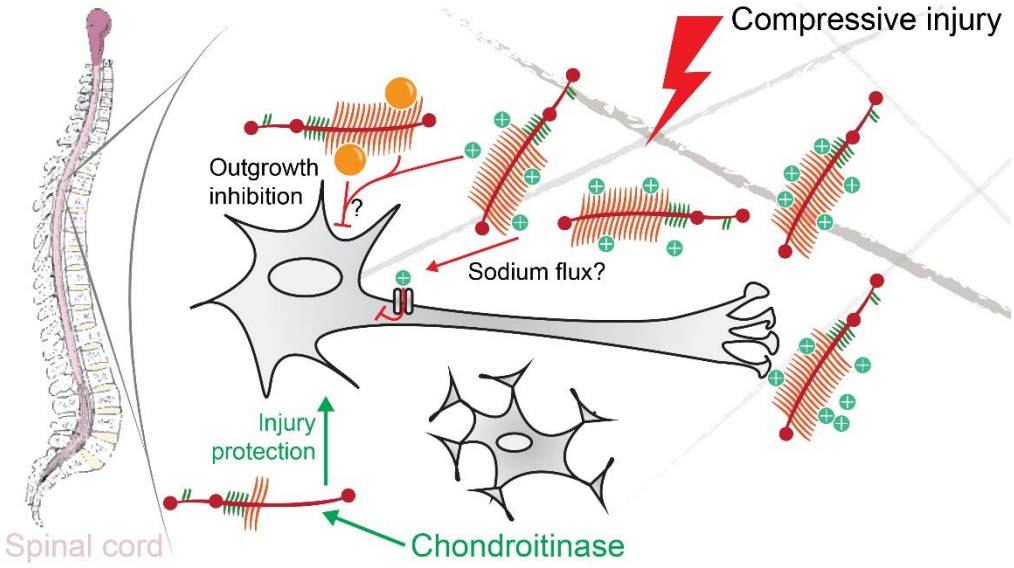

Figure 6.2 Chondroitin sulfate-mediated impact in spinal cord injury, inhibitory to repair. It is not known whether the contribution of chondroitin sulfate to inhibition of these processes is due to its influence on ion channel influxes, matrix cation dynamics, growth factors or another consequence.

In this thesis I aimed to uncover the role of HDGF in cartilage, and understand the wider role of heparan sulfate-bound matrix growth factors in cartilage injury. I have demonstrated commonalities between three heparan sulfate-bound matrix growth factors upon injury cartilage, and proposed a biophysical sodium-dependent mechanism by which their release is tuned by mechanics in healthy cartilage, and their bioavailability is lost in disease. Furthermore, I have highlighted a potential role for HDGF in the joint, with future perspectives on how to confirm the role of HDGF and utilise aspects of this novel injury response to maintain health of cartilage tissue and prevent disease.

7 Bibliography

Abouzied, M. M., Baader, S. L., Dietz, F., Kappler, J., Gieselmann, V. and Franken, S. (2004) 'Expression patterns and different subcellular localization of the growth factors HDGF (hepatoma-derived growth factor) and HRP-3 (HDGF-related protein-3) suggest functions in addition to their mitogenic activity', *Biochemical Journal*, 378(1), pp. 169–176. doi: 10.1042/bj20030916.

Abouzied, M. M., El-tahir, H. M., Prenner, L., Haberlein, H., Gieselmann, V. and Franken, S. (2005) 'Hepatoma-derived Growth Factor: Significance of amino acid residues 81-100 in cell surface interaction and proliferative activity.', *Journal of Biological Chemistry*, 280(12), pp. 10945–10954. doi: 10.1074/jbc.M414652200.

Acikara, O. B. (2013) 'Ion-Exchange Chromatography and Its Applications', in *Column Chromatography*. InTech. doi: 10.5772/55744.

Aich, U., Shriver, Z., Tharakaraman, K., Raman, R. and Sasisekharan, R. (2011) 'Competitive Inhibition of Heparinase by Persulfonated Glycosaminoglycans: A Tool to Detect Heparin Contamination', *Analytical Chemistry*. NIH Public Access, 83(20), pp. 7815–7822. doi: 10.1021/ac201498a.

Aigner, T., Fundel, K., Saas, J., Gebhard, P. M., Haag, J., Weiss, T., *et al.* (2006) 'Large-scale gene expression profiling reveals major pathogenetic pathways of cartilage degeneration in osteoarthritis', *Arthritis & Rheumatism*. John Wiley & Sons, Ltd, 54(11), pp. 3533–3544. doi: 10.1002/art.22174.

Aitken, D., Laslett, L. L., Pan, F., Haugen, I. K., Otahal, P., Bellamy, N., *et al.* (2018) 'A randomised double-blind placebo-controlled crossover trial of HUMira (adalimumab) for erosive hand OsteoaRthritis – the HUMOR trial', *Osteoarthritis and Cartilage*, 26(7), pp. 880–887. doi: 10.1016/j.joca.2018.02.899.

Allen, D. M. and Mao, J. J. (2004) 'Heterogeneous nanostructural and nanoelastic properties of pericellular and interterritorial matrices of chondrocytes by atomic force microscopy', *Journal of Structural Biology*. Academic Press Inc., 145(3), pp. 196–204. doi: 10.1016/j.jsb.2003.10.003.

Anisimov, N. V, Tarasova, A. A., Pavlova, O. S., Fomina, D. V, Makurenkov, A. M., Pavlovskaya, G. E., *et al.* (2021) 'MRI Coils Optimized for Detection of 1H and 23Na at 0.5 T', *Applied Magnetic Resonance*. Springer Vienna, pp. 1–13. doi: 10.1007/s00723-020-01306-x.

Anraku, Y., Mizuta, H., Sei, A., Kudo, S., Nakamura, E., Senba, K., *et al.* (2009) 'Analyses of early events during chondrogenic repair in rat full-thickness articular cartilage defects', *Journal of Bone and Mineral Metabolism*. J Bone Miner Metab, 27(3), pp. 272–286. doi: 10.1007/s00774-009-0038-x.

Appleton, C. T. G., Pitelka, V., Henry, J. and Beier, F. (2007) 'Global analyses of gene expression in early experimental osteoarthritis', *Arthritis & Rheumatism*. John Wiley & Sons, Ltd, 56(6), pp. 1854–1868. doi: 10.1002/art.22711.

Arai, T., Busby, W. and Clemmons, D. R. (1996) 'Binding of insulin-like growth factor (IGF) I or II to IGF-binding protein-2 enables it to bind to heparin and extracellular matrix.', *Endocrinology*. Endocrine Society, 137(11), pp. 4571–4575. doi: 10.1210/endo.137.11.8895319.

Arakawa, T. and Timasheff, S. N. (1984) 'Mechanism of Protein Salting In and Salting Out by Divalent Cation Salts: Balance between Hydration and Salt Binding', *Biochemistry*. American Chemical Society, 23(25), pp. 5912–5923. doi: 10.1021/bi00320a004.

Arikawa-Hirasawa, E., Watanabe, H., Takami, H., Hassell, J. R. and Yamada, Y. (1999) 'Perlecan is essential for cartilage and cephalic development', *Nature Genetics*. Nat Genet, 23(3), pp. 354–358. doi: 10.1038/15537.

Armelin, H. A. (1973) 'Pituitary Extracts and Steroid Hormones in the Control of 3T3 Cell Growth', *Proceedings of the National Academy of Sciences*, 70(9), pp. 2702–2706. doi: 10.1073/pnas.70.9.2702.

Armstrong, C. G. and Mow, V. C. (1982) 'Variations in the intrinsic mechanical properties of human articular cartilage with age, degeneration, and water content.', *The Journal of Bone & Joint Surgery*, 64(1), pp. 88–94. doi: 10.2106/00004623-198264010-00013.

Ataliotis, P. (2000) 'Platelet-derived growth factor A modulates limb chondrogenesis both in vivo and in vitro', *Mechanisms of Development*. Elsevier, 94(1–2), pp. 13–24. doi: 10.1016/S0925-4773(00)00321-X.

Aurich, M., Mwale, F., Reiner, A., Mollenhauer, J. A., Anders, J. O., Fuhrmann, R. A., *et al.* (2006) 'Collagen and proteoglycan turnover in focally damaged human ankle cartilage: Evidence for a generalized response and active matrix remodeling across the entire joint surface', *Arthritis & Rheumatism*. Arthritis Rheum, 54(1), pp. 244–252. doi: 10.1002/art.21535.

Awad, H. A., Halvorsen, Y. D. C., Gimble, J. M. and Guilak, F. (2003) 'Effects of Transforming Growth Factor β1 and Dexamethasone on the Growth and Chondrogenic Differentiation of Adipose-Derived Stromal Cells', *Tissue*

Engineering. Mary Ann Liebert, Inc. , 9(6), pp. 1301–1312. doi: 10.1089/10763270360728215.

Ball, D. K., Rachfal, A. W., Kemper, S. A. and Brigstock, D. R. (2003) *The heparin-binding 10 kDa fragment of connective tissue growth factor (CTGF) containing module 4 alone stimulates cell adhesion*, *Journal of Endocrinology*. Available at: http://www.endocrinology.org (Accessed: 12 November 2020).

Bao, C., Wang, J., Ma, W., Wang, X. and Cheng, Y. (2014) 'HDGF: a novel jack-of-all-trades in cancer', *Future Oncology*, 10(16), pp. 2675–2685. doi: 10.2217/fon.14.194.

Bartus, K., James, N. D., Didangelos, A., Bosch, K. D., Verhaagen, J., Yáñez-Muñoz, R. J., *et al.* (2014) 'Large-Scale Chondroitin Sulfate Proteoglycan Digestion with Chondroitinase Gene Therapy Leads to Reduced Pathology and Modulates Macrophage Phenotype following Spinal Cord Contusion Injury', *The Journal of Neuroscience*. Society for Neuroscience, 34(14), pp. 4822–4836. doi: 10.1523/JNEUROSCI.4369-13.2014.

Bashir, A., Gray, M. L. and Burstein, D. (1996) 'Gd-DTPA2− as a measure of cartilage degradation', *Magnetic Resonance in Medicine*. Magn Reson Med, 36(5), pp. 665–673. doi: 10.1002/mrm.1910360504.

Bateman, J. F., Rowley, L., Belluoccio, D., Chan, B., Bell, K., Fosang, A. J., *et al.* (2013) 'Transcriptomics of Wild-Type Mice and Mice Lacking ADAMTS-5 Activity Identifies Genes Involved in Osteoarthritis Initiation and Cartilage Destruction', *Arthritis & Rheumatism*. John Wiley & Sons, Ltd, 65(6), pp. 1547–1560. doi: 10.1002/art.37900.

Bay-Jensen, A. C., Andersen, T. L., Charni-Ben Tabassi, N., Kristensen, P. W., Kjaersgaard-Andersen, P., Sandell, L., *et al.* (2008) 'Biochemical markers of type II collagen breakdown and synthesis are positioned at specific sites in human osteoarthritic knee cartilage', *Osteoarthritis and Cartilage*. W.B. Saunders, 16(5), pp. 615–623. doi: 10.1016/j.joca.2007.09.006.

Benito, M. J., Veale, D. J., FitzGerald, O., Berg, W. B. van den and Bresnihan, B. (2005) 'Synovial tissue inflammation in early and late osteoarthritis', *Annals of the Rheumatic Diseases*. BMJ Publishing Group Ltd, 64(9), pp. 1263–1267. doi: 10.1136/ARD.2004.025270.

Blaney Davidson, E. N., van Caam, A. P. M., Vitters, E. L., Bennink, M. B., Thijssen, E., van den Berg, W. B., *et al.* (2015) 'TGF-β is a potent inducer of Nerve Growth Factor in articular cartilage via the ALK5-Smad2/3 pathway. Potential role in OA related pain?', *Osteoarthritis and Cartilage*. W.B. Saunders Ltd, 23(3), pp. 478–486. doi: 10.1016/j.joca.2014.12.005.

Blaney Davidson, E. N., Vitters, E. L., van den Berg, W. B. and van der Kraan, P. M. (2006) 'TGF β-induced cartilage repair is maintained but fibrosis is blocked in the presence of Smad7', *Arthritis Research and Therapy*. BioMed Central, 8(3), p. R65. doi: 10.1186/ar1931.

Blazek, K., Favre, J., Asay, J., Erhart-Hledik, J. and Andriacchi, T. (2014) 'Age and obesity alter the relationship between femoral articular cartilage thickness and ambulatory loads in individuals without osteoarthritis', *Journal of Orthopaedic Research*. John Wiley & Sons, Ltd, 32(3), pp. 394–402. doi: 10.1002/jor.22530.

Borthakur, A., Shapiro, E. ., Beers, J., Kudchodkar, S., Kneeland, J. . and Reddy, R. (2000) 'Sensitivity of MRI to proteoglycan depletion in cartilage: comparison of sodium and proton MRI', *Osteoarthritis and Cartilage*, 8(4), pp. 288–293. doi: 10.1053/joca.1999.0303.

Bos, P. K., Verhaar, J. A. N. and van Osch, G. J. V. M. (2006) 'Age-Related Differences in Articular Cartilage Wound Healing: A Potential Role for Transforming Growth Factor β1 in Adult Cartilage Repair', in *Advances in Experimental Medicine and Biology*. Springer New York, pp. 297–309. doi: 10.1007/978-0-387-34133-0_20.

Botter, S. M., van Osch, G. J. V. M., Waarsing, J. H., van der Linden, J. C., Verhaar, J. A. N., Pols, H. A. P., *et al.* (2008) 'Cartilage damage pattern in relation to subchondral plate thickness in a collagenase-induced model of osteoarthritis', *Osteoarthritis and Cartilage*, 16(4), pp. 506–514. doi: 10.1016/j.joca.2007.08.005.

Bradham, D. M., Igarashi, A., Potter, R. L. and Grotendorst, G. R. (1991) 'Connective tissue growth factor: A cysteine-rich mitogen secreted by human vascular endothelial cells is related to the SRC-induced immediate early gene product CEF-10', *Journal of Cell Biology*. J Cell Biol, 114(6), pp. 1285–1294. doi: 10.1083/jcb.114.6.1285.

Bremer, S., Klein, K., Sedlmaier, A., Abouzied, M., Gieselmann, V. and Franken, S. (2013) 'Hepatoma-derived growth factor and nucleolin exist in the same ribonucleoprotein complex', *BMC Biochemistry*, 14(1), p. 2. doi: 10.1186/1471-2091-14-2.

Brigstock, D. R., Goldschmeding, R., Katsube, K. I., Lam, S. C. T., Lau, L. F., Lyons, K., *et al.* (2003) 'Proposal for a unified CCN nomenclature', *Journal of Clinical Pathology - Molecular Pathology*. BMJ Publishing Group, 56(2), pp. 127–128. doi: 10.1136/mp.56.2.127.

Brigstock, D. R., Steffen, C. L., Kim, G. Y., Vegunta, R. K., Diehl, J. R. and Harding, P. A. (1997) 'Purification and Characterization of Novel Heparin-binding Growth Factors in Uterine Secretory Fluids', *Journal of Biological Chemistry*. American Society for Biochemistry and Molecular Biology, 272(32), pp. 20275–20282. doi: 10.1074/jbc.272.32.20275.

Brunner, A., Chinn, J., Neubauer, M. and Purchio, A. F. (1991) 'Identification of a Gene Family Regulated by Transforming Growth Factor-β', *DNA and Cell Biology*, 10(4), pp. 293–300. doi: 10.1089/dna.1991.10.293.

Burton-Wurster, N., Mateescu, R. G., Todhunter, R. J., Clements, K. M., Sun, Q., Scarpino, V., *et al.* (2005) 'Genes in canine articular cartilage that respond to mechanical injury: Gene expression studies with Affymetrix canine GeneChip', *Journal of Heredity*. Oxford Academic, 96(7), pp. 821–828. doi: 10.1093/jhered/esi105.

Cao, M., Pan, Q., Dong, H., Yuan, X., Li, Y., Sun, Z., *et al.* (2015) 'Adipose-derived mesenchymal stem cells improve glucose homeostasis in high-fat diet-induced obese mice', *Stem Cell Research & Therapy*. BioMed Central Ltd., 6(1), p. 208. doi: 10.1186/s13287-015-0201-3.

Carter, E. P., Fearon, A. E. and Grose, R. P. (2015) 'Careless talk costs lives: Fibroblast growth factor receptor signalling and the consequences of pathway malfunction', *Trends in Cell Biology*. Elsevier Ltd, pp. 221–233. doi: 10.1016/j.tcb.2014.11.003.

Chanalaris, A., Clarke, H., Guimond, S. E., Vincent, T. L., Turnbull, J. E. and Troeberg, L. (2019) 'Heparan Sulfate Proteoglycan Synthesis Is Dysregulated in Human Osteoarthritic Cartilage', *The American Journal of Pathology*. Elsevier Inc., 189(3), pp. 632–647. doi: 10.1016/j.ajpath.2018.11.011.

Chang, J., Liao, Z., Lu, M., Meng, T., Han, W. and Ding, C. (2018) 'Systemic and local adipose tissue in knee osteoarthritis', *Osteoarthritis and Cartilage*. W.B. Saunders Ltd, 26(7), pp. 864–871. doi: 10.1016/j.joca.2018.03.004.

Chang, K. C., Tai, M. H., Lin, J. W., Wang, C. C., Huang, C. C., Hung, C. H., *et al.* (2007) 'Hepatoma-derived growth factor is a novel prognostic factor for gastrointestinal stromal tumors', *International Journal of Cancer*. Int J Cancer, 121(5), pp. 1059–1065. doi: 10.1002/ijc.22803.

Chen, C. T., Burton-Wurster, N., Borden, C., Hueffer, K., Bloom, S. E. and Lust, G. (2001) 'Chondrocyte necrosis and apoptosis in impact damaged articular cartilage', *Journal of Orthopaedic Research*. Elsevier BV, 19(4), pp. 703–711. doi: 10.1016/S0736-0266(00)00066-8.

Chen, L.-Y., Huang, Y.-C., Huang, S.-T., Hsieh, Y.-C., Guan, H.-H., Chen, N.-C., *et al.* (2018) 'Domain swapping and SMYD1 interactions with the PWWP domain of human hepatoma-derived growth factor', *Scientific Reports*, 8(1), p. 287. doi: 10.1038/s41598-017-18510-8.

Chen, S.-C., Hu, T.-H., Huang, C.-C., Kung, M.-L., Chu, T.-H., Yi, L.-N., *et al.* (2015) 'Hepatoma-derived growth factor/nucleolin axis as a novel oncogenic pathway in liver carcinogenesis', *Oncotarget*. Impact Journals, 6(18), pp. 16253–16270. doi: 10.18632/oncotarget.3608.

Chen, S. S., Falcovitz, Y. H., Schneiderman, R., Maroudas, A. and Sah, R. L. (2001) 'Depth-dependent compressive properties of normal aged human femoral head articular cartilage: relationship to fixed charge density', *Osteoarthritis and Cartilage*. W.B. Saunders, 9(6), pp. 561–569. doi: 10.1053/joca.2001.0424.

Chen, S., Zhang, L., Xu, R., Ti, Y., Zhao, Y., Zhou, L., *et al.* (2017) 'BDKRB2 +9/−9 bp polymorphisms influence BDKRB2 expression levels and NO production in knee osteoarthritis', *Experimental Biology and Medicine*. SAGE Publications Inc., 242(4), pp. 422–428. doi: 10.1177/1535370215625471.

Chen, S., Zhou, Y., Li, J., Shan, L. Q. and Fan, Q. Y. (2012) 'The effect of bradykinin B2 receptor polymorphisms on the susceptibility and severity of osteoarthritis in a Chinese cohort', *Journal of Biomedicine and Biotechnology*, 2012. doi: 10.1155/2012/597637.

Chia, S.-L., Sawaji, Y., Burleigh, A., McLean, C., Inglis, J., Saklatvala, J., *et al.* (2009) 'Fibroblast growth factor 2 is an intrinsic chondroprotective agent that suppresses ADAMTS-5 and delays cartilage degradation in murine osteoarthritis', *Arthritis & Rheumatism*, 60(7), pp. 2019–2027. doi: 10.1002/art.24654.

Chiu, L.-Y., Hung, K.-W., Tjong, S.-C., Chiang, Y.-W. and Sue, S.-C. (2014) 'NMR characterization of the electrostatic interaction of the basic residues in HDGF and FGF2 during heparin binding', *Biochimica et Biophysica Acta (BBA) - Proteins and Proteomics*, 1844(10), pp. 1851–1859. doi: 10.1016/j.bbapap.2014.08.002.

Chlebova, K., Bryja, V., Dvorak, P., Kozubik, A., Wilcox, W. R. and Krejci, P. (2009) 'High molecular weight FGF2: the biology of a nuclear growth factor', *Cellular and Molecular Life Sciences*. NIH Public Access, 66(2), pp. 225–235. doi: 10.1007/s00018-008-8440-4.

Chong, K.-W., Chanalaris, A., Burleigh, A., Jin, H., Watt, F. E., Saklatvala, J., *et al.* (2013) 'Fibroblast Growth Factor 2 Drives Changes in Gene Expression Following Injury to Murine Cartilage In Vitro and In Vivo', *Arthritis & Rheumatism*. Wiley-Blackwell, 65(9), pp. 2346–2355. doi: 10.1002/art.38039.

Chubinskaya, S., Kumar, B., Merrihew, C., Heretis, K., Rueger, D. C. and Kuettner, K. E. (2002) 'Age-related changes in cartilage endogenous osteogenic protein-1 (OP-1)', *Biochimica et Biophysica Acta (BBA) - Molecular Basis of Disease*. Elsevier, 1588(2), pp. 126–134. doi: 10.1016/S0925-4439(02)00158-8.

Chubinskaya, S., Otten, L., Soeder, S., Borgia, J. A., Aigner, T., Rueger, D. C., *et al.* (2011) 'Regulation of

chondrocyte gene expression by osteogenic protein-1', *Arthritis Research and Therapy*. BioMed Central, 13(2), p. R55. doi: 10.1186/ar3300.

Clark, A. L., Votta, B. J., Kumar, S., Liedtke, W. and Guilak, F. (2010) 'Chondroprotective role of the osmotically sensitive ion channel transient receptor potential vanilloid 4: Age- and sex-dependent progression of osteoarthritis in Trpv4-deficient mice', *Arthritis & Rheumatism*. John Wiley & Sons, Ltd, 62(10), pp. 2973–2983. doi: 10.1002/art.27624.

Collins, A. T., Kulvaranon, M. L., Cutcliffe, H. C., Utturkar, G. M., Smith, W. A. R., Spritzer, C. E., *et al.* (2018) 'Obesity alters the in vivo mechanical response and biochemical properties of cartilage as measured by MRI', *Arthritis Research and Therapy*. BioMed Central Ltd., 20(1), pp. 1–9. doi: 10.1186/s13075-018-1727-4.

Collins, K. H., Lenz, K. L., Pollitt, E. N., Ferguson, D., Hutson, I., Springer, L. E., *et al.* (2021) 'Adipose tissue is a critical regulator of osteoarthritis', *Proceedings of the National Academy of Sciences*. National Academy of Sciences, 118(1), p. e2021096118. doi: 10.1073/pnas.2021096118.

Correa, D., Somoza, R. A., Lin, P., Greenberg, S., Rom, E., Duesler, L., *et al.* (2015) 'Sequential exposure to fibroblast growth factors (FGF) 2, 9 and 18 enhances hMSC chondrogenic differentiation', *Osteoarthritis and Cartilage*. W.B. Saunders Ltd, 23(3), pp. 443–453. doi: 10.1016/j.joca.2014.11.013.

Coste, B., Mathur, J., Schmidt, M., Earley, T. J., Ranade, S., Petrus, M. J., *et al.* (2010) 'Piezo1 and Piezo2 Are Essential Components of Distinct Mechanically Activated Cation Channels', *Science*, 330(6000), pp. 55–60. doi: 10.1126/science.1193270.

Coveney, C., Zhu, L., Miotla-Zarebska, J., Stott, B., Parisi, I., Batchelor, V., *et al.* (2020) 'The ciliary protein IFT88 controls post-natal cartilage thickness and influences development of osteoarthritis', *bioRxiv*. Cold Spring Harbor Laboratory, p. 2020.07.29.225599. doi: doi.org/10.1101/2020.07.29.225599.

Cucchiarini, M., Madry, H., Ma, C., Thurn, T., Zurakowski, D., Menger, M. D., *et al.* (2005) 'Improved Tissue Repair in Articular Cartilage Defects in Vivo by rAAV-Mediated Overexpression of Human Fibroblast Growth Factor 2', *Molecular Therapy*. Mol Ther, 12(2), pp. 229–238. doi: 10.1016/j.ymthe.2005.03.012.

Cuevas, P., Burgos, J. and Baird, A. (1988) 'Basic fibroblast growth factor (FGF) promotes cartilage repair in vivo', *Biochemical and Biophysical Research Communications*. Academic Press, 156(2), pp. 611–618. doi: 10.1016/S0006-291X(88)80887-8.

D'Lima, D. D., Hashimoto, S., Chen, P. C., Lotz, M. K. and Colwell, J. (2001) 'Cartilage injury induces chondrocyte apoptosis', in *Journal of Bone and Joint Surgery - Series A*. Journal of Bone and Joint Surgery Inc., pp. 19–21. doi: 10.2106/00004623-200100021-00004.

Daniels, J. T., Schultz, G. S., Blalock, T. D., Garrett, Q., Grotendorst, G. R., Dean, N. M., *et al.* (2003) 'Mediation of Transforming Growth Factor-β1-Stimulated Matrix Contraction by Fibroblasts', *The American Journal of Pathology*. American Society for Investigative Pathology Inc., 163(5), pp. 2043–2052. doi: 10.1016/S0002-9440(10)63562-6.

Darling, E. M., Wilusz, R. E., Bolognesi, M. P., Zauscher, S. and Guilak, F. (2010) 'Spatial Mapping of the Biomechanical Properties of the Pericellular Matrix of Articular Cartilage Measured In Situ via Atomic Force Microscopy', *Biophysical Journal*. Wiley Subscription Services, Inc., A Wiley Company, 98(12), pp. 2848–2856. doi: 10.1016/j.bpj.2010.03.037.

Davidson, E. N. B., van de Loo, F. A. J., van den Berg, W. B. and van der Kraan, P. M. (2014) 'How to build an inducible cartilage-specific transgenic mouse', *Arthritis Research & Therapy*. BioMed Central Ltd., 16(3), p. 210. doi: 10.1186/ar4573.

Davidson, E. N. B., Vitters, E. L., van Lent, P. L. E. M., van de Loo, F. A. J., van den Berg, W. B. and van der Kraan, P. M. (2007) 'Elevated extracellular matrix production and degradation upon bone morphogenetic protein-2 (BMP-2) stimulation point toward a role for BMP-2 in cartilage repair and remodeling', *Arthritis Research and Therapy*. Arthritis Res Ther, 9(5). doi: 10.1186/ar2305.

Davis, M. G., Zhou, M., Ali, S., Coffin, J. D., Doetschman, T. and Dorn, G. W. (1997) 'Intracrine and autocrine effects of basic fibroblast growth factor in vascular smooth muscle cells', *Journal of Molecular and Cellular Cardiology*. Academic Press, 29(4), pp. 1061–1072. doi: 10.1006/jmcc.1997.0383.

Deen, W. M. (1998) *Analysis of Transport Phenomena (Topics in Chemical Engineering)*.

Dell'Accio, F., De Bari, C., Eltawil, N. M., Vanhummelen, P. and Pitzalis, C. (2008) 'Identification of the molecular response of articular cartilage to injury, by microarray screening: Wnt-16 expression and signaling after injury and in osteoarthritis', *Arthritis & Rheumatism*. John Wiley & Sons, Ltd, 58(5), pp. 1410–1421. doi: 10.1002/art.23444.

Deng, T., Huang, S., Zhou, S., He, L. and Jin, Y. (2007) 'Cartilage regeneration using a novel gelatin-chondroitin-hyaluronan hybrid scaffold containing bFGF-impregnated microspheres', *Journal of Microencapsulation*. Taylor

& Francis, 24(2), pp. 163–174. doi: 10.1080/02652040701233523.

Derynck, R. and Zhang, Y. E. (2003) 'Smad-dependent and Smad-independent pathways in TGF-β family signalling', *Nature*. Nature Publishing Group, 425(6958), pp. 577–584. doi: 10.1038/nature02006.

DiDomenico, C. D., Lintz, M. and Bonassar, L. J. (2018) 'Molecular transport in articular cartilage — what have we learned from the past 50 years?', *Nature Reviews Rheumatology*. Springer US, 14(7), pp. 393–403. doi: 10.1038/s41584-018-0033-5.

Dietz, F., Franken, S., Yoshida, K., Nakamura, H., Kappler, J. and Gieselmann, V. (2002) 'The family of hepatoma-derived growth factor proteins: characterization of a new member HRP-4 and classification of its subfamilies', *Biochemical Journal*, 366(2), pp. 491–500. doi: 10.1042/bj20011811.

Ding, C., Parameswaran, V., Cicuttini, F., Burgess, J., Zhai, G., Quinn, S., *et al.* (2007) 'Association between leptin, body composition, sex and knee cartilage morphology in older adults: the Tasmanian older adult cohort (TASOAC) study', *Annals of the Rheumatic Diseases*, 67(9), pp. 1256–1261. doi: 10.1136/ard.2007.082651.

Driscoll, C., Chanalaris, A., Knight, C., Gentry, C., Bevan, S. and Vincent, T. L. (2014) 'Cartilage injury regulates nerve growth factor (NGF) in vitro and in vivo and drives painful behaviour in murine OA', *Osteoarthritis and Cartilage*. Elsevier BV, 22, p. S35. doi: 10.1016/j.joca.2014.02.084.

Driscoll, C., Chanalaris, A., Knights, C., Ismail, H., Sacitharan, P. K., Gentry, C., *et al.* (2016) 'Nociceptive Sensitizers Are Regulated in Damaged Joint Tissues, Including Articular Cartilage, When Osteoarthritic Mice Display Pain Behavior', *Arthritis & Rheumatology*. John Wiley and Sons Inc., 68(4), pp. 857–867. doi: 10.1002/art.39523.

Duchesne, L., Octeau, V., Bearon, R. N., Beckett, A., Prior, I. A., Lounis, B., *et al.* (2012) 'Transport of Fibroblast Growth Factor 2 in the Pericellular Matrix Is Controlled by the Spatial Distribution of Its Binding Sites in Heparan Sulfate', *PLoS Biology*. Edited by A. D. Lander, 10(7), p. e1001361. doi: 10.1371/journal.pbio.1001361.

Dunn, S. L., Soul, J., Anand, S., Schwartz, J. M., Boot-Handford, R. P. and Hardingham, T. E. (2016) 'Gene expression changes in damaged osteoarthritic cartilage identify a signature of non-chondrogenic and mechanical responses', *Osteoarthritis and Cartilage*. W.B. Saunders Ltd, 24(8), pp. 1431–1440. doi: 10.1016/j.joca.2016.03.007.

Eckstein, F., Kraines, J. L., Aydemir, A., Wirth, W., Maschek, S. and Hochberg, M. C. (2020) 'Intra-articular sprifermin reduces cartilage loss in addition to increasing cartilage gain independent of location in the femorotibial joint: post-hoc analysis of a randomised, placebo-controlled phase II clinical trial', *Annals of the Rheumatic Diseases*. BMJ Publishing Group, 79(4), pp. 525–528. doi: 10.1136/annrheumdis-2019-216453.

Elford, P. R. and Lamberts, S. W. J. (1990) 'Contrasting Modulation by Transforming Growth Factor-β-1 of Insulin-Like Growth Factor-I Production in Osteoblasts and Chondrocytes', *Endocrinology*. Endocrinology, 127(4), pp. 1635–1639. doi: 10.1210/endo-127-4-1635.

Eller, S., Collot, M., Yin, J., Hahm, H. S. and Seeberger, P. H. (2013) 'Automated Solid-Phase Synthesis of Chondroitin Sulfate Glycosaminoglycans', *Angewandte Chemie International Edition*, 52(22), pp. 5858–5861. doi: 10.1002/anie.201210132.

Ellman, M. B., Yan, D., Ahmadinia, K., Chen, D., An, H. S. and Im, H. J. (2013) 'Fibroblast growth factor control of cartilage homeostasis', *Journal of Cellular Biochemistry*, 114(4), pp. 735–742. doi: 10.1002/jcb.24418.

Eltawil, N. M., De Bari, C., Achan, P., Pitzalis, C. and Dell'Accio, F. (2009) 'A novel in vivo murine model of cartilage regeneration. Age and strain-dependent outcome after joint surface injury', *Osteoarthritis and Cartilage*. Elsevier, 17(6), pp. 695–704. doi: 10.1016/j.joca.2008.11.003.

Evans, R. C. and Quinn, T. M. (2005) 'Solute diffusivity correlates with mechanical properties and matrix density of compressed articular cartilage', *Archives of Biochemistry and Biophysics*. Academic Press, 442(1), pp. 1–10. doi: 10.1016/j.abb.2005.07.025.

Everett, A. D., Lobe, D. R., Matsumura, M. E., Nakamura, H. and McNamara, C. A. (2000) 'Hepatoma-derived growth factor stimulates smooth muscle cell growth and is expressed in vascular development', *Journal of Clinical Investigation.* American Society for Clinical Investigation, 105(5), pp. 567–575. doi: 10.1172/JCI7497.

Everett, A. D., Stoops, T. and McNamara, C. A. (2001) 'Nuclear Targeting Is Required for Hepatoma-derived Growth Factor-stimulated Mitogenesis in Vascular Smooth Muscle Cells', *Journal of Biological Chemistry*. American Society for Biochemistry and Molecular Biology, 276(40), pp. 37564–37568. doi: 10.1074/jbc.M105109200.

Fan, H., Tao, H., Wu, Y., Hu, Y., Yan, Y. and Luo, Z. (2010) 'TGF-β3 immobilized PLGA-gelatin/chondroitin sulfate/hyaluronic acid hybrid scaffold for cartilage regeneration', *Journal of Biomedical Materials Research Part A*. J Biomed Mater Res A, 95A(4), pp. 982–992. doi: 10.1002/jbm.a.32899.

Fisher, M. C., Li, Y., Seghatoleslami, M. R., Dealy, C. N. and Kosher, R. A. (2006) 'Heparan sulfate proteoglycans including syndecan-3 modulate BMP activity during limb cartilage differentiation', *Matrix Biology*. Matrix Biol, 25(1), pp. 27–39. doi: 10.1016/j.matbio.2005.07.008.

Flannery, C. R., Little, C. B., Hughes, C. E., Curtis, C. L., Caterson, B. and Jones, S. A. (2000) 'IL-6 and its soluble receptor augment aggrecanase-mediated proteoglycan catabolism in articular cartilage', *Matrix Biology*. Elsevier, 19(6), pp. 549–553. doi: 10.1016/S0945-053X(00)00111-6.

Fleischmann, R. M., Bliddal, H., Blanco, F. J., Schnitzer, T. J., Peterfy, C., Chen, S., *et al.* (2019) 'A Phase II Trial of Lutikizumab, an Anti–Interleukin-1α/β Dual Variable Domain Immunoglobulin, in Knee Osteoarthritis Patients With Synovitis', *Arthritis & Rheumatology*, 71(7), pp. 1056–1069. doi: 10.1002/art.40840.

Fontaine, D. A. and Davis, D. B. (2016) 'Attention to Background Strain Is Essential for Metabolic Research: C57BL/6 and the International Knockout Mouse Consortium', *Diabetes*. American Diabetes Association Inc., 65(1), pp. 25–33. doi: 10.2337/db15-0982.

Forsythe, I. D. and Redman, S. J. (1988) 'The dependence of motoneurone membrane potential on extracellular ion concentrations studied in isolated rat spinal cord.', *The Journal of Physiology*. Wiley-Blackwell, 404(1), pp. 83–99. doi: 10.1113/jphysiol.1988.sp017280.

Fortier, L. A., Barker, J. U., Strauss, E. J., McCarrel, T. M. and Cole, B. J. (2011) 'The Role of Growth Factors in Cartilage Repair', *Clinical Orthopaedics and Related Research*. Springer New York LLC, 469(10), pp. 2706–2715. doi: 10.1007/s11999-011-1857-3.

Freeman, M. A. R. (1979) 'Adult articular cartilage. M. A. R. Freeman. second edition.', *Arthritis & Rheumatism*. John Wiley & Sons, Inc. doi: 10.1002/art.1780230134.

Fukumoto, T., Sperling, J. W., Sanyal, A., Fitzsimmons, J. S., Reinholz, G. G., Conover, C. A., *et al.* (2003) 'Combined effects of insulin-like growth factor-1 and transforming growth factor-β1 on periosteal mesenchymal cells during chondrogenesis in vitro', *Osteoarthritis and Cartilage*. W.B. Saunders Ltd, 11(1), pp. 55–64. doi: 10.1053/joca.2002.0869.

Gacaferi, H., Mimpen, J. Y., Baldwin, M. J., Snelling, S. J. B., Nelissen, R. G. H. H., Carr, A. J., *et al.* (2020) 'The potential roles of high mobility group box 1 (HMGB1) in musculoskeletal disease: A systematic review', *Translational Sports Medicine*. Wiley, 3(6), pp. 536–564. doi: 10.1002/tsm2.175.

Gallitzendoerfer, R., Abouzied, M. M., Hartmann, D., Dobrowolski, R., Gieselmann, V. and Franken, S. (2008) 'Hepatoma-derived growth factor (HDGF) is dispensable for normal mouse development', *Developmental Dynamics*, 237(7), pp. 1875–1885. doi: 10.1002/dvdy.21589.

Gardiner, M. D., Vincent, T. L., Driscoll, C., Burleigh, A., Bou-Gharios, G., Saklatvala, J., *et al.* (2015) 'Transcriptional analysis of micro-dissected articular cartilage in post-traumatic murine osteoarthritis', *Osteoarthritis and Cartilage*, 23(4), pp. 616–628. doi: 10.1016/j.joca.2014.12.014.

Gardner, O. F. W., Fahy, N., Alini, M. and Stoddart, M. J. (2017) 'Joint mimicking mechanical load activates TGFβ1 in fibrin-poly(ester-urethane) scaffolds seeded with mesenchymal stem cells', *Journal of Tissue Engineering and Regenerative Medicine*. John Wiley and Sons Ltd, 11(9), pp. 2663–2666. doi: 10.1002/term.2210.

Geiger, B. C., Wang, S., Padera, R. F., Grodzinsky, A. J. and Hammond, P. T. (2018) 'Cartilage-penetrating nanocarriers improve delivery and efficacy of growth factor treatment of osteoarthritis', *Science Translational Medicine*, 10(469), p. eaat8800. doi: 10.1126/scitranslmed.aat8800.

Gendron, C., Kashiwagi, M., Lim, N. H., Enghild, J. J., Thøgersen, I. B., Hughes, C., *et al.* (2007) 'Proteolytic activities of human ADAMTS-5: comparative studies with ADAMTS-4.', *Journal of Biological Chemistry*. American Society for Biochemistry and Molecular Biology, 282(25), pp. 18294–18306. doi: 10.1074/jbc.M701523200.

Geyer, M., Grässel, S., Straub, R. H., Schett, G., Dinser, R., Grifka, J., *et al.* (2009) 'Differential transcriptome analysis of intraarticular lesional vs intact cartilage reveals new candidate genes in osteoarthritis pathophysiology', *Osteoarthritis and Cartilage*. W.B. Saunders, 17(3), pp. 328–335. doi: 10.1016/j.joca.2008.07.010.

Giri, K., Pabelick, C. M., Mukherjee, P. and Prakash, Y. S. (2016) 'Hepatoma derived growth factor (HDGF) dynamics in ovarian cancer cells', *Apoptosis*. Springer New York LLC, 21(3), pp. 329–339. doi: 10.1007/s10495-015-1200-7.

Glasson, S. S., Askew, R., Sheppard, B., Carito, B. A., Blanchet, T., Ma, H.-L., *et al.* (2004) 'Characterization of and osteoarthritis susceptibility in ADAMTS-4-knockout mice', *Arthritis & Rheumatism*. Arthritis Rheum, 50(8), pp. 2547–2558. doi: 10.1002/art.20558.

Glasson, S. S., Askew, R., Sheppard, B., Carito, B., Blanchet, T., Ma, H.-L., *et al.* (2005) 'Deletion of active ADAMTS5 prevents cartilage degradation in a murine model of osteoarthritis', *Nature*. Nature, 434(7033), pp. 644–648. doi: 10.1038/nature03369.

Glasson, S. S., Blanchet, T. J. and Morris, E. A. (2007) 'The surgical destabilization of the medial meniscus (DMM) model of osteoarthritis in the 129/SvEv mouse', *Osteoarthritis and Cartilage*. Elsevier, 15(9), pp. 1061–1069. doi: 10.1016/j.joca.2007.03.006.

Glasson, S. S., Chambers, M. G., Van Den Berg, W. B. and Little, C. B. (2010) 'The OARSI histopathology initiative – recommendations for histological assessments of osteoarthritis in the mouse', *Osteoarthritis and Cartilage*. W.B. Saunders, 18, pp. S17–S23. doi: 10.1016/j.joca.2010.05.025.

Goldring, S. R. and Goldring, M. B. (2016) 'Changes in the osteochondral unit during osteoarthritis: structure, function and cartilage–bone crosstalk', *Nature Reviews Rheumatology*. Nature Publishing Group, 12(11), pp. 632–644. doi: 10.1038/nrrheum.2016.148.

Gomes, R., Carson, M. C. F. and Carson, D. (2003) 'Perlecan-Stimulated Nodules Undergo Chondrogenic Maturation in Response to rhBMP-2 Treatment In Vitro', *Connective Tissue Research*. Taylor and Francis Ltd., 44(1), pp. 196–201. doi: 10.1080/713713591.

Gomes, R., Kirn-Safran, C., Farach-Carson, M. C. and Carson, D. D. (2002) 'Perlecan: An important component of the cartilage pericellular matrix', *Journal of Musculoskeletal Neuronal Interactions*. NIH Public Access, 2(6), pp. 511–516. Available at: /pmc/articles/PMC1387052/?report=abstract (Accessed: 13 January 2021).

Gong, X., Xie, W., Wang, B., Gu, L., Wang, F., Ren, X., *et al.* (2017) 'Altered spontaneous calcium signaling of in situ chondrocytes in human osteoarthritic cartilage', *Scientific Reports*, 7(1), p. 17093. doi: 10.1038/s41598-017-17172-w.

Gospodarowicz, D. (1974) 'Localisation of a fibroblast growth factor and its effect alone and with hydrocortisone on 3T3 cell growth.', *Nature*, 249(453), pp. 123–7. doi: 10.1038/249123a0.

Griffin, T. M., Huebner, J. L., Kraus, V. B. and Guilak, F. (2009) 'Extreme obesity due to impaired leptin signaling in mice does not cause knee osteoarthritis', *Arthritis & Rheumatism*, 60(10), pp. 2935–2944. doi: 10.1002/art.24854.

Griffin, T. M., Huebner, J. L., Kraus, V. B., Yan, Z. and Guilak, F. (2012) 'Induction of osteoarthritis and metabolic inflammation by a very high-fat diet in mice: Effects of short-term exercise', *Arthritis & Rheumatism*, 64(2), pp. 443–453. doi: 10.1002/art.33332.

Gruber, J., Vincent, T. L., Hermansson, M., Bolton, M., Wait, R. and Saklatvala, J. (2004) 'Induction of interleukin-1 in articular cartilage by explantation and cutting', *Arthritis & Rheumatism*. John Wiley & Sons, Ltd, 50(8), pp. 2539–2546. doi: 10.1002/art.20369.

Guenther, H. L., Guenther, H. E., Froesch, E. R. and Fleisch, H. (1982) 'Effect of insulin-like growth factor on collagen and glycosaminoglycan synthesis by rabbit articular chondrocytes in culture', *Experientia*. Birkhäuser-Verlag, 38(8), pp. 979–981. doi: 10.1007/BF01953688.

Guilak, F., Jones, W. R., Ting-Beall, H. P. and Lee, G. M. (1999) 'The deformation behavior and mechanical properties of chondrocytes in articular cartilage', *Osteoarthritis and Cartilage*. W.B. Saunders Ltd, 7(1), pp. 59–70. doi: 10.1053/joca.1998.0162.

Guilak, F. and Mow, V. C. (2000) 'The mechanical environment of the chondrocyte: A biphasic finite element model of cell-matrix interactions in articular cartilage', *Journal of Biomechanics*. Elsevier, 33(12), pp. 1663–1673. doi: 10.1016/S0021-9290(00)00105-6.

Guilak, F., Nims, R. J., Dicks, A., Wu, C.-L. and Meulenbelt, I. (2018) 'Osteoarthritis as a disease of the cartilage pericellular matrix', *Matrix Biology*, 71–72, pp. 40–50. doi: 10.1016/j.matbio.2018.05.008.

Guimond, S., Maccarana, M., Olwin, B. B., Lindahl, U. and Rapraeger, A. C. (1993) 'Activating and inhibitory heparin sequences for FGF-2 (basic FGF). Distinct requirements for FGF-1, FGF-2, and FGF-4.', *The Journal of Biological Chemistry*, 268(32), pp. 239906–23914. Available at: https://www.jbc.org/content/268/32/23906.short (Accessed: 18 November 2020).

Haapala, J., Lammi, M. J., Inkinen, R., Parkkinen, J. J., Agren, U. M., Arokoski, J., *et al.* (1996) 'Coordinated regulation of hyaluronan and aggrecan content in the articular cartilage of immobilized and exercised dogs.', *The Journal of rheumatology*, 23(9), pp. 1586–93. Available at: http://www.ncbi.nlm.nih.gov/pubmed/8877929.

Handel, T. M., Johnson, Z., Crown, S. E., Lau, E. K., Sweeney, M. and Proudfoot, A. E. (2005) 'Regulation of protein function by glycosaminoglycans—as exemplified by chemokines', *Annual Review of Biochemistry*. Annu Rev Biochem, 74(1), pp. 385–410. doi: 10.1146/annurev.biochem.72.121801.161747.

Handorf, A. M. and Li, W.-J. (2011) 'Fibroblast Growth Factor-2 Primes Human Mesenchymal Stem Cells for Enhanced Chondrogenesis', *PLoS ONE*. Edited by S. Shi. Public Library of Science, 6(7), p. e22887. doi: 10.1371/journal.pone.0022887.

Harding, P. A., Surveyor, G. A. and Brigstock, D. R. (1998) 'Characterization of pig connective tissue growth

factor (CTGF) cDNA, mRNA and protein from uterine tissue', *Mitochondrial DNA*. Taylor & Francis, 8(6), pp. 385–390. doi: 10.3109/10425179809020899.

Harris, H. E. and Raucci, A. (2006) 'Alarmin(g) news about danger', *EMBO reports*. European Molecular Biology Organization, 7(8), pp. 774–778. doi: 10.1038/sj.embor.7400759.

Henry, S. P., Jang, C.-W., Deng, J. M., Zhang, Z., Behringer, R. R. and de Crombrugghe, B. (2009) 'Generation of aggrecan-CreERT2 knockin mice for inducible Cre activity in adult cartilage', *genesis*. John Wiley & Sons, Ltd, 47(12), p. NA-NA. doi: 10.1002/dvg.20564.

Hiraide, A., Yokoo, N., Xin, K. Q., Okuda, K., Mizukami, H., Ozawa, K., *et al.* (2005) 'Repair of articular cartilage defect by intraarticular administration of basic fibroblast growth factor gene, using adeno-associated virus vector', *Human Gene Therapy*. Hum Gene Ther, 16(12), pp. 1413–1421. doi: 10.1089/hum.2005.16.1413.

Hochberg, M. C., Guermazi, A., Guehring, H., Aydemir, A., Wax, S., Fleuranceau-Morel, P., *et al.* (2019) 'Effect of Intra-Articular Sprifermin vs Placebo on Femorotibial Joint Cartilage Thickness in Patients With Osteoarthritis', *JAMA*. American Medical Association, 322(14), p. 1360. doi: 10.1001/jama.2019.14735.

Hollander, A., D'Onofrio, P. M., Magharious, M. M., Lysko, M. D. and Koeberle, P. D. (2012) 'Quantitative retinal protein analysis after optic nerve transection reveals a neuroprotective role for hepatoma- derived growth factor on injured retinal ganglion cells', *Investigative Ophthalmology and Visual Science*. The Association for Research in Vision and Ophthalmology, 53(7), pp. 3973–3989. doi: 10.1167/iovs.11-8350.

Hsueh, M., Zhang, X., Wellman, S. S., Bolognesi, M. P. and Kraus, V. B. (2021) 'Synergistic Roles of Macrophages and Neutrophils in Osteoarthritis Progression', *Arthritis & Rheumatology*. John Wiley and Sons Inc, 73(1), pp. 89–99. doi: 10.1002/art.41486.

Hu, H. Y., Lim, N. H., Ding-Pfennigdorff, D., Saas, J., Wendt, K. U., Ritzeler, O., *et al.* (2015) 'DOTAM Derivatives as Active Cartilage-Targeting Drug Carriers for the Treatment of Osteoarthritis', *Bioconjugate Chemistry*. American Chemical Society, 26(3), pp. 383–388. doi: 10.1021/bc500557s.

Hu, T. H., Lin, J. W., Chen, H. H., Liu, L. F., Chuah, S. K. and Tai, M. H. (2009) 'The expression and prognostic role of hepatoma-derived growth factor in colorectal stromal tumors', *Diseases of the Colon and Rectum*. Dis Colon Rectum, 52(2), pp. 319–326. doi: 10.1007/DCR.0b013e31819d1666.

Huch, K., Wilbrink, B., Flechtenmacher, J., Koepp, H. E., Aydelotte, M. B., Sampath, T. K., *et al.* (1997) 'Effects of recombinant human osteogenic protein 1 on the production of proteoglycan, prostaglandin E2, and interleukin-1 receptor antagonist by human articular chondrocytes cultured in the presence of interleukin-1β', *Arthritis and Rheumatism*. Arthritis Rheum, 40(12), pp. 2157–2161. doi: 10.1002/art.1780401209.

Hunter, D. J. and Bierma-Zeinstra, S. (2019) 'Osteoarthritis', *The Lancet*. Lancet Publishing Group, pp. 1745–1759. doi: 10.1016/S0140-6736(19)30417-9.

Im, H.-J., Muddasani, P., Natarajan, V., Schmid, T. M., Block, J. A., Davis, F., *et al.* (2007) 'Basic Fibroblast Growth Factor Stimulates Matrix Metalloproteinase-13 via the Molecular Cross-talk between the Mitogen-activated Protein Kinases and Protein Kinase Cδ Pathways in Human Adult Articular Chondrocytes', *Journal of Biological Chemistry*. J Biol Chem, 282(15), pp. 11110–11121. doi: 10.1074/jbc.M609040200.

Im, H.-J., Pacione, C., Chubinskaya, S., van Wijnen, A. J., Sun, Y. and Loeser, R. F. (2003) 'Inhibitory Effects of Insulin-like Growth Factor-1 and Osteogenic Protein-1 on Fibronectin Fragment- and Interleukin-1β-stimulated Matrix Metalloproteinase-13 Expression in Human Chondrocytes', *Journal of Biological Chemistry*. J Biol Chem, 278(28), pp. 25386–25394. doi: 10.1074/jbc.M302048200.

Inoue, A., Takahashi, K. A., Arai, Y., Tonomura, H., Sakao, K., Saito, M., *et al.* (2006) 'The therapeutic effects of basic fibroblast growth factor contained in gelatin hydrogel microspheres on experimental osteoarthritis in the rabbit knee', *Arthritis and Rheumatism*. Arthritis Rheum, 54(1), pp. 264–270. doi: 10.1002/art.21561.

Intema, F., Van Roermund, P. M., Marijnissen, A. C. A., Cotofana, S., Eckstein, F., Castelein, R. M., *et al.* (2011) 'Tissue structure modification in knee osteoarthritis by use of joint distraction: An open 1-year pilot study', *Annals of the Rheumatic Diseases*. Ann Rheum Dis, 70(8), pp. 1441–1446. doi: 10.1136/ard.2010.142364.

Ismail, H. M., Miotla-Zarebska, J., Troeberg, L., Tang, X., Stott, B., Yamamoto, K., *et al.* (2016) 'JNK2 controls aggrecan degradation in murine articular cartilage and the development of experimental osteoarthritis', *Arthritis & Rheumatology*. John Wiley and Sons Inc., 68(5), p. n/a-n/a. doi: 10.1002/art.39547.

Ismail, H. M., Yamamoto, K., Vincent, T. L., Nagase, H., Troeberg, L. and Saklatvala, J. (2015) 'Interleukin-1 Acts via the JNK-2 Signaling Pathway to Induce Aggrecan Degradation by Human Chondrocytes', *Arthritis & Rheumatology*, 67(7), pp. 1826–1836. doi: 10.1002/art.39099.

Jaccard, G., Wimperis, S. and Bodenhausen, G. (1986) 'Multiple-quantum NMR spectroscopy of S =3/2 spins in isotropic phase: A new probe for multiexponential relaxation', *The Journal of Chemical Physics*. American Institute of PhysicsAIP, 85(11), pp. 6282–6293. doi: 10.1063/1.451458.

Jackson, A. and Gu, W. (2009) 'Transport Properties of Cartilaginous Tissues', *Current Rheumatology Reviews*. Bentham Science Publishers Ltd., 5(1), pp. 40–50. doi: 10.2174/157339709787315320.

Jelic, M., Pecina, M., Haspl, M., Kos, J., Taylor, K., Maticic, D., *et al.* (2001) 'Regeneration of Articular Cartilage Chondral Defects by Osteogenic Protein-1 (Bone Morphogenetic Protein-7) in Sheep', *Growth Factors*. Harwood Academic Publishers GmbH, 19(2), pp. 101–113. doi: 10.3109/08977190109001079.

Jha, A. K., Yang, W., Kirn-Safran, C. B., Farach-Carson, M. C. and Jia, X. (2009) 'Perlecan domain I-conjugated, hyaluronic acid-based hydrogel particles for enhanced chondrogenic differentiation via BMP-2 release', *Biomaterials*. Biomaterials, 30(36), pp. 6964–6975. doi: 10.1016/j.biomaterials.2009.09.009.

Jo, C. H., Lee, Y. G., Shin, W. H., Kim, H., Chai, J. W., Jeong, E. C., *et al.* (2014) 'Intra-Articular Injection of Mesenchymal Stem Cells for the Treatment of Osteoarthritis of the Knee: A Proof-of-Concept Clinical Trial', *STEM CELLS*. Wiley-Blackwell, 32(5), pp. 1254–1266. doi: 10.1002/stem.1634.

Jørgensen, A. E. M., Kjær, M. and Heinemeier, K. M. (2017) 'The Effect of Aging and Mechanical Loading on the Metabolism of Articular Cartilage', *The Journal of Rheumatology*. The Journal of Rheumatology, 44(4), pp. 410–417. doi: 10.3899/jrheum.160226.

Kang, X., Qian, Z., Liu, J., Feng, D., Li, H., Zhang, Z., *et al.* (2020) 'Neuropeptide Y Acts Directly on Cartilage Homeostasis and Exacerbates Progression of Osteoarthritis Through NPY2R', *Journal of Bone and Mineral Research*. John Wiley and Sons Inc., 35(7), pp. 1375–1384. doi: 10.1002/jbmr.3991.

Kao, Y.-H., Chen, C.-L., Jawan, B., Chung, Y.-H., Sun, C.-K., Kuo, S.-M., *et al.* (2010) 'Upregulation of hepatoma-derived growth factor is involved in murine hepatic fibrogenesis', *Journal of Hepatology*, 52(1), pp. 96–105. doi: 10.1016/j.jhep.2009.10.002.

Kao, Y.-H., Chen, P.-H., Sun, C.-K., Chang, Y.-C., Lin, Y.-C., Tsai, M.-S., *et al.* (2018) 'Cyclic mechanical stretch up-regulates hepatoma-derived growth factor expression in cultured rat aortic smooth muscle cells', *Bioscience Reports*, 38(2), p. BSR20171398. doi: 10.1016/S0001-4575(01)00039-2.

Karlsson, C., Dehne, T., Lindahl, A., Brittberg, M., Pruss, A., Sittinger, M., *et al.* (2010) 'Genome-wide expression profiling reveals new candidate genes associated with osteoarthritis', *Osteoarthritis and Cartilage*. W.B. Saunders, 18(4), pp. 581–592. doi: 10.1016/j.joca.2009.12.002.

Kaul, G., Cucchiarini, M., Arntzen, D., Zurakowski, D., Menger, M. D., Kohn, D., *et al.* (2006) 'Local stimulation of articular cartilage repair by transplantation of encapsulated chondrocytes overexpressing human fibroblast growth factor 2 (FGF-2)in vivo', *The Journal of Gene Medicine*. John Wiley & Sons, Ltd, 8(1), pp. 100–111. doi: 10.1002/jgm.819.

Keppie, S. J., Mansfield, J. C., Tang, X., Philp, C. J., Graham, H. K., Önnerfjord, P., *et al.* (2021) 'Matrix-Bound Growth Factors are Released upon Cartilage Compression by an Aggrecan-Dependent Sodium Flux that is Lost in Osteoarthritis', *bioRxiv*. Cold Spring Harbor Laboratory, p. 2021.01.31.428791. doi: 10.1101/2021.01.31.428791.

Kiani, C., Chen, L., Wu, Y. J., Yee, A. J. and Yang, B. B. (2002) 'Structure and function of aggrecan', *Cell Research*, 12(1), pp. 19–32. doi: 10.1038/sj.cr.7290106.

Kim, B. J., Kim, D.-W., Kim, S. H., Cho, J. H., Lee, H. J., Park, D. Y., *et al.* (2013) 'Establishment of a reliable and reproducible murine osteoarthritis model', *Osteoarthritis and Cartilage*. W.B. Saunders, 21(12), pp. 2013–2020. doi: 10.1016/j.joca.2013.09.012.

Kimmerling, K. A., Oswald, S. J., Huebner, J. L., Little, D., Kraus, V. B., Kang, J. X., *et al.* (2020) 'Transgenic conversion of ω-6 to ω-3 polyunsaturated fatty acids via fat-1 reduces the severity of post-traumatic osteoarthritis', *Arthritis Research & Therapy*. BioMed Central Ltd., 22(1), p. 83. doi: 10.1186/s13075-020-02170-7.

Király, K., Lapveteläinen, T., Arokoski, J., Törrönen, K., Módis, L., Kiviranta, I., *et al.* (1996) 'Application of selected cationic dyes for the semiquantitative estimation of glycosaminoglycans in histological sections of articular cartilage by microspectrophotometry', *The Histochemical Journal*. Kluwer Academic Publishers, 28(8), pp. 577–590. doi: 10.1007/BF02331378.

Kishima, Y., Yamamoto, H., Izumoto, Y., Yoshida, K., Enomoto, H., Yamamoto, M., *et al.* (2002) 'Hepatoma-derived Growth Factor Stimulates Cell Growth after Translocation to the Nucleus by Nuclear Localization Signals', *Journal of Biological Chemistry*. American Society for Biochemistry and Molecular Biology, 277(12), pp. 10315–10322. doi: 10.1074/jbc.M111122200.

Kisiday, J. D., Frisbie, D. D., McIlwraith, C. W. and Grodzinsky, A. J. (2009) 'Dynamic Compression Stimulates Proteoglycan Synthesis by Mesenchymal Stem Cells in the Absence of Chondrogenic Cytokines', *Tissue Engineering Part A*. Mary Ann Liebert Inc., 15(10), pp. 2817–2824. doi: 10.1089/ten.tea.2008.0357.

Kiviranta, I., Jurvelin, J., Tammi, M., Säämänen, A. M. and Helminen, H. J. (1985) 'Microspectrophotometric quantitation of glycosaminoglycans in articular cartilage sections stained with Safranin O', *Histochemistry*. Springer-Verlag, 82(3), pp. 249–255. doi: 10.1007/BF00501401.

Kleinewietfeld, M., Manzel, A., Titze, J., Kvakan, H., Yosef, N., Linker, R. A., *et al.* (2013) 'Sodium chloride drives autoimmune disease by the induction of pathogenic TH17 cells', *Nature*, 496(7446), pp. 518–522. doi: 10.1038/nature11868.

Klüppel, M., Wight, T. N., Chan, C., Hinek, A. and Wrana, J. L. (2005) 'Maintenance of chondroitin sulfation balance by chondroitin-4-sulfotransferase 1 is required for chondrocyte development and growth factor signaling during cartilage morphogenesis', *Development*. Development, 132(17), pp. 3989–4003. doi: 10.1242/dev.01948.

Knight, M. M., Ross, J. M., Sherwin, A. F., Lee, D. A., Bader, D. L. and Poole, C. A. (2001) 'Chondrocyte deformation within mechanically and enzymatically extracted chondrons compressed in agarose', *Biochimica et Biophysica Acta - General Subjects*. Elsevier, 1526(2), pp. 141–146. doi: 10.1016/S0304-4165(01)00118-0.

Korhonen, R. K., Julkunen, P., Jurvelin, J. S. and Saarakkala, S. (2011) 'Structural and Compositional Changes in Peri- and Extracellular Matrix of Osteoarthritic Cartilage Modulate Chondrocyte Morphology', *Cellular and Molecular Bioengineering*. Springer, 4(3), pp. 484–494. doi: 10.1007/s12195-011-0178-7.

Kuo, A. C., Rodrigo, J. J., Reddi, A. H., Curtiss, S., Grotkopp, E. and Chiu, M. (2006) 'Microfracture and bone morphogenetic protein 7 (BMP-7) synergistically stimulate articular cartilage repair', *Osteoarthritis and Cartilage*. Osteoarthritis Cartilage, 14(11), pp. 1126–1135. doi: 10.1016/j.joca.2006.04.004.

Kuo, W. J., Digman, M. A. and Lander, A. D. (2010) 'Heparan sulfate acts as a bone morphogenetic protein coreceptor by facilitating ligand-induced receptor hetero-oligomerization', *Molecular Biology of the Cell*. American Society for Cell Biology, 21(22), pp. 4028–4041. doi: 10.1091/mbc.E10-04-0348.

Lai, W. M., Hou, J. S. and Mow, V. C. (1991) 'A Triphasic Theory for the Swelling and Deformation Behaviors of Articular Cartilage', *Journal of Biomechanical Engineering*. American Society of Mechanical Engineers, 113(3), p. 245. doi: 10.1115/1.2894880.

Lane, N. E., Schnitzer, T. J., Birbara, C. A., Mokhtarani, M., Shelton, D. L., Smith, M. D., *et al.* (2010) 'Tanezumab for the Treatment of Pain from Osteoarthritis of the Knee', *New England Journal of Medicine*. New England Journal of Medicine (NEJM/MMS), 363(16), pp. 1521–1531. doi: 10.1056/nejmoa0901510.

Lee, G. M. and Loeser, R. F. (1998) *Interactions of the Chondrocyte with its Pericellular Matrix*, *Cells and Materials*.

Lee, G. M., Poole, C. A., Kelley, S. S., Chang, J. and Caterson, B. (1997) 'Isolated chondrons: a viable alternative for studies of chondrocyte metabolism in vitro', *Osteoarthritis and Cartilage*, 5(4), pp. 261–274. doi: 10.1016/S1063-4584(97)80022-2.

Lee, J. H., Fitzgerald, J. B., DiMicco, M. A. and Grodzinsky, A. J. (2005) 'Mechanical injury of cartilage explants causes specific time-dependent changes in chondrocyte gene expression', *Arthritis & Rheumatism*. John Wiley & Sons, Ltd, 52(8), pp. 2386–2395. doi: 10.1002/art.21215.

Lee, W., Leddy, H. A., Chen, Y., Lee, S. H., Zelenski, N. A., McNulty, A. L., *et al.* (2014) 'Synergy between Piezo1 and Piezo2 channels confers high-strain mechanosensitivity to articular cartilage', *Proceedings of the National Academy of Sciences*, 111(47), pp. E5114–E5122. doi: 10.1073/pnas.1414298111.

Lew, E. D., Furdui, C. M., Anderson, K. S. and Schlessinger, J. (2009) 'The Precise Sequence of FGF Receptor Autophosphorylation Is Kinetically Driven and Is Disrupted by Oncogenic Mutations', *Science Signaling*, 2(58), pp. ra6–ra6. doi: 10.1126/scisignal.2000021.

Li, D., Han, Z., Liu, J., Zhang, X., Ren, J., Yan, L., *et al.* (2013) 'Upregulation of nucleus HDGF predicts poor prognostic outcome in patients with penile squamous cell carcinoma bypass VEGF-A and Ki-67', *Medical Oncology*. Med Oncol, 30(4). doi: 10.1007/s12032-013-0702-9.

Li, S. Z., Zhao, Y. B., Cao, W. D., Qu, Y., Luo, P., Zhen, H. N., *et al.* (2013) 'The expression of hepatoma-derived growth factor in primary central nervous system lymphoma and its correlation with angiogenesis, proliferation and clinical outcome', *Medical Oncology*. Med Oncol, 30(3). doi: 10.1007/s12032-013-0622-8.

Li, X., Ellman, M. B., Kroin, J. S., Chen, D., Yan, D., Mikecz, K., *et al.* (2012) 'Species-specific biological effects of FGF-2 in articular cartilage: Implication for distinct roles within the FGF receptor family', *Journal of Cellular Biochemistry*. NIH Public Access, 113(7), pp. 2532–2542. doi: 10.1002/jcb.24129.

Li, Y., Frank, E. H., Wang, Y., Chubinskaya, S., Huang, H. H. and Grodzinsky, A. J. (2013) 'Moderate dynamic compression inhibits pro-catabolic response of cartilage to mechanical injury, tumor necrosis factor-α and interleukin-6, but accentuates degradation above a strain threshold', *Osteoarthritis and Cartilage*. W.B. Saunders, 21(12), pp. 1933–1941. doi: 10.1016/j.joca.2013.08.021.

Li, Z., Kupcsik, L., Yao, S.-J., Alini, M. and Stoddart, M. J. (2010) 'Mechanical load modulates chondrogenesis of human mesenchymal stem cells through the TGF-β pathway', *Journal of Cellular and Molecular Medicine*. J Cell Mol Med, 14(6a), pp. 1338–1346. doi: 10.1111/j.1582-4934.2009.00780.x.

Liao, Y., Zeng, Z., Lu, F., Dong, Z., Chang, Q. and Gao, J. (2015) 'In vivo dedifferentiation of adult adipose cells', *PLOS ONE*. Edited by G. López Lluch. Public Library of Science, 10(4), p. e0125254. doi: 10.1371/journal.pone.0125254.

Lin, T.-S., Hsieh, C.-H., Kuo, C., Juang, Y.-P., Hsieh, Y. S. Y., Chiang, H., *et al.* (2020) 'Sulfation pattern of chondroitin sulfate in human osteoarthritis cartilages reveals a lower level of chondroitin-4-sulfate', *Carbohydrate Polymers*. Elsevier Ltd, 229, p. 115496. doi: 10.1016/j.carbpol.2019.115496.

Linn, F. C. and Sokoloff, L. (1965) 'Movement and composition of interstitial fluid of cartilage', *Arthritis & Rheumatism*. John Wiley & Sons, Ltd, 8(4), pp. 481–494. doi: 10.1002/art.1780080402.

Little, C. B., Barai, A., Burkhardt, D., Smith, S. M., Fosang, A. J., Werb, Z., *et al.* (2009) 'Matrix metalloproteinase-13 deficient mice are resistant to osteoarthritic cartilage erosion but not chondrocyte hypertrophy or osteophyte development', *Arthritis & Rheumatism*, 60(12), pp. 3723–3733. doi: 10.1002/art.25002.

Little, C. B., Mittaz, L., Belluoccio, D., Rogerson, F. M., Campbell, I. K., Meeker, C. T., *et al.* (2005) 'ADAMTS-1-Knockout mice do not exhibit abnormalities in aggrecan turnover in vitro or in vivo', *Arthritis & Rheumatism*, 52(5), pp. 1461–1472. doi: 10.1002/art.21022.

Loeser, R. F. (2014) 'Integrins and chondrocyte–matrix interactions in articular cartilage', *Matrix Biology*, 39, pp. 11–16. doi: 10.1016/j.matbio.2014.08.007.

Loeser, R. F., Chubinskaya, S., Pacione, C. and Im, H.-J. (2005) 'Basic fibroblast growth factor inhibits the anabolic activity of insulin-like growth factor 1 and osteogenic protein 1 in adult human articular chondrocytes', *Arthritis & Rheumatism*. John Wiley & Sons, Ltd, 52(12), pp. 3910–3917. doi: 10.1002/art.21472.

Loeser, R. F., Olex, A. L., McNulty, M. A., Carlson, C. S., Callahan, M., Ferguson, C., *et al.* (2013) 'Disease Progression and Phasic Changes in Gene Expression in a Mouse Model of Osteoarthritis', *PLoS ONE*. Edited by F. Rannou. Public Library of Science, 8(1), p. e54633. doi: 10.1371/journal.pone.0054633.

Loeser, R. F., Pacione, C. A. and Chubinskaya, S. (2003) 'The combination of insulin-like growth factor 1 and osteogenic protein 1 promotes increased survival of and matrix synthesis by normal and osteoarthritic human articular chondrocytes', *Arthritis and Rheumatism*. Arthritis Rheum, 48(8), pp. 2188–2196. doi: 10.1002/art.11209.

Loeser, R. F., Shanker, G., Carlson, C. S., Gardin, J. F., Shelton, B. J. and Sonntag, W. E. (2000) 'Reduction in the chondrocyte response to insulin-like growth factor 1 in aging and osteoarthritis: Studies in a non-human primate model of naturally occurring disease', *Arthritis & Rheumatism*. Arthritis Rheum, 43(9), pp. 2110–2120. doi: 10.1002/1529-0131(200009)43:9<2110::AID-ANR23>3.0.CO;2-U.

Loga, I. S., Batchelor, V., Driscoll, C., Burleigh, A., Chia, S. L., Stott, B., *et al.* (2020) 'Does Pain at an Earlier Stage of Chondropathy Protect Female Mice Against Structural Progression After Surgically Induced Osteoarthritis?', *Arthritis & Rheumatology*. John Wiley and Sons Inc, 72(12), pp. 2083–2093. doi: 10.1002/art.41421.

Von Loga, I. S., El-Turabi, A., Jostins, L., Miotla-Zarebska, J., Mackay-Alderson, J., Zeltins, A., *et al.* (2019) 'Active immunisation targeting nerve growth factor attenuates chronic pain behaviour in murine osteoarthritis', *Annals of the Rheumatic Diseases*. BMJ Publishing Group, 78(5), pp. 672–675. doi: 10.1136/annrheumdis-2018-214489.

Lohmander, S. L., Neame, P. J. and Sandy, J. D. (1993) 'The structure of aggrecan fragments in human synovial fluid. evidence that aggrecanase mediates cartilage degradation in inflammatory joint disease, joint injury, and osteoarthritis', *Arthritis & Rheumatism*. Arthritis Rheum, 36(9), pp. 1214–1222. doi: 10.1002/art.1780360906.

Louwerse, R. T., Heyligers, I. C., Klein-Nulend, J., Sugihara, S., van Kampen, G. P. J., Semeins, C. M., *et al.* (2000) 'Use of recombinant human osteogenic protein-1 for the repair of subchondral defects in articular cartilage in goats', *Journal of Biomedical Materials Research*. John Wiley & Sons Inc, 49(4), pp. 506–516. doi: 10.1002/(SICI)1097-4636(20000315)49:4<506::AID-JBM9>3.0.CO;2-A.

Lu, X., Chen, Z. and Qiu, S. (2015) 'The expression and clinical significance of HDGF in osteosarcoma', *OncoTargets and Therapy*. Dove Medical Press Ltd., 8, p. 2509. doi: 10.2147/OTT.S91708.

Lukasik, S. M. (2006) 'High resolution structure of the HDGF PWWP domain: A potential DNA binding domain', *Protein Science*, 15(2), pp. 314–323. doi: 10.1110/ps.051751706.

Ma, H., Blanchet, T. J., Peluso, D., Hopkins, B., Morris, E. A. and Glasson, S. S. (2007) 'Osteoarthritis severity is sex dependent in a surgical mouse model', *Osteoarthritis and Cartilage*, 15(6), pp. 695–700. doi: 10.1016/j.joca.2006.11.005.

Malda, J., de Grauw, J. C., Benders, K. E. M., Kik, M. J. L., van de Lest, C. H. A., Creemers, L. B., *et al.* (2013) 'Of Mice, Men and Elephants: The Relation between Articular Cartilage Thickness and Body Mass', *PLoS ONE*. Edited by J. P. R. O. Orgel, 8(2), p. e57683. doi: 10.1371/journal.pone.0057683.

Maldonado, D. C., Silva, M. C. P. da, Neto, S. E.-R., de Souza, M. R. and de Souza, R. R. (2013) 'The effects of joint immobilization on articular cartilage of the knee in previously exercised rats', *Journal of Anatomy*. Wiley-Blackwell, 222(5), pp. 518–525. doi: 10.1111/joa.12036.

Manzano, S., Manzano, R., Doblaré, M. and Doweidar, M. H. (2015) 'Altered swelling and ion fluxes in articular cartilage as a biomarker in osteoarthritis and joint immobilization: a computational analysis', *Journal of The Royal Society Interface*, 12(102), p. 20141090. doi: 10.1098/rsif.2014.1090.

Maroudas, A. (1972) 'X-Ray Microprobe Analysis of Articular Cartilage', *Connective Tissue Research*. Informa Healthcare, 1(2), pp. 153–163. doi: 10.3109/03008207209152069.

Maroudas, A. (1976) 'Balance between swelling pressure and collagen tension in normal and degenerate cartilage', *Nature*, 260(5554), pp. 808–809. doi: 10.1038/260808a0.

Maroudas, A. and Bollough, P. (1968) 'Permeability of Articular Cartilage', *Nature*, 219(5160), pp. 1260–1261. doi: 10.1038/2191260a0.

Maroudas, A. and Evans, H. (1972) 'A Study of Ionic Equilibria in Cartilage', *Connective Tissue Research*, 1(1), pp. 69–77. doi: 10.3109/03008207209152058.

Maroudas, A. and Freeman, M. A. R. (1979) 'Physico-Chemical Properties of Articular Cartilage', in *Adult Articular Cartilage*. Tunbridge Wells: Pitman Medical, pp. 215–290.

Maroudas, A., Ziv, I., Weisman, N. and Venn, M. (1985) 'Studies of hydration and swelling pressure in normal and osteoarthritic cartilage', *Biorheology*. Biorheology, 22(2), pp. 159–169. doi: 10.3233/BIR-1985-22206.

Martin, J. A., Miller, B. A., Scherb, M. B., Lembke, L. A. and Buckwalter, J. A. (2002) 'Co-localization of insulin-like growth factor binding protein 3 and fibronectin in human articular cartilage', *Osteoarthritis and Cartilage*. Osteoarthritis Cartilage, 10(7), pp. 556–563. doi: 10.1053/joca.2002.0791.

Martin, P., D'Souza, D., Martin, J., Grose, R., Cooper, L., Maki, R., *et al.* (2003) 'Wound healing in the PU.1 null mouse--tissue repair is not dependent on inflammatory cells.', *Current biology : CB*, 13(13), pp. 1122–8. doi: 10.1016/s0960-9822(03)00396-8.

Mason, J. M., Breitbart, A. S., Barcia, M., Porti, D., Pergolizzi, R. G. and Grande, D. A. (2000) 'Cartilage and Bone Regeneration Using Gene-Enhanced Tissue Engineering', *Clinical Orthopaedics and Related Research*. Lippincott Williams and Wilkins, 379, pp. S171–S178. doi: 10.1097/00003086-200010001-00023.

Matta, C. (2013) 'Calcium signalling in chondrogenesis implications for cartilage repair', *Frontiers in Bioscience*, S5(1), p. S374. doi: 10.2741/S374.

Maudsley, A. A. and Hilal, S. K. (1984) 'Biological aspects of sodium-23 imaging', *British Medical Bulletin*. Br Med Bull, 40(2), pp. 165–166. doi: 10.1093/oxfordjournals.bmb.a071964.

McAlindon, T. E., LaValley, M. P., Gulin, J. P. and Felson, D. T. (2000) 'Glucosamine and Chondroitin for Treatment of Osteoarthritis: A Systematic Quality Assessment and Meta-analysis', *JAMA*. American Medical Association, 283(11), p. 1469. doi: 10.1001/jama.283.11.1469.

McCulloch, R. S., Mente, P. L., O'Nan, A. T. and Ashwell, M. S. (2018) 'Articular cartilage gene expression patterns in the tissue surrounding the impact site following applications of shear and axial loads', *BMC Musculoskeletal Disorders*. BioMed Central Ltd., 19(1), p. 449. doi: 10.1186/s12891-018-2374-2.

McKeon, R. J., Höke, A. and Silver, J. (1995) 'Injury-induced proteoglycans inhibit the potential for laminin-mediated axon growth on astrocytic scars', *Experimental Neurology*. Exp Neurol, 136(1), pp. 32–43. doi: 10.1006/exnr.1995.1081.

McLeod, M. A., Wilusz, R. E. and Guilak, F. (2013) 'Depth-dependent anisotropy of the micromechanical properties of the extracellular and pericellular matrices of articular cartilage evaluated via atomic force microscopy', *Journal of Biomechanics*. Elsevier, 46(3), pp. 586–592. doi: 10.1016/j.jbiomech.2012.09.003.

McNamee, K. E., Burleigh, A., Gompels, L. L., Feldmann, M., Allen, S. J., Williams, R. O., *et al.* (2010) 'Treatment of murine osteoarthritis with TrkAd5 reveals a pivotal role for nerve growth factor in non-inflammatory joint pain', *Pain*. No longer published by Elsevier, 149(2), pp. 386–392. doi: 10.1016/j.pain.2010.03.002.

McNulty, A. L., Leddy, H. A., Liedtke, W. and Guilak, F. (2015) 'TRPV4 as a therapeutic target for joint diseases', *Naunyn-Schmiedeberg's Archives of Pharmacology*. Springer Verlag, pp. 437–450. doi: 10.1007/s00210-014-1078-x.

McQuillan, D. J., Handley, C. J., Campbell, M. A., Bolis, S., Milway, V. E. and Herington, A. C. (1986) 'Stimulation of proteoglycan biosynthesis by serum and insulin-like growth factor-I in cultured bovine articular cartilage', *Biochemical Journal*. Biochem J, 240(2), pp. 423–430. doi: 10.1042/bj2400423.

Meier, S. D., Kovalchuk, Y. and Rose, C. R. (2006) 'Properties of the new fluorescent Na+ indicator CoroNa Green:

Comparison with SBFI and confocal Na+ imaging', *Journal of Neuroscience Methods*, 155(2), pp. 251–259. doi: 10.1016/j.jneumeth.2006.01.009.

Montero, A., Okada, Y., Tomita, M., Ito, M., Tsurukami, H., Nakamura, T., *et al.* (2000) 'Disruption of the fibroblast growth factor-2 gene results in decreased bone mass and bone formation', *Journal of Clinical Investigation*. The American Society for Clinical Investigation, 105(8), pp. 1085–1093. doi: 10.1172/JCI8641.

Moore, E. E., Bendele, A. M., Thompson, D. L., Littau, A., Waggie, K. S., Reardon, B., *et al.* (2005) 'Fibroblast growth factor-18 stimulates chondrogenesis and cartilage repair in a rat model of injury-induced osteoarthritis', *Osteoarthritis and Cartilage*. W.B. Saunders, 13(7), pp. 623–631. doi: 10.1016/j.joca.2005.03.003.

Moscatelli, D. (1992) 'Basic fibroblast growth factor (bFGF) dissociates rapidly from heparan sulfates but slowly from receptors. Implications for mechanisms of bFGF release from pericellular matrix.', *The Journal of biological chemistry*, 267(36), pp. 25803–9. Available at: http://www.jbc.org/content/267/36/25803.full.pdf (Accessed: 21 August 2017).

Mouaddab, M., Foucat, L., Donnat, J. P., Renou, J. P. and Bonny, J. M. (2007) 'Absolute quantification of Na+ bound fraction by double-quantum filtered 23Na NMR spectroscopy', *Journal of Magnetic Resonance*. Academic Press, 189(1), pp. 151–155. doi: 10.1016/j.jmr.2007.09.003.

Mouw, J. K., Imler, S. M. and Levenston, M. E. (2007) 'Ion-channel Regulation of Chondrocyte Matrix Synthesis in 3D Culture Under Static and Dynamic Compression', *Biomechanics and Modeling in Mechanobiology*, 6(1–2), pp. 33–41. doi: 10.1007/s10237-006-0034-1.

Mow, V. C., Kuei, S. C., Lai, W. M. and Armstrong, C. G. (1980) 'Biphasic Creep and Stress Relaxation of Articular Cartilage in Compression: Theory and Experiments', *Journal of Biomechanical Engineering*, 102(1), pp. 73–84. doi: 10.1115/1.3138202.

Mow, V. C., Ratcliffe, A. and Poole, R. A. (1992) 'Cartilage and diarthrodial joints as paradigms for hierarchical materials and structures', *Biomaterials*, 13(2), pp. 67–97. doi: 10.1016/0142-9612(92)90001-5.

Muddasani, P., Norman, J. C., Ellman, M., van Wijnen, A. J. and Im, H.-J. (2007) 'Basic Fibroblast Growth Factor Activates the MAPK and NFκB Pathways That Converge on Elk-1 to Control Production of Matrix Metalloproteinase-13 by Human Adult Articular Chondrocytes', *Journal of Biological Chemistry*. J Biol Chem, 282(43), pp. 31409–31421. doi: 10.1074/jbc.M706508200.

Muhammad, H., Schminke, B., Bode, C., Roth, M., Albert, J., Von Der Heyde, S., *et al.* (2014) 'Human migratory meniscus progenitor cells are controlled via the TGF-β pathway', *Stem Cell Reports*. Cell Press, 3(5), pp. 789–803. doi: 10.1016/j.stemcr.2014.08.010.

Murdoch, A. D., Grady, L. M., Ablett, M. P., Katopodi, T., Meadows, R. S. and Hardingham, T. E. (2007) 'Chondrogenic Differentiation of Human Bone Marrow Stem Cells in Transwell Cultures: Generation of Scaffold-Free Cartilage', *Stem Cells*. Wiley, 25(11), pp. 2786–2796. doi: 10.1634/stemcells.2007-0374.

Nakamura, H., Izumoto, Y., Kambe, H., Kuroda, T., Mori, T., Kawamura, K., *et al.* (1994) 'Molecular cloning of complementary DNA for a novel human hepatoma-derived growth factor: Its homology with high mobility group-1 protein'. Available at: https://pubmed.ncbi.nlm.nih.gov/7929202/ (Accessed: 6 January 2021).

Nakamura, H., Kambe, H., Egawa, T., Kimura, Y., Ito, H., Hayashi, E., *et al.* (1989) 'Partial purification and characterization of human hepatoma-derived growth factor.', *Clinica chimica acta; international journal of clinical chemistry*, 183(3), pp. 273–84. Available at: http://www.ncbi.nlm.nih.gov/pubmed/2553304 (Accessed: 1 February 2017).

Nakamura, H., Yoshino, S., Kato, T., Tsuruha, J. and Nishioka, K. (1999) 'T-cell mediated inflammatory pathway in osteoarthritis', *Osteoarthritis and Cartilage*, 7(4), pp. 401–402. doi: 10.1053/joca.1998.0224.

Nakamura, N., Horibe, S., Toritsuka, Y., Mitsuoka, T., Natsu-Ume, T., Yoneda, K., *et al.* (2008) 'The location-specific healing response of damaged articular cartilage after ACL reconstruction: Short-term follow-up', *Knee Surgery, Sports Traumatology, Arthroscopy*, 16(9), pp. 843–848. doi: 10.1007/s00167-008-0565-3.

Nameki, N. (2005) 'Solution structure of the PWWP domain of the hepatoma-derived growth factor family', *Protein Science*, 14(3), pp. 756–764. doi: 10.1110/ps.04975305.

Navon, G., Shinar, H., Eliav, U. and Seo, Y. (2001) 'Multiquantum filters and order in tissues', *NMR in Biomedicine*, 14(2), pp. 112–132. doi: 10.1002/nbm.687.

Neidel, J. and Zeidler, U. (1993) 'Independent effects of interleukin 1 on proteoglycan synthesis and proteoglycan breakdown of bovine articular cartilage in vitro.', *Agents and actions*, 39(1–2), pp. 82–90. doi: https://doi.org/10.1007/BF01975718.

Nelson, F., Dahlberg, L., Laverty, S., Reiner, A., Pidoux, I., Ionescu, M., *et al.* (1998) 'Evidence for altered synthesis of type II collagen in patients with osteoarthritis', *Journal of Clinical Investigation*. The American Society

for Clinical Investigation, 102(12), pp. 2115–2125. doi: 10.1172/JCI4853.

Nieminen, M. T., Rieppo, J., Silvennoinen, J., Töyräs, J., Hakumäki, J. M., Hyttinen, M. M., *et al.* (2002) 'Spatial assessment of articular cartilage proteoglycans with Gd-DTPA-enhanced T 1 imaging', *Magnetic Resonance in Medicine*. John Wiley and Sons Inc., 48(4), pp. 640–648. doi: 10.1002/mrm.10273.

Nieminen, M. T., Rieppo, J., Töyräs, J., Hakumäki, J. M., Silvennoinen, J., Hyttinen, M. M., *et al.* (2001) 'T 2 relaxation reveals spatial collagen architecture in articular cartilage: A comparative quantitative MRI and polarized light microscopic study', *Magnetic Resonance in Medicine*. John Wiley and Sons Inc., 46(3), pp. 487–493. doi: 10.1002/mrm.1218.

Nishida, T., Kawaki, H., Baxter, R. M., DeYoung, R. A., Takigawa, M. and Lyons, K. M. (2007) 'CCN2 (Connective Tissue Growth Factor) is essential for extracellular matrix production and integrin signaling in chondrocytes', *Journal of Cell Communication and Signaling*. Kluwer Academic Publishers, 1(1), pp. 45–58. doi: 10.1007/s12079-007-0005-z.

Nishida, T., Kubota, S., Kojima, S., Kuboki, T., Nakao, K., Kushibiki, T., *et al.* (2004) 'Regeneration of Defects in Articular Cartilage in Rat Knee Joints by CCN2 (Connective Tissue Growth Factor)', *Journal of Bone and Mineral Research*. John Wiley & Sons, Ltd, 19(8), pp. 1308–1319. doi: 10.1359/JBMR.040322.

Nomura, M., Sakitani, N., Iwasawa, H., Kohara, Y., Takano, S., Wakimoto, Y., *et al.* (2017) 'Thinning of articular cartilage after joint unloading or immobilization. An experimental investigation of the pathogenesis in mice', *Osteoarthritis and Cartilage*. W.B. Saunders Ltd, 25(5), pp. 727–736. doi: 10.1016/j.joca.2016.11.013.

Noyes, F. R. and Stabler, C. L. (1989) 'A system for grading articular cartilage lesions at arthroscopy', *The American Journal of Sports Medicine*, 17(4), pp. 505–513. doi: 10.1177/036354658901700410.

Nüße, J., Blumrich, E.-M., Mirastschijski, U., Kappelmann, L., Kelm, S. and Dietz, F. (2017) 'Intra- or extra-exosomal secretion of HDGF isoforms: the extraordinary function of the HDGF-A N-terminal peptide', *Biological Chemistry*, 0(0). doi: 10.1515/hsz-2016-0315.

Nuttall, M. E., Shah, F., Singh, V., Thomas-Porch, C., Frazier, T. and Gimble, J. M. (2014) 'Adipocytes and the regulation of bone remodeling: A balancing act', *Calcified Tissue International*. Springer, pp. 78–87. doi: 10.1007/s00223-013-9807-6.

O'Conor, C. J., Leddy, H. A., Benefield, H. C., Liedtke, W. B. and Guilak, F. (2014) 'TRPV4-mediated mechanotransduction regulates the metabolic response of chondrocytes to dynamic loading', *Proceedings of the National Academy of Sciences*. National Academy of Sciences, 111(4), pp. 1316–1321. doi: 10.1073/pnas.1319569111.

O'Hara, B. P., Urban, J. P. and Maroudas, A. (1990) 'Influence of cyclic loading on the nutrition of articular cartilage.', *Annals of the Rheumatic Diseases*. BMJ Publishing Group, 49(7), pp. 536–539. doi: 10.1136/ard.49.7.536.

Ojanen, S. P., Finnilä, M. A. J., Reunamo, A. E., Ronkainen, A. P., Mikkonen, S., Herzog, W., *et al.* (2018) 'Site-specific glycosaminoglycan content is better maintained in the pericellular matrix than the extracellular matrix in early post-traumatic osteoarthritis', *PLOS ONE*. Public Library of Science, 13(4), p. e0196203. doi: 10.1371/JOURNAL.PONE.0196203.

Olczyk, P., Mencner, Ł. and Komosinska-Vassev, K. (2015) 'Diverse Roles of Heparan Sulfate and Heparin in Wound Repair', *BioMed Research International*. Hindawi Limited, 2015, pp. 1–7. doi: 10.1155/2015/549417.

Omoto, S., Nishida, K., Yamaai, Y., Shibahara, M., Nishida, T., Doi, T., *et al.* (2004) 'Expression and localization of connective tissue growth factor (CTGF/Hcs24/CCN2) in osteoarthritic cartilage', *Osteoarthritis and Cartilage*. Elsevier, 12(10), pp. 771–778. doi: 10.1016/j.joca.2004.06.009.

Ooi, B. N. S., Mukhopadhyay, A., Masilamani, J., Do, D. V., Lim, C. P., Cao, X. M., *et al.* (2010) 'Hepatoma-derived growth factor and its role in keloid pathogenesis', *Journal of Cellular and Molecular Medicine*. Wiley-Blackwell, 14(6a), pp. 1328–1337. doi: 10.1111/j.1582-4934.2009.00779.x.

Ori, A., Wilkinson, M. C. and Fernig, D. G. (2011) 'A Systems Biology Approach for the Investigation of the Heparin/Heparan Sulfate Interactome', *Journal of Biological Chemistry*, 286(22), pp. 19892–19904. doi: 10.1074/jbc.M111.228114.

Ortega, S., Ittmann, M., Tsang, S. H., Ehrlich, M. and Basilico, C. (1998) 'Neuronal defects and delayed wound healing in mice lacking fibroblast growth factor 2', *Proceedings of the National Academy of Sciences of the United States of America*. National Academy of Sciences, 95(10), pp. 5672–5677. doi: 10.1073/pnas.95.10.5672.

Otsuki, S., Hanson, S. R., Miyaki, S., Grogan, S. P., Kinoshita, M., Asahara, H., *et al.* (2010) 'Extracellular sulfatases support cartilage homeostasis by regulating BMP and FGF signaling pathways', *Proceedings of the National Academy of Sciences*. National Academy of Sciences, 107(22), pp. 10202–10207. doi: 10.1073/pnas.0913897107.

Palmoski, M., Perricone, E. and Brandt, K. D. (1979) 'Development and Reversal of a Proteoglycan Aggregation Defect In Normal Canine Knee Cartilage After Immobilization', *Arthritis & Rheumatism*. Arthritis Rheum, 22(5), pp. 508–517. doi: 10.1002/art.1780220511.

Parvizi, J., Parpura, V., Greenleaf, J. F. and Bolander, M. E. (2002) 'Calcium signaling is required for ultrasound-stimulated aggrecan synthesis by rat chondrocytes', *Journal of Orthopaedic Research*, 20(1), pp. 51–57. doi: 10.1016/S0736-0266(01)00069-9.

Pellegrini, L. (2001) 'Role of heparan sulfate in fibroblast growth factor signalling: A structural view', *Current Opinion in Structural Biology*. Elsevier Ltd, pp. 629–634. doi: 10.1016/S0959-440X(00)00258-X.

Pellegrini, L., Burke, D. F., Delft, F. von, Mulloy, B. and Blundell, T. L. (2000) 'Crystal structure of fibroblast growth factor receptor ectodomain bound to ligand and heparin', *Nature*. Nature Publishing Group, 407(6807), pp. 1029–1034. doi: 10.1038/35039551.

Pelletier, J.-P., Martel-Pelletier, J. and Abramson, S. B. (2001) 'Osteoarthritis, an inflammatory disease: Potential implication for the selection of new therapeutic targets', *Arthritis & Rheumatism*. John Wiley & Sons, Ltd, 44(6), pp. 1237–1247. doi: 10.1002/1529-0131(200106)44:6<1237::AID-ART214>3.0.CO;2-F.

Penn, J. W., Grobbelaar, A. O. and Rolfe, K. J. (2012) 'The role of the TGF-β family in wound healing, burns and scarring: a review.', *International journal of burns and trauma*. e-Century Publishing Corporation, 2(1), pp. 18–28. Available at: http://www.ncbi.nlm.nih.gov/pubmed/22928164 (Accessed: 21 December 2020).

Pers, Y.-M., Rackwitz, L., Ferreira, R., Pullig, O., Delfour, C., Barry, F., *et al.* (2016) 'Adipose Mesenchymal Stromal Cell-Based Therapy for Severe Osteoarthritis of the Knee: A Phase I Dose-Escalation Trial', *STEM CELLS Translational Medicine*. Wiley, 5(7), pp. 847–856. doi: 10.5966/sctm.2015-0245.

Phillips, E. R., Haislup, B. D., Bertha, N., Lefchak, M., Sincavage, J., Prudnikova, K., *et al.* (2019) 'Biomimetic proteoglycans diffuse throughout articular cartilage and localize within the pericellular matrix', *Journal of Biomedical Materials Research Part A*. John Wiley and Sons Inc., 107(9), pp. 1977–1987. doi: 10.1002/jbm.a.36710.

Plaas, A. H. K., West, L. A., Wong-Palms, S. and Nelson, F. R. T. (1998) 'Glycosaminoglycan Sulfation in Human Osteoarthritis', *Journal of Biological Chemistry*. American Society for Biochemistry and Molecular Biology, 273(20), pp. 12642–12649. doi: 10.1074/jbc.273.20.12642.

Poole, A. R., Pidoux, I., Reiner, A. and Rosenberg, L. (1982) 'An immunoelectron microscope study of the organization of proteoglycan monomer, link protein, and collagen in the matrix of articular cartilage.', *Journal of Cell Biology*, 93(3), pp. 921–937. doi: 10.1083/jcb.93.3.921.

Reddy, R., Insko, E. K. and Leigh, J. S. (1997) 'Triple quantum sodium imaging of articular cartilage', *Magnetic Resonance in Medicine*. John Wiley & Sons, Ltd, 38(2), pp. 279–284. doi: 10.1002/mrm.1910380218.

Redman, S. N., Dowthwaite, G. P., Thomson, B. M. and Archer, C. W. (2004) 'The cellular responses of articular cartilage to sharp and blunt trauma', *Osteoarthritis and Cartilage*. W.B. Saunders Ltd, 12(2), pp. 106–116. doi: 10.1016/j.joca.2002.12.001.

Reker, D., Siebuhr, A. S., Thudium, C. S., Gantzel, T., Ladel, C., Michaelis, M., *et al.* (2020) 'Sprifermin (rhFGF18) versus vehicle induces a biphasic process of extracellular matrix remodeling in human knee OA articular cartilage ex vivo', *Scientific Reports*. Nature Research, 10(1), pp. 1–9. doi: 10.1038/s41598-020-63216-z.

Ren, H., Tang, X., Lee, J. J., Feng, L., Everett, A. D., Waun, K. H., *et al.* (2004) 'Expression of hepatoma-derived growth factor is a strong prognostic predictor for patients with early-stage non-small-cell lung cancer', *Journal of Clinical Oncology*. J Clin Oncol, 22(16), pp. 3230–3237. doi: 10.1200/JCO.2004.02.080.

Reynard, L. N. and Loughlin, J. (2013) 'The genetics and functional analysis of primary osteoarthritis susceptibility', *Expert Reviews in Molecular Medicine*, 15, p. e2. doi: 10.1017/erm.2013.4.

Richy, F., Bruyere, O., Ethgen, O., Cucherat, M., Henrotin, Y. and Reginster, J. Y. (2003) 'Structural and symptomatic efficacy of glucosamine and chondroitin in knee osteoarthritis: A comprehensive meta-analysis', *Archives of Internal Medicine*. Arch Intern Med, 163(13), pp. 1514–1522. doi: 10.1001/archinte.163.13.1514.

Roberts, S., Hollander, A. P., Caterson, B., Menage, J. and Richardson, J. B. (2001) 'Matrix turnover in human cartilage repair tissue in autologous chondrocyte implantation', *Arthritis & Rheumatism*. Arthritis Rheum, 44(11), pp. 2586–2598. doi: 10.1002/1529-0131(200111)44:11<2586::AID-ART439>3.0.CO;2-I.

Roelofs, A. J., Zupan, J., Riemen, A. H. K., Kania, K., Ansboro, S., White, N., *et al.* (2017) 'Joint morphogenetic cells in the adult mammalian synovium', *Nature Communications*. Nature Publishing Group, 8(1), p. 15040. doi: 10.1038/ncomms15040.

Romanzetti, S., Mirkes, C. C., Fiege, D. P., Celik, A., Felder, J. and Shah, N. J. (2014) 'Mapping tissue sodium concentration in the human brain: A comparison of MR sequences at 9.4Tesla', *NeuroImage*, 96, pp. 44–53. doi:

10.1016/j.neuroimage.2014.03.079.

Rothenfluh, D. A., Bermudez, H., O'Neil, C. P. and Hubbell, J. A. (2008) 'Biofunctional polymer nanoparticles for intra-articular targeting and retention in cartilage', *Nature Materials*. Nature Publishing Group, 7(3), pp. 248–254. doi: 10.1038/nmat2116.

Roughley, P. J. and Lee, E. R. (1994) 'Cartilage proteoglycans: Structure and potential functions', *Microscopy Research and Technique*. Microsc Res Tech, 28(5), pp. 385–397. doi: 10.1002/jemt.1070280505.

Ruckh, T. T., Mehta, A. A., Dubach, J. M. and Clark, H. A. (2013) 'Polymer-Free Optode Nanosensors for Dynamic, Reversible and Ratiometric Sodium Imaging in the Physiological Range', *Scientific Reports*. Nature Publishing Group, 3(1), p. 3366. doi: 10.1038/srep03366.

Ryseck, R. P., Macdonald-Bravo, H., Mattéi, M. G. and Bravo, R. (1991) 'Structure, mapping, and expression of fisp-12, a growth factor-inducible gene encoding a secreted cysteine-rich protein.', *Cell growth & differentiation : the molecular biology journal of the American Association for Cancer Research*, 2(5), pp. 225–33. Available at: http://europepmc.org/article/med/1888698 (Accessed: 12 November 2020).

Salter, D. M., Hughes, D. E., Simpson, R. and Gardner, D. L. (1992) 'Integrin expression by human articular chondrocytes', *Rheumatology*, 31(4), pp. 231–234. doi: 10.1093/rheumatology/31.4.231.

Sato, T., Konomi, K., Yamasaki, S., Aratani, S., Tsuchimochi, K., Yokouchi, M., *et al.* (2006) 'Comparative analysis of gene expression profiles in intact and damaged regions of human osteoarthritic cartilage', *Arthritis & Rheumatism*. John Wiley & Sons, Ltd, 54(3), pp. 808–817. doi: 10.1002/art.21638.

Sawaji, Y., Hynes, J., Vincent, T. and Saklatvala, J. (2008) 'Fibroblast growth factor 2 inhibits induction of aggrecanase activity in human articular cartilage', *Arthritis & Rheumatism*. John Wiley & Sons, Ltd, 58(11), pp. 3498–3509. doi: 10.1002/art.24025.

Schepkin, V. D. (2016) 'Sodium MRI of glioma in animal models at ultrahigh magnetic fields', *NMR in Biomedicine*. John Wiley and Sons Ltd, 29(2), pp. 175–186. doi: 10.1002/nbm.3347.

Schepkin, V. D., Neubauer, A., Nagel, A. M. and Budinger, T. F. (2017) 'Comparison of potassium and sodium binding in vivo and in agarose samples using TQTPPI pulse sequence', *Journal of Magnetic Resonance*. Academic Press Inc., 277, pp. 162–168. doi: 10.1016/j.jmr.2017.03.003.

Schinagl, R. M., Gurskis, D., Chen, A. C. and Sah, R. L. (1997) 'Depth-dependent confined compression modulus of full-thickness bovine articular cartilage', *Journal of Orthopaedic Research*, 15(4), pp. 499–506. doi: 10.1002/jor.1100150404.

Schlessinger, J., Plotnikov, A. N., Ibrahimi, O. A., Eliseenkova, A. V, Yeh, B. K., Yayon, A., *et al.* (2000) 'Crystal Structure of a Ternary FGF-FGFR-Heparin Complex Reveals a Dual Role for Heparin in FGFR Binding and Dimerization', *Molecular Cell*, 6(3), pp. 743–750. doi: 10.1016/S1097-2765(00)00073-3.

Schmal, H., Zwingmann, J., Fehrenbach, M., Finkenzeller, G., Stark, G. B., Südkamp, N. P., *et al.* (2007) 'bFGF influences human articular chondrocyte differentiation', *Cytotherapy*. Elsevier, 9(2), pp. 184–193. doi: 10.1080/14653240601182846.

Schneider, C. A., Rasband, W. S. and Eliceiri, K. W. (2012) 'NIH Image to ImageJ: 25 years of image analysis', *Nature Methods*. Nature Publishing Group, pp. 671–675. doi: 10.1038/nmeth.2089.

Schott, E. M., Farnsworth, C. W., Grier, A., Lillis, J. A., Soniwala, S., Dadourian, G. H., *et al.* (2018) 'Targeting the gut microbiome to treat the osteoarthritis of obesity', *JCI Insight*. NLM (Medline), 3(8). doi: 10.1172/jci.insight.95997.

Scrimgeour, J., McLane, L. T., Chang, P. S. and Curtis, J. E. (2017) 'Single-Molecule Imaging of Proteoglycans in the Pericellular Matrix', *Biophysical Journal*, 113(11), pp. 2316–2320. doi: 10.1016/j.bpj.2017.09.030.

Seif-Naraghi, S. B., Horn, D., Schup-Magoffin, P. J. and Christman, K. L. (2012) 'Injectable extracellular matrix derived hydrogel provides a platform for enhanced retention and delivery of a heparin-binding growth factor', *Acta Biomaterialia*. Elsevier, 8(10), pp. 3695–3703. doi: 10.1016/j.actbio.2012.06.030.

Serrat, M. A. and Ion, G. (2017) 'Imaging IGF-I uptake in growth plate cartilage using in vivo multiphoton microscopy', *Journal of Applied Physiology*. American Physiological Society, 123(5), pp. 1101–1109. doi: 10.1152/japplphysiol.00645.2017.

Setton, L. A., Elliott, D. M. and Mow, V. C. (1999) 'Altered mechanics of cartilage with osteoarthritis: human osteoarthritis and an experimental model of joint degeneration', *Osteoarthritis and Cartilage*, 7(1), pp. 2–14. doi: 10.1053/joca.1998.0170.

Shapiro, E. M., Borthakur, A., Dandora, R., Kriss, A., Leigh, J. S. and Reddy, R. (2000) 'Sodium Visibility and Quantitation in Intact Bovine Articular Cartilage Using High Field 23Na MRI and MRS', *Journal of Magnetic*

Resonance, 142(1), pp. 24–31. doi: 10.1006/jmre.1999.1932.

Shapiro, E. M., Borthakur, A., Gougoutas, A. and Reddy, R. (2002) '23Na MRI accurately measures fixed charge density in articular cartilage', *Magnetic Resonance in Medicine*, 47(2), pp. 284–291. doi: 10.1002/mrm.10054.

Shapiro, E. M., Borthakur, A., Kaufman, J. H., Leigh, J. S. and Reddy, R. (2001) 'Water distribution patterns inside bovine articular cartilage as visualized by 1 H magnetic resonance imaging', *Osteoarthritis and Cartilage*, 9, pp. 533–538. doi: 10.1053/joca.2001.0428.

Shen, J., Li, J., Wang, B., Jin, H., Wang, M., Zhang, Y., *et al.* (2013) 'Deletion of the Transforming Growth Factor β Receptor Type II Gene in Articular Chondrocytes Leads to a Progressive Osteoarthritis-like Phenotype in Mice', *Arthritis & Rheumatism*, 65(12), pp. 3107–3119. doi: 10.1002/art.38122.

Shepherd, C., Zhu, D., Skelton, A. J., Combe, J., Threadgold, H., Zhu, L., *et al.* (2018) 'Functional Characterization of the Osteoarthritis Genetic Risk Residing at ALDH1A2 Identifies rs12915901 as a Key Target Variant', *Arthritis & Rheumatology*. John Wiley and Sons Inc., 70(10), pp. 1577–1587. doi: 10.1002/art.40545.

Shi, S., Mercer, S., Eckert, G. J. and Trippel, S. B. (2009) 'Growth Factor Regulation of Growth Factors in Articular Chondrocytes', *Journal of Biological Chemistry*. J Biol Chem, 284(11), pp. 6697–6704. doi: 10.1074/jbc.M807859200.

Shinar, H., Knubovets, T., Eliav, U. and Navon, G. (1993) 'Sodium interaction with ordered structures in mammalian red blood cells detected by Na-23 double quantum NMR', *Biophysical Journal*, 64(4), pp. 1273–1279. doi: 10.1016/S0006-3495(93)81492-9.

Shriver, Z., Capila, I., Venkataraman, G. and Sasisekharan, R. (2012) 'Heparin and Heparan sulfate: Analyzing structure and microheterogeneity', *Handbook of Experimental Pharmacology*. NIH Public Access, 207(207), pp. 159–176. doi: 10.1007/978-3-642-23056-1_8.

Silver, J. and Miller, J. H. (2004) 'Regeneration beyond the glial scar', *Nature Reviews Neuroscience*. European Association for Cardio-Thoracic Surgery, pp. 146–156. doi: 10.1038/nrn1326.

Snelling, S., Rout, R., Davidson, R., Clark, I., Carr, A., Hulley, P. A., *et al.* (2014) 'A gene expression study of normal and damaged cartilage in anteromedial gonarthrosis, a phenotype of osteoarthritis', *Osteoarthritis and Cartilage*. Elsevier, 22(2), pp. 334–343. doi: 10.1016/j.joca.2013.12.009.

Sö, S., Hambach, L., Lissner, R., Kirchner, T. and Aigner, T. (2002) 'Ultrastructural localization of type VI collagen in normal adult and osteoarthritic human articular cartilage', *Osteoarthritis and Cartilage*, 10, pp. 464–470. doi: 10.1053/joca.2001.0512.

Sokolove, J. and Lepus, C. M. (2013) 'Role of inflammation in the pathogenesis of osteoarthritis: latest findings and interpretations', *Therapeutic Advances in Musculoskeletal Disease*, 5(2), pp. 77–94. doi: 10.1177/1759720X12467868.

Solchaga, L. A., Penick, K., Porter, J. D., Goldberg, V. M., Caplan, A. I. and Welter, J. F. (2005) 'FGF-2 enhances the mitotic and chondrogenic potentials of human adult bone marrow-derived mesenchymal stem cells', *Journal of Cellular Physiology*, 203(2), pp. 398–409. doi: 10.1002/jcp.20238.

Stannus, O. P., Cao, Y., Antony, B., Blizzard, L., Cicuttini, F., Jones, G., *et al.* (2015) 'Cross-sectional and longitudinal associations between circulating leptin and knee cartilage thickness in older adults', *Annals of the Rheumatic Diseases*, 74(1), pp. 82–88. doi: 10.1136/annrheumdis-2013-203308.

Starkman, B. G., Cravero, J. D., DelCarlo, M. and Loeser, R. F. (2005) 'IGF-I stimulation of proteoglycan synthesis by chondrocytes requires activation of the PI 3-kinase pathway but not ERK MAPK', *Biochemical Journal*. Portland Press, 389(3), pp. 723–729. doi: 10.1042/BJ20041636.

Stockwell, R. A. (1970) 'Changes in the acid glycosaminoglycan content of the matrix of ageing human articular cartilage.', *Annals of the Rheumatic Diseases*, 29(5), pp. 509–515. doi: 10.1136/ard.29.5.509.

Stracke, J. O., Fosang, A. J., Last, K., Mercuri, F. A., Pendás, A. M., Llano, E., *et al.* (2000) 'Matrix metalloproteinases 19 and 20 cleave aggrecan and cartilage oligomeric matrix protein (COMP)', *FEBS Letters*. No longer published by Elsevier, 478(1–2), pp. 52–56. doi: 10.1016/S0014-5793(00)01819-6.

Sue, S.-C., Chen, J.-Y., Lee, S.-C., Wu, W.-G. and Huang, T.-H. (2004) 'Solution Structure and Heparin Interaction of Human Hepatoma-derived Growth Factor', *Journal of Molecular Biology*, 343(5), pp. 1365–1377. doi: 10.1016/j.jmb.2004.09.014.

Sue, S.-C., Lee, W.-T., Tien, S.-C., Lee, S.-C., Yu, J.-G., Wu, W.-J., *et al.* (2007) 'PWWP Module of Human Hepatoma-derived Growth Factor Forms a Domain-swapped Dimer with Much Higher Affinity for Heparin', *Journal of Molecular Biology*, 367(2), pp. 456–472. doi: 10.1016/j.jmb.2007.01.010.

Suzuki, T., Bessho, K., Fujimura, K., Okubo, Y., Segami, N. and Iizuka, T. (2002) 'Regeneration of defects in the

articular cartilage in rabbit temporomandibular joints by bone morphogenetic protein-2', *British Journal of Oral and Maxillofacial Surgery*. Churchill Livingstone, 40(3), pp. 201–206. doi: 10.1054/bjom.2001.0720.

Szmacinski, H. and Lakowicz, J. R. (1997) 'Sodium green as a potential probe for intracellular sodium imaging based on fluorescence lifetime', *Analytical Biochemistry*. Academic Press Inc., 250(2), pp. 131–138. doi: 10.1006/abio.1997.2203.

Tachmazidou, I., Hatzikotoulas, K., Southam, L., Esparza-Gordillo, J., Haberland, V., Zheng, J., *et al.* (2019) 'Identification of new therapeutic targets for osteoarthritis through genome-wide analyses of UK Biobank data', *Nature Genetics*, 51(2), pp. 230–236. doi: 10.1038/s41588-018-0327-1.

Takigawa, M. (2013) 'CCN2: a master regulator of the genesis of bone and cartilage', *Journal of Cell Communication and Signaling*. Springer, 7(3), pp. 191–201. doi: 10.1007/s12079-013-0204-8.

Tan, Q., Wang, Q., Kuang, L., Zhang, J., Peng, X., Liang, S., *et al.* (2021) 'TGF-β/Alk5 signaling prevents osteoarthritis initiation via regulating the senescence of articular cartilage stem cells', *Journal of Cellular Physiology*. J Cell Physiol, p. jcp.30231. doi: 10.1002/jcp.30231.

Tang, J., Su, N., Zhou, S., Xie, Y., Huang, J., Wen, X., *et al.* (2016) 'Fibroblast Growth Factor Receptor 3 Inhibits Osteoarthritis Progression in the Knee Joints of Adult Mice', *Arthritis and Rheumatology*. John Wiley and Sons Inc., 68(10), pp. 2432–2443. doi: 10.1002/art.39739.

Tang, X., Muhammad, H., McLean, C., Miotla-Zarebska, J., Fleming, J., Didangelos, A., *et al.* (2018) 'Connective tissue growth factor contributes to joint homeostasis and osteoarthritis severity by controlling the matrix sequestration and activation of latent TGFβ', *Annals of the Rheumatic Diseases*, 77(9), pp. 1372–1380. doi: 10.1136/annrheumdis-2018-212964.

Tesche, F. and Miosge, N. (2004) 'Perlecan in late stages of osteoarthritis of the human knee joint', *Osteoarthritis and Cartilage*. W.B. Saunders, 12(11), pp. 852–862. doi: 10.1016/j.joca.2004.07.004.

Tong, W., Zeng, Y., Chow, D. H. K., Yeung, W., Xu, J., Deng, Y., *et al.* (2019) 'Wnt16 attenuates osteoarthritis progression through a PCP/JNK-mTORC1-PTHrP cascade', *Annals of the Rheumatic Diseases*. BMJ Publishing Group, 78(4), pp. 551–561. doi: 10.1136/annrheumdis-2018-214200.

Towheed, T., Maxwell, L., Anastassiades, T. P., Shea, B., Houpt, J., Welch, V., *et al.* (2005) 'Glucosamine therapy for treating osteoarthritis', *Cochrane Database of Systematic Reviews*. Cochrane Database Syst Rev, (4). doi: 10.1002/14651858.CD002946.pub2.

Uchisawa, H., Okuzaki, B., Ichita, J. and Matsue, H. (2001) 'Binding between calcium ions and chondroitin sulfate chains of salmon nasal cartilage glycosaminoglycan', *International Congress Series*. Elsevier, 1223(C), pp. 205–220. doi: 10.1016/S0531-5131(01)00458-7.

Urban, J. P. G., Hall, A. C. and Gehl, K. A. (1993) 'Regulation of matrix synthesis rates by the ionic and osmotic environment of articular chondrocytes', *Journal of Cellular Physiology*, 154(2), pp. 262–270. doi: 10.1002/jcp.1041540208.

Uyama, H., Tomita, Y., Nakamura, H., Nakamori, S., Zhang, B., Hoshida, Y., *et al.* (2006) 'Hepatoma-Derived Growth Factor Is a Novel Prognostic Factor for Patients with Pancreatic Cancer', *Clinical Cancer Research*, 12(20), pp. 6043–6048. doi: 10.1158/1078-0432.CCR-06-1064.

Venn, M. and Maroudas, A. (1977) 'Chemical composition and swelling of normal and osteoarthrotic femoral head cartilage. I. Chemical composition.', *Annals of the Rheumatic Diseases*, 36(2), pp. 121–129. doi: 10.1136/ard.36.2.121.

Vincent, T., Hermansson, M., Bolton, M., Wait, R. and Saklatvala, J. (2002) 'Basic FGF mediates an immediate response of articular cartilage to mechanical injury', *Proceedings of the National Academy of Sciences*, 99(12), pp. 8259–8264. doi: 10.1073/pnas.122033199.

Vincent, T. L. (2019) 'Mechanoflammation in osteoarthritis pathogenesis', *Seminars in Arthritis and Rheumatism*. W.B. Saunders, 49(3), pp. S36–S38. doi: 10.1016/j.semarthrit.2019.09.018.

Vincent, T. L., Hermansson, M. A., Hansen, U. N., Amis, A. A. and Saklatvala, J. (2004) 'Basic fibroblast growth factor mediates transduction of mechanical signals when articular cartilage is loaded', *Arthritis & Rheumatism*. Wiley Subscription Services, Inc., A Wiley Company, 50(2), pp. 526–533. doi: 10.1002/art.20047.

Vincent, T. L., McLean, C. J., Full, L. E., Peston, D. and Saklatvala, J. (2007) 'FGF-2 is bound to perlecan in the pericellular matrix of articular cartilage, where it acts as a chondrocyte mechanotransducer', *Osteoarthritis and Cartilage*, 15(7), pp. 752–763. doi: 10.1016/j.joca.2007.01.021.

Vincent, T. L. and Wann, A. K. T. (2018) 'Mechanoadaptation: articular cartilage through thick and thin', *The Journal of Physiology*. John Wiley & Sons, Ltd (10.1111). doi: 10.1113/JP275451.

Virag, J. A. I., Rolle, M. L., Reece, J., Hardouin, S., Feigl, E. O. and Murry, C. E. (2007) 'Fibroblast growth factor-2 regulates myocardial infarct repair: Effects on cell proliferation, scar contraction, and ventricular function', *American Journal of Pathology*. American Society for Investigative Pathology Inc., 171(5), pp. 1431–1440. doi: 10.2353/ajpath.2007.070003.

Wang, C.-H., Davamani, F., Sue, S.-C., Lee, S.-C., Wu, P., Tang, F.-M., *et al.* (2011) 'Cell surface heparan sulfates mediate internalization of the PWWP/HATH domain of HDGF via macropinocytosis to fine-tune cell signalling processes involved in fibroblast cell migration', *Biochemical Journal*, 433(1), pp. 127–138. doi: 10.1042/BJ20100589.

Wang, L., Jiang, Q., Hua, S., Zhao, M., Wu, Q., Fu, Q., *et al.* (2014) 'High nuclear expression of HDGF correlates with disease progression and poor prognosis in human endometrial carcinoma', *Disease Markers*. Hindawi Limited, 2014. doi: 10.1155/2014/298795.

Wang, Q. G., El Haj, A. J. and Kuiper, N. J. (2008) 'Glycosaminoglycans in the pericellular matrix of chondrons and chondrocytes', *Journal of Anatomy*. Wiley-Blackwell, 213(3), pp. 266–273. doi: 10.1111/j.1469-7580.2008.00942.x.

Wann, A. K. T., Zuo, N., Haycraft, C. J., Jensen, C. G., Poole, C. A., McGlashan, S. R., *et al.* (2012) 'Primary cilia mediate mechanotransduction through control of ATP-induced Ca 2+ signaling in compressed chondrocytes', *The FASEB Journal*, 26(4), pp. 1663–1671. doi: 10.1096/fj.11-193649.

Watt, F. E., Hamid, B., Garriga, C., Judge, A., Hrusecka, R., Custers, R. J. H., *et al.* (2020) 'The molecular profile of synovial fluid changes upon joint distraction and is associated with clinical response in knee osteoarthritis', *Osteoarthritis and Cartilage*. W.B. Saunders Ltd, 28(3), pp. 324–333. doi: 10.1016/j.joca.2019.12.005.

Watt, F. E., Paterson, E., Freidin, A., Kenny, M., Judge, A., Saklatvala, J., *et al.* (2016) 'Acute Molecular Changes in Synovial Fluid Following Human Knee Injury: Association With Early Clinical Outcomes', *Arthritis & Rheumatology*, 68(9), pp. 2129–2140. doi: 10.1002/art.39677.

Wei, T., Kulkarni, N. H., Zeng, Q. Q., Helvering, L. M., Lin, X., Lawrence, F., *et al.* (2010) 'Analysis of early changes in the articular cartilage transcriptisome in the rat meniscal tear model of osteoarthritis: pathway comparisons with the rat anterior cruciate transection model and with human osteoarthritic cartilage', *Osteoarthritis and Cartilage*. W.B. Saunders, 18(7), pp. 992–1000. doi: 10.1016/j.joca.2010.04.012.

Weng, T., Yi, L., Huang, J., Luo, F., Wen, X., Du, X., *et al.* (2012) 'Genetic inhibition of fibroblast growth factor receptor 1 in knee cartilage attenuates the degeneration of articular cartilage in adult mice', *Arthritis & Rheumatism*. John Wiley & Sons, Ltd, 64(12), pp. 3982–3992. doi: 10.1002/art.34645.

Wetterling, F., Corteville, D. M., Kalayciyan, R., Rennings, A., Konstandin, S., Nagel, A. M., *et al.* (2012) 'Whole body sodium MRI at 3T using an asymmetric birdcage resonator and short echo time sequence: first images of a male volunteer', *Physics in Medicine and Biology*. Phys Med Biol, 57(14), pp. 4555–4567. doi: 10.1088/0031-9155/57/14/4555.

Whang, J., Katz, J., Boxt, L. M., Reagan, K., Sorce, D. J., Sciacca, R. R., *et al.* (1994) 'Multiple-Quantum-Filtered NMR Determination of Equilibrium Magnetization for 23Na Quantitation in Model Phantoms', *Journal of Magnetic Resonance, Series B*. Academic Press, 103(2), pp. 175–179. doi: 10.1006/jmrb.1994.1026.

Widhalm, H. K., Apprich, S., Welsch, G. H., Zbyn, S., Sadoghi, P., Vekszler, G., *et al.* (2016) 'Optimized cartilage visualization using 7-T sodium (23Na) imaging after patella dislocation', *Knee Surgery, Sports Traumatology, Arthroscopy*. Springer Verlag, 24(5), pp. 1601–1609. doi: 10.1007/s00167-014-3455-x.

Wiegant, K., van Roermund, P. M., Intema, F., Cotofana, S., Eckstein, F., Mastbergen, S. C., *et al.* (2013) 'Sustained clinical and structural benefit after joint distraction in the treatment of severe knee osteoarthritis', *Osteoarthritis and Cartilage*. Osteoarthritis Cartilage, 21(11), pp. 1660–1667. doi: 10.1016/j.joca.2013.08.006.

Wilusz, R. E., DeFrate, L. E. and Guilak, F. (2012) 'A biomechanical role for perlecan in the pericellular matrix of articular cartilage', *Matrix Biology*. Elsevier, 31(6), pp. 320–327. doi: 10.1016/j.matbio.2012.05.002.

Wilusz, R. E. and Guilak, F. (2014) 'High resistance of the mechanical properties of the chondrocyte pericellular matrix to proteoglycan digestion by chondroitinase, aggrecanase, or hyaluronidase', *Journal of the Mechanical Behavior of Biomedical Materials*. Elsevier Ltd, 38, pp. 183–197. doi: 10.1016/j.jmbbm.2013.09.021.

Wilusz, R. E., Sanchez-Adams, J. and Guilak, F. (2014) 'The structure and function of the pericellular matrix of articular cartilage', *Matrix Biology*, 39, pp. 25–32. doi: 10.1016/j.matbio.2014.08.009.

Wilusz, R. E., Zauscher, S. and Guilak, F. (2013) 'Micromechanical mapping of early osteoarthritic changes in the pericellular matrix of human articular cartilage', *Osteoarthritis and Cartilage*. Osteoarthritis Cartilage, 21(12), pp. 1895–1903. doi: 10.1016/j.joca.2013.08.026.

van der Woude, J.-T. A. D., Wiegant, K., van Roermund, P. M., Intema, F., Custers, R. J. H., Eckstein, F., *et al.* (2017) 'Five-Year Follow-up of Knee Joint Distraction: Clinical Benefit and Cartilaginous Tissue Repair in an

Open Uncontrolled Prospective Study', *CARTILAGE*. SAGE Publications Inc., 8(3), pp. 263–271. doi: 10.1177/1947603516665442.

Wright, M. O., Nishida, K., Bavington, C., Godolphin, J. L., Dunne, E., Walmsley, S., *et al.* (1997) 'Hyperpolarisation of cultured human chondrocytes following cyclical pressure-induced strain: Evidence of a role for α5β1 integrin as a chondrocyte mechanoreceptor', *Journal of Orthopaedic Research*. Raven Press Ltd, 15(5), pp. 742–747. doi: 10.1002/jor.1100150517.

Wu, C.-L., Jain, D., McNeill, J. N., Little, D., Anderson, J. A., Huebner, J. L., *et al.* (2015) 'Dietary fatty acid content regulates wound repair and the pathogenesis of osteoarthritis following joint injury', *Annals of the Rheumatic Diseases*. BMJ Publishing Group, 74(11), pp. 2076–2083. doi: 10.1136/annrheumdis-2014-205601.

Wu, C., Yosef, N., Thalhamer, T., Zhu, C., Xiao, S., Kishi, Y., *et al.* (2013) 'Induction of pathogenic TH17 cells by inducible salt-sensing kinase SGK1', *Nature*, 496(7446), pp. 513–517. doi: 10.1038/nature11984.

Wu, H., Zeng, H., Lam, R., Tempel, W., Amaya, M. F., Xu, C., *et al.* (2011) 'Structural and Histone Binding Ability Characterizations of Human PWWP Domains', *PLoS ONE*. Edited by P. Kursula, 6(6), p. e18919. doi: 10.1371/journal.pone.0018919.

Yamamoto, K., Troeberg, L., Scilabra, S. D., Pelosi, M., Murphy, C. L., Strickland, D. K., *et al.* (2013) 'LRP-1-mediated endocytosis regulates extracellular activity of ADAMTS-5 in articular cartilage', *The FASEB Journal*. John Wiley & Sons, Ltd, 27(2), pp. 511–521. doi: 10.1096/fj.12-216671.

Yamamoto, S., Tomita, Y., Hoshida, Y., Morii, E., Yasuda, T., Doki, Y., *et al.* (2007) 'Expression level of hepatoma-derived growth factor correlates with tumor recurrence of esophageal carcinoma', *Annals of Surgical Oncology*. Ann Surg Oncol, 14(7), pp. 2141–2149. doi: 10.1245/s10434-007-9369-9.

Yamamoto, T., Wakitani, S., Imoto, K., Hattori, T., Nakaya, H., Saito, M., *et al.* (2004) 'Fibroblast growth factor-2 promotes the repair of partial thickness defects of articular cartilage in immature rabbits but not in mature rabbits', *Osteoarthritis and Cartilage*. W.B. Saunders, 12(8), pp. 636–641. doi: 10.1016/j.joca.2004.04.007.

Yan, D., Chen, D., Cool, S. M., van Wijnen, A. J., Mikecz, K., Murphy, G., *et al.* (2011) 'Fibroblast growth factor receptor 1 is principally responsible for fibroblast growth factor 2-induced catabolic activities in human articular chondrocytes', *Arthritis Research & Therapy*. Arthritis Res Ther, 13(4), p. R130. doi: 10.1186/ar3441.

Yang, X., Chen, L., Xu, X., Li, C., Huang, C. and Deng, C. X. (2001) 'TGF-β/Smad3 signals repress chondrocyte hypertrophic differentiation and are required for maintaining articular cartilage', *Journal of Cell Biology*. The Rockefeller University Press, 153(1), pp. 35–46. doi: 10.1083/jcb.153.1.35.

Yang, X. and Momot, K. I. (2016) *Biophysics and Biochemistry of Cartilage by NMR and MRI*. Edited by Y. Xia and K. Momot. Cambridge: Royal Society of Chemistry (New Developments in NMR). doi: 10.1039/9781782623663.

Yi, W., Zhou, H., Li, A., Yuan, Y., Guo, Y., Li, P., *et al.* (2019) 'A NIR-II fluorescent probe for articular cartilage degeneration imaging and osteoarthritis detection', *Biomaterials Science*. Royal Society of Chemistry, 7(3), pp. 1043–1051. doi: 10.1039/c8bm01440j.

Zeggini, E., Panoutsopoulou, K., Southam, L., Rayner, N. W., Day-Williams, A. G., Lopes, M. C., *et al.* (2012) 'Identification of new susceptibility loci for osteoarthritis (arcOGEN): a genome-wide association study', *The Lancet*. Lancet Publishing Group, 380(9844), pp. 815–823. doi: 10.1016/S0140-6736(12)60681-3.

Zengini, E., Hatzikotoulas, K., Tachmazidou, I., Steinberg, J., Hartwig, F. P., Southam, L., *et al.* (2018) 'Genome-wide analyses using UK Biobank data provide insights into the genetic architecture of osteoarthritis', *Nature Genetics*, 50(4), pp. 549–558. doi: 10.1038/s41588-018-0079-y.

Zhang, A., Long, W., Guo, Z., Liu, G., Hu, Z., Huang, Y., *et al.* (2010) 'Development and clinical evaluation of a multi-purpose mAb and a sandwich ELISA test for hepatoma-derived growth factor in lung cancer patients', *Journal of Immunological Methods*. J Immunol Methods, 355(1–2), pp. 61–67. doi: 10.1016/j.jim.2010.02.011.

Zhang, C., Chang, X., Chen, D., Yang, F., Li, Z., Li, D., *et al.* (2019) 'Downregulation of HDGF inhibits the tumorigenesis of bladder cancer cells by inactivating the PI3K-AKT signaling pathway', *Cancer Management and Research*. Dove Medical Press Ltd, 11, pp. 7909–7923. doi: 10.2147/CMAR.S215341.

Zhang, J., Chen, N., Qi, J., Zhou, B. and Qiu, X. (2014) 'HDGF and ADAM9 are novel molecular staging biomarkers, prognostic biomarkers and predictive biomarkers for adjuvant chemotherapy in surgically resected stage I non-small cell lung cancer', *Journal of Cancer Research and Clinical Oncology*. Springer Verlag, 140(8), pp. 1441–1449. doi: 10.1007/s00432-014-1687-2.

Zhen, G., Wen, C., Jia, X., Li, Y., Crane, J. L., Mears, S. C., *et al.* (2013) 'Inhibition of TGF-β signaling in mesenchymal stem cells of subchondral bone attenuates osteoarthritis', *Nature Medicine*, 19(6), pp. 704–712. doi: 10.1038/nm.3143.

Zhou, Z., Yamamoto, Y., Sugai, F., Yoshida, K., Kishima, Y., Sumi, H., *et al.* (2004) 'Hepatoma-derived Growth Factor Is a Neurotrophic Factor Harbored in the Nucleus', *Journal of Biological Chemistry*, 279(26), pp. 27320–27326. doi: 10.1074/jbc.M308650200.

Zhu, L., Chanalaris, A., Lympany, S. and Vincent, T. L. (2017) 'Cartilage injury regulates inflammatory gene expression in part by suppressing cellular retinoic acid signaling', *Osteoarthritis and Cartilage*, 25, p. S168. doi: 10.1016/j.joca.2017.02.288.

8 Appendix

8.1 Achievements

Achievement	Details	Description
Cutting Edge OA 2017 Conference		Conference attendance
Osteoarthritis Research Society International (OARSI) 2018 Conference		Conference attendance
BBSRC *in vivo* Skills Award	Grant awarded 2018	Research Award Grant
Kennedy Institute 3-Minute Thesis Award	Awarded April 2019	Oral Presentation Award
Oxford DTC Bioscience Best Poster Award	Awarded April 2019	Poster Presentation Award
BSMB 2019 Stroma, Niche and Repair Conference		Poster Presentation
Cutting Edge OA 2019 Conference		Short Oral Presentation & Poster
Cutting Edge OA Runner Up Poster Award	Awarded June 2019	Poster Presentation Award
Matrix Biology Europe Conference 2020	Postponed	Oral Invitation
Osteoarthritis and Cartilage Abstract Publication	doi.org/10.1016/j.joca.2020.02.291	Abstract Publication
BBSRC PIPS Internship: Roche (Product Development: Clinical Science)	July–October 2020	Industry Work Experience
STEM Ambassador	2018–2021 https://www.stem.org.uk/stem-ambassadors	Big Bang Fair 2018 Big Bang Eastern Science Judge 2019 STEM Outreach
BioRxiv pre-print	doi.org/10.1101/2021.01.31.428791	Journal Publication

Matrix-Bound Growth Factors are Released upon Cartilage Compression by an Aggrecan-Dependent Sodium Flux that is Lost in Osteoarthritis

Stuart J. Keppie[a], Jessica C. Mansfield[b], Xiaodi Tang[a], Christopher J. Philp[c], Helen K. Graham[d], Patrik Önnerfjord[e], Alanna Wall[a], Celia McLean[a], C. Peter Winlove[b], Michael J. Sherratt[d], Galina E. Pavlovskaya[c], Tonia L Vincent[a,1].

[a] Kennedy Institute of Rheumatology, University of Oxford, Oxford, OX3 7FY
[b] School of Physics and Astronomy, University of Exeter, Exeter, EX4 4QL
[c] Sir Peter Mansfield Imaging Centre, University of Nottingham, Nottingham, NG7 2QX
[d] School of Biological Sciences, The University of Manchester, Manchester, M13 9PT
[e] Rheumatology and Molecular Skeletal Biology, Department of Clinical Sciences Lund, Lund University, Lund, Sweden
[1] Correspondence: Tonia.Vincent@Kennedy.ox.ac.uk, Kennedy Institute of Rheumatology, Centre for OA Pathogenesis Versus Arthritis, University of Oxford, Roosevelt Drive, OX3 7FY, United Kingdom

Abstract

Articular cartilage is a dense extracellular matrix-rich tissue that degrades following chronic mechanical stress, resulting in osteoarthritis (OA). The tissue has low intrinsic repair especially in aged and osteoarthritic joints. Here we describe three pro-regenerative factors; fibroblast growth factor 2 (FGF2), connective tissue growth factor, bound to transforming growth factor-beta (CTGF-TGFβ), and hepatoma-derived growth factor (HDGF), that are rapidly released from the pericellular matrix (PCM) of articular cartilage upon mechanical injury. All three growth factors bound heparan sulfate, and were displaced by exogenous NaCl. We hypothesised that sodium, sequestered within the aggrecan-rich matrix, was freed by injurious compression, thereby enhancing the bioavailability of pericellular growth factors. Indeed, growth factor release was abrogated when cartilage aggrecan was depleted by IL-1 treatment, and in severely damaged human osteoarthritic cartilage. A flux in free matrix sodium upon mechanical compression of cartilage was visualised by ^{23}Na magnetic resonance imaging (MRI) just below the articular surface. This corresponded to a region of reduced tissue stiffness, measured by scanning acoustic microscopy and second harmonic generation microscopy, and where Smad2/3 was phosphorylated upon cyclic compression. Our results describe a novel intrinsic repair mechanism, controlled by matrix stiffness and mediated by the free sodium concentration, in which heparan sulfate-bound growth factors are released from cartilage upon injurious load. They identify aggrecan as a depot for sequestered sodium, explaining why osteoarthritic tissue loses its ability to repair. Treatments that restore matrix sodium to allow appropriate release of growth factors upon load are predicted to enable intrinsic cartilage repair in osteoarthritis.

Significance Statement

Osteoarthritis is the most prevalent musculoskeletal disease, affecting 250 million people worldwide [1]. We identify a novel intrinsic repair response in cartilage, mediated by aggrecan-dependent sodium flux, and dependent upon matrix stiffness, which results in the release of a cocktail of pro-regenerative growth factors after injury. Loss of aggrecan in late-stage osteoarthritis prevents growth factor release and likely contributes to disease progression. Treatments that restore matrix sodium in osteoarthritis may recover the intrinsic repair response to improve disease outcome.

Keywords: Growth Factor, Osteoarthritis, Injury, Repair, Cartilage, Extracellular Matrix, Sodium

Introduction

Articular cartilage is a highly mechanosensitive tissue that overlies the ends of bone in all articulating joints. It is predominantly composed of extracellular matrix, with the remaining tissue containing sparsely distributed cells (chondrocytes) that constitute 5–10% of the tissue by volume. Articular cartilage contains an abundance of type II collagen, a fibrillar collagen responsible for providing tensile strength to the tissue, and proteoglycans. The most abundant proteoglycan of articular cartilage is aggrecan, to whose core protein are attached ~100 chondroitin sulfate glyscosaminoglycan (GAG) chains [2], which generate a net negative fixed charge to the tissue. This negative charge contributes to the osmotic retention of water in the tissue by attracting sodium cations, and provides intermolecular electrostatic repulsion between GAGs, contributing to tissue stiffness and elasticity. The aggrecan-rich extracellular matrix is divided into the territorial matrix (TM) and interterritorial matrix (ITM) and these are separated from the cell by a distinct region of matrix termed the pericellular matrix (PCM), which is rich in collagen VI and the heparan sulfate proteoglycan perlecan [3].

Loss of aggrecan is an early pathological feature of cartilage matrix breakdown that occurs in osteoarthritis (OA), a disease estimated to

affect over 250 million people worldwide [4], and a leading cause of disability and societal burden. Other disease features of the OA joint include synovial hypertrophy, osteophyte formation and subchondral bone sclerosis. Degradation of aggrecan can be detected histologically using cationic dyes, as well as in patients *in vivo* by sodium-MRI imaging [5]. A number of pathogenic mechanisms contribute to the development of OA, which can be broadly divided into those that drive proteolytic degradation of the matrix and those that suppress the intrinsic repair of the tissue. Both are closely linked to the two major aetiological factors in disease; abnormal mechanical joint loading and ageing.

In exploring the response of articular cartilage to mechanical stress, our group has observed that sequestered matrix-bound growth factors are released from the pericellular matrix of cartilage following mechanical injury. The best characterised of these is fibroblast growth factor 2 (FGF2), which is chondroprotective *in vivo* in multiple animal models of OA [6–12]. The second molecule identified was connective tissue growth factor (CTGF), which is in a covalently bound complex with latent transforming growth factor beta (TGFβ) [13]. When the latent complex is released from cartilage upon injury, latent TGFβ is activated by binding to the cell surface receptor TGFβR3 [13]. TGFβ is a strong chondrogenic growth factor [14,15] and is implicated in intrinsic tissue repair responses elsewhere in the body [16–18]. TGFβ and FGF2 exhibit binding affinities to heparin and heparan sulfate [19]. In our previous studies both growth factors were released rapidly upon injury (within 5 minutes), and this was independent of cell viability [13,20].

In this study, we characterise a third growth factor released upon cartilage injury, hepatoma-derived growth factor (HDGF). We reveal the common mechanism by which these growth factors are released upon tissue injury and how this goes awry in OA.

Results

PCM Growth Factors, Including Hepatoma Derived Growth Factor (HDGF) are Bound to Heparan Sulfate and Released Rapidly upon Cartilage Injury

We previously identified HDGF from a proteomic analysis of human isolated PCM and tested whether HDGF was released upon cartilage injury in a similar fashion to release of FGF2 and CTGF. FGF2, CTGF and HDGF were all released from human knee cartilage within 30 minutes of recutting injury (Figure 1A), and were not detected in the medium of uninjured, rested cartilage explants. HDGF release into the medium occurred largely within the first 5 minutes (Figure 1B). We confirmed our previous observation of co-localisation of FGF2 and CTGF in the type VI collagen and perlecan-rich pericellular matrix (Figure 1C) and confirmed heparin binding of all three growth factors by showing their depletion from the injury conditioned medium (recut CM) on a heparin column, and elution with 2.5M NaCl (Figure 1D). They were also released from articular cartilage following treatment with heparitinase (Figure 1E). The injurious release of growth factors occurred irrespective of whether the tissue was alive or dead (Figure 1F), at 4 °C or 37 °C, or after pre-incubation with an inhibitor of matrix metalloproteases, or a broad-spectrum protease inhibitor (Figure 1G). These results suggested that there was a common mechanism of release of PCM-bound growth factors upon cartilage injury, which did not require viable cells or involve cell-dependent protease activity.

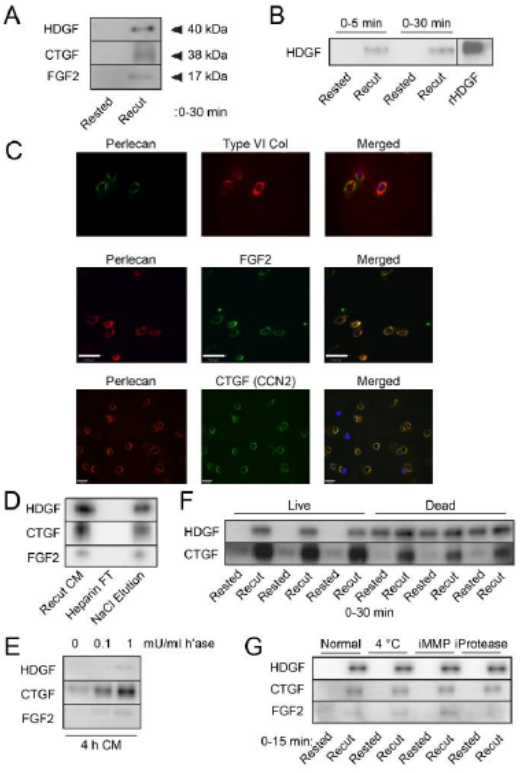

Fig. 1. Heparan sulfate-bound growth factors are released upon cartilage injury. (A) Immunoblots of medium conditioned (30 min) by rested (48 h post dissection) or recut (Recut CM) human articular cartilage. (B) Medium conditioned by rested and recut cartilage for 5 or 30 minutes. Recombinant HDGF (rHDGF). (C) confocal microscopy showing co-immunolocalisation of type VI collagen/perlecan, perlecan/FGF2 and perlecan/CTGF (CCN2) in the PCM. (D) Injury CM (recut) was passed through a heparin-agarose column and eluted with 2.5M NaCl. Starting material (Recut CM), column flow through (Heparin FT) and eluted fractions (NaCl Elution) were immunoblotted for CTGF, HDGF and FGF2. (E) Rested porcine articular cartilage was treated with 0, 0.1 or 1 mU/ml heparitinase I for 4 h and the conditioned medium immunoblotted for growth factors. (F) Immunoblots showing release of FGF2, CTGF and HDGF in rested or recut CM (30 mins) from live or dead (3 cycles of freeze-thawing) porcine articular cartilage. (G) Porcine articular cartilage explants were pre-treated with 10 μM batimastat (MMP inhibitor) or with protease inhibitor cocktail, or were incubated at 4°C or 37°C prior to recutting.

Manipulation of Tissue Sodium Affects Growth Factor Release upon Cartilage Injury

As the interaction of heparin-bound growth factors with heparan sulfate is ionic and the growth factors in injury CM were displaced by elution from a heparin column with sodium chloride (Figure 1D), we hypothesised that growth factor release after injury was dependent upon mobilisation of tissue sodium. This hypothesis was supported by the fact

that the PCM was devoid of chondroitin sulfate (Figure 2A), indicating a cation gradient from the territorial to the pericellular matrix.

To test the hypothesis, we studied the injury response after manipulating tissue sodium levels. Addition of exogenous sodium chloride, at supraphysiological concentrations, displaced HDGF and CTGF from cartilage in a concentration dependent manner and enhanced the release of HDGF and CTGF after injury (Figure 2B, C). Conversely, depletion of aggrecan from cartilage following prolonged treatment with interleukin-1 (IL-1), reduced the fixed charge of the tissue (Figure 2D) and abrogated the release of HDGF, CTGF and FGF2 upon recutting (Figure 2E–H). The reduction in release upon injury occurred despite there being no difference in total growth factor extracted from untreated and IL-1 treated tissue (Figure 2I).

Bound Sodium is Mobilised upon Cartilage Compression

We next examined the effect of cartilage mechanical compression on sodium mobilisation using multi-modal MRI methods (Figure A). Porcine knee osteochondral plugs were imaged using a Bruker AVANCE III 9.4T microimaging system at micron length scales to obtain anatomical, free and bound sodium scans of cartilage plugs during compressive loading. A strong sodium signal was seen in the articular cartilage, but not subchondral bone (Figure 3B). The MRI signal contribution from bound sodium was determined by inserting a multiple quantum filter before applying localising gradients (Supplementary Figure S2). Tissue compression (28% strain) caused redistribution of both free and bound sodium within articular cartilage (Figure 3B). Compression led to a heterogeneous distribution in free sodium in the cartilage matrix, specifically just below the superficial layer. Compression reduced bound sodium levels, with partial restoration of these levels upon relaxation of the cartilage. This was further confirmed by two dimensional ^{23}Na TQTPPI spectroscopy (details in supplementary - ^{23}Na MRS) where sodium signals in both free and bound states are recorded, providing information about bulk sodium levels in each state. Tissue compression caused a significant increase in free sodium of 46%, with a concomitant significant decrease in the bound sodium fraction ($F(2,9) = 9.709$, $p=0.0057$) (Figure 3C). Upon relaxation of the tissue, the free and bound sodium fractions were lower than in the compressed state, with a tendency towards uncompressed levels.

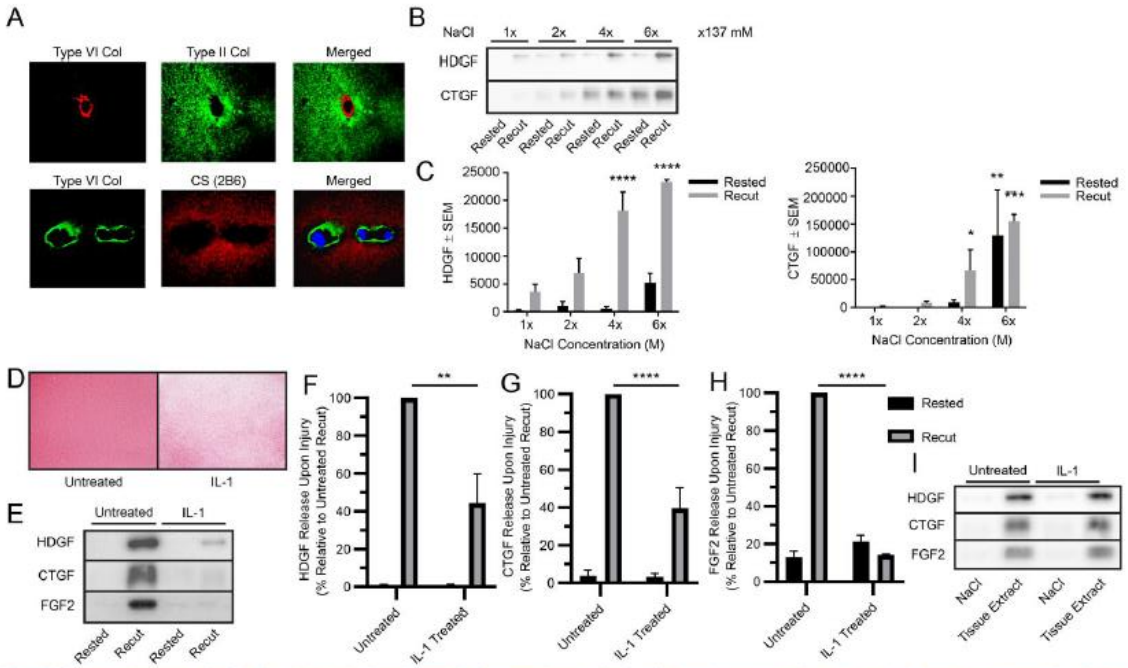

Fig. 2. Changes in tissue NaCl affect injury-induced growth factor release. (A) Confocal microscopy delineating pericellular matrix (type VI collagen) and territorial matrix (type II collagen and chondroitin sulfate (CS)), in human articular cartilage. (B) Western blot of CM (0–15 mins) from rested and recut porcine articular cartilage generated in medium with physiological NaCl (0.137 mM) or supraphysiological NaCl concentrations (2–6 fold). (C) Quantification for HDGF and CTGF (Two-Way ANOVA with Sidak multiple comparisons compared to 1x NaCl, n=3 biological replicates). (D-I) Aggrecan was depleted from articular cartilage by 7 day IL-1 treatment. (D) Safranin O staining of porcine cartilage after 7 days. (E) Immunoblots of growth factors of rested and injury CM after recutting (0–15 min). (F-H) Quantification of western blots for HDGF, CTGF and FGF2 respectively (T-test, n=6 biological replicates). (I) Western blots of tissue extracts (2.5M NaCl or dissociative lysis buffer) of control and IL-1-treated explants (representative experiment of four independent experiments). (*=p<0.05, **=p<0.01, ***=p<0.001, ****=p<0.0001).

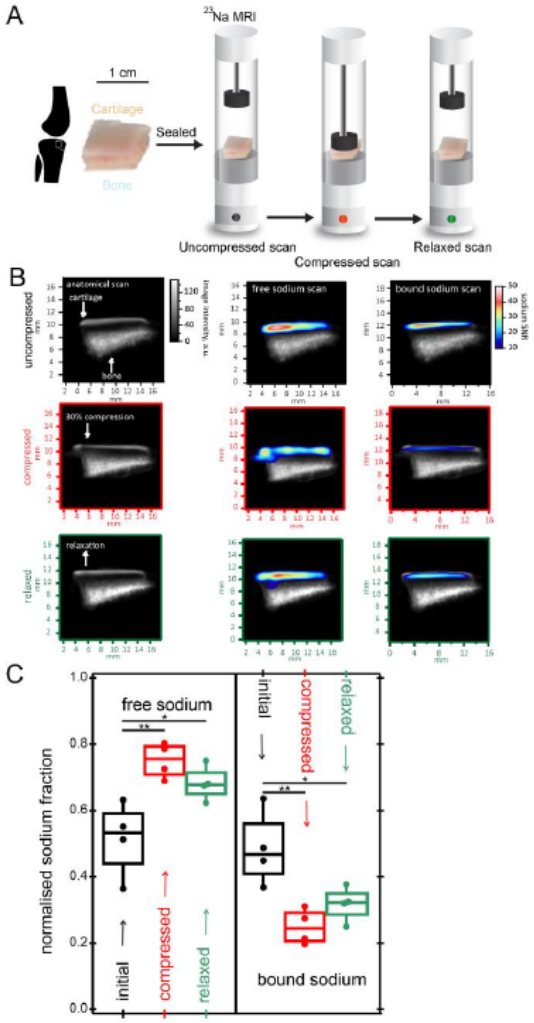

Fig. 3. Sodium is reversibly mobilised from bound stores upon cartilage compression. (A) Schematic of tibial plateau osteochondral plugs for ^{1}H (anatomical) and ^{23}Na (free and bound) MRI performed at microscale resolution in initial (uncompressed), compressed (28% strain) and relaxed states. All images were recorded at steady state. (B) Anatomical, free and bound sodium scans overlaid with corresponding anatomical scans of vacuum-sealed porcine osteochondral plugs during loading cycle depicted in A. (C) Free and bound sodium fractions (n=4) quantified with 2D TQTPPI ^{23}Na spectroscopy (details in supplementary) in the initial, compressed and relaxed states as depicted in A. One-Way ANOVA with Tukey multiple comparisons (*=p<0.05, **=p<0.01).

Compression-Induced Growth Factor Release is Preferentially in Areas of Low Matrix Stiffness

To explore further the possibility that regional differences exist within the tissue, cyclically compressed porcine knee cartilage was examined by immunohistochemistry for evidence of growth factor dependent cell activation. SMAD2 phosphorylation, indicative of TGFβ activation, was evident in the superficial zone of cartilage from just below the articular surface (between 50 and 300 µm from the surface) in compressed, but not non-compressed cartilage explants (Figure 4A–C). Regional activation was not due to differences in the amount of growth factor present in the tissue at different levels, as all three PCM growth factors were identified throughout the deeper parts of the tissue by proteomic analysis (Figure 4D). Full proteomic dataset of each cartilage layer shown in supplementary file and raw data available via ProteomeXchange with identifier PXD023890.

As the region of SMAD2 activation was not apparently limited by growth factor distribution within the tissue, we next explored whether regional differences in tissue stiffness might explain differential activation upon compression. Scanning acoustic microscopy wave speeds were recorded across the depth of the tissue in compressed and non-compressed tissue sections. Variations in stiffness through the depth of the tissue were observed, with the highest stiffness (highest wave speed) in the most superficial 50 µm and a region of reduced stiffness below this from 50–350µm, which became more evident upon compression (Figure 4E). This region also contained a higher polarised light microscopy signal, consistent with disordered collagen fibres in this region (Figure 4F).

Differential stiffness and response to compression was further investigated in human articular cartilage by second harmonic generation, to explore the collagen organisation and arrangement upon compression. Following compressive load of the tissue (0–21% strain), a marked loss of tissue volume was observed in the superficial zone (Figure 5A, upper box), compressive load led to marked loss of tissue volume (Figure 5B-D), with reorganisation of the collagen fibre orientation (Figure 5E). In contrast, compression of the tissue led to no discernible volume loss in the deep region (Figure 5A lower box, Figure 5F-H), with no change in the collagen orientation (Figure 5I). In both regions of interest, the submicron organisation parameter I_2, which represents the degree of order of individual collagen fibrils within a focal spot, remained constant (data not shown). Taken together, these data confirm region-specific difference in tissue stiffness and response to compression in human cartilage, similar to that seen in pig.

Severely Damaged Osteoarthritic Tissue Exhibits Impaired Release of Heparan Sulfate Bound Growth Factors after Injury

Proteolytic degradation of aggrecan in OA occurs through the actions of aggrecanases [21–23] and results in a reduction of the fixed charge density of the tissue reflected by the loss of safranin O staining (Figure 6A). We explored whether release of growth factors after injury was blunted in OA and whether it was dependent upon severity of disease in an aggrecan-dependent manner. Cartilage biopsies were taken from human osteoarthritic cartilage obtained from knee arthroplasty surgery (Figure 6B) and scored for macroscopic disease severity using the Outerbridge classification. Proteoglycan content (as assessed by amount of GAG) inversely correlated with Outerbridge score (Figure 6C), confirming that severe macroscopic damage was associated with reduced GAG (aggrecan) content. Uniform biopsy punches (matched by wet weight) from severely diseased regions (Outerbridge score 3–4) released significantly less HDGF, CTGF and FGF2 upon injury compared with

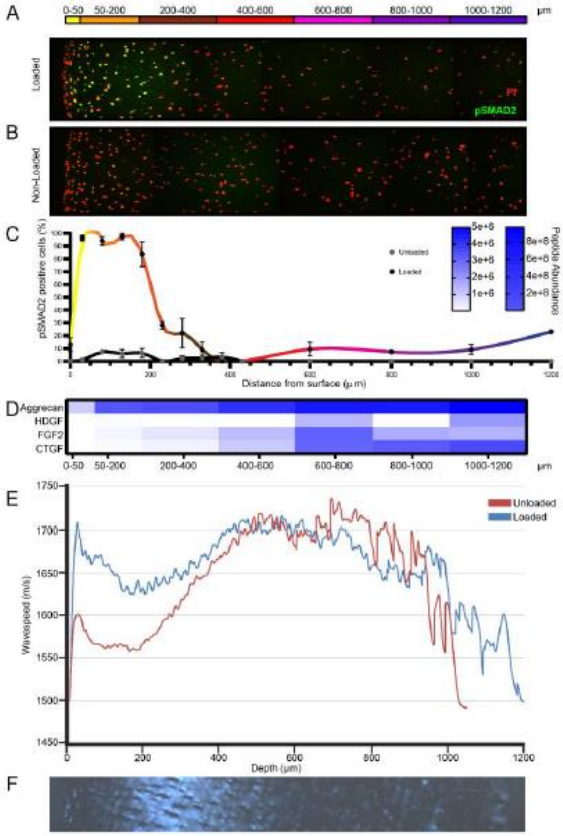

Fig. 4. TGFβ/CTGF mediated SMAD2 activation occurs after cyclical compression in a region of cartilage with low tissue stiffness. Porcine articular cartilage was (A) cyclically loaded for 45 min or (B) left unloaded. (A,B) Coronal sections perpendicular to the articular surface were immunostained for phosphorylated SMAD2 (green) and (C) quantified (n=6 separate experiments). Nuclei were counterstained with propidium iodide. (D) Slices of articular cartilage, parallel with the articular surface were removed by cryosection and analysed by proteomics. (E) Scanning acoustic microscopy (SAM) was performed across the depth of porcine knee cartilage sections, where wavespeed denotes tissue stiffness from the surface (left) to the deep zone (right). (F) Articular cartilage sections were imaged for collagen alignment by polarised light microscopy.

biopsies taken from relatively undamaged regions of the same joint (Outerbridge score 0–1) (Figure 6E–H). This was not due to reduced growth factor content as protein extracted from the matrix with 2.5M NaCl indicated that the more damaged cartilage contained higher Na-extractable growth factor compared with tissue with mild disease (Figure 6I–L).

Discussion

To date our group has identified three growth factors that are released rapidly following mechanical injury of articular cartilage [3,13,20]. Here we characterise, for the first time, the release of HDGF, a lesser known heparan sulfate bound growth factor, identified in a proteomic analysis of articular cartilage PCM. Like CTGF and FGF2, HDGF was released rapidly, in a cell-independent manner, from a heparan sulfate bound matrix store. Commonality between the three growth factors, in terms of release by injury and sequestration on heparan sulfate within the PCM, suggested a common mechanism of release.

Three distinct properties of cartilage led us to hypothesise that release upon injury was due to a shift in the matrix sodium concentration. Firstly, the extracellular sodium content in cartilage is high compared with other tissues, at around 250-350mM [24–27], which we confirmed by ^{23}Na MRI imaging (Figure 3B). Secondly, we identified a gradient of sodium between the territorial/interterritorial matrix and pericellular matrix due to absence of aggrecan (chondroitin sulfate) in the PCM (Figure 2A). Thirdly, all three growth factors were bound to heparan sulfate in cartilage (Figure 1F, G) and had previously been shown to elute from heparin using NaCl [19,28]. Our previous studies had demonstrated that perlecan is the major heparan sulfate proteoglycan in cartilage and is exclusively found in the PCM [3]. Though we were unable to immunolocalise HDGF in the PCM (data not shown), it was highly likely that it was also bound to perlecan along with CTGF and FGF2.

Our data support a sodium dependent release of growth factors upon injury by demonstrating that modulating sodium directly (by exogenous NaCl addition) or indirectly (by depleting aggrecan), increases or decreases, respectively, the release of growth factors after injury. Moreover, a shift in free sodium, relative to bound sodium, within the tissue was demonstrated after cartilage compression using ^{23}Na MRI. This indicates that pathological type mechanical loading (28% unconfined strain) leads to a relative increase in free sodium levels and decrease in the bound sodium levels.

Regional changes in sodium observed by ^{23}Na MRI suggested that sodium mobilisation occured non-uniformly in the cartilage upon compression. This was consistent with regional CTGF/TGFβ activation (Smad 2 phosphorylation), which occurred just below the articular surface upon loading, and differences in matrix stiffness. Indeed, this region of matrix had a different polarised microscopy appearance, consistent with the known random alignment of collagen fibres in this region [29], and displayed reduced tissue stiffness, which became more evident upon compression (Figure 4F). These observations were also confirmed in human cartilage, where a marked reduction in volume was observed in the area just below the superficial zone, but not the deep zone, which was associated with marked collagen fibre realignment (Figure 5). Our data are consistent with previous findings that the region just below the surface is lower in fixed charge density [24,30], has increased

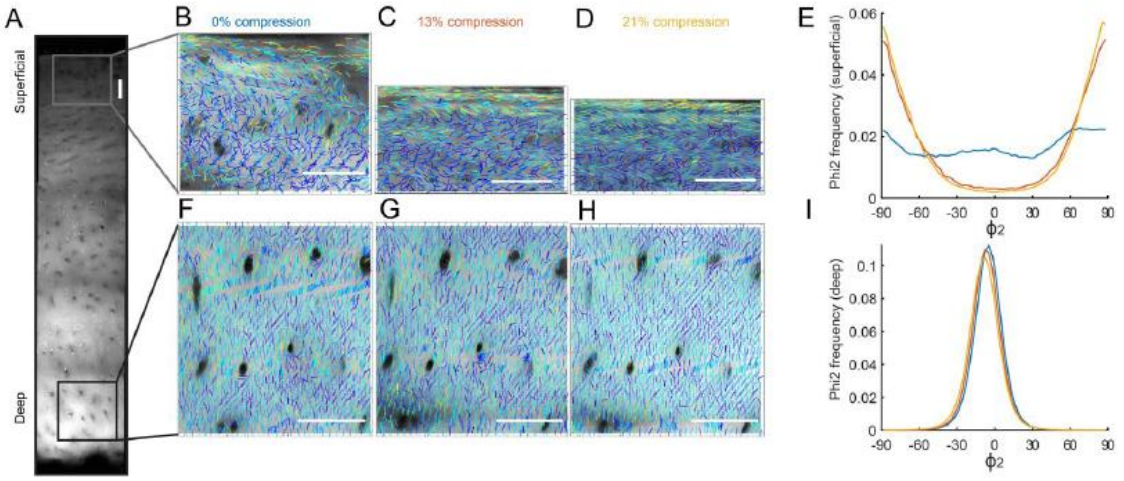

Fig. 5. Polarisation sensitive second harmonic generation (SHG) measurement of collagen organisation of human articular cartilage under compressive load. (A) Full depth image of the unloaded region of cartilage, highlighting the 2 areas where polarisation SHG analysis was carried out at 0% (B, F), 13% (C, G) and 12% (D, H). These correspond to the unloaded samples and then the overall strain in the full thickness of the cartilage. Maps of the collagen organisation in the (B–D) superficial region and (F–H) deep region, as a function of load. The direction of the sticks indicates the collagen fibre direction and the colour of the sticks indicates I_2 (level of submicron organisation). ϕ_2 measurements, indicating a change in orientation of collagen fibres upon compression, are shown in the (E) superficial layer and the (I) deep layer. Blue line (0% stain), orange line (13% strain), yellow line (21% strain). Note the marked change in compression and collagen orientation in the superficial, but not deep, region. Scale 100 µm.

permeability [31], and is more likely to compress upon load [30,32,33]. It is also where the tissue exhibits high cation fluxes [34].

Fluid flows away from more readily compressed regions to unloaded regions [35]. Fluid flow is also high in osteoarthritic tissue which loses its fixed charge density, has a lower compressive modulus (more susceptible to compression) and becomes more permeable [36–38]. However, fluid transport is not thought to significantly affect the transport rate of small solutes in cartilage, as diffusion coefficients are the dominant factor for small solute transport [39]. Therefore, we suggest that displacement of growth factors upon loading occurs as a result of the net change in the local concentration of free sodium in the tissue rather than due to movement of sodium mediated by fluid flow. Taken together, we suggest that the region just below the articular surface selectively loses water, causing a local increase in the concentration of free sodium, and this drives growth factor release when compression is applied.

This mechanism fails in osteoarthritis where severe loss of proteoglycan leads to an inability to release growth factors upon injury. Growth factors are still present in the tissue and can be extracted by NaCl; indeed these appear to be increased in severe disease compared with less diseased osteoarthritic tissue. Proteoglycan loss and loss of fixed charge density are well established pathological features of osteoarthritis [40,41], and this is mediated by specific aggrecan degrading enzymes such as a disintegrin and metalloproteinase with thrombospondin motif-5 (ADAMTS5) [22]. Aggrecanase activity is an early feature of disease and may precede collagen degradation [42]. Early partial GAG loss, when the collagen network is still intact, can render cartilage more sensitive to load and increased fluid loss [43] suggesting that in early disease there may be enhanced release of growth factors. This could explain why observed release of growth factors was strong from the less affected osteoarthritic cartilage explants (Outerbridge score 0–1) (Figure 6D). We were unable to test whether this was higher than the amount released from completely normal articular cartilage, due to difficulties obtaining such tissue. Enhancement of release early in disease might therefore represent a previously unrecognised role for aggrecanases in promoting the intrinsic repair response of articular cartilage. Once proteoglycan is severely depleted, osteoarthritic tissue loses this mechanism of growth factor release and this presumably then contributes to the failure of the tissue.

Loss of cartilage repair due to reduced growth factor bioavailability is emerging as an important mechanism in osteoarthritis pathogenesis. Both FGF2 and TGFβ have disease modifying roles in pre-clinical models *in vivo* [11–13]. FGF2 signalling is known to enhance the chondrogenic potential of mesenchymal stem cells by priming them for chondrogenesis [44–46], and TGFβ drives chondrogenic differentiation [14,15,47]. Both FGF and TGFβ pathways have been identified in osteoarthritis genome wide association studies, where hypomorphic variants are associated with increased risk of disease [48,49]. Both growth factors, FGF2 and TGFβ, predict clinical response to surgical joint distraction in OA patients; a procedure that drives regeneration of articular cartilage [50]. The therapeutic potential of intrinsic growth factors is reflected in the recent successful phase 2 FORWARD trial (NCT01919164) of a truncated form of recombinant fibroblast growth factor 18 (sprifermin). This study is the first structure modifying drug to demonstrate efficacy by building back articular cartilage in osteoarthritis [51,52]. The role of HDGF is currently unknown, but it has been implicated in the tissue injury response in smooth muscle cells of vascular tissue [53,54]. Its functional role *in vivo* is being explored.

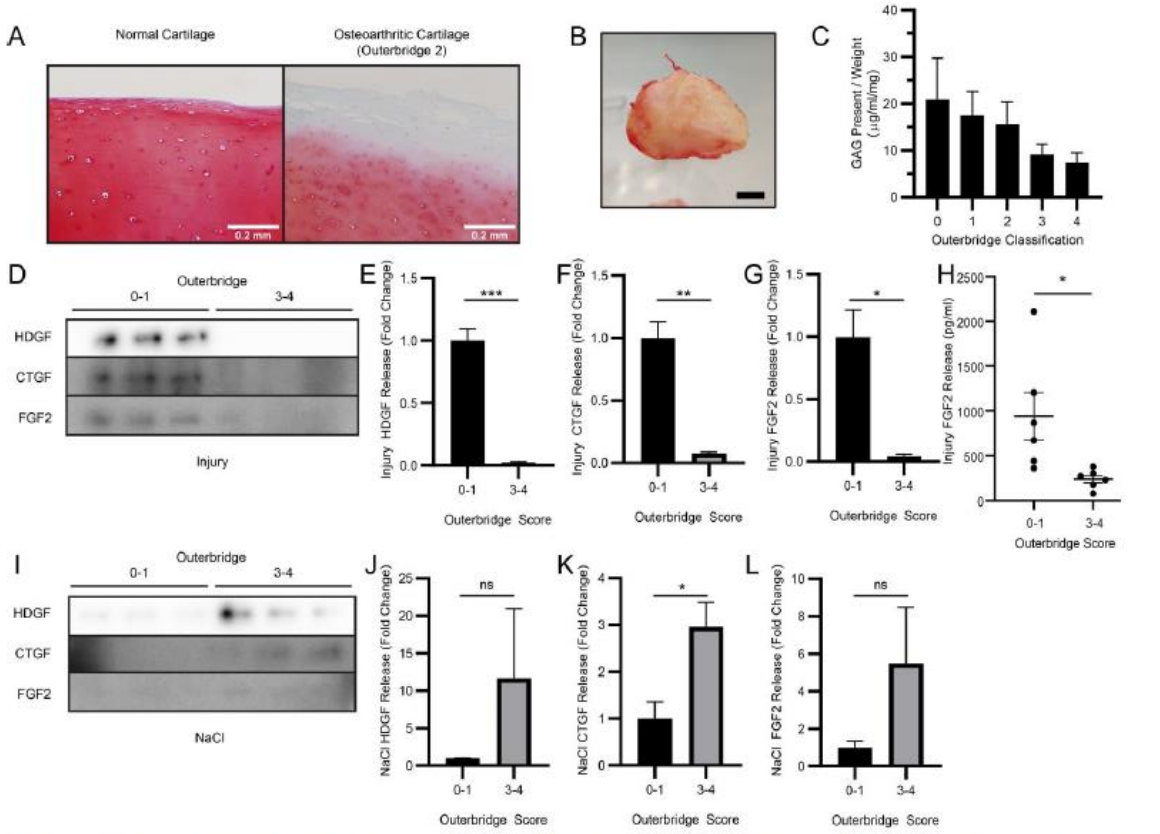

Fig. 6. Release of heparan sulfate-bound growth factors is reduced from diseased osteoarthritic tissue compared to less damaged tissue after cutting injury. (A) Healthy and osteoarthritic human articular cartilage stained with Safranin O (0.2 mm scale). (B) Human osteochondral samples were collected from arthroplasty speciments and osteoarthritis severity scored macroscopically according to the Outerbridge Classification (1 cm scale). (C) Individual explants were digested with proteinase K and assessed for GAG content by the dimethylmethylene blue assay. (D–G) Injury conditioned medium (15 mins) was collected from osteoarthritic cartilage samples from mildly damaged (0–1) or severely diseased (3–4) areas and immunoblotted for growth factors, (H) or assessed by ELISA (FGF2). (E–G) Quantified from D (representative image, n=3 biological replicates). Injured cartilage explants were extracted with 2.5 M NaCl. (I) Matrix extract was immunoblotted for growth factor release. (J–L) Quantified from I (representative image, n=3 biological replicates). T-test (*=p<0.05, **=p<0.01, ***=p<0.001).

Our data, supported by historical studies on tissue composition, response to mechanical load and solute transport, support a model whereby cartilage compression expels water preferentially from less stiff regions of the matrix, causes an increase in free sodium concentration, and enables the release of growth factors from the PCM. This study identifies an important intrinsic repair mechanism of normal cartilage that is lost in osteoarthritis, but could be exploited to recover reparative activities to improve disease outcome.

Materials and Methods

Tissue

Porcine articular cartilage was from the metacarpophalangeal joint for injury and recutting experiments, or from the medial tibial knee joint for imaging experiments, of 7-month-old pigs obtained from an abattoir after slaughter. Human articular cartilage was obtained from knee arthroplasty surgery of osteoarthritic patients.

Cartilage Injury

For recutting injury experiments, uniform cartilage discs were explanted using a 4 mm biopsy punch (Stiefel #BI1500). Explants were rested in serum-free Dulbecco's Modified Eagle's medium (DMEM) for 48 h. Rested explants remained uncut (rested) or were injured (recut into 4 pieces by cutting twice with a scalpel (Swann-Morton, 15 blade) for 30 min, or specified time, in serum-free DMEM, after which time the conditioned medium was removed for immediate use or stored at -20 °C. Dead cartilage was freeze-thawed after dissection and washed thoroughly before recutting experiments. Cartilage injured at 4 °C or in the presence of inhibitors were pre-treated for 15 min prior to remaining uncut (rested) or being injury (recut), using batimastat from AbCam (ab142087) or protease inhibitor from Roche/Sigma (#4693132001). Recutting experiments in the presence of exogenous NaCl were conducted by placing explants in serum-free DMEM containing added NaCl to a total of (137 mM; 1x, 274 mM; 2x, 548 mM; 4x, 822 mM; 6x). After 15 min, conditioned medium was removed for immediate use or stored at -20 °C.

Aggrecan depletion of chondroitin sulfate (sodium depletion)

Uniform cartilage discs were explanted using a 4 mm biopsy punch and rested in serum-free Dulbecco's Modified Eagle's medium (DMEM) for 24 h. Explants were treated either with serum-free DMEM or with serum-free DMEM containing 50 ng/ml interleukin-1 for 7 days. Conditioned medium was collected and replenished every 24 h, and assessed for GAG release by DMMB assay. After 7 days, recutting injury was performed as described, or explants were stained with safranin O to assess fixed charge density. Alternatively, after 7 days, explants were extracted using a dissociative whole tissue lysis buffer (RIPA), or matrix extraction buffer (2.5 M NaCl).

Sodium ^{23}MRI Loaded Imaging

Osteochondral cubes of 1 cm^3 were dissected from the porcine knee medial tibial plateau, then vacuum sealed and placed in a custom-made compression cell. Imaging and spectroscopy were conducted for both proton and sodium nuclei on a Bruker 9.4T Ultra-high field microimaging system. Samples were imaged firstly uncompressed, then after 28% deformation compressive load to the cartilage surface, and finally after relaxation with no compression.

Loading in MRI experiments was performed after placing samples into a custom-made compression cell. The cartilage specimen was placed in the centre of the cell and compressed to approximately 30% of the original cartilage thickness using a screw-driven plunger entering the cell from the top. The compression was released by returning the screw-driven plunger into its original position. Samples were imaged firstly uncompressed, then after 28% deformation compressive load to the cartilage surface (as monitored by proton MRI), and finally after relaxation with no compression.

Anatomical images were acquired with home written gradient echo code (TopSpin3.2, Bruker, Germany) using dual tuned 1H/23Na microimaging coil to ensure proper co-registration of anatomical and sodium images. Each anatomical imaging protocol was performed without slice selection in order to match best sodium scan parameters. Time domain data were acquired into 256x128 matrices and were processed using Prospa 3.2 (Magritek, Germany) to result in the magnitude images with FOV = 19.52 mm2 and in plane image resolution of 76 µm2. Further experimental details are reported in the Supplementary.

Sodium imaging was performed after ^{1}H scans. Localisation of free and bound sodium was performed with TopSpin 3.2 (Bruker, Germany) using a home written non-selective Gradient Echo (GE) MRI protocol. Bound sodium was visualised during loading cycle by inserting multiple quantum filter (MQF) into GE protocol before applying localising gradients. MQF time duration was determined from a series of triple quantum filtered experiments and set to the evolution time τ where the triple quantum filtered signal was at maximum. Achieved in plane resolution in sodium images was (117 × 0.109) μm^2 for free and (62 × 86) μm^2 for bound sodium. All details pertinent to sodium imaging including MQF imaging are given in the Supplementary.

Two dimensional (2D) ^{23}Na MRS TQ TPPI spectroscopy was performed during loading cycles in order to determine changes in free and bound sodium levels upon compression and relaxation. All details of these experiments and analysis of the obtained spectra to yields fractions of sodium in the free and bound states during the loading cycle are reported in the Supplementary.

Cartilage Depth Loaded Imaging

Porcine articular cartilage explants were taken from the pig knee joint by a 4 mm biopsy punch (Stiefel #BI1500). Explants were washed in serum-free DMEM and serum starved for 48 h. Cartilage explants were either cyclically loaded (0.1Hz) or rested in serum free DMEM for 45 min at 37°C and snap frozen in liquid nitrogen. Frozen explants were mounted in optimal cutting temperature compound (OCT) and cut by cryostat into 7 µm frozen sections (through the full thickness) on Surgipath snowcoat Xtra slides.

Alternatively, rested porcine knee joint cartilage samples were cut across specified depths for mass spectrometry analysis or scanning acoustic microscopy and polarised light microscopy.

Sample preparation for mass spectrometry analysis

4M Gu-HCl tissue extracts of sectioned regions (from superficial zone towards the bone) were precipitated with ethanol (9:1) overnight at 4°C and collected after centrifugation at 13,200 g at 4°C for 30 minutes. The precipitate was dissolved in 100 µL of buffer (25 mM ammonium bicarbonate (AmBic), pH:7.8) /0,2% Rapigest (Waters) reduced with 2mM DTT at 56°C for 30 minutes on an orbital shaker and alkylated with 8 mM iodoacetamide at room temperature for 1h in the dark. Trypsin digestion was performed with 2µg of trypsin gold (Promega, Madison, WI) at 37°C on a shaker for 16h. Subsequently, samples were diluted to 200µl with 1M AmBic and filtered through a 30kDa filter (Pall Life Sciences, Port Washington, NY) by centrifugation at 2060 x g for 8 minutes. The filter was then washed with an additional 100µl 0.5M AmBic buffer to optimize recovery. The filtrates were then desalted using a reversed-phase C18 column (UltraMicro Spin C18, The Nest group, Southborough, MA) according to the manufacturer's instructions.

Discovery mass spectrometry

The samples were analyzed on a quadrupole Orbitrap benchtop mass spectrometer (Q Exactive™) (Thermo Fisher Scientific, Waltham, WA) equipped with an Easy nano-LC 1000 system (Thermo Scientific, Waltham MA). Separation was performed on 75 µm × 25 cm capillary columns (Acclaim Pepmap™ RSLC, C18, 2µm, 100Å, Thermo Scientific, Waltham, WA). A spray voltage of +2000 V was used with a heated ion transfer setting of 275°C for desolvation. On-line reversed-phase separation was performed using a flow rate of 300 nl/min and a linear binary gradient from 3% solvent B for 60 min to 35% solvent B, then to 90% solvent B for 5 min and finally isocratic 90% solvent B for 5 min. An MS scan (400–1200 m/z) was recorded in the Orbitrap mass analyzer set at a resolution of 70,000 at 200 m/z, $1\times10E^6$ automatic gain control (AGC) target and 100 ms maximum ion injection time. The MS was followed by data-dependent collision induced dissociation MS/MS scans at a resolution of 15,000 on the 15 most intense multiply charged ions at $2 \times 10E^4$ intensity threshold, 2 m/z isolation width and dynamic exclusion enabled for 30 seconds.

Database search

Identification was performed using the sus scrofa taxonomy (22,166 sequences) setting of the Uniprot database (Proteome UP000008227) with Proteome Discoverer 2.5 (version 2.5.0.400,Thermo Scientific). The processing workflow consisted of the following nodes: Spectrum recalibration; Minora Feature detection; Spectrum Selector for spectra pre-processing (350–5000 Da); Spectrum Properties Filter (S/N Threshold: 1.5); Spectrum Properties (charges 2–6); Sequest-HT search engine (Protein Database: see above; Enzyme: Trypsin; Max. missed cleavage sites: 2; Peptide length range 6–144 amino acids; Precursor mass tolerance: 10 ppm; Fragment mass tolerance: 0.02 Da; Static modification: cysteine carbamidomethylation; Dynamic modification: methionine and proline oxidation; INFERYS Rescoring and Percolator for peptide validation (FDR<1% based on peptide q-value). Results were filtered to keep only the Master protein and protein FDR <1%. The

quantification workflow was based on protein abundance using top-3 peptide intensities average allowing only unique peptides.

The mass spectrometry proteomics data have been deposited to the ProteomeXchange Consortium via the PRIDE [55] partner repository with the dataset identifier PXD023890.

Immunohistochemistry

Frozen tissue sections were fixed in methanol for 10min, blocked with 10% goat serum/PBS for 60min at room temperature, and incubated with anti-phospho-Smad2 antibody from Cell Signaling (#138D4) (1:1000 dilution in goat serum) for 1hr at room temperature. Sections were washed three times with PBS and incubated with secondary Alexa 647-conjugated IgG, goat anti rabbit antibody from Invitrogen (#A-31852) for 1h at room temperature. After wash and mounting in 50% glycerol, florescence signals were detected by Ultraview confocal microscopy (Perkin-Elmer, x60 oil immersion lens).

Protein Analysis

Growth factor proteins were analysed in conditioned medium and dissociative tissue extracts by Western blotting using anti-HDGF from AbCam (ab131064), anti-CTGF from Santa Cruz (sc-14939) and anti-FGF2 from PeproTech (#500-P18). FGF2 in condioned medium was also analysed by FGF2 V-PLEX ELISA from MSD (#K151MDD).

Scanning Acoustic Microscopy Loaded Imaging

Loaded and rested porcine articular cartilage was sectioned to 5 microns thickness. Sections were air dried overnight onto a charged glass slide. Sections were rehydrated and imaged under scanning acoustic microscopy (SAM) to measures acoustic wave speed, positively correlated to tissue stiffness. Images were taken from the articular (STZ) to the deep zone in normal and damaged samples to assess wave speed across the tissue by sampling 5 boxed regions (50x50 pixels) every 200µm. The same tissue region was imaged by polarised light microscopy.

Human Osteoarthritic Cartilage

Human osteoarthritic cartilage was macroscopically graded for severity of disease by modified Outerbridge classification (Grade 0; normal cartilage, Grade 1; cartilage with softening and swelling, Grade 2; partial-thickness defect with superficial fissuring, Grade 3; deep fissuring, Grade 4; exposed subchondral bone).
Human osteoarthritic articular cartilage biopsies were taken using a 4 mm biopsy punch, assigned to an Outerbridge classification. Explants were injured in 200 µl serum-free DMEM, after 30 min the conditioned medium was stored at -20 °C, then explants were fully digested with 50 µg/ml proteinase K and assessed for GAG content by DMMB assay. Alternatively, explant matrix proteins were extracted with 2.5 M NaCl for 30 min, then total tissue protein extracted with RIPA tissue dissociative lysis buffer for 1 h.

Polarization sensitive SHG imaging of collagen fibres under compression

Polarization sensitive Second Harmonic Generation (PSHG) was used to investigate the collagen fibre realignments under compressive load on the microscopic scale. The strength of the SHG signal from collagen is highly dependent on the polarisation of the laser fundamental with respect to the collagen fibre axis. Therefore by taking a series of images at different polarization angles it is possible to extract detailed information on the collagen organisation within the tissue on the microscopic scale. This analysis provides two parameters, I_2 and ϕ_2, which describe the collagen fibre organisation on the microscopic scale. ϕ_2 is the predominant collagen fibre orientation in a given pixel, and I_2 is a measure of the molecular organisation at a submicron scale (I_2=0 when the collagen fibre arrangement is isotropic, and increasing values of I_2 indicate a more parallel collagen fibre arrangement). A full description of how the measurements are taken and how the parameters I_2 and ϕ_2 are derived is given in [56]. 1 mm thick sections of human articular cartilage with the underlying bone attached were compressed on a bespoke loading rig which attached onto the stage of the multiphoton microscope (Supplementary Figure S3), after compressive loading the samples were left for 30 min to equilibrate.

Acknowledgements

This work was supported by funding from the Biotechnology and Biological Sciences Research Council (BBSRC) [grant number BB/M011224/1].

This work has been supported by the Centre for Osteoarthritis Pathogenesis Versus Arthritis (Grant 20205 and 21621).

Tissue samples and/or data were collected with informed donor consent in full compliance with national and institutional ethical requirements, the UK Human Tissue Act, and the Declaration of Helsinki (HTA Licence 12217 and REC 07/H0706/81).

The research was supported by the National Institute for Health Research (NIHR) Oxford Biomedical Research Centre (BRC). Disclaimer: The views expressed are those of the author(s) and not necessarily those of the NHS, the NIHR or the Department of Health.

Medical Research Council grant G1001398 [Quantifying age-related changes in the mechanical properties of tissues].

This work was partly funded by Arthritis Research UK grant No. 20714 and by a Leverhulme Trust Visiting Professorship (S. Brasselet) Grant No. VP2-2015-025.The collection and storage of human cartilage samples from total knee replacement surgery was carried out by the RD&E Tissue Bank, part of the NIHR Exeter Clinical Research Facility.

G.E.P thanks the Medical Research Council for funding (Grant No. MC_PC_15074) for developing sodium imaging methods.

This article contains supporting information online.

References

1. James, S. L. *et al.* Global, regional, and national incidence, prevalence, and years lived with disability for 354 diseases and injuries for 195 countries and territories, 1990–2017: a systematic analysis for the Global Burden of Disease Study 2017. *Lancet* **392**, 1789–1858 (2018).
2. Kiani, C., Chen, L., Wu, Y. J., Yee, A. J. & Yang, B. B. Structure and function of aggrecan. *Cell Res.* **12**, 19–32 (2002).
3. Vincent, T. L., McLean, C. J., Full, L. E., Peston, D. & Saklatvala, J. FGF-2 is bound to perlecan in the pericellular matrix of articular cartilage, where it acts as a chondrocyte mechanotransducer. *Osteoarthr. Cartil.* **15**, 752–763 (2007).
4. Hunter, D. J. & Bierma-Zeinstra, S. Osteoarthritis. *The Lancet* **393**, 1745–1759 (2019).
5. Wheaton, A. J. *et al.* Proteoglycan loss in human knee cartilage: Quantitation with sodium MR imaging - Feasibility study. *Radiology* **231**, 900–905 (2004).

6. Cuevas, P., Burgos, J. & Baird, A. Basic fibroblast growth factor (FGF) promotes cartilage repair in vivo. *Biochem. Biophys. Res. Commun.* **156**, 611–618 (1988).
7. Cucchiarini, M. *et al.* Improved Tissue Repair in Articular Cartilage Defects in Vivo by rAAV-Mediated Overexpression of Human Fibroblast Growth Factor 2. *Mol. Ther.* **12**, 229–238 (2005).
8. Hiraide, A. *et al.* Repair of articular cartilage defect by intraarticular administration of basic fibroblast growth factor gene, using adeno-associated virus vector. *Hum. Gene Ther.* **16**, 1413–1421 (2005).
9. Inoue, A. *et al.* The therapeutic effects of basic fibroblast growth factor contained in gelatin hydrogel microspheres on experimental osteoarthritis in the rabbit knee. *Arthritis Rheum.* **54**, 264–270 (2006).
10. Kaul, G. *et al.* Local stimulation of articular cartilage repair by transplantation of encapsulated chondrocytes overexpressing human fibroblast growth factor 2 (FGF-2)in vivo. *J. Gene Med.* **8**, 100–111 (2006).
11. Chia, S.-L. *et al.* Fibroblast growth factor 2 is an intrinsic chondroprotective agent that suppresses ADAMTS-5 and delays cartilage degradation in murine osteoarthritis. *Arthritis Rheum.* **60**, 2019–2027 (2009).
12. Yamamoto, T. *et al.* Fibroblast growth factor-2 promotes the repair of partial thickness defects of articular cartilage in immature rabbits but not in mature rabbits. *Osteoarthr. Cartil.* **12**, 636–641 (2004).
13. Tang, X. *et al.* Connective tissue growth factor contributes to joint homeostasis and osteoarthritis severity by controlling the matrix sequestration and activation of latent TGFβ. *Ann. Rheum. Dis.* **77**, 1372–1380 (2018).
14. Fukumoto, T. *et al.* Combined effects of insulin-like growth factor-1 and transforming growth factor-β1 on periosteal mesenchymal cells during chondrogenesis in vitro. *Osteoarthr. Cartil.* **11**, 55–64 (2003).
15. Murdoch, A. D. *et al.* Chondrogenic Differentiation of Human Bone Marrow Stem Cells in Transwell Cultures: Generation of Scaffold-Free Cartilage. *Stem Cells* **25**, 2786–2796 (2007).
16. Bos, P. K., Verhaar, J. A. N. & van Osch, G. J. V. M. Age-Related Differences in Articular Cartilage Wound Healing: A Potential Role for Transforming Growth Factor β1 in Adult Cartilage Repair. in *Advances in Experimental Medicine and Biology* **585**, 297–309 (Springer New York, 2006).
17. Daniels, J. T. *et al.* Mediation of Transforming Growth Factor-β1-Stimulated Matrix Contraction by Fibroblasts. *Am. J. Pathol.* **163**, 2043–2052 (2003).
18. Penn, J. W., Grobbelaar, A. O. & Rolfe, K. J. The role of the TGF-β family in wound healing, burns and scarring: a review. *Int. J. Burns Trauma* **2**, 18–28 (2012).
19. Ori, A., Wilkinson, M. C. & Fernig, D. G. A Systems Biology Approach for the Investigation of the Heparin/Heparan Sulfate Interactome. *J. Biol. Chem.* **286**, 19892–19904 (2011).
20. Vincent, T., Hermansson, M., Bolton, M., Wait, R. & Saklatvala, J. Basic FGF mediates an immediate response of articular cartilage to mechanical injury. *Proc. Natl. Acad. Sci.* **99**, 8259–8264 (2002).
21. Glasson, S. S. *et al.* Characterization of and osteoarthritis susceptibility in ADAMTS-4-knockout mice. *Arthritis Rheum.* **50**, 2547–2558 (2004).
22. Glasson, S. S. *et al.* Deletion of active ADAMTS5 prevents cartilage degradation in a murine model of osteoarthritis. *Nature* **434**, 644–648 (2005).
23. Troeberg, L. & Nagase, H. Proteases involved in cartilage matrix degradation in osteoarthritis. *Biochim. Biophys. Acta - Proteins Proteomics* **1824**, 133–145 (2012).
24. Maroudas, A. & Freeman, M. A. R. Physico-Chemical Properties of Articular Cartilage. in *Adult Articular Cartilage* 215–290 (Pitman Medical, 1979).
25. Shapiro, E. M. *et al.* Sodium Visibility and Quantitation in Intact Bovine Articular Cartilage Using High Field 23Na MRI and MRS. *J. Magn. Reson.* **142**, 24–31 (2000).
26. Shapiro, E. M., Borthakur, A., Gougoutas, A. & Reddy, R. 23Na MRI accurately measures fixed charge density in articular cartilage. *Magn. Reson. Med.* **47**, 284–291 (2002).
27. Bashir, A., Gray, M. L. & Burstein, D. Gd-DTPA2− as a measure of cartilage degradation. *Magn. Reson. Med.* **36**, 665–673 (1996).
28. Chiu, L.-Y., Hung, K.-W., Tjong, S.-C., Chiang, Y.-W. & Sue, S.-C. NMR characterization of the electrostatic interaction of the basic residues in HDGF and FGF2 during heparin binding. *Biochim. Biophys. Acta - Proteins Proteomics* **1844**, 1851–1859 (2014).
29. Nieminen, M. T. *et al.* T 2 relaxation reveals spatial collagen architecture in articular cartilage: A comparative quantitative MRI and polarized light microscopic study. *Magn. Reson. Med.* **46**, 487–493 (2001).
30. Chen, S. S., Falcovitz, Y. H., Schneiderman, R., Maroudas, A. & Sah, R. L. Depth-dependent compressive properties of normal aged human femoral head articular cartilage: relationship to fixed charge density. *Osteoarthr. Cartil.* **9**, 561–569 (2001).
31. Maroudas, A. & Bollough, P. Permeability of Articular Cartilage. *Nature* **219**, 1260–1261 (1968).
32. Yang, X. & Momot, K. I. *Biophysics and Biochemistry of Cartilage by NMR and MRI*. (Royal Society of Chemistry, 2016). doi:10.1039/9781782623663
33. Schinagl, R. M., Gurskis, D., Chen, A. C. & Sah, R. L. Depth-dependent confined compression modulus of full-thickness bovine articular cartilage. *J. Orthop. Res.* **15**, 499–506 (1997).
34. Manzano, S., Manzano, R., Doblaré, M. & Doweidar, M. H. Altered swelling and ion fluxes in articular cartilage as a biomarker in osteoarthritis and joint immobilization: a computational analysis. *J. R. Soc. Interface* **12**, 20141090 (2015).
35. Linn, F. C. & Sokoloff, L. Movement and composition of interstitial fluid of cartilage. *Arthritis Rheum.* **8**, 481–494 (1965).
36. Armstrong, C. G. & Mow, V. C. Variations in the intrinsic mechanical properties of human articular cartilage with age, degeneration, and water content. *J. Bone Jt. Surg.* **64**, 88–94 (1982).
37. Mow, V. C., Ratcliffe, A. & Robin Poole, A. Cartilage and diarthrodial joints as paradigms for hierarchical materials and structures. *Biomaterials* **13**, 67–97 (1992).
38. DiDomenico, C. D., Lintz, M. & Bonassar, L. J. Molecular transport in articular cartilage — what have we learned from the past 50 years? *Nat. Rev. Rheumatol.* **14**, 393–403 (2018).
39. O'Hara, B. P., Urban, J. P. & Maroudas, A. Influence of cyclic loading on the nutrition of articular cartilage. *Ann. Rheum. Dis.* **49**, 536–539 (1990).
40. Venn, M. & Maroudas, A. Chemical composition and swelling of normal and osteoarthrotic femoral head cartilage. I. Chemical composition. *Ann. Rheum. Dis.* **36**, 121–129 (1977).
41. Madelin, G. *et al.* Articular Cartilage: Evaluation with Fluid-suppressed 7.0-T Sodium MR Imaging in Subjects with and Subjects without Osteoarthritis. *Radiology* **268**, 481–491 (2013).
42. Little, C. B. *et al.* Matrix metalloproteinase-13 deficient mice are resistant to osteoarthritic cartilage erosion but not chondrocyte hypertrophy or osteophyte development. *Arthritis Rheum.* **60**, 3723–3733 (2009).
43. Nia, H. T. *et al.* High-Bandwidth AFM-Based Rheology Reveals that Cartilage is Most Sensitive to High Loading Rates at Early Stages of Impairment. *Biophys. J.* **104**, 1529–1537 (2013).

44. Correa, D. *et al.* Sequential exposure to fibroblast growth factors (FGF) 2, 9 and 18 enhances hMSC chondrogenic differentiation. *Osteoarthr. Cartil.* **23**, 443–453 (2015).

45. Handorf, A. M. & Li, W.-J. Fibroblast Growth Factor-2 Primes Human Mesenchymal Stem Cells for Enhanced Chondrogenesis. *PLoS One* **6**, e22887 (2011).

46. Solchaga, L. A. *et al.* FGF-2 enhances the mitotic and chondrogenic potentials of human adult bone marrow-derived mesenchymal stem cells. *J. Cell. Physiol.* **203**, 398–409 (2005).

47. Muhammad, H. *et al.* Human migratory meniscus progenitor cells are controlled via the TGF-β pathway. *Stem Cell Reports* **3**, 789–803 (2014).

48. Zengini, E. *et al.* Genome-wide analyses using UK Biobank data provide insights into the genetic architecture of osteoarthritis. *Nat. Genet.* **50**, 549–558 (2018).

49. Tachmazidou, I. *et al.* Identification of new therapeutic targets for osteoarthritis through genome-wide analyses of UK Biobank data. *Nat. Genet.* **51**, 230–236 (2019).

50. Watt, F. E. *et al.* The molecular profile of synovial fluid changes upon joint distraction and is associated with clinical response in knee osteoarthritis. *Osteoarthr. Cartil.* **28**, 324–333 (2020).

51. Hochberg, M. C. *et al.* Effect of Intra-Articular Sprifermin vs Placebo on Femorotibial Joint Cartilage Thickness in Patients With Osteoarthritis. *JAMA* **322**, 1360 (2019).

52. Eckstein, F. *et al.* Intra-articular sprifermin reduces cartilage loss in addition to increasing cartilage gain independent of location in the femorotibial joint: post-hoc analysis of a randomised, placebo-controlled phase II clinical trial. *Ann. Rheum. Dis.* **79**, 525–528 (2020).

53. Everett, A. D., Lobe, D. R., Matsumura, M. E., Nakamura, H. & McNamara, C. A. Hepatoma-derived growth factor stimulates smooth muscle cell growth and is expressed in vascular development. *J. Clin. Invest.* **105**, 567–575 (2000).

54. Narron, J. V, Stoops, T. D., Barringhaus, K., Matsumura, M. & Everett, A. D. Hepatoma-Derived Growth Factor Is Expressed after Vascular Injury in the Rat and Stimulates Smooth Muscle Cell Migration. *Pediatr. Res.* **59**, 778–783 (2006).

55. Perez-Riverol, Y. *et al.* The PRIDE database and related tools and resources in 2019: improving support for quantification data. *Nucleic Acids Res.* **47**, D442–D450 (2019).

56. Mansfield, J. C., Mandalia, V., Toms, A., Winlove, C. P. & Brasselet, S. Collagen reorganization in cartilage under strain probed by polarization sensitive second harmonic generation microscopy. *J. R. Soc. Interface* **16**, 20180611 (2019).

8.2 Reagents

Table 8.1 Listed reagents

Reagent	**Source**	**Catalogue Number**
Batimastat	AbCam, Cambridge, UK	Ab142087
BD Vacutainer EDTA 18 mg	Fisher Scientific, Waltham, USA	367525
Collagenase II	Thermo Fisher	17101-015
cOmplete EDTA-free Protease Inhibitor Cocktail	Roche (Merck, Sigma)	4693132001
Dispase	Thermo Fisher	17105-041
DMEM	Lonza	BE12-604F
Float-A-Lyzer G2 Dialysis Device	Spectra/Por	G235029
FGFR inhibitor SB402451	GSK	Non-catalogue
Heparitinase I	Sigma Aldrich	H8891-5UN
HiTrap Heparin HP affinity columns	GE Healthcare	17040601 GE
Recombinant FGF2	Peprotech	100-18C-10
Recombinant TGFβ3		
RNase Inhibitor	Thermo Fisher	N8080119
RNeasy Mini Kit	QIAGEN	
RNEasy Micro Kit	QIAGEN	
PowerUp SYBR Green Master Mix	Applied Biosystems	A25778
Proteinase K	QIAGEN	19131
TGFβ3	Bio-Techne	243-B3
TGFβR inhibitor SB431542	Bio-Techne	1614/1

Table 8.2 Listed antibodies

Antibody	**Source**	**Catalogue Number**	**Usage**
Anti-HDGF	AbCam	Ab131046	1:1000 milk WB
Anti-CTGF	Santa Cruz	Sc14939	1:500 milk WB
Anti-FGF2	PeproTech	500-P18	1:1000 milk WB
Anti-α-Tubulin	AbCam	Ab7291	1:1000 milk WB
Anti-β-Actin	Novus	8H10D10	1:1000 milk WB
Anti-Perlecan	Merck	MAB1948P	IHC
Anti-Collagen VI	AbCam	Ab6588	IHC
AlexaFluor 594 Anti-rat	Thermo Fisher	A11007	IHC
AlexaFluor 488 anti-rabbit	Thermo Fisher	A11034	IHC
Anti-pERK1/2	Cell Signalling	4370	1:1000 BSA WB
Anti-pSGK1 (T256)	Thermo Fisher	44-1260G	1:1000 BSA WB
Anti-pSGK1 (S422)	Thermo Fisher	44-1264G	1:1000 BSA WB
Goat anti-Rabbit HRP	Thermo Fisher	31460	1:5000 milk WB
Rabbit anti-Goat HRP	Dako	P0449	1:1000 milk WB

8.3 Equipment

Table 8.3 Listed equipment

Equipment	**Source**	**Version**
9.4T Ultra-high field microimaging system	Bruker	
Accu-Cut SRM 200 microtome	Sakura	
Cryostat	Leica	CM1900UV
ImageJ	NIH	1.52p Java 1.8.0_172 (64bit)
Nanodrop One	Thermo Scientific	
Olympus BX61 Brightfield microscope	Olympus	
Olympus FV1200 IX83 Confocal microscope	Olympus	
ViiA7 PCR Machine	Applied Biosystems	

8.4 Supplementary

Table 8.4 Hepatoma-Derived Growth Factor published structures

PDB ID	DESCRIPTION	METHOD	REFERENCE
1N27	Solution Structure of PWWP Domain of Mouse HDGFRP3	Solution NMR	(Nameki, 2005)
1RI0	NMR Structure of N Terminal HATH Domain of HDGF	Solution NMR	(Sue *et al.*, 2004)
2B8A	High Resolution Structure of HDGF PWWP Domain	Solution NMR	(Lukasik, 2006)
2NLU	Domain Swapped Dimer PWWP of HDGF	Solution NMR	(Sue *et al.*, 2007)
3QBY	Crystal Structure of PWWP Domain of HDGF2 in Complex with H4K20me3 peptide	X-Ray Diffraction	(Wu *et al.*, 2011)
3QJ6	Crystal structure of PWWP domain of HDGF2 in complex with H3K79me3	X-Ray Diffraction	(Wu *et al.*, 2011)
5XSK	Crystal structure of HDGF bound to SMYD1 promoter	X-Ray Diffraction	(Chen *et al.*, 2018)
5XSL	Crystal structure of *apo* inactive unbound HDGF	X-Ray Diffraction	(Chen *et al.*, 2018)

Table 8.5 Microfluidic TaqMan array gene list

GENE	PROTEIN	TAQMAN ASSAY ID	(CARTILAGE) FUNCTION
18S	Eukaryotic 18S rRNA	Hs99999901_s1	Ribosomal RNA
ADAMTS1	A Disintegrin-Like And Metallopeptidase (Reprolysin Type) With Thrombospondin Type 1 Motif, 1	Mm00477355_m1	
ADAMTS15	A Disintegrin-Like And Metallopeptidase (Reprolysin Type) With Thrombospondin Type 1 Motif, 15	Mm01176187_m1	
ADAMTS4	A Disintegrin-Like And Metallopeptidase (Reprolysin Type) With Thrombospondin Type 1 Motif, 4	Mm00556068_m1	Aggrecanase that cleaves aggrecan and mediates cartilage degradation (Glasson *et al.*, 2004)
ADAMTS5	A Disintegrin-Like And Metallopeptidase (Reprolysin Type) With Thrombospondin Type 1 Motif, 5 (Aggrecanase-2)	Mm00478620_m1	Aggrecanase that cleaves aggrecan and mediates cartilage degradation (Glasson *et al.*, 2005)
AGTR2	Angiotensin II Receptor, Type 2	Mm01341373_m1	
ALDH1A2	Aldehyde Dehydrogenase Family 1, Subfamily A2	Mm00501306_m1	Retinoic acid regulatory gene, hand osteoarthritis genetic risk variant (Shepherd *et al.*, 2018)
ARG1	Arginase, Liver	Mm00475988_m1	M2-macrophage related gene, upregulated 4h post-DMM (Ismail *et al.*, 2016), hydrolysis of arginine to ornithine and urea
BDKRB1	Bradykinin Receptor, Beta 1	Mm04207315_s1	Pain regulatory gene
BDKRB2	Bradykinin Receptor, Beta 2	Mm00437788_s1	Pain regulatory gene
BMPR2	Bone Morphogenetic Protein Receptor, Type II (Serine/Threonine Kinase)	Mm00432134_m1	Bone and cartilage development gene

CCL2	Chemokine (C-C Motif) Ligand 2	Mm00441242_m1	Monocyte chemoattractant protein-1 (MCP-1)
CCR2	Chemokine (C-C Motif) Receptor 2	Mm01216173_m1	Receptor for CCL2/MCP-1
CD68	Macrophage Antigen CD68	Mm03047340_m1	Monocyte/macrophage marker
CTGF	Connective Tissue Growth Factor	Mm01192932_g1	Heparin-binding growth factor, released upon injury, chondroprotective in OA (Tang *et al.*, 2018)
CYP26A1	Cytochrome P450, Family 26, Subfamily A, Polypeptide 1	Mm00514486_m1	
CYP26B1	Cytochrome P450, Family 26, Subfamily B, Polypeptide 1	Mm00558507_m1	
CYP26C1	Cytochrome P450, Family 26, Subfamily C, Polypeptide 1	Mm03412454_m1	
FGF18	Fibroblast Growth Factor 18	Mm00433286_m1	ECM formation, chondrogenic cell differentiation, inhibiting cell proliferation, chondroprotective growth factor in OA (Ellman *et al.*, 2013)
FGF2	Fibroblast Growth Factor 2	Mm00433287_m1	Heparin-binding growth factor. Anabolic and catabolic regulator of cartilage (Ellman *et al.*, 2013). Protective in OA (Chia *et al.*, 2009).
FGFR1	Fibroblast Growth Factor Receptor 1	Mm00438930_m1	
FGFR2	Fibroblast Growth Factor Receptor 2	Mm00438941_m1	
FGFR3	Fibroblast Growth Factor Receptor 3	Mm00433294_m1	
FGFR4	Fibroblast Growth Factor Receptor 4	Mm01341852_m1	
FMOD	Fibromodulin	Mm00491215_m1	Cartilage matrix component, interacts with collagen I and II
GAPDH	Glyceraldehyde-3-Phosphate Dehydrogenase	Hs99999905_m1	
HAS1	Hyaluronan Synthase1	Mm03048195_m1	Cartilage matrix synthesis enzyme
HAS2	Hyaluronan Synthase 2	Mm00515089_m1	Cartilage matrix synthesis enzyme

IL1A	Interleukin 1 Alpha	Mm00439620_m1	Catabolic inflammatory cytokine, inhibits matrix synthesis, induces aggrecanase matrix degradation (Neidel and Zeidler, 1993; Gruber *et al.*, 2004; Ismail *et al.*, 2015)
IL1B	Interleukin 1 Beta	Mm00434228_m1	Catabolic pro-inflammatory cytokine, inhibits matrix synthesis, induces aggrecanase matrix degradation (Neidel and Zeidler, 1993; Ismail *et al.*, 2015)
IL33	Interleukin 33	Mm00505403_m1	Pro-Inflammatory cytokine, neutrophil migration in synovial fluid, binds IL1RL1/ST2 receptor, Th2 maturation, innate cell activation
IL6	Interleukin 6	Mm00446190_m1	Inflammatory cytokine, aggrecanase-mediated proteoglycan catabolism (Flannery *et al.*, 2000)
INHBA	Inhibin Beta-A	Mm00434339_m1	Subunit of Inhibin A, Activin A and Activin AB, inhibit aggrecanase-mediated cleavage of aggrecan in human and rat articular cartilage, regulator of TGFβ superfamily
LRP1	Low Density Lipoprotein Receptor-Related Protein 1	Mm00464608_m1	Extracellular protein endocytosis, ADAMTS-5 clearance (Yamamoto *et al.*, 2013)
LTBP1	Latent Transforming Growth Factor Beta Binding Protein 1	Mm00498234_m1	Targets latent complexes of TGFβ to the extracellular matrix
LTBP2	Latent Transforming Growth Factor Beta Binding Protein 2	Mm01307379_m1	Targets latent complexes of TGFβ to the extracellular matrix
MMP13	Matrix Metallopeptidase 13	Mm00439491_m1	Collagenase, implicated in early OA cartilage erosion (Little *et al.*, 2009),

			cleaves fibrillar collagen, fibronectin, TNC, ACAN, type I, type II and type III collagen, collagen type IV, type XIV and type X, activation of TGFβ1 and degradation
MMP19	Matrix Metallopeptidase 19	Mm00491300_m1	Matrix aggrecan and COMP cleavage (Stracke *et al.*, 2000), hydrolyses collagen type IV, laminin, nidogen, nascin-C isoform, fibronectin, and type I gelatin
MMP3	Matrix Metallopeptidase 3	Mm00440295_m1	(Stromelysin) Collagenase enzyme
NGF	Nerve Growth Factor	Mm00443039_m1	Neurotrophic factor, nerve growth and differentiation, regulates pain in OA (Von Loga *et al.*, 2019)
NPY	Neuropeptide Y	Mm03048253_m1	Pain-related neuropeptide, cartilage homeostasis (Kang *et al.*, 2020)
PMEPA1	Prostate Transmembrane Protein, Androgen Induced 1	Mm00452229_m1	Negative regulator of TGFβ signalling
PTGS2	Prostaglandin-Endoperoxide Synthase 2	Mm00478374_m1	Cyclooxygenase (COX2), cartilage injury responsive
SOST	Sclerostin	Mm04208528_m1	Bone growth negative regulator, Wnt signalling inhibitior
TAC1	Tachykinin 1	Mm01166996_m1	Tachykinin precursor: Substance P, Neurokinin A, Neuropeptide K, Neuropeptide Gamma.
TGFB1	Transforming Growth Factor, Beta 1	Mm01178820_m1	TGFβ family ligand
TGFB2	Transforming Growth Factor, Beta 2	Mm00436955_m1	TGFβ family ligand
TGFB3	Transforming Growth Factor, Beta 3	Mm00436960_m1	TGFβ family ligand
TGFBI	Transforming Growth Factor, Beta Induced	Mm01337605_m1	Collagen-binding (I, II, IV) induced by TGFβ and acts to inhibit cell adhesion in other cell types

TGFBR1	Transforming Growth Factor, Beta Receptor I	Mm00436964_m1	(ALK-5), TGFβ1 (and TGFβ2) signalling, heterodimerises with TFGβR2 upon TGFβ-binding
TGFBR2	Transforming Growth Factor, Beta Receptor II	Mm00436977_m1	TGFβ1 and TGFβ2 signalling, binds TGFβ, heterodimerises with TGFβR1
TGFBR3	Transforming Growth Factor, Beta Receptor III	Mm00803538_m1	(Betaglycan), cell surface heparan sulfate proteoglycan, TGFβ co-receptor
TIMP1	Tissue Inhibitor Of Metalloproteinase 1	Mm00441818_m1	Secreted inhibitor of MMPs and ADAMTSs
TNC	Tenascin C	Mm00495662_m1	Matrix glycoprotein, involved in early cartilage maturation
TNFAIP6	Tumor Necrosis Factor Alpha Induced Protein 6	Mm00493736_m1	(TSG-6) FGF2-dependent, associated with inflammatory markers in synovial fluid of knee OA, upregulated in OA, mildly chondroprotective
TNFRSF12A	Tumor Necrosis Factor Receptor Superfamily, Member 12a	Mm00489103_m1	(Tweak) Matrix-cell adhesion,
TNN	Tenascin N	Mm01284101_m1	(Tenascin-W) Matrix protein, bone Wnt signalling, upregulated post-DMM (Gardiner *et al.*, 2015)
TRPV4	Transient Receptor Potential Cation Channel, Subfamily V, Member 4	Mm01203726_m1	Sensor of mechanical or osmotic signals (McNulty *et al.*, 2015), mechanotransduction
TSPAN2	Tetraspanin 2	Mm00510514_m1	Regulated post-DMM (Gardiner *et al.*, 2015), cell surface protein with four hydrophobic domains
WNT16	Wingless-Type MMTV Integration Site Family, Member 16	Mm00446420_m1	Bone regulation, inhibits chondrocyte hypertrophy (Tong *et al.*, 2019).